UNIVERSITY OF SOUTHAMPTON

FACULTY OF ENGINEERING, SCIENCE AND MATHEMATICS

School of Ocean and Earth Science

IRON BIOGEOCHEMISTRY IN THE WATERS SURROUNDING THE CROZET ISLANDS, SOUTHERN OCEAN.

by

Hélène Planquette

Thesis for the degree of Doctor of Philosophy

February 2008

UNIVERSITY OF SOUTHAMPTON

ABSTRACT

FACULTY OF ENGINEERING, SCIENCE, AND MATHEMATICS

SCHOOL OF OCEAN AND EARTH SCIENCE

Doctor of Philosophy

Iron biogeochemistry in the waters surrounding the Crozet Islands, Southern Ocean.

By Hélène Planquette

The aim of this thesis was to improve our understanding of the natural iron fertilisation processes that can alleviate the High Nutrient Low Chlorophyll conditions normally associated with the Southern Ocean. The annual phytoplankton bloom occurring north of the Crozet Plateau (46˚26'S - 52˚18'E) provided a good opportunity to study these phenomena during CROZEX, a multidisciplinary study performed in austral summers 2004/2005 and 2005/2006. Particular emphasis has been placed on the sources of Fe to the upper water column, and on the different processes that drive the distribution of iron, such as mixing with deeper waters, advection of Fe rich waters from the islands, or particles and atmospheric inputs.

A flow-injection analyser with DPD catalytic spectrophotometric detection (FIA-DPD) was first set up for the determination of total dissolved Fe (DFe, ≤ 0.2 µm) and careful assessment of data demonstrated the high quality of the information obtained in this study. Analytical measurements of DFe were performed in twenty vertical profiles from the North to the South of the islands that show evidence of a range of processes influencing the iron distributions. Most significantly, an enrichment of DFe (>1 nM) has been identified at close proximity to the islands, which suggests that the plateau and the associated sediments are a source of iron. Waters further north also appear to be affected by this input of both coastal and shelf origin, although dissolved iron concentrations decrease as a function of distance to the north of the plateau with a gradient of 0.07 $nM.km^{-1}$ as a result of dispersion and mixing. This gradient was then combined with short-lived Radium isotopes profiles, allowing the determination of a horizontal advective flux of Fe. Estimates of atmosphere and vertical fluxes of Fe to surface waters were also calculated. It was then possible to estimate a pre-bloom concentration of ~ 0.44 nM, which is sufficient to drive the inferred level of the new production in the bloom area.

Labile iron has been distinguished from the refractory fraction of iron in the suspended particulate matter exported from the mixed layer by developing a two-stage leaching technique. The resulting solutions were analyzed using ICP-MS. By using associated ^{234}Th fluxes, vertical fluxes of particulate iron in both phases were determined as well as their residence times. Data clearly show that carbon export was linked to the iron residence time and enhanced in the northern region where iron inputs occur.

This thesis therefore provides a comprehensive data set of DFe and particulate iron in waters surrounding the Crozet Islands. It also presents the first attempt to establish an iron budget that can be developed into a model and provides a good reference point for subsequent studies of natural iron fertilization processes that occur around these islands.

LIST OF CONTENTS

LIST OF FIGURES

Chapter Three

Chapter Four

Chapter Five

LIST OF TABLES

Chapter Two

Chapter Four

Chapter Five

LIST OF APPENDICES

DECLARATION OF AUTHORSHIP

I, **Hélène Planquette**, declare that the thesis entitled:

Iron biogeochemistry in the waters surrounding the Crozet Islands, Southern Ocean

and the work presented in it are my own. I confirm that:

- this work was done wholly or mainly while in candidature for a research degree at this University;
- where any part of this thesis has previously been submitted for a degree or any other qualification at this University or any other institution, this has been clearly stated;
- where I have consulted the published work of others, this is always clearly attributed;
- where I have quoted from the work of others, the source is always given. With the exception of such quotations, this thesis is entirely my own work;
- I have acknowledged all main sources of help;
- where the thesis is based on work done by myself jointly with others, I have made clear exactly what was done by others and what I have contributed myself;
- Parts of this work have been published as:

H. Planquette, Statham P.J., Fones G.R., Charette M.A., Moore C.M., Salter I., Nédélec F.H., Taylor S.L., French M., Baker A.R., Mahowald N. and Jickells T.D., 2007. Dissolved iron in the vicinity of the Crozet Islands, Southern Ocean. Deep-Sea Research II, 54, 1999-2019

C.M. Moore, Seeyave S., Hickman A.E., Allen J.T., Lucas M.I., Planquette H., Pollard R.T. and Poulton A.J., 2007. Iron-light interactions during the CROZet natural iron bloom and EXport experiment (CROZEX) I: phytoplankton growth and photophysiology. Deep-Sea Research II, 54, 2045-2065

M.A. Charette, Gonneea M.E., Morris P. , Statham P.J., Fones G.R., Planquette H., Salter I., Naveira Garabato A., 2007. Radium isotopes as tracers of iron sources fueling a Southern Ocean phytoplankton bloom. Deep-Sea Research II, 54, 1989-1998

Signed: Hélène Planquette

Date: 12th February 2008

AUTHOR'S DECLARATION

At no time during the registration for the degree of Doctor of Philosophy has the author been registered for any other University award without prior agreement of the Graduate Committee.

This study was financed with the aid of a studentship from the University of Southampton and carried out in collaboration with the National Oceanography Centre, Southampton.

A programme of advanced study was undertaken, which included postgraduate courses in demonstrating and communication skills. Additional skills were acquired for working at sea with courses in personal survival techniques, risk assessments, and manual handling and lifting awareness. The author participated to three major cruises: CROZEX legs 1 and 2 Transect (RRS Discovery, D285&D286, 12 weeks, November 2004- January 2005) and Benthic Crozet (RRS Discovery, D300, 6 weeks, November 2005-January 2006).

The author also has been demonstrating during practicals in Environmental Analytical Chemistry, Chemical Oceanography, and during the Falmouth field trip organised by the National Oceanography Centre.

Relevant scientific meetings, seminars, and conferences were regularly attended at which work was often presented and several papers prepared for publication.

Publications: *see previous page*

Presentation and Conferences Attended:

National Oceanography Centre, CROZEX meeting, March 2006. "Iron sources and distribution around the Crozet Islands". **H Planquette**

Challenger Conference (Scottish Association for Marine Sciences), Oban, Scotland, September 2006. "A biogeochemical study in the context of the iron hypothesis" **H. Planquette**, P. J. Statham, G.R. Fones, M. A. Charette, A.R. Baker, T.D. Jickells

Challenger Conference (Scottish Association for Marine Sciences), Oban, Scotland, September 2006. "Distribution of dissolved iron around the Crozet Islands, Southern Ocean". **H. Planquette**, P. J. Statham, G.R. Fones, M. A. Charette

AGU Fall meeting 2006 San Francisco, U.S.A., "Evidence of a Natural Source of Iron around the Crozet Islands, Southern Ocean" **H. Planquette**, P.J. Statham, G.R. Fones, R. Sanders

EGU general assembly 2007 Vienna, Austria, "Dissolved iron in the vicinity of the Crozet Islands, Southern Ocean", **H. Planquette**, P.J. Statham, Gary R. Fones, M.A. Charette.

External Contacts:

Dr Matt Charette, WHOI, U.S.A.
Pr Tim Jickells, School of Environmental Sciences, University of East Anglia, U.K.
Dr Alex Baker, School of Environmental Sciences, University of East Anglia, U.K.

Word count of main body of thesis: 48,192 words

Signed: Hélène Planquette
Date: 12th February 2008

GRADUATE SCHOOL OF THE NATIONAL OCEANOGRAPHY CENTRE, SOUTHAMPTON

This PhD dissertation by

Hélène Planquette

has been produced under the supervision of the following persons

Supervisors Professor Peter J. Statham

Doctor Gary R. Fones

Doctor Richard Sanders

Chair of Advisory Panel: Doctor Rachel Mills

Internal Examiner: Professor Eric Achterberg

External Examiner: Professor Stéphane Blain

ACKNOWLEDGMENTS

These three years as a PhD student have been fantastic for my knowledge of oceanography and on a personal level. I would like to express my gratitude to my supervisors, Peter Statham, Gary Fones and Richard Sanders, who offered me the chance to do this PhD. I am really grateful to Peter for his advices and support, especially during the last 6 months, to Gary for his help with the ICP-MS and encouragements throughout these years, and to Richard for helping out reaching the 5% left. I would like to thank too Doug Connelly, Paul Gooddy, Bob Head and Tina Hayes for their assistance with the lab work.

Few months after I started my PhD, I was embarking on my first cruise in the Southern Ocean. To every single person who was on Discovery during CROZEX, thank you. It was such a wonderful and powerful experience that I will always remember. I am particularly thankful to Raymond Pollard, as well as Mike Lucas and John Allen who were always there when needed.

I can't forget Alain Saliot, Laurence Méjanelle and Richard Camilli who introduced me to oceanography several years ago and encouraged me to go ahead with my thesis even if they wouldn't recognize it!

I would like to thank my friends at NOCs particularly Isa, Sophie, Ross, Will and his bikes, and the so famous british german duet of moustaches: Ian and Joerg. I can't forget Julie and her incredible energy, Tristan and his poetry, Didier, Eric, Clément, Caroline, Hughes, Amélie and Mathieu who were always around.

I would like to send a huge thank you to my family, in particular to my parents to whom this thesis is dedicated. Without their constant support, love, and feel for work, none of this would have been possible. I would like to thank equally my brother Guillaume (as well as Couin-couin and Couine-couine) for his presence and advices during all these years. A particular thought on contemplative moments spent on the family sailing boats Belle Insula and Far. They are not so strangers to this.

Finally my thoughts are going to Florent, who crossed the channel so many times, who by his extreme support, patience and understanding made my writing hermit retirement in Normandy a great experience, and whom I am proud to be with.

LIST OF ABBREVIATIONS

ARC Algulhas return current

BA Baie Américaine (Ile de la Possession, Archipel Crozet)

CL Chemiluminescence

Chl *a* Chlorophyll a

CROZEX Crozet natural iron fertilisation and carbon export experiment

CTD Conductivity temperature depth

DPD *N,N*-dimethyl-*p*-phenylenediamine

EIFEX European Iron Fertilization Experiment in the subpolar South Atlantic Ocean

EISENEX Eisen (iron) experiment

FIA Flow injection analyser

FIA-CL Flow injection analyser with chemiluminescence detection

FIA-DPD Flow injection analyser with catalytic spectrophotometric detection of the oxidation of DPD by hydrogen peroxide

FIA-DPD-NTA Flow injection analyser with catalytic spectrophotometric detection of the oxidation of DPD by hydrogen peroxide using a NTA chelating resin

HAc-Me: Acid leachable (labile) Metal

HNLC High-nutrient low-chlorophyll

8-HQ 8-Hydroxyquinoline

ICP-MS Inductively coupled plasma mass spectrometry

LDPE Low-density polyethylene

LISW Low-iron sea water

LPFe Leachable Particulate iron

NASS-5 North Atlantic surface seawater – 5

NOCS National Oceanography Centre, Southampton

OTE Ocean technology equipment

PML Plymouth marine laboratory

PFe: Particulate iron

PFZ Polar front Zone

POC Particulate organic carbon

PON Particulate organic nitrogen

PTFE Polytetrafluoroethylene (Teflon)

Q-HCl Quartz distilled hydrochloric acid

Ref-Me- Refractory fraction of a metal

RSD Relative standard deviation

SAF Sub-Antarctic front

SBDW Sub-boiled distilled water

SeaWiFS Sea-viewing Wide Field-of-view Sensor

SEEDS Subarctic Pacific iron experiment for ecosystem dynamics study

SEM Scanning electron microscopy

SERIES Sub-arctic ecosystem response to iron enrichment study

SOFeX Southern Ocean iron fertilisation experiment

SOIREE Southern Ocean iron-release experiment

SPFe Iron concentration in suspended particulate matter

SPM Suspended particulate matter

TDFe Total dissolved iron

UoS University of Southampton

CHAPTER ONE:

INTRODUCTION AND OBJECTIVES

Over the last two decades, studying the role and the distribution of iron in marine ecosystems has been one of the most expanding areas of oceanography. Our knowledge of this element has been considerably improved by a number of major investigations in many parts of the world oceans and in different biogeochemical environments. Prior to announcing the main objectives of this thesis, various aspects of iron biogeochemistry are presented, starting with a brief history of iron investigations in marine systems and finishing with a detailed presentation of our current understanding of the marine iron cycle.

1 Rationale

1.1 A little bit of an iron history

The initial ideas on the potential role of iron as a limiting factor for primary production were suggested by Gran in 1931, Hart in 1934 and Harvey in 1938 but it was only in the early 1990s that scientists were able to investigate the role of iron (see Chapter Two) after the advent of clean sampling techniques and analytical methods that allowed the determination of natural iron concentrations in seawater at sub-nanomolar levels.

Curiously, whilst iron is the fourth most abundant element in the Earth's crust, its combined high reactivity and very low solubility in the oxidised form reduces it to

nanomolar or sub-nanomolar concentrations in dissolved form for most of the open ocean surface waters (Johnson et al., 1997). Where such low iron concentrations occur in spite of high macro-nutrient concentrations, these regions are called "High Nutrient Low Chlorophyll" (HNLC hereafter). They are mainly present in the Southern Ocean, the Equatorial Pacific and the North Pacific (Martin et al., 1993; de Baar et al, 1999; Watson, 2001) and represent nearly 40% of the oceans. The phytoplankton species in the HNLC zones behave as they do in areas of the ocean where the levels of the standard nutrients are low. John Martin was convinced there was something else that explained the absence of phytoplankton in these areas other than low nitrogen or phosphorus levels. Half a century after Gran, J. Martin proposed the hypothesis (Martin and Fitzwater, 1988; Martin and Gordon, 1988) that low concentrations of iron could be one limiting factor explaining the low primary productivity observed in these HNLC regions. This is known nowadays as the "iron hypothesis" (Martin, 1990a). To test this hypothesis, Martin sent his team to the Southern Ocean where they undertake incubations in which samples had iron added and others were left untreated for roughly a week, at simulated *in situ* light and temperature conditions. The phytoplankton in the iron enriched bottles flourished after a few days. He also measured the iron levels in seawater collected from these regions and found that they were exceedingly low (Martin et al., 1990b). This hypothesis led to many controversies (Martin et al., 1991) but Martin suggested that it could be possible to perform an *in situ* experiment, by artificially fertilizing the oceans by dumping tonnes of iron in the ocean. He argued that such fertilization would have a broader implication for climate. By stimulating primary production iron can increase the efficiency of the biological pump, by increasing the sinking of dead organisms and promoting drawdown of atmospheric carbon dioxide and thus possibly modify the climate (Martin et al., 1991). Such an iron addition experiment was conducted in October 1993 in the equatorial Pacific and was named IronEx-I (Martin et al., 1994) and was followed by many others. A summary of results is presented in the next section.

1.2 Artificial iron addition experiments

IronEx-I was the first experiment of a long series of such scientific investigations. 445 kg of iron were dumped over a 64 km^2 patch of oligotrophic water near the Galapagos Islands. The experiment was a success in that chlorophyll-*a* levels increased threefold (Martin et al., 1994). IronEx-II was performed in summer 1995 in the same area (Coale et al., 1996) and led to phytoplankton productivity enhancement. Such experiments took

place in other parts of the world's ocean over the last decade to try and understand the relationship between iron and the biogeochemical functioning of HNLC regions. In the Southern Ocean, SOIREE (Boyd et al., 2000) was conducted in February 1999, EISENEX in November 2000 (Gervais et al., 2002) and SOFeX (Coale et al., 2004) in January and February 2002. The HNLC region of the sub-arctic Pacific was fertilized in SEEDS which took place in summer 2001 (Takeda and Tsuda, 2005; Kinugasa et al., 2005) then by SERIES in July 2002 (Boyd et al, 2004). These experiments are summarized by de Baar et al. (2005) and Boyd et al. (2007): they all showed a significant increase in biological activity after addition of iron, therefore highlighting the importance of iron availability for phytoplankton communities in these types of system. However, the potential role of iron in carbon sequestration was demonstrated to be less important than expected (Buesseler et al., 2004; Blain et al., 2007). The possibility of performing large-scale fertilization experiments known as "geo-engineering" or "ocean farming" to reduce the green-house effect has emerged in the last few years. This tantalizing option is offered by a number of companies (Planktos, Green sea venture, Climos) that are trying to turn the cultivation of ocean-based algae into billion-dollar businesses (Foucart, 2007). In addition to the fact that such an experiment does not necessarily enhance the carbon sequestration, these artificial enrichments cannot mimic the natural processes that are adding iron continuously and slowly. Moreover, these perturbations could lead to many unintended side effects such as a modification of trophic chains or release of other than carbon dioxide greenhouse gases, as pointed out for example by Chisholm et al. (2001), Johnson and Karl (2002), Buesseler and Boyd (2003) or Zeebe and Archer (2005).

Sites of natural and continuous fertilisation by iron do exist where there is permanent interaction between water masses and margins of land masses; this phenomenon is generally called "the island mass effect". In particular, enhanced phytoplankton blooms occur in close proximity to islands such as South Georgia (Atkinson et al., 2001; Korb et Whitehouse, 2004; Holeton et al, 2005), Bouvet Island (Perissinotto et al., 1992, Kerguelen Islands (Blain et al, 2001; Bucciarelli et al., 2001; Blain et al, 2007; Blain et al., submitted) and the Crozet Islands (Sedwick et al., 2002; Pollard et al., 2007a). These studies have provided the first insights into the concentration of dissolved iron in these water columns and the response of the phytoplankton community to natural iron enrichment.

A detailed knowledge of biological and geochemical reservoirs, along with the cycling and fluxes of Fe is thus essential to first obtain a complete understanding of carbon and nutrient biogeochemistry in these regimes, and then to determine the environmental effect and efficiency of large scale iron fertilization of the ocean.

2 The iron cycle in the modern ocean.

Fe exists in seawater in two oxidation states. The dominant form of iron is Fe III in oxygenated waters, however Fe II can be formed in the upper ocean through photochemical (Rijkenberg, 2006) and biological processes (Maldonado and Price, 2000). The distribution of iron and its biogeochemical behaviour is driven by a complex combination of processes such as inputs, solubility of Fe(II) and Fe(III) under oxidising and reducing conditions, rates of chemical transformations, rates of transport within basins, uptake and release of Fe by planktonic organisms or internal cycling (de Baar and de Jong, 2001). Therefore, iron can be found in the ocean as soluble (free Fe (II) and Fe (III), weak ionic complexes) and insoluble inorganic species, dissolved organic complexes, colloidal forms, mineral particles and in living cells (Moffett, 2001). It is important to be aware that an arbitrary frontier has been defined, between particulate iron (>0.2 μm) and dissolved iron (<0.2 μm) (Wells et al. 1983), which appears to be complexed by naturally occurring organic or inorganic ligands (Rue and Bruland 1995). However, not all these forms are biologically available to phytoplankton in the water column. It is therefore necessary to determine the importance of the various sources, removal processes and speciation, when studying a particular environment. The major sources, transport and recycling processes controlling the iron cycle are illustrated in Figure I - 1 and are described below.

2.1 Role of iron in marine biota

Iron is a vital constituent of phytoplankton, because of its involvement in cellular metabolism. In cells, iron is present in more than one oxidation state. It is a catalyst of redox reactions and plays a major role in electron transport, in nitrogen reductase and nitrate fixation (Sunda and Huntsman, 1995; 1997) therefore having a huge impact on the assimilation of nitrogen by phytoplankton. Its presence in active centres of cytochromes

and iron-sulphur proteins, like ferrodoxin, makes it an essential component of the photosynthetic and respiratory electron transport chain.

As the amount of cellular iron needed to support phytoplankton growth is higher under low-light intensities, phytoplankton requires more iron-based redox proteins for photosynthesis, leading to the growth of small cells (Moore et al., 2007). This can have the consequence to increase the grazing by the micro zooplankton (Henjes et al., 2007), thus minimising the loss of fixed carbon and nitrogen from surface waters in settling particles (algal cells or faecal pellets), and finally increases nutrient cycling and decreases carbon export. To understand the uptake processes of iron, it is necessary to be able to quantify the amount of iron present, and thus to identify the various input and removal factors.

2.2 Sources of iron

The sources of iron are multiple and of high complexity. Depending on the physical and the chemical forms in which iron enters the marine system, the impact on the phytoplankton will be different. These sources can be external such as rivers and atmospheric deposition or in the ocean itself, for example, by resuspension of sediments.

Atmospheric deposition - The deposition of atmospheric aerosols to the surface ocean plays a significant role in supplying bioactive elements, including iron, and the major nutrients N and P to the remote ocean (Duce et al., 1991; Jickells et al., 2005). Natural sources from desert soils are believed to dominate emissions of atmospheric iron and aluminium, thus representing an important source of this micronutrient to many open ocean areas (Bruland et al, 1994; Duce and Tindale, 1991; Mahowald et al., 2005). The largest sources (e.g. Saharan desert) are located in the northern hemisphere (Jickells et al., 2005). However, the global distribution of atmospheric deposition shows large regional and temporal variability.

In terms of biogeochemical response to atmospheric deposition, only the readily soluble fraction is presumed to be available for biological uptake, and it is necessary to know the aerosol iron solubility to assess the impact of this source. Current global ocean biogeochemical models estimate that Fe solubilities are between 1–10% when specifying

bioavailable Fe fluxes from simulated aeolian dust deposition (Gregg et al., 2003; Moore et al., 2004). However, measurements of iron solubility in aerosols and rain reveal a greater variability and in a much wider range from 0.01 to 80% (Baker et al., 2006; Fan et al., 2006). The "true" solubility of aerosol Fe is still largely debated and this solubility related to the fraction of deposited Fe that is available for phytoplankton growth is still to be investigated (Jickells et al., 2005; Mahowald et al., 2005). A number of factors such as for example, the type of the aerosol source (Spokes et al, 1994), the suspended particle concentrations (Bonnet and Guieu, 2004) or the pH of rainwater (Baker et al., 2006) can influence the solubility. High Fe solubility has often been measured at low dust concentrations (Chen and Siefert, 2004). As dust concentrations decrease with distance of transport, Fe solubility would appear to increase with particle age in the atmosphere (Baker and Jickells, 2006). As for HNLC regions, it seems that atmospheric deposition may be important enough to relieve temporarily iron limitation (Blain et al., 2004; Planquette et al., 2007) although the atmospheric inputs are estimated to be small (e.g. 6% of the total dust input in the Southern Ocean, Jickells et al., 2005). In rainwater, the solubility of iron is estimated to be 14% at pH 8 (Baker et al., 2006). Therefore, even if 70% of the atmospheric deposition is dry, wet deposition dominates the flux of soluble iron in the ocean (Jickells and Spokes, 2001).

Riverine input – Riverine inputs are also variable and are relatively important in the global iron transport (Figure I – 1). Following mobilization from soils and rocks, iron can be transported via rivers to the coastal environments. Particulate and dissolved iron concentrations in rivers are typically in the order of 1 mM and 1 μM respectively ((Ussher et al. (2004), Figure I -1). The increase in salinity and the presence of the major seawater cations lead to the flocculation and sedimentation of both phases (dissolved and particulate) when they enter in contact with seawater. These processes reduce the flux of iron to the sea by about 70 to 95 % (Sholkovitz, 1978). Rivers and land run-off are estimated to deliver approximately half of the surface global iron input to the oceans, despite a high percentage of mobilized iron being lost in estuaries by scavenging. Although this pathway is likely to provide the main source of bioavailable iron to many coastal and shelf waters, the proportion of soluble iron originating from land run-off transported to open ocean remain unknown, making it difficult to estimate realistically the actual input (Ussher et al., 2004).

Hydrothermal activity -The two metals most enriched in hydrothermal vent fluids are iron and manganese. Vent fluids are strongly enriched in iron (1mmol L^{-1}), a million times greater than open-ocean values (Statham et al., 2005). When these metals enter the ocean, they are instantaneously cooled from temperatures greater than 350 °C down to temperatures lower than 30 °C. Precipitation of a range of iron rich metal sulfides occurs. In addition, high concentrations of suspended iron oxyhydroxide particulate material are precipitated (German and Von Damm, 2004). The hydrothermal inputs of iron and manganese, consequently, is argued to be essentially all scavenged and removed in the deep sea prior to have a chance to mix back into the surface waters (Bruland and Lohan, 2004), although this inference is yet to be fully demonstrated.

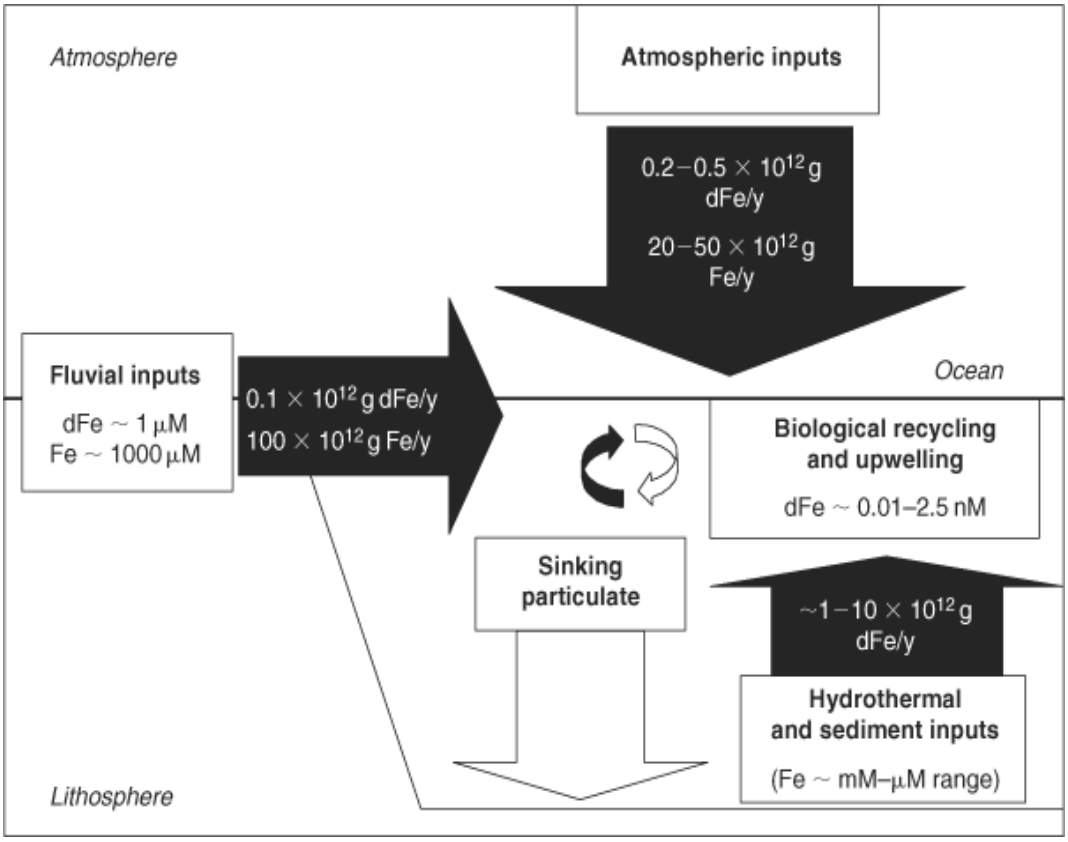

Figure I - 1: Global iron transport

Ambient concentrations of dissolved iron (dFe) and particulate iron (Fe) are in white boxes and approximate annual fluxes are shown in black and white arrows. Riverine flux is estimated on the basis of 90% loss from estuarine mixing. From Ussher et al., 2004.

Sea-ice melting - In polar waters, melting of sea ice can release some dissolved iron, up to concentrations greater than 1 nmol L^{-1} (Grotti et al., 2001; Sedwick and di Tullio, 1997) but this input is very localised. The mechanisms releasing dissolved iron from particles is still unclear, and a recent modelling study by Tagliabue and Arrigo (2006) reveal that photoreduction is the key process governing the supply of bioavailable Fe to the resident phytoplankton in the areas affected by this type of input such as the Ross Sea.

2.3 Removal processes

The removal of iron from the upper ocean occurs via two main pathways: biological and physical processes and are described below.

Biological uptake – Due to its involvement in biological cycles as previously described in Section 2.1, iron is usually highly depleted in surface waters (Bruland and Lohan, 2004). Depending on the plankton species and on the initial concentration available the biota adopts different strategies to acquire iron (Whitfield, 2001). Consequently, species have different minimum iron requirements for growth (Sunda and Huntsman, 1995; Price, 2005), depending on the location, the time of the year and the possible competition with other species (Hutchins et al., 1999) thus making iron requirements and uptake hard to define (Martin and Fitzwater, 1988). To further complicate this aspect, there is still an inability to define which forms are bioavailable to cells and some external influences on the iron availability such as light (Rijkenberg et al., 2005) or chemical speciation (Gerringa et al., 2000, 2007) can also affect the bioavailability of iron. These influences will be discussed in Section 2.5 of this chapter. Several assimilation and uptake mechanisms have been identified. For example, there is evidence that diatoms manage to extracellularly reduce the organically bound Fe(III). This reduction promotes the liberation of Fe(II) which can then become available for assimilation (Maldonado and Price, 1999; Barbeau et al., 2001). In regions where the phytoplankton community is iron stressed, iron must be recycled very rapidly by the biota. One consequence is that an individual iron atom may be in a different form each day (Bruland and Lohan, 2004). Interestingly, it has been argued that Fe(III)-binding organic ligands observed in the deep sea (Rue and Bruland, 1997) play an important role in allowing the dissolved iron in the deep sea to exist at concentrations on the order of nmol kg^{-1}. Uptake by marine

phytoplankton for primary productivity is a very important aspect of iron cycling as it affects its removal as well as the release of organic ligands that can influence the uptake.

Physical removal processes - In addition to the role of active assimilation of required trace metals by phytoplankton, the physical removal of iron and its subsequent export can happen simultaneously (de Baar and de Jong, 2001). In surface waters, iron can be scavenged onto a wide variety of relatively high affinity surface sites on both living and dead particulate materials. For example undissolved mineral particles, settling phytoplankton, and skeletal materials are good carriers of iron out the photic zone. Moreover, in surface waters, aqueous Fe rapidly precipitates into the more thermodynamically stable particulate ferric hydroxides (Fe(OH)x), which have a very low solubility, and therefore limit the levels of biologically available iron. These forms also can aggregate and be removed by scavenging. However, recycling processes allow a small fraction of iron to remain dissolved and/or to be available to phytoplankton.

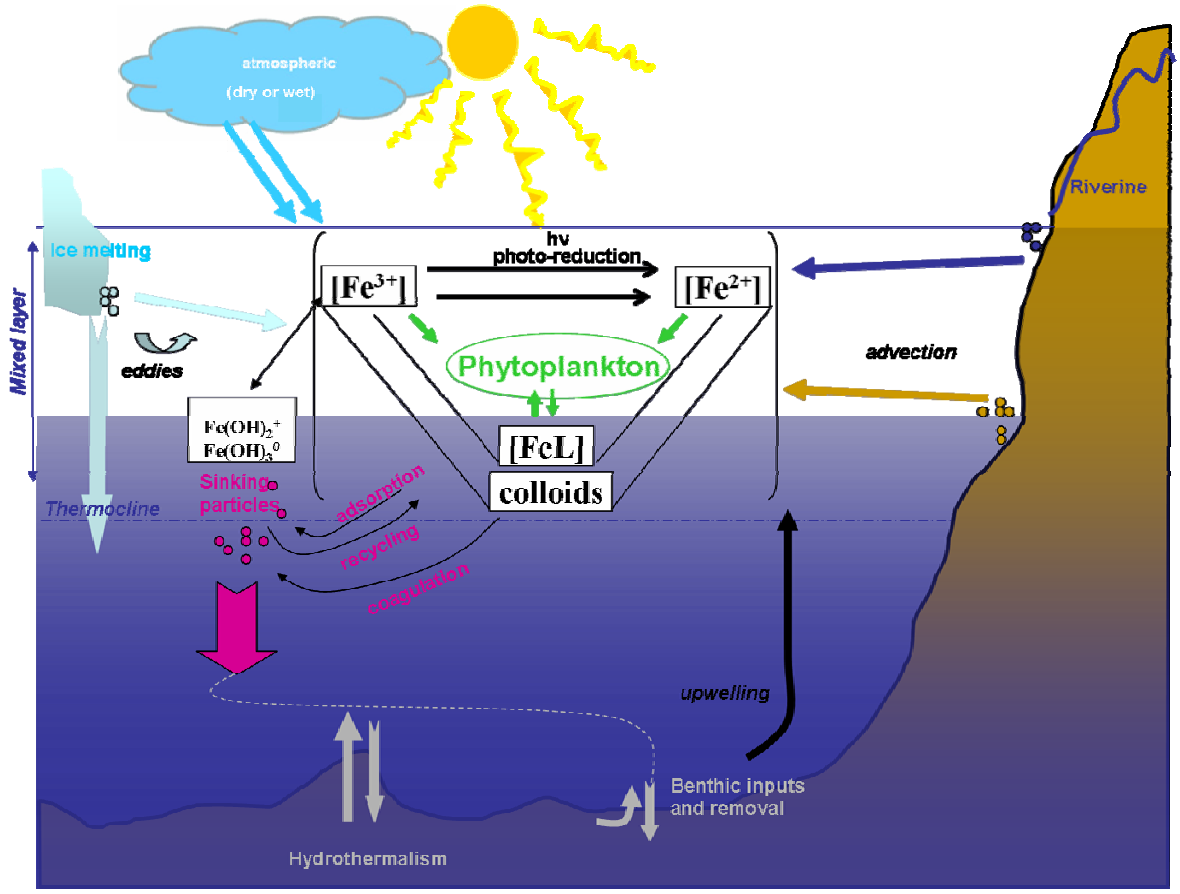

Figure I - 2: Schematic of the iron biogeochemical cycle in the modern ocean. FeL stands for iron associated with ligands

2.4 Recycling processes

Recycling processes occur at all depths of the water column. They encompass multiple cycles of assimilation into the biogenic pool in surface waters, by respiration of heterotrophic bacteria, followed by a release or remineralisation at greater depths before being buried in sediments (Hutchins et al., 1993). Iron can be recycled back into the dissolved phase and acts as a source to the deep-ocean as well, where relatively high concentrations can be observed above the sea floor and shelf areas (Elrod et al., 2004). Moreover, pore water concentrations of trace metals can be significantly higher than those observed in the overlying water column. Elevated pore-water concentrations suggested a potential for benthic fluxes of dissolved metals out of the sediment, which has been verified by direct measurements (Westerlund et al., 1986). These deep waters that are iron enriched have the potential to supply iron into the surface waters via upwelling processes and to be used by the phytoplankton. This phenomenon has been reported for example in the upwelled waters off coast of California (Johnson et al., 1999) or around the Kerguelen Islands (Blain et al, 2007) where sediments are resuspended then iron enriched water upwelled. This supply is not continuous and is limited to restricted events leading to various iron stress levels in the HNLC areas.

Another type of transport that may be particularly important at shelf edges is the horizontal advection of resuspended sediments (Johnson et al., 1997) and the influence of eddies (Johnson et al., 2005).

In the next section, external factors that influence iron availability in surface waters are presented.

2.5 Influence of light and chemical speciation

Light influence - Field and laboratory studies have shown the role of solar radiation on the formation of dissolved and biologically available iron species (Faust, 1994). UV radiation enhances the dissolution of particulate iron oxides/hydroxides and colloids (Sulzberger and Laubscher, 1995; Waite and Morel, 1984) by suitable reductants such as humic, fulvic and hydroxycarboxylic acids, as long as they are present in excess. These light-induced reductive reactions control to a large extent the chemical speciation and thus, the

biological availability of iron in surface waters. These reactions are also in competition with precipitation processes. For example, O_2 is an important oxidant of Fe(II), as well as the photochemically produced H_2O_2. The resultant Fe(III) can be then re-chelated by organic ligands or precipitated as iron hydroxides that are not directly bioavailable. Finally, Rijkenberg et al. (2006) showed that the photochemistry of Fe(III) and the resulting photo-produced Fe(II) concentration is strongly dependent on the type of chemical speciation of iron, i.e., the identity of the Fe-binding organic ligands. As a direct consequence, changes in UV radiation and accompanying changes in photochemical reactions (Rijkenberg et al., 2005), are an important element of global change impact on marine biogeochemical cycles (Moore et al., 2007).

Chemical speciation - In the surface of the oceans, it has been shown that complexation of iron and many other trace metals with relatively specific and strong metal binding organic ligands, leads to complexed forms being in excess of the ionic forms (Rue and Bruland, 1995). As mentioned earlier, iron exists in seawater in two oxidation states. Although the dominant form in oxic water is Fe(III), greater than 99% of this Fe(III) is complexed with strong organic ligands existing at sub-nanomolar concentrations but in slight excess of dissolved iron (Van den Berg, 1995; Boye et al., 2003). Recent advances have been made in the knowledge of marine siderophores that appear to constitute a significant fraction of the natural Fe(III) binding ligands (Macrellis et al, 2001; Gledhill et al., 2004). Siderophores are defined as low molecular weight organic chelators with a very high and specific affinity for Fe(III) (Bruland and Lohan, 2004). They are produced by marine heterotrophic and photosynthetic bacteria (Barbeau et al, 2003). However, even if the organic ligands appear to dominate the speciation, little is known about their identity, their chemical structure or their biogeochemical cycles.

2.6 Summary

The processes governing the marine iron cycle are summarized on Figure I - 2. Iron oceanic distributions and biogeochemical behaviour are controlled by complex interactions between inputs, internal recycling and removal processes (de Baar and de Jong, 2001; Ussher et al., 2004) coupled with physical transport and mixing in the oceans that affect the distribution in the water column of all forms of iron. Over the last ten years,

the use of relatively contamination free sampling and analytical methods have resulted in a significant increase in our understanding of the marine biogeochemistry of iron (Bruland and Lohan, 2005).

In surface oxic waters, the thermodynamically stable form of iron is Fe (III). However, Fe(II) seems to be the form in which iron is the most available to phytoplankton. Therefore, in order to maintain iron in solution, several reductive mechanisms occur such as enzymatic reduction at cell surfaces (Maldonado and Price, 2000); photoreduction (Moffett, 2001) that seems to be influenced by the nature of organic ligands (Rijkenberg et al., 2006); presence of organic matter (Rose and Waite, 2002) or the microbial community in anoxic basins and sediments (Ussher et al., 2004). Iron has been shown to be 99% complexed by organic ligands, but knowledge of their sources and identity remains unclear. Another major difficulty in assessing the dissolved iron concentration in environmental systems is the filtration processes. An arbitrary frontier has been set at 0.2µm but his fraction includes the colloidal fraction and what is measured is the filterable iron and not the truly dissolved iron. Together with other macro and micro nutrients, dissolved iron is then taken up by the phytoplankton for photosynthesis before being recycled throughout the water column. Remineralization processes (Berelson et al, 2003) of exported particulate organic matter can release some dissolved iron, as well as diffusion or resuspension of Fe(II) rich pore waters (Canfield, 1989). Iron in suspended sediments can be returned to the surface waters via different kind of transport including upwelling. Residence times for iron range from days in surface waters to a few years in deeper waters (de Baar and de Jong, 2001).

In remote areas, a characteristic iron profile show very low concentrations (picomolar) in the surface, increasing in deeper waters (Johnson et al., 1997; Ussher et al., 2004). However, the distribution of dissolved iron cannot be uniform in the world's ocean as it is considerably modified depending on the nature of sources and removal mechanisms, highlighting the complexity of all these previously described processes that influence the iron cycle. This complexity of processes cannot be mimicked during artificial iron fertilization experiments and the need to study places where natural iron fertilization occurs has recently been appreciated. A particular zone in which hypothesized natural iron release has been associated with blooms around islands is in the HNLC Southern Ocean.

3 The case of the Crozet Islands and thesis objectives

A major objective of this thesis is to test the hypothesis that the phytoplankton blooms occurring every year north of the Crozet Islands in the Southern Ocean are stimulated by a source of iron originating from or associated with the islands and to identify these sources.

3.1 The Crozet Islands

To place this objective in context, the Crozet Islands are located in the Southern Ocean which is one of the so-called HNLC regions. This volcanic archipelago is located on a shallow Plateau on the eastern flank of the southwest Indian ridge (Figure I - 3) and comprises two main islands, "Île de la Possession "and "Île de l'Est" in the east and three smaller islands 100 km to the west.

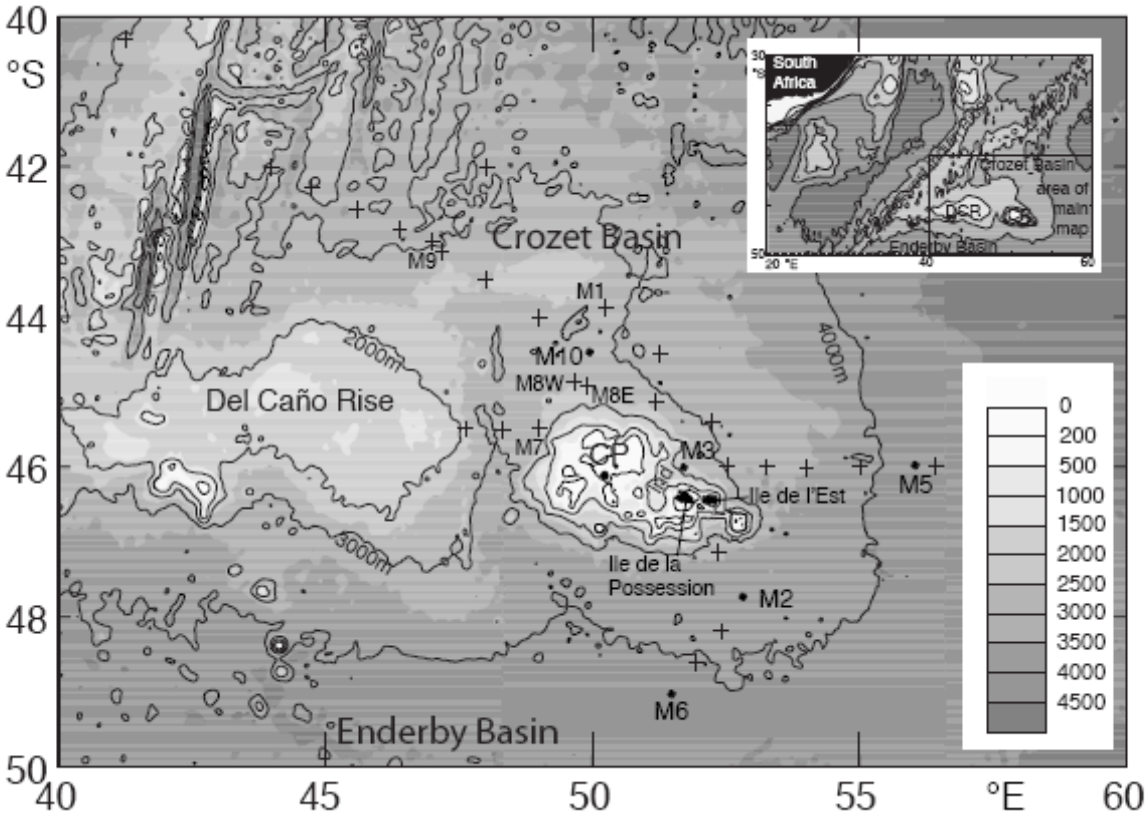

Figure I - 3: Bathymetry of the survey area between 40-50°S and 40-60°E.
The inset shows the location of the Crozet Archipelago relative to South Africa and the Southwest Indian Ridge. Black filled circles mark the five sites M2, M3, M5, M6 and M10 and crosses mark the main sampling stations that were sampled during CROZEX. Map courtesy of R. Pollard from Pollard et al., 2007b

The phytoplankton bloom which occurs annually north of the Crozet Plateau (Figure I – 4) provides an opportunity to examine the hypothesis that natural iron fertilization can alleviate HNLC conditions normally associated with the Southern Ocean. The bloom is located in the Polar Front Zone (Pollard et al., 2002 and Figure I - 4) with macronutrients present in non-limiting quantities at the end of the winter (Banse, 1996). The bloom usually peaks in October (up to 6 µg L^{-1}), although it is sometimes delayed until November (e.g., 2003-2004. It then decays away from the islands, but nearly every year there is a second bloom in late December of January that appears to be constrained closely to the two main islands. To the south of the Plateau, chlorophyll levels are low (< 0.5 µg L^{-1}), similar to background Southern Ocean levels. Over the Plateau itself, levels are intermediate (Venables et al., 2007).

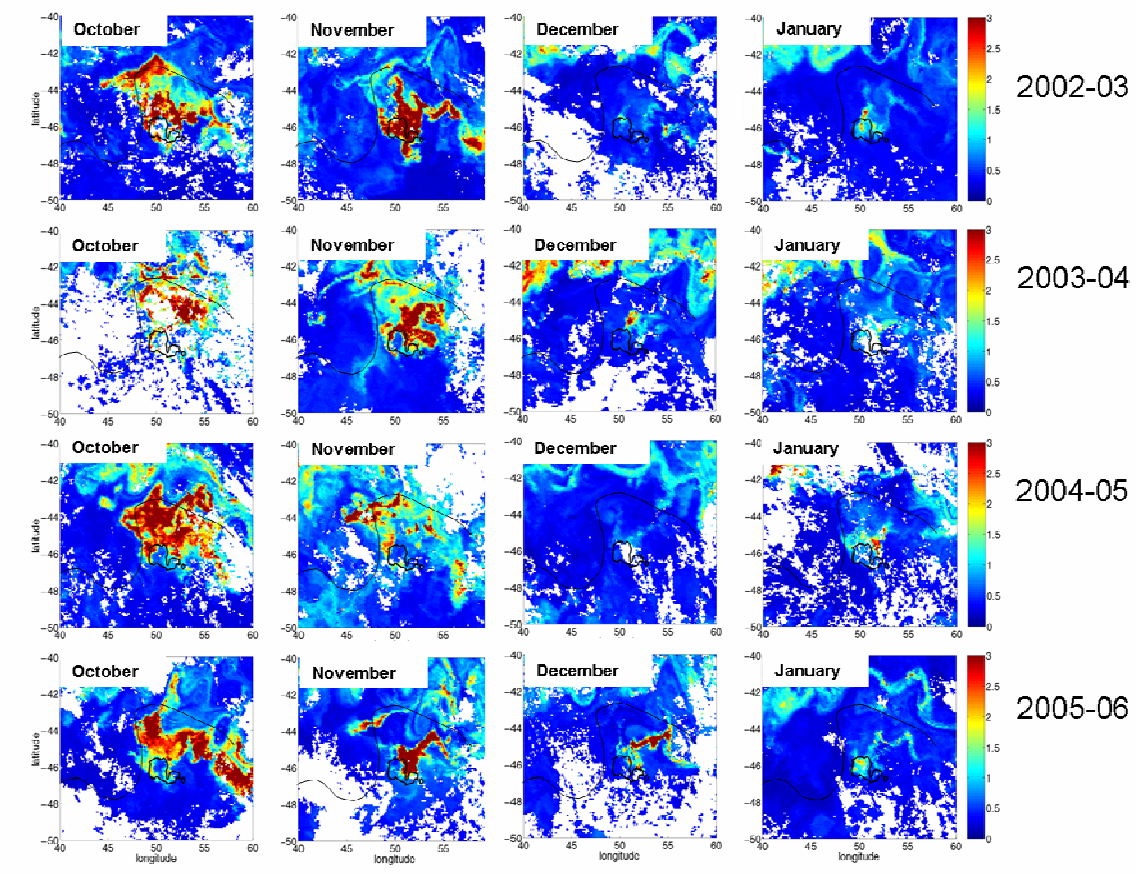

Figure I - 4: SeaWIFS/MODIS images around Crozet of Autral summers 2002-2203 to 2005-2006. The Crozet Plateau (contour at 500m) is represented by a light black solid line. The northern branch of the Sub Antartic Front is also represented by a thin black line. Satellite images were provided by Hugh Venables (NOCS/BAS)

Nitrates were non-limiting over the sampling period (Lucas et al., 2007) and remained in a concentration range of 18-30 µmol L^{-1}. Silicates concentrations were initially of 20

μmol L^{-1} and became almost depleted in December. This area is particularly suited for the study of iron distributions and sources because of the way in which the topography and the zonal winds constrain the local circulation patterns and the extent of the bloom (Pollard et al., 2007b) to the north west and to the north as explained below.

Figure I - 5 shows the main features of the ocean circulation in the area. The path of the Sub Antarctic Front (SAF) is initially deflected by the Del Caño rise before reflecting eastwards and then moving slightly southwards and to the east. This path, together with the plateau to the south creates a mostly enclosed area with a long water residence time, which is on the order of 100 days (Venables et al., 2007). Therefore, as the bloom is constrained to the west and north by the SAF, it is easier to survey. It is also likely that the surface flow over and past the Crozet Plateau and Islands is weak and to the north. Thus south of Crozet is "upstream", north of Crozet is "downstream" of the islands.

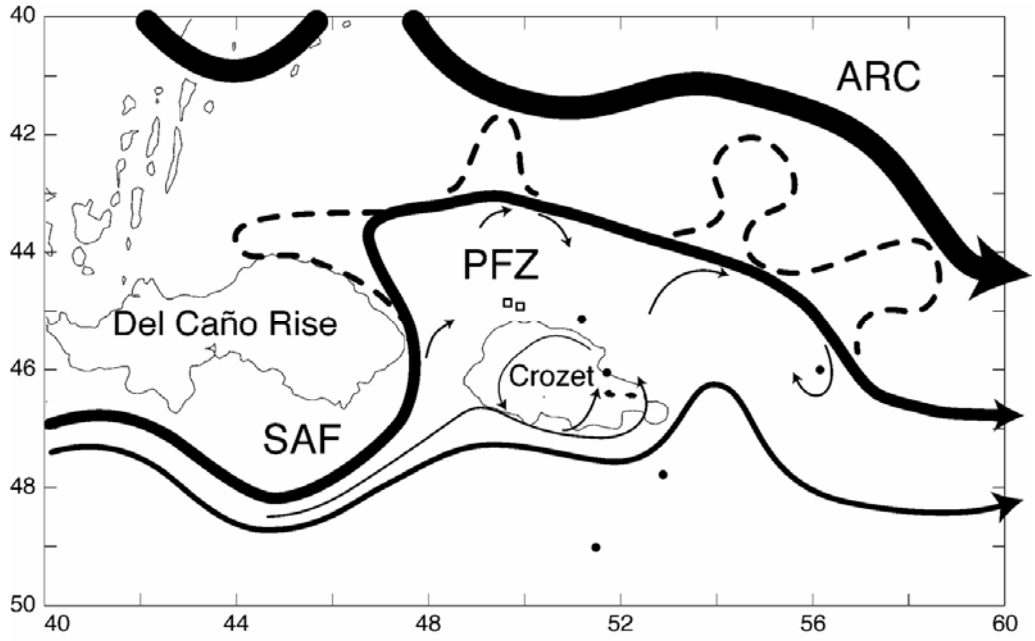

Figure I - 5: Schematic of the circulation around Crozet.
The thick black line marks the Agulhas Return Current (ARC), the bold solid line is the SubAntarctic Front (SAF), with dashed lines between them marking transient, propagating eddies. Thin arrows represent the very weak circulation in the Polar Frontal Zone (PFZ) between the SAF and Crozet. They show anticyclonic circulation round Crozet, Ekman flow past the islands, meanders breaking off the SAF into the region and re-entrainment of eddies into the SAF. Eastward flow south of Crozet is also shown. For spatial reference, the 2000 m contour is the light solid line. From Pollard et al., 2007b.

Therefore, the three-leg *CROZEX* cruises on *RRS Discovery* in the austral summer of 2004/05 (2 legs) and 2005/06 (1 leg) in the waters surrounding the Crozet Islands provided an excellent opportunity to examine how the natural sources of iron, originating

either from the islands directly or from the relatively shallow surrounding sediments, can relieve iron stress and therefore promote phytoplankton growth, particularly by the larger cells typically responsible for the export of particulate carbon and nitrogen.

This thesis was an integral part of the CROZEX research program and started by collecting a range of samples between November 2004 and January 2005 during the first two legs of the program, including total dissolved iron, particulate iron in large suspended particles (>53µm) and atmospheric samples. A year later, only large suspended particles were collected during Benthic Crozet.

3.2 Major objectives of the thesis

1) Development of an analyzer for measurement of very low concentrations of dissolved iron (DFe)

For the study of dissolved iron no appropriate analytical tool was available and the first goal was to build a system that could measure very low concentrations of dissolved iron. The decision was made to build a flow injection system based on catalytic spectrophotometric detection (FIA-NTA-DPD) similar to the analyser developed by Lohan et al. (2006). Matt Mowlem (OED, NOCS) offered his help for the design of the software and instrument control. A short review of available techniques and the development of this analyzer are described in Chapter Two and the full analytical description is given in Appendix I.

2) Study the distribution of dissolved iron in the vicinity of the Crozet Islands in order to elucidate DFe pathways.

The objective was to investigate the distribution of total dissolved iron by analyzing the samples taken during the two first legs of CROZEX. In Chapter Three, new data on total dissolved iron concentration (< 0.2µm) are presented. Particular emphasis has been placed on the sources of iron to the upper water column and on the different processes driving its distribution, such as biological uptake, mixing with deeper waters, advection of iron rich waters from the islands and atmospheric inputs. This work has been done in collaboration with Mark Moore, NOCS, Matt Charette, WHOI and with Alex Baker and Tim Jickells, UEA. This work led to three publications, Charette et al. (2007), Moore et

al. (2007) and Planquette et al. (2007) and the main findings are presented in Chapter Five.

3) Study the distribution, nature and vertical fluxes of iron and aluminium in the > 53µm fraction around the Crozet Islands.

The third objective was to look at the distribution of particulate iron in large suspended particles (>53µm) collected just below the mixed layer during the three legs of the CROZEX program in order to determine which fraction of iron was biogenic, and to examine the variability of iron export in the survey area. Analyses were carried out by ICP-MS allowing the determination of iron and aluminium. Results are presented in Chapter Four.

Vertical fluxes for iron relative to carbon have been calculated using ^{234}Th data in collaboration with Paul Morris. An iron budget has then been established, and residence times estimates for iron are given in Chapter Five.

CHAPTER TWO:

DEVELOPING ANALYTICAL METHODS FOR DETERMINING DIFFERENT PHASES OF IRON IN SEAWATER

Determining the concentration of iron in seawater samples is a difficult exercise. This is due to the contamination risks throughout all stages of sampling and analysis originating from various sources such as equipment in the lab, atmospheric dust, reagents or the research vessel. Therefore extreme caution must be adopted through each step of the sampling and analytical processes. This has not been the case up to the 1970s, and as ultra clean conditions were not adopted, poor quality data sets resulted (Achterberg et al., 2001). For the last thirty years, various methods have been developed with the aim of generating good iron data, and trace metal research groups started to develop more sensitive analytical methods. It is now possible to detect and determine iron concentrations in seawater at levels of a few picomoles per litre depending on the area of sampling. Particular efforts have also been made by several teams in order to get new pieces of sampling equipment. Some discrepancies still exist between the teams and the need to "develop an implementation framework that ensures methodological continuity and reproducibility at all levels from sample acquisition and processing through to

analytical protocols" has been raised recently in the GEOTRACES program (Geotraces Science Plan 2006). During CROZEX, all the labware as well as the sampling equipment was rigorously cleaned, these aspects being covered in this chapter for both phases investigated during the program, i.e. total dissolved iron (TDFe) and particulate iron in suspended particulate matter (SPFe).

Cleaning, sampling and analytical techniques for determining TDFe are first reported, this includes the development of the flow injection method which was used to produce the results of this thesis. The second part concerns the cleaning and the sequential leaching technique used for the determination of SPFe.

1 Total Dissolved iron

All critical operations were performed in a class-100 clean-air laboratory, following the current protocol used at the National Oceanography Centre in Southampton (NOCs) which is similar to that of Achterberg et al. (2001) and as described in the section below.

1.1 Sampling and pre-treatment procedures

Prior to the cruises, clean low density polyethylene bottles (LDPE, Nalgene, 1L, 500mL, 250mL, 125 mL) sample bottles were soaked in ~5% (v/v) aqueous Decon detergent for three days and subsequently soaked for three days each in 50% (v/v) HCl and 50% (v/v) HNO_3 (Fisher Scientific). In between steps, the bottles were rinsed three times with Milli-Q water. After removal from the acid bath, the sample bottles were rinsed with sub-boiled distilled water and then filled with Milli-Q water acidified with quartz sub-boiling distilled Q-HCl down to pH 2 and stored in double clean zipper seal polyethylene bags until use. Polycarbonate filters were soaked for two weeks in 10% (v/v) Q-HCl, rinsed and stored in sub-boiled distilled water.

Sampling - A titanium CTD rosette mounted with 10L Ocean Technology Equipment (OTE) bottles was used for obtaining the vertical profiles presented in Chapter three. All pieces of electronic equipment were housed in titanium cases. These OTE bottles were washed with care before use at sea and then rinsed with seawater. Between casts, the rosette was protected with a plastic cover on the deck to minimize contamination from the

particles generated on board. After collection, OTE bottles were carried inside the clean container on the after deck for filtration.

However, the highest risk when sampling remains the ship itself. Contamination problems have been reported for the samples taken in the first 25m, showing that the surrounding waters around the ship could be contaminated whilst on station. These data have been discarded from the final results discussed in this thesis (Appendix III).

Filtration - As reported in Chapter One, the biogeochemistry of iron is highly complex, and the two oxidation states of iron, Fe(II) and Fe(III) are involved in the formation of soluble inorganic and organic complexes, colloids and particulate phases (Figure II-1). However the size distribution of iron species, as well as their true chemical solubility and biological availability in seawater are still under investigation (Bruland and Rue, 2001). Moreover, the recognition of the existence of colloids that represent much of the operationally defined dissolved iron (Wu and Luther, 1994; Nishioka et al., 2001) has made the dissolved particle size boundary particularly difficult to establish, varying from 0.1 to 0.4 µm (Figure II-1). It is common to set the operational distinction for the particulate phase at 0.4 µm and the dissolved at 0.2 µm (Wu et al., 2001). During Crozex, polycarbonate Nuclepore 0.2 µm filters were used.

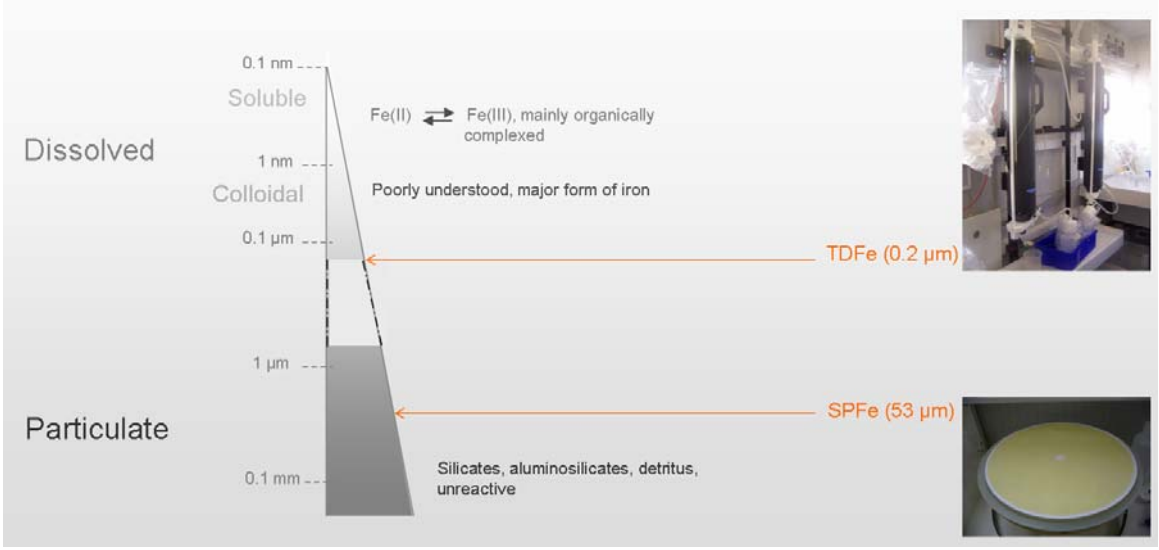

Figure II - 1: Diagram of the different phases of iron.
Top right corner: OTE bottles for the filtration of dissolved iron. Bottom right corner: example of a SAPS filter after deployment.

Inside the clean container, OTE bottles were maintained on a rack, using Delrin clamps (Figure II - 1, top right corner) to allow pressurization with filtered nitrogen (BOC) to

~0.8 atm. After opening the Teflon tap, samples were filtered in line using acid washed silicone rubber tubing with Teflon connections and acid washed Teflon filter holders containing Nuclepore filters (0.2 μm). The filtrate was collected in the storage bottle (typically 0.5L or 1L) after rinsing it three times with the seawater sample.

Acidification of samples - During CROZEX, it was not possible to proceed directly to the analysis of the samples on board, due to equipment and time constraints. All the samples were acidified on board with Q-HCl to pH ~ 2, representing typically 1mL of Q-HCl per litre of seawater, then adjusted to pH 1.7 in the lab, and stored double bagged in the dark until analysis. It has been shown that storage of acidified seawater samples is necessary to maintain iron in solution and avoid its adsorption onto the bottle walls (Moody, 1982). An intercomparison study (Bowie, 2004) has argued that it is useful to consider extended storage (i.e. > 6months) of filtered, acidified samples as a potential protocol for the determination of dissolved iron in seawater. After a few weeks up to years, this acidification enable full detection of all organically complexed iron and any potential colloidal iron present within the dissolved phase (Bowie et al., 2006). Lohan et al. (2005) demonstrated that acidification to pH 1.7 to 1.8 releases iron from two strong iron binding ligands, such as desferrioxamine B and rhodotorulic acid. However acidification changes some aspect of speciation like organic complexation (Weeks and Bruland, 2002) making it necessary to take specific samples for this purpose only.

1.1 Total dissolved iron (TDFe) analysis

Measurement of dissolved iron concentrations is a difficult task (Bruland and Rue, 2001) despite numerous efforts from many research teams. However, following a first inter-comparison exercise by Bowie et al. (2006), experiments from the recent SAFe cruise (Johnson et al., 2007) showed a good agreement between analytical methods, where differences in measured concentration were less than 0.05 nM for the surface sample. For the analysis of the CROZEX samples, an analyzer similar to the one described by Lohan et al. (2006) has been developed. In this section the different flow injection systems available to date are first succinctly presented and in a second phase, the development of the analyzer used in this study is described.

Overview of the flow injection systems - When taken to sea, an analyzer should ideally be relatively compact, portable and resistant to variations of temperature and movements of

the sea. Most of the methods taken to sea involve the use of flow injection analysis (FIA) with or without in-line preconcentration depending on the ambient concentrations. These methods are generally low cost, portable and allow the utilisation of small amounts of reagents, but the main advantage is the reduction of contamination risk.

The principal land based and ship based techniques are described by Achterberg et al. (2001) and in the table below are described the main characteristics of the flow injection systems used to date.

Distinct Features	Preconcentration resin	Species	Detection limit	Reference
FIA-CL (sulfoflavin)	8-HQ	Fe(II) and TDFe	0.45 nM	Elrod et al. (1991)
FIA-CL (luminol)	-	Fe(III)	0.050 nM	Obata et al. (1993)
FIA-DPD	8-HQ	TDFe	0.025 nM	Measures et al. (1995)
FIA- Ferrozine	C-18	Fe(II) and Fe(III)	0.3 nM	Blain and Tréguer (1995)
FIA-CL (luminol)	8-HQ	Fe(III)	0.021 nM	De Jong et al. (1998)
FIA-CL (sulfoflavin)	XAD-4-HEED	Fe(II)	0.8 nM	Hirata et al. (1999)
FIA-CL (luminol)	-	Fe(II)	0.025 nM	Croot and Laan (2002)
FIA-CL (luminol)	8-HQ	Fe(II) or Fe (II+III)	0.008-0.012 nM	Bowie et al. (2002)
FIA-DPD *in situ*	8-HQ	TDFe	0.15 nM	Laës et al. (2005)
FIA-DPD	NTA	TDFe	0.024 nM	Lohan et al. (2006)

Table II - 1: Overview of the major flow injection techniques in use for determining iron. FIA, Flow injection analyser; CL, Chemiluminescence; 8-HQ, 8-Hydroxyquinoline; DPD, N,N-dimethyl-*p*-phenylenediamine; XAD, Amberlite; HEED, N,hydroxyethylethylenediamine; NTA, nitrilotriacetic acid

During this thesis, the first goal was to build a Fe analyzer over a short period of time in order to analyze the numerous seawater samples collected during the two first legs of CROZEX. The choice of an in line flow injection preconcentration system has been preferred as it allows the analysis of a fairly high number of samples per hour, with a low consumption of reagents, making it relatively low cost and offers good precision as these systems are computer controlled. The method developed by Lohan et al. (2006), referred

here as FIA-DPD-NTA (flow injection analyzer with DPD catalytic spectrophotometric detection using a nitrilotriacetic resin preconcentration step) and based on the technique of Measures et al. (1995) has been selected for its practicality and efficiency as it only requires one spectrophotometer for its instrumentation. The principle of this technique is presented in the following section.

Catalytic oxidation of DPD by hydrogen peroxide – Principle

Hirayama and Unohara introduced in 1988 a batch spectrophotometric method based on the catalytic action of Fe(III) on the oxidation of N,N-dimethyl-*p*-phenylenediamine (DPD) by hydrogen peroxide (H_2O_2) in weakly acidic media. DPD can be oxidised by hydrogen peroxide and can form two reddish semiquinone derivatives (DPDQ) but this reaction proceeds very slowly without the action of a catalyst, which can be Fe(III). Fe (III) reacts with DPD to form DPDQ, and is reduced to Fe(II) (Figure II - 2). The optimum pH of this reaction was found between 5.5 and 6.

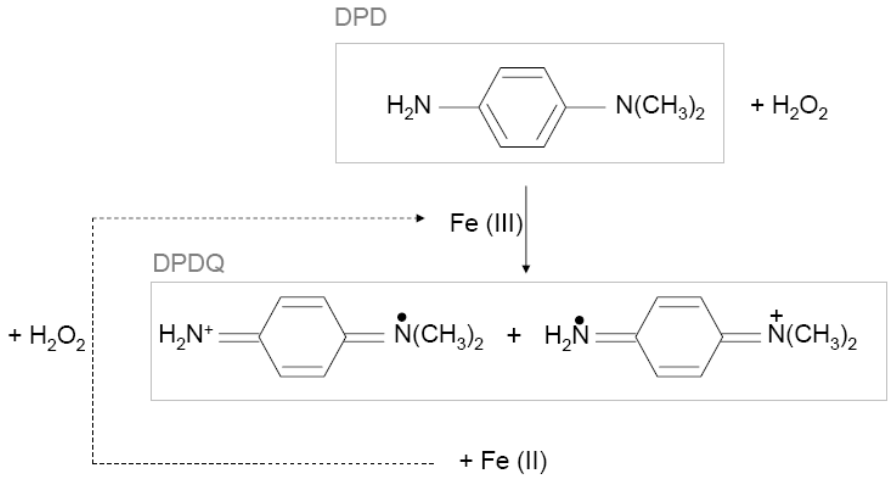

Figure II - 2: Schematic of the oxidation of DPD by hydrogen peroxide with the catalytic action of Fe(III) (after Hirayama et al., 1988).

Then, Fe(II) can be oxidized by hydrogen peroxide back to Fe(III) and the reformed Fe(III) is allowed to act with DPD again (Equations 1, 2, 3). Therefore, the two species of iron can act as catalysts and the coloured products are determined spectrophotochemically.

$$Fe(III) + H_2O_2 \rightarrow Fe(II) + {}^{\bullet}OOH + H^+ \quad (1)$$

$$Fe(II) + H_2O_2 \rightarrow Fe(III) + {}^{\bullet}OH + OH^- \quad (2)$$

$$2\ {}^{\bullet}OOH \rightarrow O_2 + H_2O_2 \quad (3)$$

The catalytic nature of the reaction enhances the sensitivity of the method since the amount of the oxidized DPD is proportional to the amount of Fe(II) and Fe(III) and the length of reaction time. This reaction is the basis of all the flow injection methods that use DPD oxidation by H_2O_2 (Measures et al., 1995; Sedwick et al.,2002; Weeks and Bruland, 2002; Lohan et al., 2006).

Measures et al. (1995) presented a flow injection adaptation of this manual method, including the in-line preconcentration of iron onto a column containing 8-hydroxyquinoline (8-HQ). The optimal reaction pH was found to be between 5.5 and 6, as in the Hirayama and Unohara method (1988). Columns of 8-HQ were found to remove iron in the pH range 3-6, so the sample was buffered to a target pH of 5.2 prior to the adsorption on the 8-HQ column. This preconcentration step is a critical one as it allows both the concentration and separation of iron from some of the interfering metal cations (Measures et al., 1995) with quantitative recovery of the element, and the separation from the seawater matrix that could precipitate in the manifold. Several types of chelating resins exist and 8-HQ columns have been extensively used in flow injection systems, but the recovery is highly pH specific. For example, Fe(III) is quantitatively recovered between pH values from 2.6 to 4 with no recovery of Fe(II) (Obata et al., 1993; de Jong et al., 1998) whereas Fe(II) is recovered along with Fe(III) at pH 5.2 to 6 (Obata et al., 1997). Another important factor, the presence of organic ligands in seawater, can affect the preconcentration step and has been recently investigated by Ndung'u et al. (2003) and Ussher et al. (2005) following the study by Obata et al. (1997). For example, a poor recovery at pH 3 to 4 in the presence of EDTA was shown. In order to ensure that all Fe complexes are destroyed and dissolved iron is loaded onto the resin, micro-wave treatment (Weeks and Bruland, 2002) or UV-digestion (Guéguen et al., 1999; Ndung'u et al., 2003) of the acidified sample prior to analysis have been recommended. Alternatively, it has been suggested that stored samples should not be analysed before a minimum of 6-months after collection to allow complete release of iron from organic complexes and colloids (Bowie et al., 2004). Lohan et al. (2005) demonstrated that acidification at pH 1.7 to 1.8 allows Fe in the samples to be preconcentrated directly and quantitatively onto an nitriolotriacetic (NTA) chelating resin even in the presence of two strong binding ligands, desferrioxamine B and rhodotulic acid.

1.2 Development of a FIA-DPD-NTA analyser

The FIA-DPD-NTA analyzer was chosen because it allows near real-time determination of total dissolved Fe(II+III), the use of the commercially available NTA resin and the relatively low cost of the apparatus. The construction of the analyser is based on the manifold described in Lohan et al. (2006) with optimisation of various parameters. The different steps were operated in the clean room facility and are described below.

Description of the manifold - As described in the previous section, this method is based on the in-line preconcentration of total dissolved iron on a nitriloacetic acid (NTA (Quiagen)) resin, placed in a Global FIA 2cm mini-column. Eluted Fe(III) then catalyzes the oxidation of *N*,*N*-dimethyl-*p*-phenylenediamine dihydrochloride (DPD, Sigma-Aldrich) by hydrogen peroxide (H_2O_2, Trace metal Grade, Fisher Scientific). This catalyzed reaction is followed spectrometrically by monitoring the change of the absorbance at 514nm (1cm flow through cell in a UNICAM 8625 spectrophotometer).

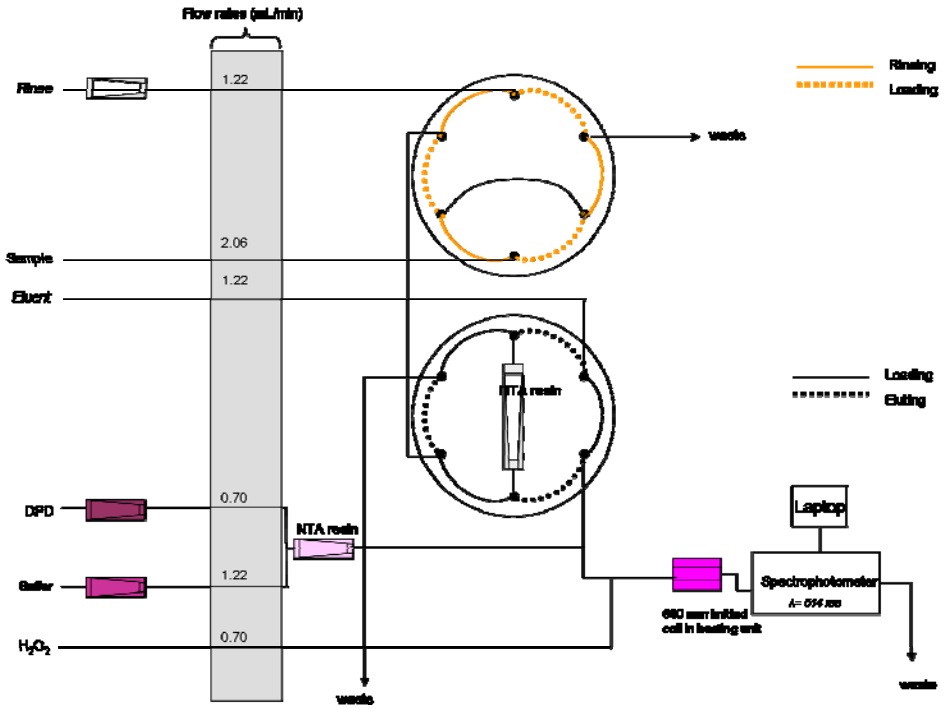

Figure II - 3: Schematic of the final version of the manifold of the FIA-DPD-NTA analyser.

This system is divided into two parts: the flow injection system including a peristaltic pump, and two 6-port valves and the detection system including a flow through cell, a spectrophotometer set at 514 nm and a laptop. Details about instrumentation, reagent preparation, and the analytical sequence are given in Appendix I. The signal from the

spectrophotometer is acquired through a National Instrument DAQ-MX USB 6009 card powered up when connected to the host laptop. The valves are controlled by the same card and operated by a LabView 7.0 software written by Dr Matt Mowlem (NOCS). The spectrophotometer showed very good linearity but it became unstable after a relatively short time of analysis (5 hours maximum), probably due to its age.

Several parameters have been optimised to reduce the blank, maximise the reaction and obtain a better sensitivity and stability. The reagents should be as clean as possible to minimise the blank, the pH of the buffer should be optimised to give the best peak area and the mixing loops lengths must be adjusted as well as the temperature of reaction, as discussed below.

Optimisation of the blank - In order to estimate the various contributions of each reagent on the signal, no cleaning columns were used at first. Then, progressively, one column on each line of reagent was added. When no cleaning columns were in line, the baseline immediately saturated (Figure II-5) as the absorbance reached the highest limit (1V). The first reagent to be cleaned in-line was the DPD and the cleaning columns were the same as used by Nédélec et al. (2006) (Figure II-4)

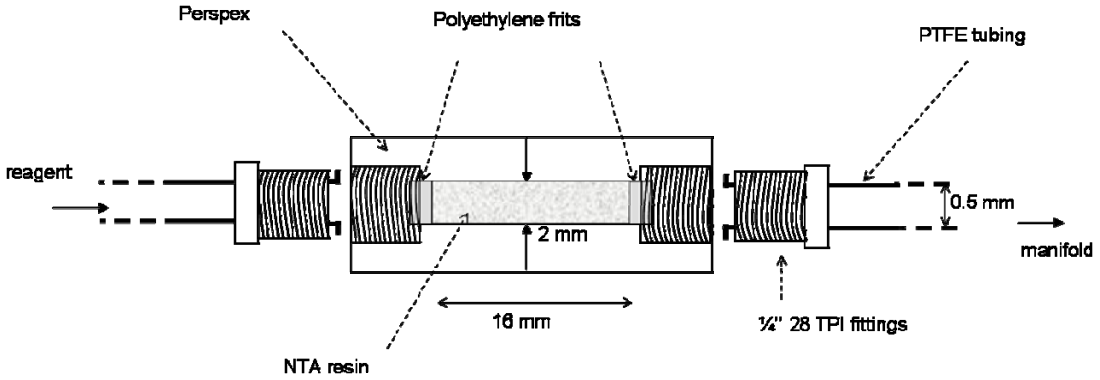

Figure II - 4: Cleaning columns used in the analyser (after Nédélec et al., 2006)

These columns were made of clear Perspex (Polymethylmethacrylate) and the resin was kept inside the column by two polyethylene frits at either end. Packing the NTA resin in the columns was carried out by pipetting carefully 100µL into the column. Then the supernatant was removed using a syringe and more NTA was added if the column was not fully filled. Then another column was added on the buffer line and finally an extra one after the T-piece joining the buffer and the DPD stream. The effect on each column is

shown in Figure II – 5, and the DPD solution appears to account at least for 0.35 V of the baseline level. The buffer accounts for ~0.25V of the baseline level. This infers that the DPD solution has the biggest contribution to the baseline level.

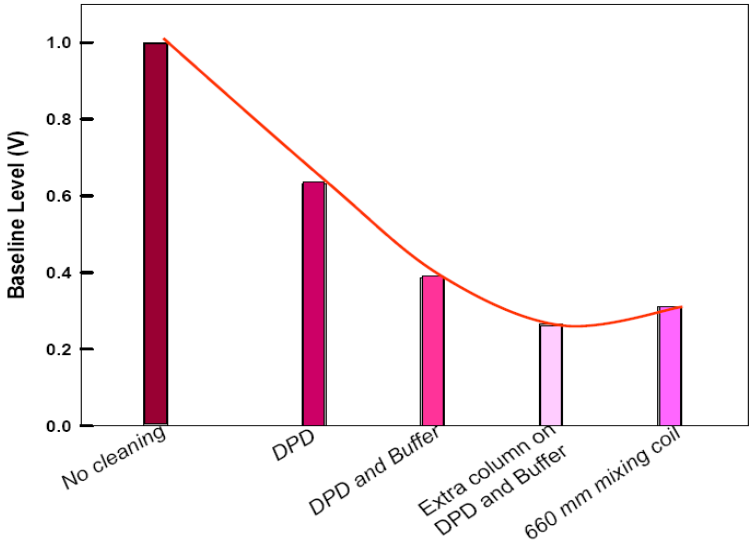

Figure II - 5: Baseline level as a function of the number of cleaning columns added in-line without a mixing coil, as well as the influence of a mixing coil at 30°C.

Optimisation of the reaction – As explained in section 1.2.2, the oxidation of DPD by H_2O_2 is pH dependant. The optimum pH for the reaction which will provide the greatest peak area is at pH 5.8, as observed by Measures et al. (1995). This can be explained by the fact that the reaction chemistry downstream from the resin is identical to that developed by Measures et al. (1995). To obtain a final pH of 5.8, it is necessary to adjust the ammonium acetate buffer (3.5 M) at pH 9.3. Details of preparation of the buffer are given in Appendix I.

The length of the mixing coil has been investigated as it can facilitate the final catalytic reaction. Three lengths were available in the heating unit system: 660mm, 1150mm and 1700mm. The choice of the shortest one was a good compromise between the peak area and the baseline level, as shown in Figure II – 6.

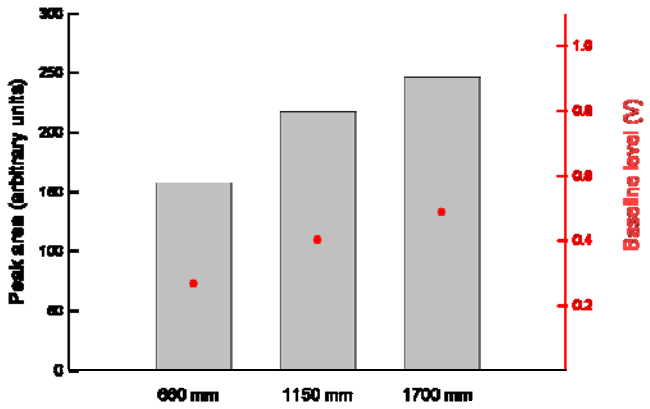

Figure II - 6: Effect of the length of the mixing coil on the peak area and on the baseline level for a 1 nM standard solution at 30°C.

The temperature has been investigated as well, the ambient temperature being usually around 15°C in the lab. Various settings were tested from 15°C to 37°C. The benefit of increasing the temperature is to increase the peak area. However it has a side effect which is to generate some bubbles which affect the quality of the peaks. When a bubble is passing through the detection cell, the absorbance drops to 0, affecting the shape of the peal, then making difficult its integration afterwards. Again, a compromise has been achieved by setting up the heating unit at 30°C.

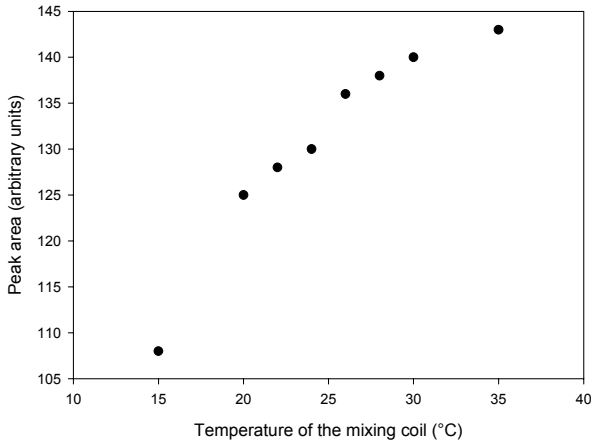

Figure II - 7: Effect of the temperature of the mixing coil on the peak area of a 2nM standard solution, with a 660mm length mixing coil.

Rinsing and conditioning the NTA resin – As demonstrated by Lohan et al. (2006) it is necessary to elute the resin with 1.5 M HCl in order to ensure a rapid desorption of iron. The same strength eluting acid has been used in this analyser; the only difference is that it

has been prepared with sub-boiled distilled water instead of Milli-Q water to minimize the blank, as sometimes, the Milli-Q appears to be slightly contaminated.

The seawater matrix is complex and may potentially create interferences during the detection step and there is a need of a rinsing step after passing the sample through the column to remove sea-salts still present in the dead volume of the column. The dead volume in the preconcentration column (Figure II - 8) used in this system is 170µL.

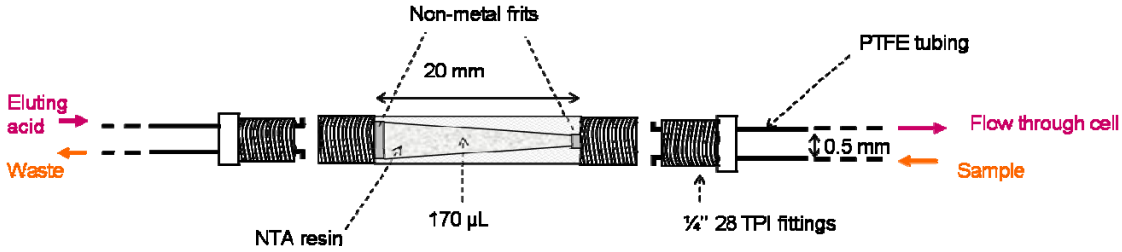

Figure II - 8: Schematic of the preconcentration column used in the system (Global-FIA).

Any change in the pH is automatically reflected in the absorbance signal and the consequence of mixing 170 µL of rinsing solution with the reagent stream is to produce a depression in the absorbance signal. To minimize this effect the pH of the 1.5 M ammonium acetate rinsing solution was adjusted to pH 3.2 as its ionic strength matches that of the 1.5 M HCl eluting acid (Lohan et al., 2006). The pH of the rinse is a little lower than the one used in Lohan et al. (2006) (pH 3.5) as the peak shape was better at this pH. At this pH, no iron bound on the resin will be eluted accidentally during the rinse step.

The optimal time for both rinsing and conditioning was set at 15s in the manifold, corresponding to 35s and 25s respectively in the Labview program (see Appendix I). An example of peak shapes obtained is shown in Figure II-9.

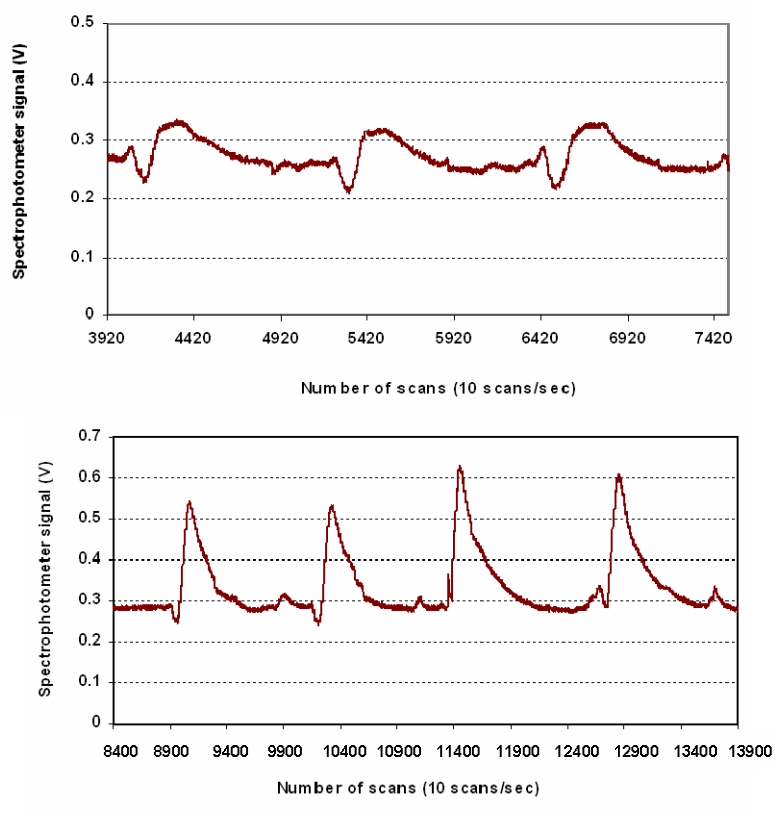

Figure II - 9: Elution profile for a 3 blank runs (top) and two samples with a 25s rinse step. The samples are low iron seawater (2 first peaks) and low iron seawater with 0.25 nmol L^{-1} of iron added (2 last peaks)

Standardisation – Prior to each batch of analyses, a calibration was performed daily, using standards additions of iron to low iron seawater (LISW), ranging from 0.1 nM to up to 2 nM using serial dilutions of 1000 µg L^{-1} Fe stock solution in acidified (pH 1.7) sub-boiled distilled water. Standards were run at the start and when possible (if reagents were left) at the end of each day of analysis. Concentrations were calculated from these standards based on the absorbance peaks (Appendix I). The internal low-iron seawater standard (LISW-IS) was used to monitor changes in sensitivity of the analyser as well as giving another indicator of the reliability of the system. This LISW was filtered and acidified near surface seawater collected during CROZEX (Station 15491, 300m). This internal standard had the double advantage of being acidified to the same degree as standards and samples, minimising changes in the loading pH; and having a lower concentration than NASS-5 seawater. The LISW (0.43 ± 0.042 nM) was generally analysed on several occasions during each day of analysis: after the blank, after the NASS-5 seawater, and randomly during the samples sequence (Appendix I)

Blanks and detection limits – As seen in the section "*Optimisation of the blank"*, reagents represent the major contribution to the baseline signal and are cleaned in-line with several NTA columns. This blank was investigated by running no sample in the manifold. The contribution of the addition of H_2O_2 (25 µL of 30% (v/v) of H_2O_2 to a 25 mL sample) has been investigated by spiking acidified low internal standard seawater with 50, 100 and 200 µL following a similar protocol to Lohan et al. (2006). The doubling of the H_2O_2 caused the iron concentration to increase by 0.02 nM, which was used as the H_2O_2 blank. Two sub samples out of the three Q-HCl bottles that were used for the acidification of the samples have been kept and analysed by ICP-MS and their contribution to the blank has been estimated negligible. Therefore, the rinsing solution with the NTA preconcentration column and the H_2O_2 are mainly contributing to the blank value. Blank values varied from 0.058 to 0.09 nM with a mean value of 0.073 ± 0.016 nM.

The detection limit was estimated as three time the standard deviation of the blank, resulting in a detection limit of 0.048 nM.

Accuracy and precision – NASS-5 certified seawater (National Research Council, Canada) was first used to test the accuracy of the method and good accordance was found as the value obtained with this method was: 3.67 ± 0.18 nM compared to 3.71 ± 0.63 nM. However, this concentration is relatively high compared to the concentrations found during CROZEX. Therefore some reference seawater from the recent iron intercomparison exercise (Sampling and Analysis of Fe (SAFe, Johnson et al., 2007) were ordered. Concentrations for the SAFe deep standard (0.91± 0.09 nM) fell within the quoted ranged of 0.95 ± 0.11 nM). When the peak areas had a standard deviation of more than 7%, another replicate was run. Unfortunately, the surface SAFe standard appeared to be contaminated and has not been used in this work.

Overall, the time for one analytical cycle was approximatively 15 min (with 7 mins of preconcentration for a ~0.1 nM sample) and a minimum of two replicate analyses per sample were made.

2 Suspended Particulate Iron

A central problem in marine geochemistry is to understand the global distribution, sources and sinks and reactions of elements involved in biogeochemical cycles. In surface waters, active fixation of dissolved substances during phytoplankton growth converts many chemical elements into particulate matter, which is then transported as large aggregates or particles to deep-ocean, where remineralisation and oxidation processes release the elements back into the dissolved state. Chemical species that are passively adsorbed, complexed or co-precipitated in particulate matter also follow similar routes. As explained in Chapter One, the aim was to collect particles sinking from the biologically productive mixed layer of the water column using large *in situ* pumps in order to measure C and Fe export from the upper ocean.

2.1 Sampling and pre-treatment procedures

Filtering large volume of seawater allows the collection of sufficient material for a representative sample. Most particles that dominate the vertical transport of material in the water column have a diameter greater than 50 μm (Bishop et al., 1985), justifying the choice of a 53 μm nylon filter as used here in the Stand Alone Pump Systems (SAPS, Challenger Oceanic, Figure II - 10). These filters have been used by several other workers (e.g., Lam et al., 2006). The parameters used for the determination of each deployment depth were water temperature, fluorescence and transmission. SAPS were placed at a depth that would collect the sinking particles that were falling out of the biologically productive surface layers of the water column, and were therefore deployed below the thermal mixed layer, i.e. below the chlorophyll maximum and below the point of increasing transmission corresponding to decreasing chlorophyll concentrations and rapid changes in density. The sampling details for the three legs of CROZEX are given in Chapter Four (Table IV - 1).

Figure II - 10: Example of two SAPS systems mounted on a stainless steel cable ready for deployment during D300. The top SAPS is for iron and trace metals analysis, the bottom SAPS is for POC/PON and ^{234}Th analysis.

Pumps were set to run for typically 1.5 hour, except at two stations where the biomass had a high concentration and a 60 minutes pump time was chosen (D285, Station 15499#2; D300. Station 15777#1) to preserve the filters from any clogging or breaking.

The filter holder was made of Polypropylene (PP), the filter head was made of PVC, and butyl O-rings sealed the assembly. The filter used in the SAPS was a 53 μm nylon mesh monofilament screen (300 mm diameter). Each filter was acid washed in 10% HCl solution, rinsed, dried, pre-weighed and stored in two plastic bags. Before each deployment, the PP filter holder was soaked in 10% Deacon solution for 2 to 3 days depending of the frequency of the stations during the cruises and rinsed with freshly taken Milli-Q just before deployment. The pump head was covered with a plastic bag to exclude any aerosol particles until the last minute of the deployment.

Immediately after recovery and separation of the head from the SAPS body, excess water in the housing was drawn off under vacuum in a flow laminar hood. Various "swimmers" (i.e. copepods mainly) were removed manually with cleaned tweezers and placed in vials, and then the filter was immediately put in a freezer at –20°C to avoid any physical or

chemical changes until analysis back in the lab. At the same time, except during D300, samples for the determination of Particulate Organic Carbon (POC), Particulate Organic Nitrogen (PON) and ^{234}Th were taken by Paul Morris (Morris et al., 2007).

2.2 Leaching and total digest method

Rationale - The environmental reactivity of an element cannot be assessed solely by its total concentration, and identification and quantification of elements present in different phases or fractions within a sample is of more interest. Numerous carrier phases and types of associations are possible between trace elements and suspended particulate matter (SPM). SPM may consist of biological and mineral phases, that will each contain different coordination sites to bind metals (Stumm, 1992). For example, the particulate iron pool is comprised of biogenic, lithogenic and detrital iron (Morel and Price, 2003), which are derived from terrigenous material scavenged by biogenic particles, specific biochemical functions, or included with structural materials such as calcite, opal, and scavenging processes at active surfaces (Collier and Edmond, 1984). It is therefore useful to distinguish a "potentially biologically active" carrier phase from a "refractory" phase (Landing and Bruland, 1987).

The majority of trace element analytical procedures involve highly sensitive spectroscopic techniques, such as atomic absorption spectroscopy (AAS, GFAAS), inductively coupled plasma optical emission and mass spectrometry (ICP-AES and ICP-MS). The drawback of these techniques is that they require first the solid sample to be transformed into a solution in which the metal content is then determined. Total sample digestion is mainly carried out by a fusion or a wet procedure based on an acid digestion with a heated mixture of mineral acids. There is not any universal dissolution procedure valid for every type of sample. Ideally, such a procedure should:

- be able to dissolve the sample completely, without any insoluble residue,
- exclude any possible source of sample loss through volatility, and adsorption onto the wall of the vessel,
- avoid sample contamination from the reagents used in the dissolution process.
- be reasonably quick and safe.

The aim here was to determine the concentration of iron associated with SPM in order to estimate the vertical flux of Fe relative to Carbon (Fe/C ratio) as discussed in Chapter Five and to better understand the biogeochemistry of Fe in this system.

The decision was made to distinguish:

- the labile fraction, which comprises those metals bound by organic matter weakly sorbed to surfaces, associated with amorphous metal oxyhydroxides (Fe, Mn) and carbonate minerals,
- the more refractory fraction, such as aluminosilicates and crystalline Fe oxyhydroxides.

This analysis determines the first fraction by a 25% acetic acid leach, with the residue after this extraction being carried over to the next step and being completely digested with aqua regia and hydrofluoric acid (HF).

Protocol - The whole protocol of this two-step sequential leach is detailed in Appendix II, the major steps being described here. All the following operations were performed in a clean room laboratory.

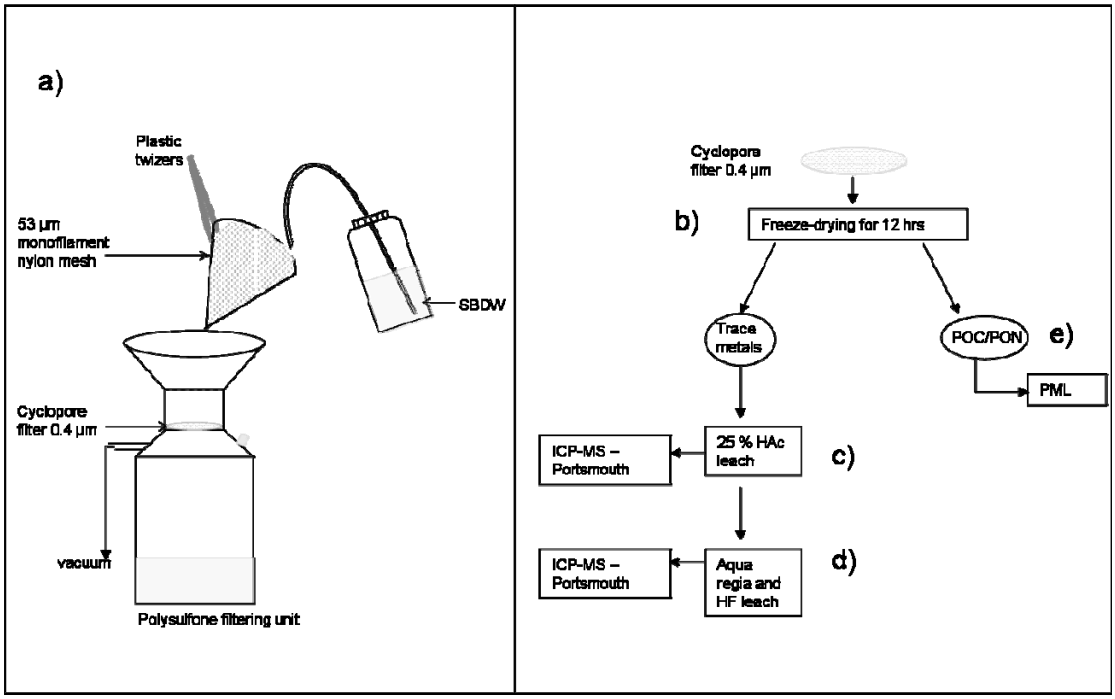

Figure II - 11: Schematic of the various steps of the sequential leaching technique.

Sea-salt removal: As the nylon filters were stored frozen and folded into quarters, the first step was to remove any sea salts that could interfere from the particulate matter. It was decided to dislodge the particles from the nylon filter for three main reasons:

- some high blanks for nylon mesh have been reported (Weinstein and Moran, 2004)
- it is not possible to fully digest them
- it is very difficult to handle the nylon filters due to their large diameter.

Therefore the particles from the nylon filter were washed off with SBDW (Figure I – 11a) and collected onto one or several pre-weighed 0.4µm Cyclopore filters depending on the mass of material. A sub-sample was sometimes taken for Scanning Electron Microscopy (SEM) (Appendix II).

The nylon mesh and the Cyclopore filters were then freeze dried for 12 hours (Figure I – 11b) and weighed using an electromicrobalance (Metler AE240) for mass determination of the SPM.
Sub-samples were taken for Particulate Organic Carbon and Nitrogen (POC/PON) (Figure I -11e).

1st leach: 25% Acetic acid (HAc)
The "labile" fraction of the particulate iron pool was characterised with the use of 25% Acetic acid (HAc), as it can extract the soluble, exchangeable and carbonate bound metal fraction (Fitzwater et al., 2003; Lewis and Landing, 1992; Löscher, 1999; Wells et al., 2000). The dried Cyclopore filters were placed in Teflon vials with 5 to 12 mL of 25% Quartz-distilled HAc (Q-HAc) and soaked for 2h at room temperature according to the protocol of Wells et al. (2000) (FigureII-11c, Table, Appendix II). They were then transferred with the solution into 10mL polypropylene centrifuge tubes and centrifuged (2500 rpm for 15 mins). The overlying solution was transferred to clean Teflon pots (30 mL screw cap) and taken to dryness on a hotplate (110°C). The residues were brought into solution by addition of 4 mL of 2% Q-HNO_3, this solution being kept for analysis on the ICP-MS.

The refractory residue was rinsed out of the tube with SBDW directly into a Teflon pot (15 mL screw cap) then dried on a hot plate at 140°C, ready for the second leach.

2nd leach: total digestion

The refractory fraction was brought into solution by a total digestion using aqua regia and hydrofluoric acid (HF) (Eggiman and Betzer, 1976), which fully releases the trace elements including the aluminosilicate phases. Because of the possibility of trace element loss due to volatilization at higher temperatures, all processing steps were done in closed Teflon pots (15mL screw cap, Savillex).

The reagents (HCl, HNO_3, HF) used in the dissolution procedures were all high purity, as they were double-sub-boiled distilled acid and all operations were performed in a clean room.

The first digestion was made with 2.4 mL of concentrated aqua regia for 24 hours at 140°C. The solution was then taken to dryness. Following this, residues were dissolved with hydrofluoric acid (HF)/nitric (HNO_3) for 24 hours at 140°C in order to dissolve any opal or silicates which may have been present. With a few samples, any residual organic matter was further digested by a heating evaporation cycle with more Q-HNO_3 and HF (samples from Stations 15777 and 15595).

Finally, a reduction step with 2mL of 6M HCl was done to drive off the fluorides for 24 hours. Following complete dissolution, the solution was evaporated to dryness and redissolved in 2% HNO_3 and kept in clean 15mL LDPE bottles (Nalgene) until analysis. Blank filters (n=6) were treated in the same manner as the sample and represent a total chemistry and procedural blank. A very small amount of acid migration through the threads was noted occasionally but blank runs indicated no significant contamination from the pots (Table II - 2).

A dilution factor of 10-4600 depending on iron concentrations was applied to each sample and standard. These solutions were analyzed by inductively coupled plasma–mass spectrometry (ICP-MS, Agilent 7500 series) at the facilities of the School of Earth and Environmental Sciences in Portsmouth. A wide range of elements were analysed, including: Al, Cr, Mn, Fe, Co, Ni, Cu, Zn, As, Se, Sr, Ag, Cd, Ba, Pb, Bi, Th, U, but only Fe and Al data will be presented and discussed in this thesis.

The data processing procedure includes linear drift correction, interference corrections, blank subtraction, calibration with international standards, and a dilution correction all software controlled. A full description of the protocol is given in Appendix II.

Blanks, precision and accuracy - Accuracy and precision of chemical analyses of trace elements in SPM were determined by using Certified International Standard Reference Materials (JA-2; JB-2; MAG-1; SGR-1; BIR-1, TORT-2 and No.9 (NIES) and replicate analyses performed at the same time as for the samples. The values are reported in Table II -2 with the blank values (n=5). All data are blank corrected. The recoveries from CRM ranged between 98 and 108% of the recommended concentrations for all trace metals. The concentrations of metals in the analytical blank was about 0.00031 ppm for Al and 0.0011 ppm for Fe, and this value is much lower than the concentrations analysed in samples.

	Blank	BIR-1	JA-2	MAG-1	JB-2	No. 9 NIES	SGR-1	TORT-2
Al	**0.00031 ± 0.00012 (n=5)**	*8.12 ± 0.27* *	*8.15* *	*16.64 ± 0.3* *	*7.74* *	*215*	*6.52 ± 0.21* *	-
		10.2 ± 0.35 (n=4)	**9.35 ± 0.29 (n=3)**	**18.4 ± 0.11 (n=3)**	**7.45 ± 0.75 (n=3)**	**213 ± 3.92 (n=3)**	**6.58 ± 0.14 (n=3)**	**5.18 ± 0.23 (n=4)**
		118 %	111 %	108%	100%	100%	100%	-
Fe	**0.0011 ± 0.00075 (n=5)**	*7.87 ± 0.16* *	*4.34* *	*6.8 ± 0.6*	*9.96* *	*187 ± 6*	*3.03 ± 0.14* *	*105 ±13*
		8.47 ± 2.6 (n=4)	**4.25 ± 0.66 (n=3)**	**8.47 ± 0.84 (n=3)**	**10.35 ± 0.37 (n=3)**	**180 ± 9.2 (n=3)**	**2.70 ± 0.12 (n=3)**	**104 ± 6.05 (n=4)**
		100%	100%	103%	100%	100%	98%	100%

Table II - 2: Quality control results of replicate analyses of metals in standard reference materials. All concentrations are expressed in ppm except for *: weight %. Certified concentrations are in italics. Concentrations obtained in this study are in bold. % recovery is in blue.

MAG-1: *Marine mud, United States Geological Survey (USGS)*

SGR-1: *Oil Shale of the Green River Formation, USGS*

BIR-1*: Icelandic basalt, Reykjavik dolerites, 12 km east of Reykjavik, Iceland*

JB-2: *Basalt from Oshima volcano erupted in 1950-51, Oshima, Tokyo, Geological Survey of Japan*

JA-2: *Andesite, Goshikidai sanukitoid, 14Ma, Sakaide, Kagawa Prefecture, GSJ*

No. 9 NIES: *Sargasso Seaweed, National Institute for Environmental Studies (NIES), Japan*

TORT-2: *Hepatopancreas of lobster, NRC Canada*

CHAPTER THREE:

DISSOLVED IRON DISTRIBUTION AROUND THE CROZET ISLANDS, SOUTHERN OCEAN

As reported in Chapter one, during the last decade, mesoscale iron enrichment experiments in the Southern Ocean (summarized by de Baar et al. (2005) and Boyd et al. (2007)), have clearly demonstrated that iron availability controls phytoplankton productivity. Without exception, these experiments have resulted in increased chlorophyll-a (Chl *a*) biomass after Fe additions. However, as pointed out by Chisholm (2000), such artificial enrichments cannot represent natural processes effectively, as the form of iron added is different from the forms naturally present in seawater. Furthermore the perturbation could lead to many unintended side effects such as changing the structure of the marine ecosystem, or generating greenhouse gases other than carbon dioxide, like DMS for example.

Studying regions exhibiting high phytoplankton biomass resulting from a natural release of iron is an alternative way to determine the role of iron in regulating the biological carbon pump (Blain et al., 2007; Pollard et al., 2007a). The Crozet Islands are a good *in situ* laboratory, as interaction between water masses and margins of land masses is extensive therefore leading to a potential "island mass effect". The CROZEX project provided an excellent opportunity to study in more detail the distribution and pathways of

iron around the Crozet islands as well as extend our collection of data as few data have been reported in the past for this area (Metzl et al, 1999; Sedwick et al.,2002).

In the present chapter new data on dissolved iron (DFe, < 0.2 µm) distributions around the Crozet islands are presented. Sampling sites are first briefly described before presenting the results in detail. Key results have led to a publication in Deep-Sea Research II (Appendix III, Planquette et al., 2007).

1 Presentation of the study area and sampling sites

A full description of the Crozet Islands and associated Plateau is given in Chapter One and Appendix Three, including the main circulation features, and information on major nutrients and phytoplankton distribution over the survey area. The sampling strategy then the different analytical methods for nutrients, Chl *a* and DFe are described below.

Figure III-1 represents the sites sampled during the first two legs of CROZEX in the austral summer 2004-2005. The bloom is likely to be constrained to the west and north by a branch of the Antarctic Circumpolar Current (ACC): the SubAntarctic Front (SAF). Surface flow over and past the Crozet Plateau and Islands is weak as suggested by surface drifter data (Pazan and Niiler, 2004) and the residence time of water is estimated at about 100 days in this area (Venables et al., 2007; Pollard et al., 2007b).

During the austral summer 2004-2005, the bloom peaked in late October just before the cruises began then decayed away from the islands, and a second bloom occurred in January. Chl *a* concentrations reached a local maximum of 8 µg L^{-1} at the beginning of November north of the islands, with a maximum of 1.4 µg L^{-1} at very close proximity of the islands. During the second bloom, Chl *a* concentrations reached 1.8 µg L^{-1} at station M3 (Venables et al., 2007). The minimum concentrations of 0.6 µg L^{-1} were found in the southern sites (Stations M2 and M6) that are not influenced by the islands.

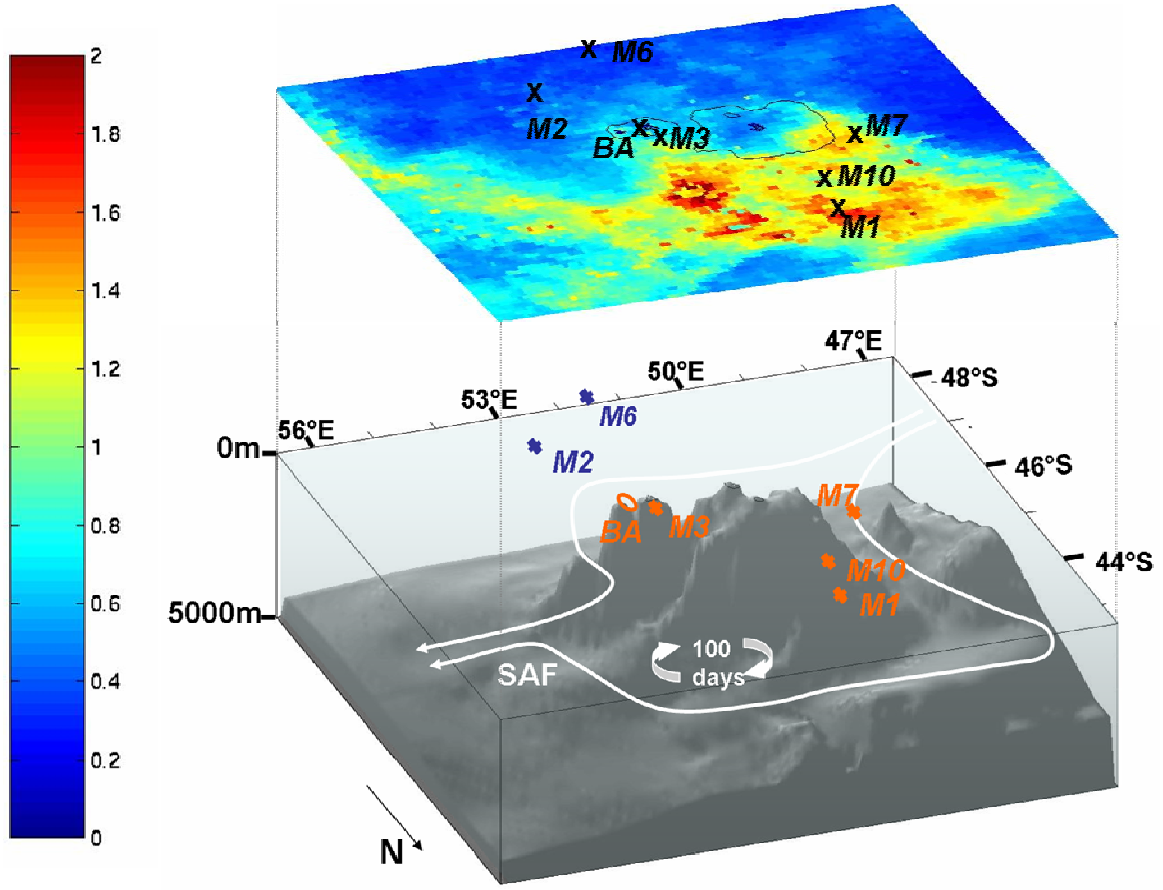

Figure III - 1 Crozet Islands topography combining the main circulation paths (white lines), stations sampling sites and a SeaWIFS Chl *a* image for the austral summer 2005-2005. Stations located in the bloom area are in orange and purple. Stations out of the bloom area are in dark blue. Note that station M6 is outside the main grid. The residence time of 60 days is indicated in green. SAF stands for Sub Antarctic Front. BA stands for the 3 stations occupied in Baie Américaine on île de la Possession.

Three main regions were sampled between 3rd November 2004 and 21st January 2005 (Figure III - 1):

- one to the north of the islands, in the bloom area (Stations M1, M3, M7 and M10),
- one to the south of the island, which is the HNLC "control" region (Stations M2 and M6) ,
- one in close proximity to the main island île de la Possession (Baie Américaine (BA) transect).

Station M3 was sampled several times, providing an opportunity to assess the temporal evolution of conditions at one site (for full station details please see Table 1 in Appendix III).

Dissolved iron concentrations were determined by flow injection analysis with catalytic spectrophotometric detection (FIA-NTA-DPD method presented in Chapter Two) and other routine measurements such as nutrients and Chl *a* were processed on board by R. Sanders, M. Stinchcombe and P.J. Morris (Sanders et al., 2007) and C. Mark Moore and A. E. Hickman, (Moore et al., 2007); a summary of procedures can be found in Appendix II.

2 Results

Vertical profiles of DFe are shown and discussed below. They are grouped together for three broad locations as introduced above: an oligotrophic control area south of the plateau (Stations M2 and M6), a productive area north east of the plateau (Station M3, M1, M7, and M10) and Baie Américaine stations (BA, BA+1, BA+2) in close proximity to the plateau. Density, Chl *a,* macronutrients and iron concentrations are reported in Table III-1 below.

Station details	Depth (m)	DFe (nM)	Density σ_0	Chl *a* ($mg.m^{-3}$)	Nitrates and Nitrites ($\mu mol\ L^{-1}$)	Silicates ($\mu mol\ L^{-1}$)	Phosphates ($\mu mol\ L^{-1}$)
M1 (491)	5	0.22	26.566	0.90	-	-	-
11/11/2004	10	-	26.566	0.76	-	-	-
43.92049 °S	20	0.31	26.566	0.79	18.5	0.74	1.33
50.26742 °E	40	-	26.567	0.77	-	-	-
3118m	50	0.34	26.570	-	-	-	-
	60	-	26.571	0.73	18.38	0.86	1.31
	70	-	26.576	0.76	-	-	-
	110	0.38	26.882	-	27.95	26.18	2.00
	250	0.30	27.117	-	28.96	24.46	2.04
	500	0.29	27.347	-	32.91	48.98	2.28
M3 (496)	5	-	26.822	0.61	23.01	6.12	1.66
13/11/2004	10	-	26.822	0.87	-	-	-
46.06809 °S	15	0.10	26.822	0.68	22.91	6.11	1.64
51.78529 °E	42	0.09	26.839	1.1	22.84	6.43	1.60
2287m	65	-	26.839	1.03	-	-	-
	175	0.09	26.938	-	24.77	13.25	1.74
	218	0.10	26.981	-	25.56	16.63	1.80
	300	0.12	27.114	-	27.90	23.91	1.95

M2 (502)	5	0.27	26.871	0.34	25.06	15.49	1.78
19/11/2004	10	0.24	26.881	0.39	23.93	15.90	1.75
47.79537 °S	20	-	26.890	0.35	23.83	15.89	1.79
52.86216 °E	40	0.24	26.903	0.42	24.38	15.86	1.83
3870m	60	(4.38)a	26.912	0.43	24.43	15.61	1.75
	80	0.22	26.914	0.43	24.64	16.00	1.78
M6 (511)	5		26.948	0.27	24	18.40	1.75
22/11/2004	10	0.20	26.948	0.25	-	-	-
49.00557 °S	20	-	26.960	0.25	-	-	-
51.50046 °E	40	0.25	26.966	0.45	25.28	18.67	1.83
4275m	60	-	26.974	0.27	24.56	18.18	1.77
	80	0.21	26.976	0.38	24.62	18.52	1.81
	250	0.40	27.129	-	-	-	-
M3 (516)	5	-	26.826	0.47	21.65	9.10	1.68
25/11/2004	10	-	26.826	0.48	21.07	9.02	1.56
46.05961 °S	20	(2.08)a	26.826	0.49	21.34	8.84	1.55
51.79093 °E	40	0.19	26.841	0.49	21.24	9.46	1.54
3986m	60	(0.40)	26.894	0.49	21.74	8.98	1.60
	80	0.28	26.928	0.41	22.28	11.21	1.64
M7 (524)	5	-	26.675	1.34	19.05	0.06	1.26
27/11/04	10	(1.65)a	26.675	1.34	19.26	0.14	1.38
45.49943 °S	15	(0.63)	26.675	1.39	19.69	0.18	1.30
49.00242 °E	25	(0.73)	26.675	1.41	19.15	0.11	1.32
2749m	35	0.29	26.677	1.38	19.13	0.25	1.32
	55	0.27	26.748	1.22	23.23	6.53	1.79
	75	0.44	26.920	-	25.93	13.88	1.84
	100	0.34	26.971	-	28.13	17.21	1.96
	125	0.23	27.013	-	27.48	18.90	1.87
	150	0.46	27.038	-	28.19	20.14	1.87
	200	0.20	27.103	-	29.7	22.99	1.99
	300	0.26	27.214	-	32.15	29.70	2.23
	400	0.46	27.293	-	32.83	39.41	2.36
	500	0.23	27.355	-	35.05	48.75	2.44
M10 (563)	5	0.48	26.578	0.80	21.75	3.87	1.48
21/12/2004	10	-	26.577	0.73	-	-	-
44.52528 °S	15	0.40	26.576	-	21.69	3.91	1.46
49.96059 °E	25	-	26.578	0.8	-	-	-
2943m	35	0.31	26.595	0.81	22.01	3	1.51
	55	-	26.666	-	-	-	-
	75	0.30	26.789	0.20	23.27	5.9	1.68
	125	0.16	26.943	-	26.15	15.16	1.80

	200	0.30	27.075	0.037	29.03	22.54	1.97
BA (567)	5	1.05	26.830	0.57	23.95	7.91	1.71
22/12/2004	25	0.68	26.834	0.56	24.03	7.83	1.70
46.36854 °S	50	2.16	26.863	0.54	24.04	8.74	1.72
51.82754 °E	80	1.13	26.874	0.47	24.43	10.25	1.71
83m							
BA+1 (568)	5	0.60	26.819	0.60	22.28	5.13	1.61
22/12/2004	25	0.52	26.819	0.62	22.42	4.91	1.60
46.32332 °S	50	0.56	26.823	0.62	22.14	4.68	1.64
51.89459 °E	100	0.39	26.924	0.27	23.77	8.77	1.68
379m	200	1.01	27.034	0.30	28.35	25.27	2.00
	300	2.08	27.151	0.19	-	-	-
	376	0.56	27.262	0.06	30.34	35.99	2.14
BA+2 (569)	5	0.16	26.796	0.88	22.52	3.75	-
22/12/2004	25	0.15	26.810	1.00	22.58	4	1.56
46.26997 °S	50	0.32	26.899	0.45	24.80	10.73	1.68
51.97083 °E	100	0.15	27.007	0.18	26.32	15.61	1.81
1491m	300	0.42	27.199	0.04	29.59	29.26	2.08
	750	0.29	27.476	-	-	-	-
M3 (572)	5	(1.71)a	26.720	1.01	22.64	1.85	1.53
22/12/2004	10	-	26.725	0.948	-	-	-
46.06223 °S	15	-	26.725	1.01	-	-	-
51.78169 °E	25	0.26	26.725	0.95	22.86	1.70	1.53
2375m	35	0.38	26.725	0.97	22.80	1.77	1.55
	55	-	26.756	0.82	-	-	-
	75	0.26	26.829	-	23.65	5.83	1.71
	175	0.31	27.023	-	27.64	19.98	1.87
	500	0.22	27.316	-	32.56	43.25	2.39
M3 (592)	5	0.24	26.725	0.61	22.52	2.72	1.49
31/12/2004	10	-	26.741	0.62	-	-	-
46.05134 °S	15	-	26.747	0.72	-	-	-
51.77591 °E	25	0.27	26.763	0.78	22.68	2.89	1.52
2404m	35	-	26.774	0.73	-	-	-
	55	0.12	26.795	0.79	23.43	3.50	1.59
	100	0.41	26.933	-	25.65	11.13	1.70
	200	0.15	27.094	-	29.18	23.67	1.92
M2 (605)	10	(0.52)	26.690	0.26	22.55	2.04	1.54
06/01/2005	20	-	26.691	0.30	-	-	-
47.80111°S	40	-	26.714	0.32	-	-	-

52.84952 °E	50	0.09	26.719	-	22.41	1.84	1.57
3883m	60	-	26.734	0.43	-	-	-
	80	-	26.789	0.72	-	-	-
	100	0.16	26.846	0.35	23.90	11.56	1.80
	150	-	27.008	0.13	-	-	-
	160	0.17	27.027	-	-	-	-
	200	0.11	27.097	-	-	-	-
M3 (622)	5	0.15	26.619	4.94	17.68	0.19	1.12
10/01/2005	10	-	26.620	5.10	-	-	-
46.03412 °S	20	0.23	26.619	4.95	17.78	0.37	1.18
51.86656 °E	40	-	26.705	3.94	-	-	-
2322m	50	-	26.833	0.88	-	-	-
	60	-	26.889	-	-	-	-
	80	0.10	26.945	0.29	25.48	15.05	1.81
	100	-	27.006	-	25.97	17.27	1.84
	150	0.09	27.057	-	27.43	23.80	1.94
	200	-	27.133	-	-	-	-
	300	0.34	27.205	-	29.95	31.79	2.09
	400	-	27.264	-	-	-	-
	500	0.20	27.337	-	32.78	49.04	2.37

Table III-1: Station locations, depth, dissolved iron concentrations (<0.2µm), density, Chl *a*, and macronutrients concentrations during D285 and D286. A dash indicates that no sample was collected; (a) denotes that the sample was grossly contaminated from OTE bottle, ( ) denotes that the sample is thought to be contaminated from the ship by a specific comparison with the rest of the profile.

2.1 Southern Sites (M6&M2)

Stations M2 and M6 (502, 605 and 511) are located south of the islands in HNLC water masses. Nitrates and Phosphates were non-limiting, with concentrations been comprised between 24 and 26 µmol L^{-1} and 1.7 and 1.9 µmol L^{-1} respectively (Figure III-3). Silicates concentrations were non-limiting at the beginning of the survey, reaching up to 18 µmol L^{-1} in the upper water column, but became depleted down to 2 µmol L^{-1} at the second occupation of M2 (Stn 605) in early January 2005 (Figure III-3).

These water masses are not believed to be influenced by the plateau as they have not been in contact with the islands (Figure III - 1). Consequently, the phytoplankton productivity for this region was low (< 0.5 gC m^{-2} d^{-1}) (Seeyave et al., 2007).

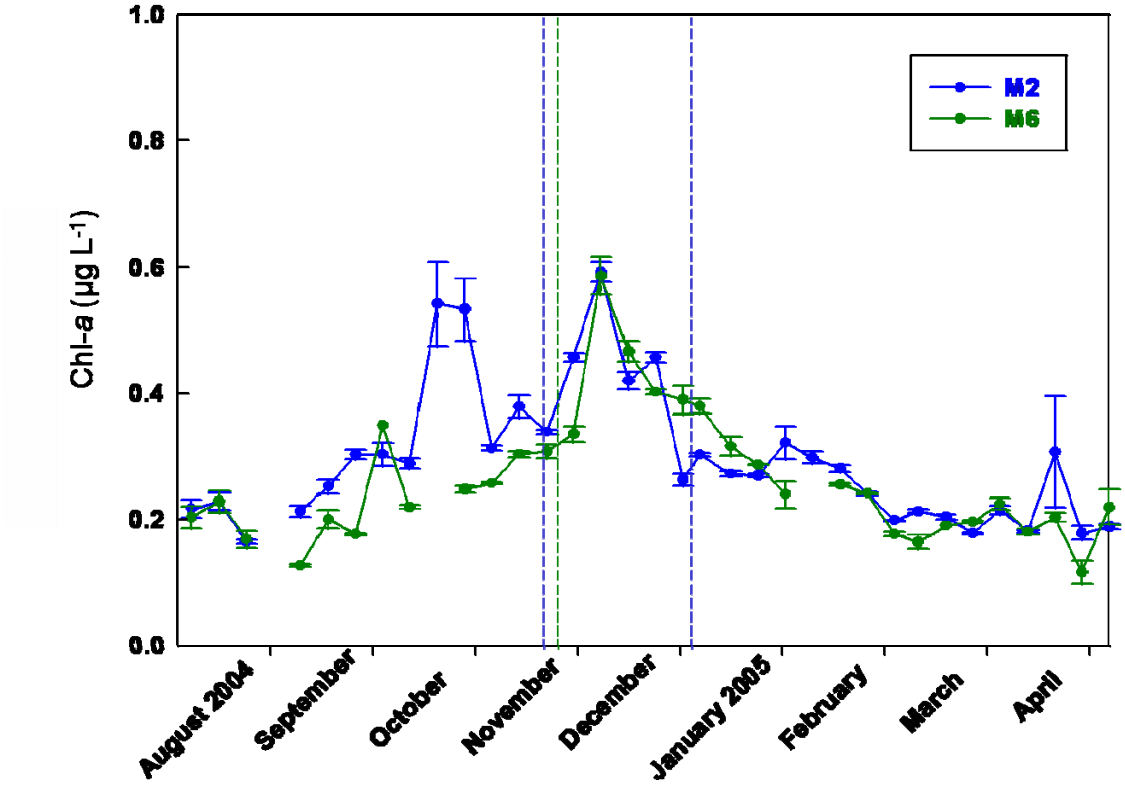

Figure III - 2: Variation of surface Chl *a* (merged MODIS/SeaWIFS data, courtesy of Hugh Venables) at stations M2 and M6 during the austral summer 2004-2005.
Long dashed vertical bars represent the sampling dates for DFe vertical profiles.

Figure III - 2 shows the variations of surface Chl *a* concentrations during the austral summer 2004-2005 as well as the specific days of sampling for DFe. The mean Chl *a* was obtained for each 8-day merged SeaWIFS/MODIS image, which improved coverage. All non non-cloud pixels were averaged in a 18.2 km radius circle about each station. Error bars give the standard deviation of the mean of these pixels (data provided by Hugh Venables). Only shallow depths (down to 200m) samples were analyzed for these stations.

M6 (Figure III-3, a)- Surface water temperatures were close to 2°C and the constant density down to ~125m implies deep mixing. Consequently, DFe concentrations above this depth exhibit little variability (range 0.21- 0.25 nM), as well as macronutrients that are present in non-limiting concentrations. Chl *a* concentrations are also low (0.18-0.26 µg L^{-1}), which can be explained by a low light regime at this time of the year.

M2 (Figure III-3, b and c) is located north east of M6. Surface water temperatures varied from 3.3 and 5 °C. Between mid November (b) and early January (c), Chl *a* values varied between 0.26 and 0.35 μg L^{-1} whilst DFe decreased from 0.22 nM to 0.09 nM during this period in the top hundred meters. This decrease corresponds to a small bloom (Figure III - 2 and in Venables et al., 2007) that occurred in late December, with the phytoplankton community presumably removing the available iron and the silicates that became depleted in early January (Figure III-3). Overall, these values are consistent with this being a typical HNLC region in contrast to the north of the plateau described hereafter.

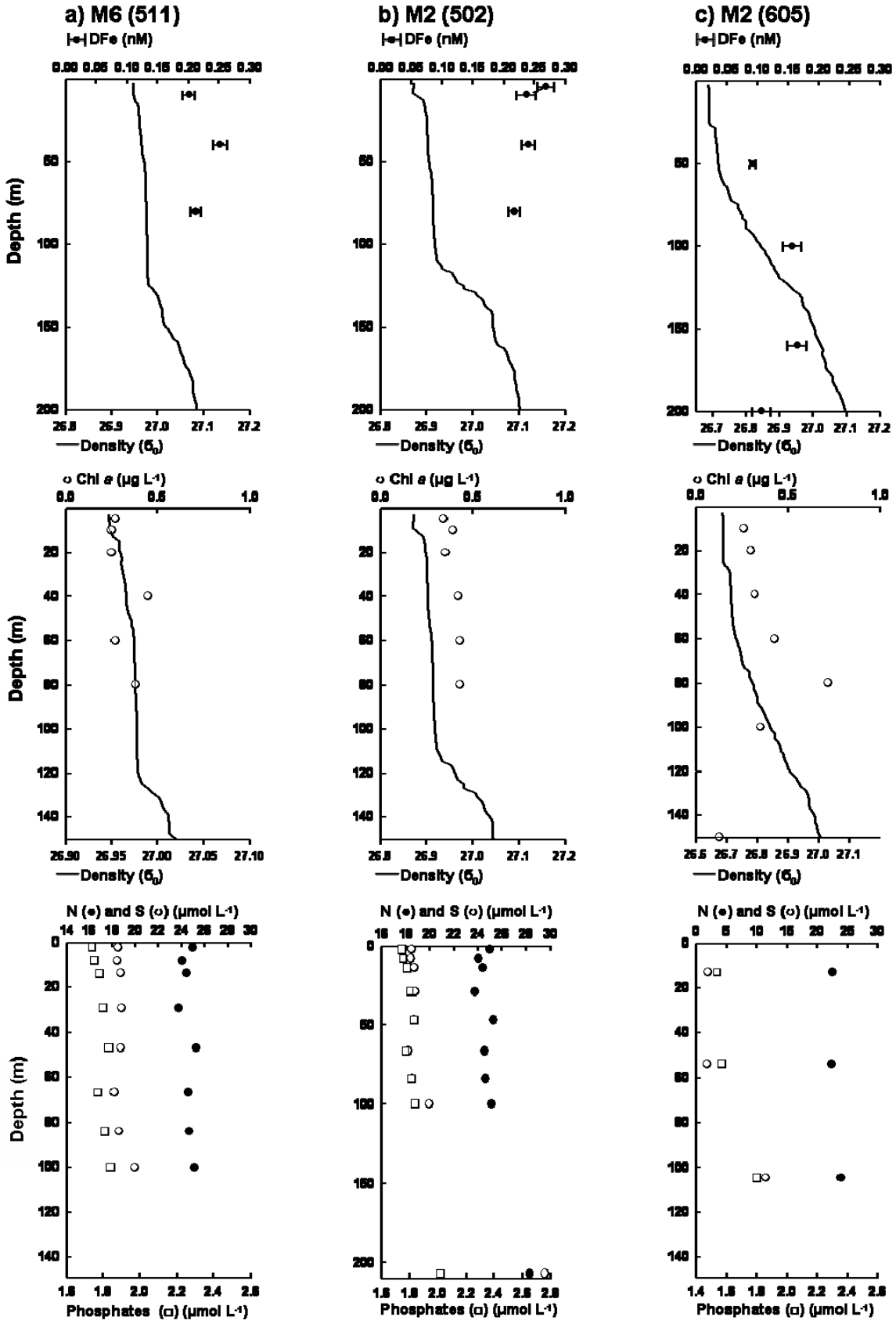

Figure III - 3: Water column profiles of DFe (top), density (black lines), chlorophyll *a* (middle), macronutrients (bottom) at the Southern sites ((a) M6. Stn 511 (22/11/2004); b) M2.1, Stn 502 (19/11/2004); c) M2.2, Stn 605 (06/01/2005)).

2.2 Northern Sites

Four stations (M1, M3, M7 and M10) were sampled in the area located north of the plateau (Figure III - 1), where they can be potentially affected by a natural "island mass effect". As Station M3 was sampled on 5 occasions, it will be described in a separate section. The three other sites will be presented later.

*M3 (*Figure III - 5*):* This station is located ~35km north of the plateau in an area where it was hypothesised that the bloom developed in direct response to an input of dissolved iron from the islands. This station was occupied 5 times and at each occupation of this station, major nutrients as well as productivity were measured. The main observation was that nitrate concentrations decreased from 24 µM to 18 µM over the sampling period and initial silicate concentrations of 18.5 µM became almost totally depleted (0.2 µM) in this region by mid January (Pollard et al., 2007a), which marked the end of the bloom (Figure III-5).

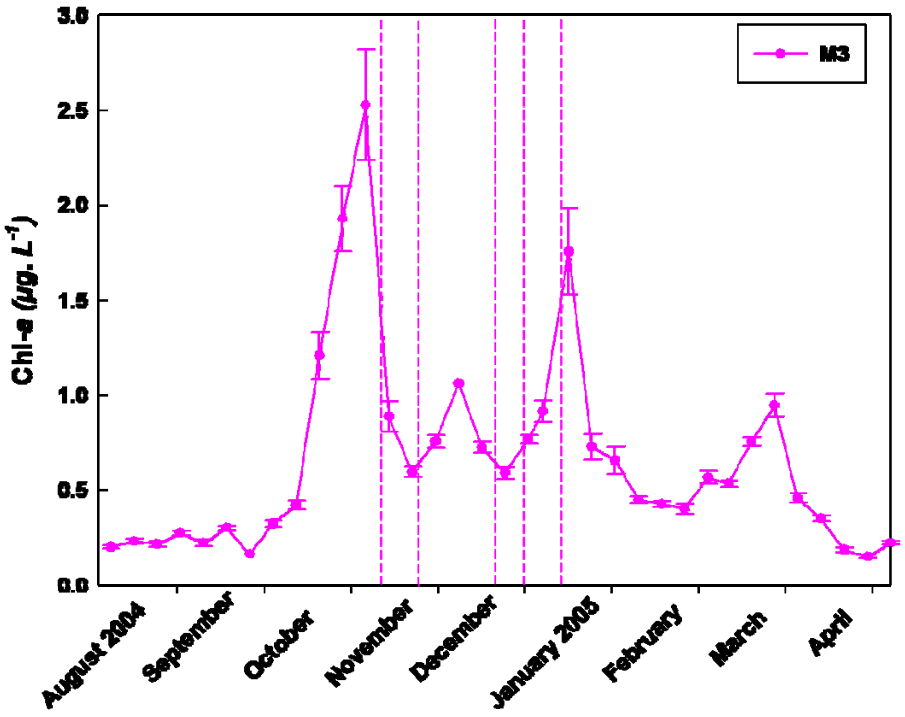

Figure III - 4: Variation of surface Chl *a* (merged MODIS/SeaWIFS data, courtesy of Hugh Venables) at stations M3 during the austral summer 2004-2005. Long dashed vertical bars represent the sampling dates for DFe vertical profiles

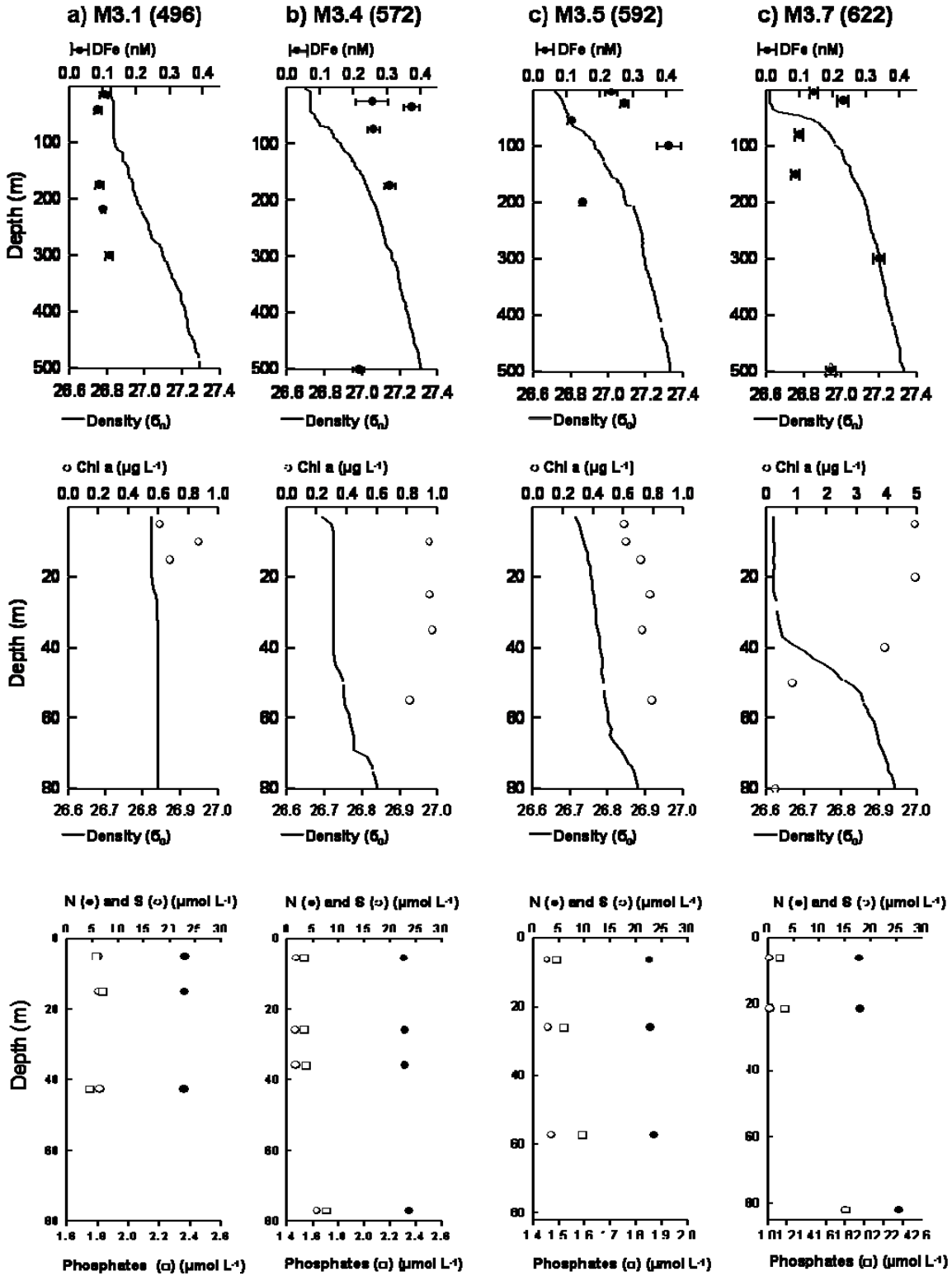

Figure III - 5: Water column profiles of DFe (top), density, chlorophyll *a* (middle) and macronutrients (bottom) at M3 ((a) Stn 496 (13/11/2004), b) Stn 572 (22/12/2004), c) Stn 592 (31/12/2004), d) Stn 622 (10/01/2005)).

The production was estimated at ~3 gC m^{-2} d^{-1} during the secondary bloom in January (Seeyave et al., 2007).

Sea surface temperature varied from 4.4 °C at the beginning of the sampling period (Stn 496, 13/11/2004) to 6.1 °C at the end (Stn 622, 10/01/2005). The mixed layer depths were relatively shallow (40-70m) for all the occupations.

Four stations are shown on Figure III - 5, as too few data were available for Station 516 (Table 1, Appendix III). The first occupation (496, Figure III - 5a) was in the declining stage of the first main bloom event in mid October. At this time, this station appeared to be under the influence of an influx of new water coming from the South (Pollard et al., 2007b). Consequently, surface chlorophyll concentrations were low at this station, with a maximum of 0.15 µg L^{-1} at 42m depth. DFe concentrations above the mixed layer depth had a mean value of 0.1 nM, this depletion being due to uptake by phytoplankton. Silicates were also depleted down to 5 µmol L^{-1}. The later two occupations (Stations 572, Figure III - 5b and 592, Figure III - 5c) exhibit low chlorophyll concentrations, varying from 0.58 to 0.85 µg L^{-1} within the mixed layer. Silicates were depleted down to 2 µmol L^{-1}, and in parallel, DFe concentrations in the upper water column varied with time, and had a mean value of 0.26 nM within the mixed layer. At station 592, a DFe maximum of 0.4 nM was observed just below the pycnocline at 100m depth which may be due to active recycling, or lateral advection. Unfortunately, no precise answer can be given and it could be as well a combination of both processes.

The last occupation in January 2005, (Station 622, Figure III - 5d) was sampled right before the maximum of Chl *a* during the secondary bloom event (Figure III - 4), with Chl *a* concentrations reaching 5 µg L^{-1} at 20m depth with DFe and silicates concentrations depleted down to 0.1 nM and 0.2 µmol L^{-1} within the mixed layer. Another DFe maximum of 0.34 nM was observed at 300m maybe due to remineralisation processes or advection of iron enriched waters. No values as high at this depth were found at the Southern sites.

Other northern sites: *M1, M10, M7*

These stations are located downstream of the plateau, Station M7 being the most western one, located right above the edge of the Plateau. A main bloom event occurred from the end of September until the end of October (Figure III - 6), with Chl *a* concentrations reaching up to 6 µg L^{-1} in surface.

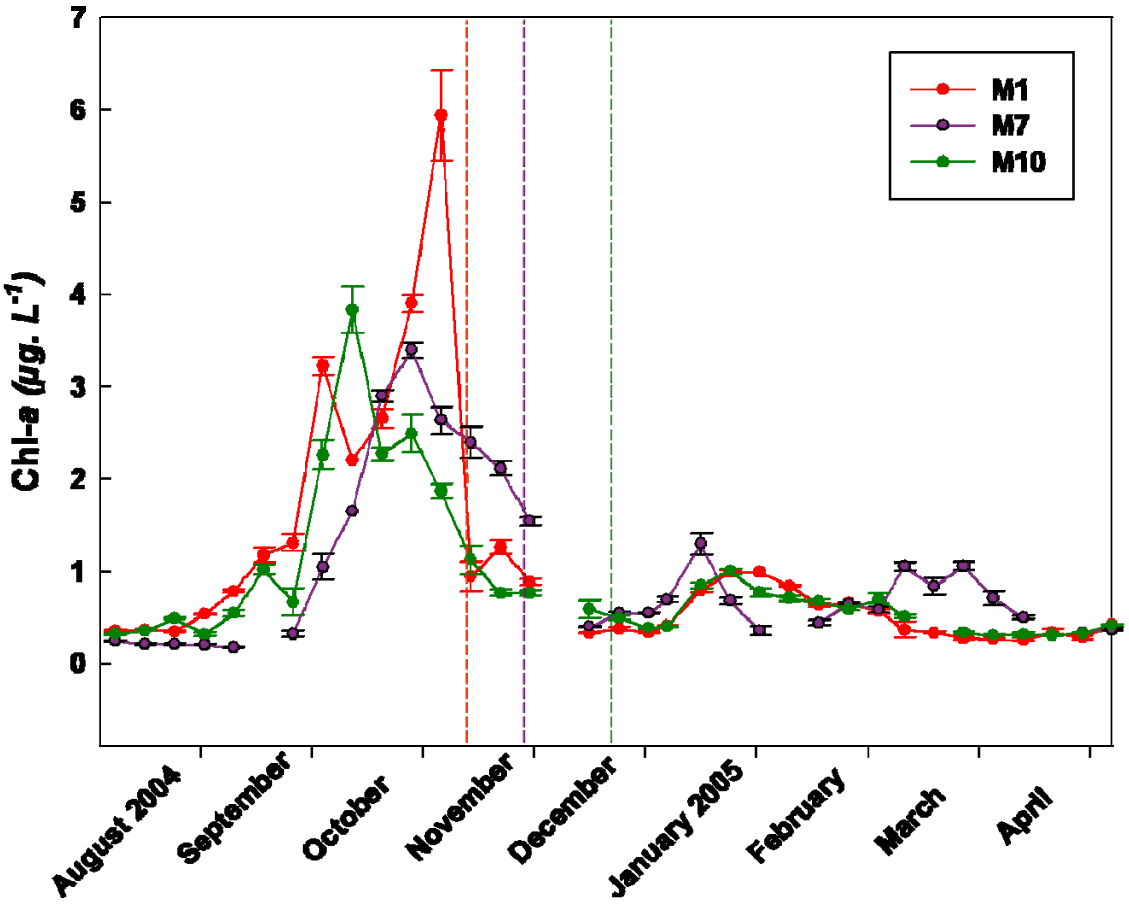

Figure III - 6: Variation of surface Chl *a* (merged MODIS/SeaWIFS data, courtesy of Hugh Venables) at stations M1, M7 and M10 during the austral summer 2004-2005.
Long dashed vertical bars represent the sampling dates for DFe vertical profiles

M1 and M7 were sampled in November; during the declining stage of the main bloom event, when the concentrations of Chl *a* were quite high for both, 0.79 for M1 and up to 1.20 µg L^{-1} at M7 respectively.

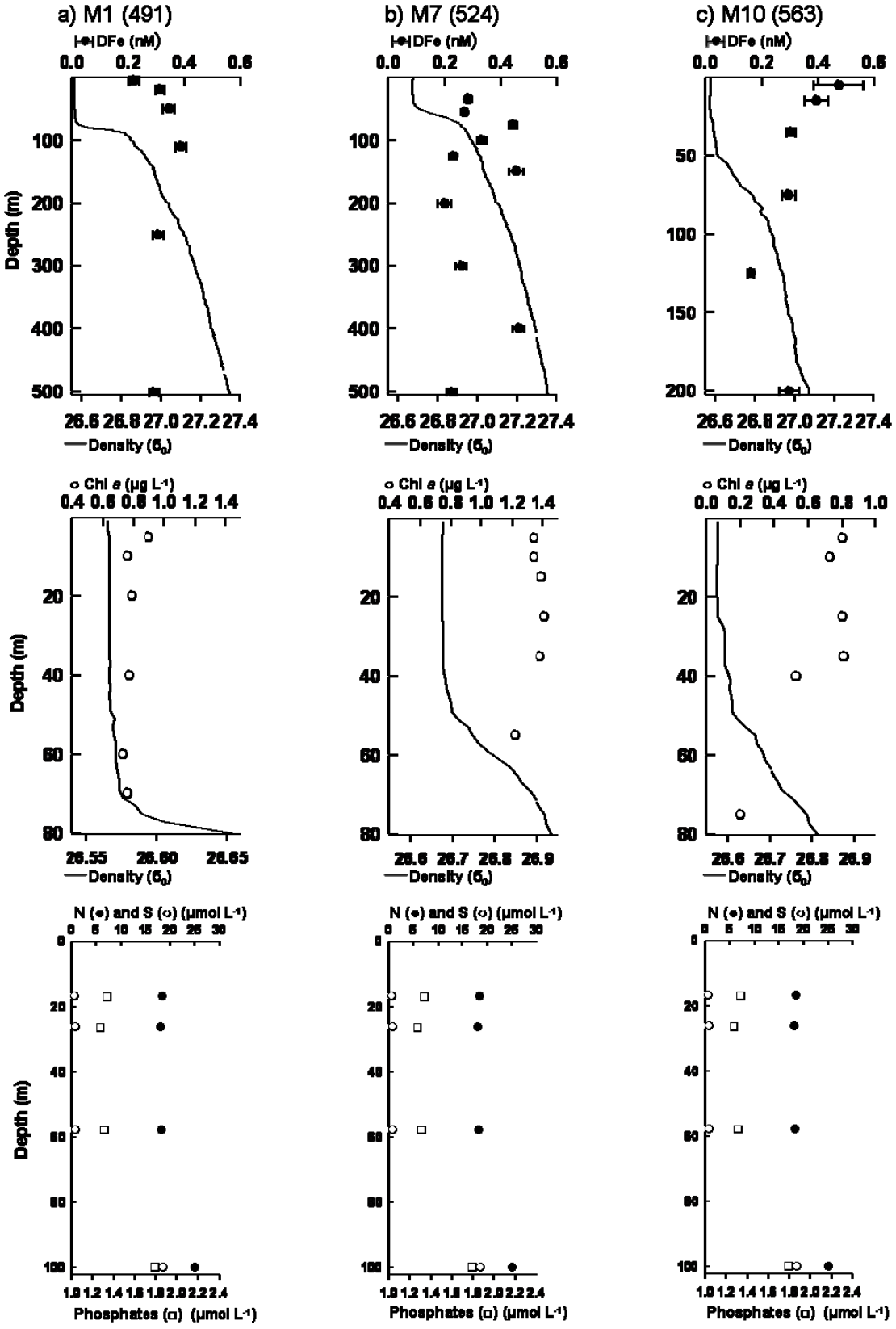

Figure III - 7: Water column profiles of DFe (top), density, chlorophyll *a* (middle) and macronutrients (bottom) at M1 (a,Stn 491), 11/11/2004), M7 (b, Stn 524, 27/11/2004), and M10 (c, Stn 563, 21/12/2004).

DFe concentrations were in a similar range at all these stations, around 0.3 nM in the upper water column with no evident depth related trends (Figure III - 7). M10 was sampled after the major bloom in late December. Concentrations of iron are higher, around 0.5 nM and chlorophyll concentrations are very low, 0.3 µg L^{-1}. DFe concentrations exhibit similar concentrations to those reported by Croot et al. (2004a) along a 6°E transect in the Southern Ocean and Sedwick et al. (2002) around the Crozet Islands for the 0.4 µm filtered fraction with concentrations ranging from 0.1 nM in surface waters to 0.5 nM at greater depths. A low level variability is evident between these stations, with concentrations ranging from 0.2 nM to 0.4 nM in the upper water column.

2.3 Baie Américaine

This bay is located at the north eastern flank of Île de la Possession, which is one of the main islands of the Crozet Archipelago. A series of 3 CTD casts were performed on the same day, in order to provide a near shore data set of DFe.

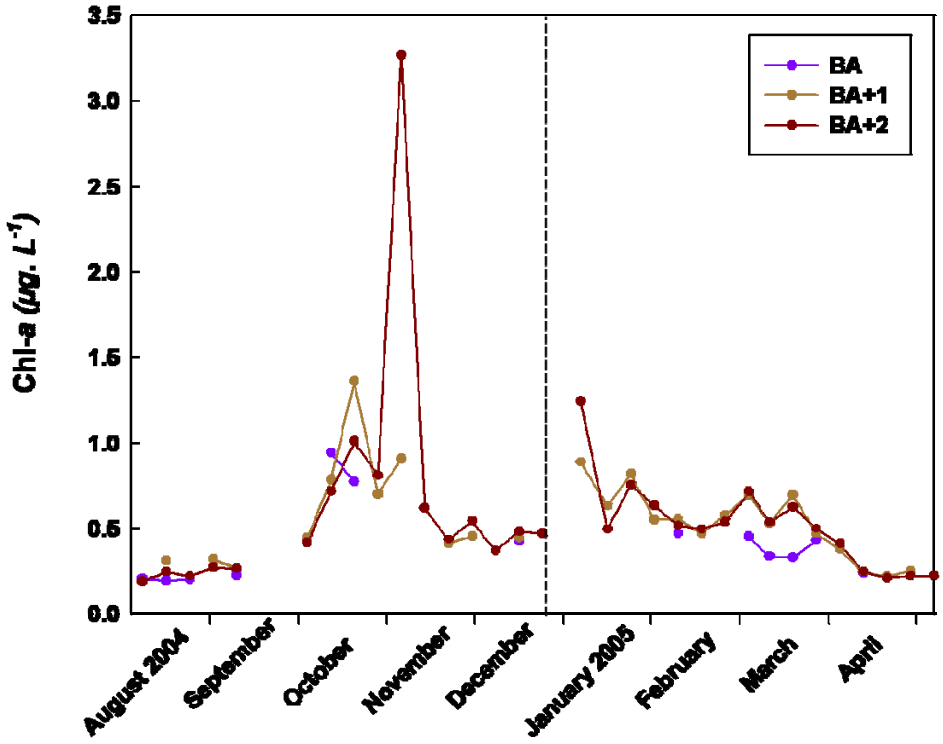

Figure III - 8: Variation of surface Chl *a* (merged MODIS/SeaWIFS data, courtesy of Hugh Venables) at stations BA, BA+1 and BA+2 during the austral summer 2004-2005. Long dashed vertical bars represent the sampling dates for DFe vertical profiles.

This corresponds to 3 stations that were occupied: 567 (Figure III - 9a), 568 (Figure III - 9b), and 569 (Figure III - 9c), which were located progressively further away from the shore. Station 567 was approximately 1 km from the shore, in shallow waters (80m).

At Station 567, DFe concentrations were remarkably high (> 0.5 nM), with a 2.16 nM peak at 50m depth and surface values were close to 1 nM (Figure III - 9a). Interestingly, Chl *a* concentration within this mixed, and potentially turbid, water column were low, with a mean value of 0.5 μg L^{-1}, suggesting the potential for light limitation within near shore waters.

Station 568 is located north east of 567 and at ~8.2 km distance from the shore. Within the mixed layer (80m), DFe and Chl *a* concentrations were relatively constant, at around 0.5 nM and 0.5 μg L^{-1} respectively. Elevated DFe concentrations of 1nM at 200 m then 2 nM at 300 m, and a lower value of 0.5 nM near the bottom (376m) were observed.

The last station (569) offshore in this transect was located 16 km away from the shore. Here again, within the mixed layer (50m) DFe and Chl *a* concentrations were relatively constant. An increase in the DFe concentration of 0.4 nM was observed at 300 m depth. Chl *a* concentration were higher at station 569, up to 1.67 μg L^{-1}, which corresponded to a low DFe concentration (0.18 nM) in surface waters.

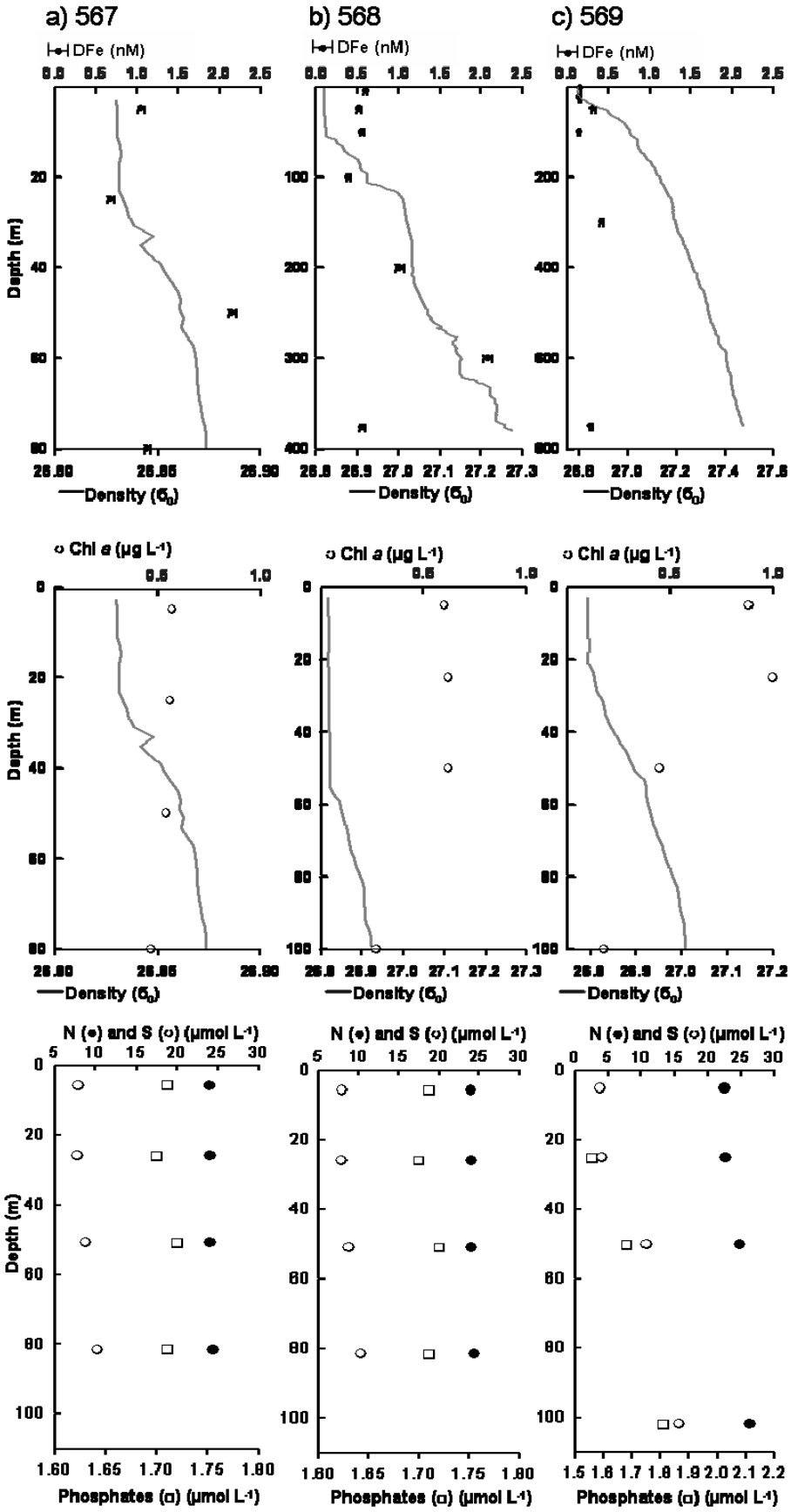

Figure III - 9: Water column profiles of DFe (top), density, chlorophyll *a* (middle) and macronutrients (bottom) along a transect from Baie Américaine on 22/12/2004.

(a) BA, Stn 567, (b) BA + 1, Stn 568, (c) BA + 2, Stn 569.

3 Discussion

This new data set allows a comparison with other studies conducted in other parts of the Southern Ocean. Moreover, repeated occupations of Station M3 provide a quasi time series and highlight the complexity of the processes influencing the bloom. Therefore, the relationship between Chl *a* and DFe distribution will be discussed at this station. Finally, using the Baie Americaine profile, the possible island source that can fertilize the semi-enclosed area north of the Crozet Islands will be presented.

3.1 Comparison with other studies

The surface concentrations of DFe are similar to recently reported values in this sector of the Southern Ocean. In late summer 1998, Croot et al. (2004a) using chemiluminescence detection found dissolved iron (<0.4 μm) concentrations ranging from 0.04 nM outside the fertilized area to 0.58 nM along a 6°E transect. Sedwick et al. (2002), during ANTARES IV (Jan-Feb 1999) around the Crozet Islands, reported DFe concentrations varying between 0.09 nM and 0.50 nM over the top 300m (<0.4 μm) using catalytic spectrophotometric detection (Measures et al. 1995.). More recently, Blain et al. (2007) reported a mean concentration around the Kerguelen Islands of 0.09 ± 0.034 nM over the top 500m. However, a study conducted around the Kerguelen Islands (Bucciarelli et al. 2001) observed considerably higher concentrations of DFe, in the order of 7 nM. This difference may be explained by the time of sampling, which was prior to the bloom event in October therefore prior to the main uptake by the phytoplankton, and as well by the presence of high concentrations of lithogenic material emanating from coastal wheathering, river discharge and inputs noted within the coastal waters of Kerguelen (Blain et al., 2001). As iron is considered to be the main limiting nutrient, one might expect that a high input of iron will promote a bloom which will cause an increase in chlorophyll and gradually a decrease in iron concentrations. However, we do not expect a simple relationship between DFe and Chl *a*. This may reflect changes in iron uptake and the fact that the phytoplankton community is affected by other factors such as light availability and grazing (Lancelot et al. 2000). For example, the fact that the Chl *a* concentrations are low at very close proximity to the shore (station 567) and where DFe

are the highest could indicate that the light mixing regime is not favourable to the phytoplankton community in these turbid waters.

3.2 Upper water column (50m) distributions of DFe and their relationship to Chl *a* at M3

M3 station is located downstream of the Crozet Islands (Figure III - 1) but is occasionally influenced by advection of near surface waters from the South (Pollard et al., 2007b).

Figure III - 10 represents the variation of integrated Chl *a* and DFe over time at M3. The first occupation of this station (M3.1, Stn 572, Table III-1) was sampled at the end of the main bloom, when biological uptake has certainly reduced the bioavailable DFe and silicates to a concentration resulting in limitation of the phytoplankton population by mid November (Lucas et al., 2007). A change in the phytoplankton community structure has also been observed by Poulton et al. (2007), the colony evolving from diatoms to *Phaeocystis*. A temporally and spatially variable Fe resupply proximal to the Plateau may have occurred and reinitiated or maintained small bloom regions. It is also likely that some DFe recycling processes occurred. A combination of these factors may thus explain the high integrated Chl *a* observed in mid January and simultaneous decrease in integrated DFe (Station 622). An additional factor of importance seems to be the ambient irradiance which appeared to be the component which initiates the bloom and early development (Venables et al., 2007), usually in October.

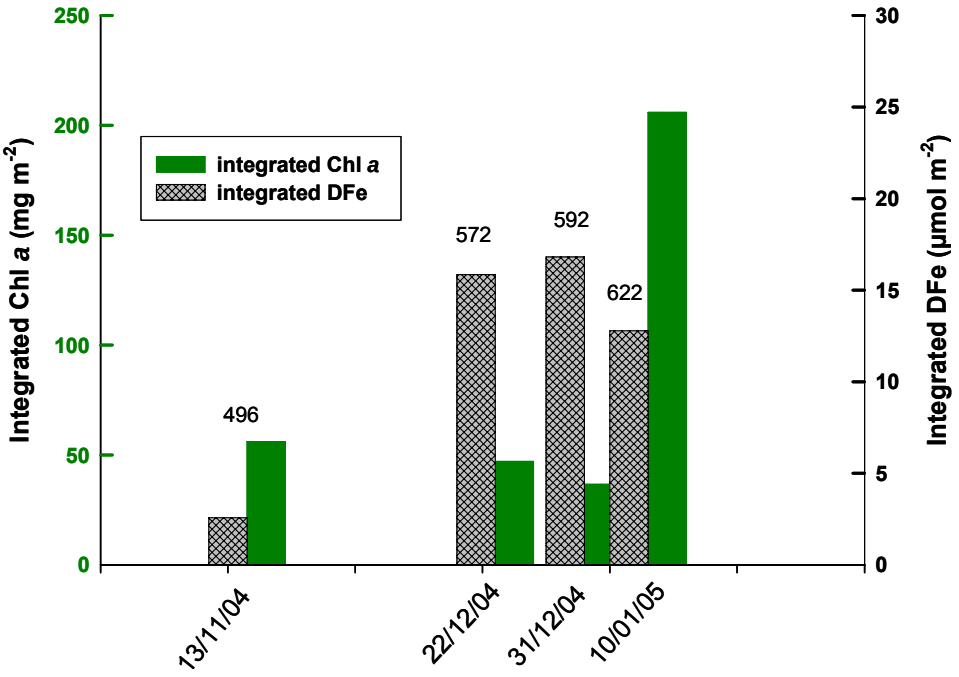

Figure III - 10: Variation of integrated Chl *a* and DFe at station M3 (496 refers to M3.1, 572 to M3.4, 592 to M3.5 and 622 to M3.7)

Moore et al. (2007a, 2007b) calculated the growth rates of phytoplankton species after different addition of DFe, under low and high light conditions. The reported values to the north of the plateau were of comparable magnitudes to the maximal growth rates estimated for the natural population around the Kerguelen Islands.

Within the declinging stages of the bloom in the northern area, growth rates were low, presenting the evidence for Fe limitation. Enhanced phytoplankton photochemical efficiencies (Fv/Fm) with higher DFe concentrations were also observed *in situ*.

At any particular time the relationship between DFe and Chl *a* will also depend on the stage of bloom progression and the amount of biological Fe uptake which has occurred.

3.3 Lateral sources of Fe from the island system

The first station sampled immediately in the vicinity of Baie Américaine was Station 567, which had average DFe concentration of 1.25 nM. The next station, located

approximatively 3 kms away from the shore was Station 568 and had average DFe concentration of 0.81 nM. These are the highest concentrations found during this study and indicate that the island system is a source of iron. This source can be from sediments on the shelf (Elrod et al., 2004), direct runoff and there is also the possibility that soluble Fe can be leached from suspended particles as they are laterally advected through the water column (Lam et al , 2006).

Moreover, Stations 567, 568, 569 (Baie Américaine) and 572 (M3) show a clear decreasing gradient (Figure III - 11) of DFe concentrations at all depths.

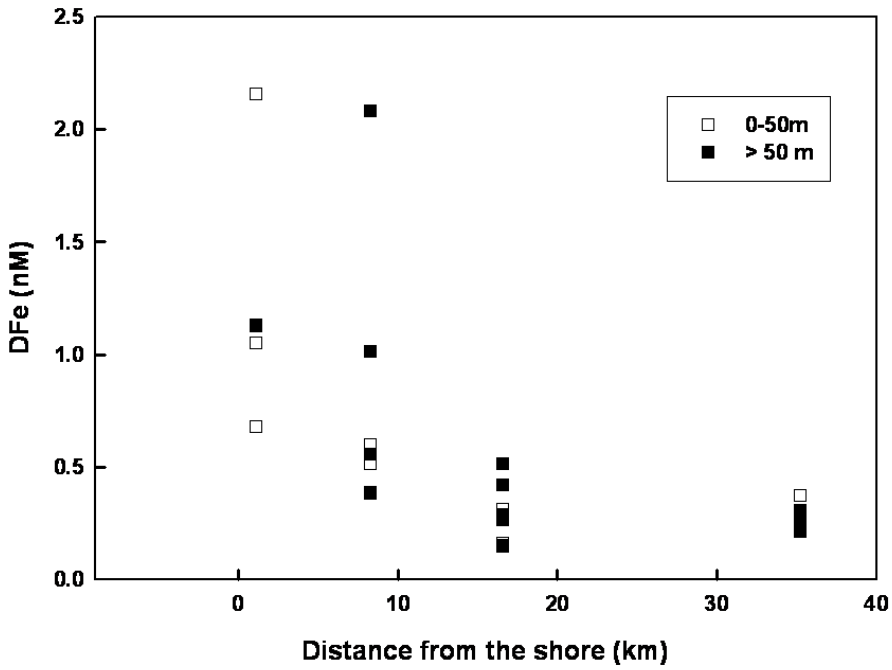

Figure III - 11: DFe versus distance from the shore along the Baie Américaine transect extended out to M3 (Stn 572).

Using the same approach as Johnson et al. (1997), it is possible to estimate a scale length which is defined as "the distance over which concentrations drop to 1/e of the initial value". Looking at the upper 50m, the scale length here is 25 km, which is considerably lower than the scale length of 151 km estimated by Bucciarelli et al. (2001) in the vicinity of Kerguelen Islands in the near shore waters. This difference may be explained by a different circulation pattern around the two islands and by the difference between the respective surface areas of the islands as well as a different sampling time. The magnitude of natural iron fertilization may well depend on the surface area of the islands: the

Kerguelen Islands have a surface area of 7000 km^2 and the Crozet Islands only 350 km^2 , which could explain the smaller scale length calculated here. Significant loss of iron advected from the sediments and shelf can occur too, in particular with scavenging onto sinking particles, which can remove iron before it can be distributed to the entire bloom region which extends well north of M3.

Despite a relatively short scale length, it is possible to suggest the following fertilizing scenario. The circulation, as described by Pollard et al. (2007b) has the consequence of semi-enclosing the area to the north of the Crozet Plateau (Figure III - 1) where the residence time of surface water is ~100 days. Consequently the large bloom observed in this HNLC area is clearly constrained by this northern branch as well as any dissolved iron from the islands and the associated plateau. If one considers the island and the plateau systems to be a source of iron throughout the year then, during the low light conditions of the winter when primary production is low, the concentration of iron can build up and disperse laterally to then be readily available to phytoplankton in spring time. A detailed explanation of this hypothesis and resulting calculations is presented in Chapter Five, together with other inputs that can be considered, such as atmospheric inputs, particulate inputs or vertical mixing.

4 Conclusion

The distribution of DFe in the study area revealed that there were not significant differences in surface concentration between the northern sites and the southern sites. However, the concentrations of DFe observed in this study are the net effect of the inputs, the biological cycling as well as the removal processes.

The vertical profiles obtained at the transect of stations from Baie Américaine shows a distinct concentrations gradient, thus providing strong evidence for the island shelf system being a source of Fe. Due to the circulation patterns and low light levels in the winter, it is anticipated that the iron liberated from this source can accumulate during the winter and be available for phytoplankton when the spring arises.

Other input terms to the surface water will have to be considered including for example atmospheric deposition input and vertical mixing. This will be developed in Chapter Five.

It is also necessary to look at the potential role of suspended particles. Scavenging processes are likely to occur and it is reported that soluble Fe can be leached from large suspended particles as they are laterally advected through the water column as recently described by Lam et al. (2006). It is also possible that colloidal iron may be released from sediments and added to the Fe advected to the bloom area. These additional sources would increase the iron budget at the end of the winter and require further investigation. Unfortunately, no samples for smaller particles (0.4 - 53μm) were taken so this potential source will remain unknown for the moment.

The case of iron in suspended particulate matter sinking out of the mixed layer is investigated in the next chapter.

CHAPTER FOUR:

THE DISTRIBUTION OF IRON AND ALUMINIUM IN LARGE SUSPENDED PARTICLES

As detailed in Chapter One, iron exists in seawater in different chemical and physical forms; these determine its bioavailability to organisms as well as its transport. Until recently, the majority of research has focused on DFe even if the total iron in a seawater sample is heavily dominated by the particulate fraction (De Baar and De Jong, 1991; Coale et al., 2005).

The particulate pool is highly complex to study, because both biogenic and non biogenic particles are present, and because trace metal distributions are controlled by several processes including surface adsorption, biological uptake, and particle sinking (Collier and Edmond, 1984). For example, iron bound to particles can be quickly incorporated into the sediments whereas free iron and iron bound to ligands in solution should have a longer residence time in water and may be transported over long distances or interact more readily with organisms and surfaces. Therefore, the content of iron can be high in seawater but its bioavailability is probably limited.

A better understanding of potentially bioactive iron concentrations and fluxes around the Crozet Islands is of importance when looking at the effect of natural iron fertilization on particulate organic carbon (POC) export. It is crucial to examine the downward flux of Fe, as it could be a major sink in the iron cycle, therefore contributing to the control of phytoplankton ecology in HNLC regions. It could help in answering whether or not increased iron supply will elevate carbon sequestration to the deep ocean. It is also important to note that the downward flux and content of iron remains poorly studied in the Southern ocean.

Here, a two step sequential leach (Chapter Two and Appendix II) is used to investigate the concentrations of aluminium and iron in a series of samples of large suspended particles (>53 μm) taken just below the mixed layer during CROZEX (Austral summer 2004/2005) and Benthic Crozet (Austral summer 2005/2006). This larger size class of particles (>50 μm) is considered to represent the bulk (90 %) of particles rapidly settling out of the water column (Bishop et al., 1977, Clegg and Whitfield 1990, Buesseler et al., 2006). Aluminium concentrations in particles are important to determine as they can be used to provide a clear indication of what fraction of the iron present is associated with aluminosilicate phases. It has been conventionally used to estimate the continental contribution to marine sediments (Saito et al., 1992), which could help to identify the island source.

This sequential leach was applied to each sample of large particles and gave both “acid leachable” or “labile” and “refractory” metal concentrations, elsewhere referred to as “reactive” and “non reactive” forms by Landing and Bruland (1987).

Results are presented according to the three zones predefined in the previous chapter, i.e., north and south of the islands, and in close proximity to them. Concentrations of particulate aluminium and iron in the filtered seawater are presented as well as their concentrations within the particles. Scanning Electronic Microscopy (SEM hereafter) images are shown for several stations too. Both phases will be discussed in relation to Particulate Organic Carbon (POC).

1 Sampling sites

SPM concentrations in seawater vary over at least five orders of magnitude depending on the region where they are sampled. Minimum concentrations of 0.5 µg L^{-1} have been observed in oligotrophic areas of the open ocean whereas SPM content in coastal waters can exceed 50 mg L^{-1} (Eggiman and Betzer, 1976; Helmers, 1996). Therefore, in HNLC regions away from land masses, there is a need to filter large volumes of seawater in order to get enough material to process. In this study, SPM was collected in the waters surrounding the Crozet Islands, to the North, South and East during the austral summers 2004/2005 and 2005/2006, in the framework of the CROZEX program (Figure IV-1). Sampling was generally carried out just below the mixed layer depth, typically 5 to 10m below the density discontinuity. During the surveys, the mixed layer depth ranged from 30 to 225m (Table IV - 1).

Large particles (>53 µm) were collected on 293mm diameter nylon meshes using Challenger Oceanics Systems and Services *in situ* pumps (see Chapter Two). There was one particular deployment during D300 where two SAPS were deployed at the same time, one close to the bottom (340m) and the other one at 70m depth. Only one sample was found to be contaminated (Station 15775#9, D300). The concentrations of Fe in the 1st leach were too high (840 µg g^{-1}) compared to the range of the concentrations observed elsewhere (0.2-110 µg g^{-1}, see Table IV-2). This is probably due to some contamination during the handling after deployment.

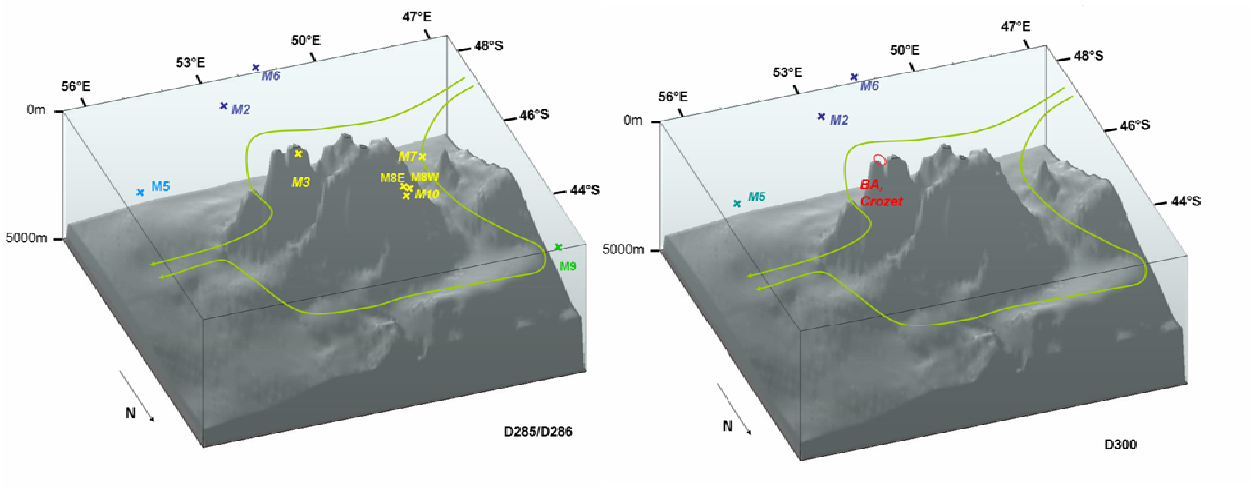

Figure IV - 1: Sampling sites during CROZEX (D285/D286, left) and Benthic Crozet (D300, right). The major currents are represented by the solid green lines superimposed on the topography.

Station #	Latitude (°S)	Longitude (°E)	Depth (m)	Volume filtered (L)	Mass collected (mg)	Station #	Latitude (°S)	Longitude (°E)	Depth (m)	Volume filtered (L)	Mass collected (mg)
15494#2 M3	46.05766	51.78060	225	1933	173.8	15554 M9	42.99510	47.02378	120	1861	14.3
15499#2 M3	46.02599	51.81050	155	1502	19.28	15563 M10	44.52528	49.96059	110	1817	21.6
15503#2 M2	47.79552	52.85540	150	2017	61.15	15573#2 M3	46.06834	51.77819	180	1945	16.0
15511#1 M6	49.00557	51.50046	200	2053	68.85	15580 M5	45.99740	56.15210	125	1001	15.8
15517#2 M3	46.07007	51.77153	200	1990	43.25	15591 M3	46.04319	51.77791	100	1909	33.6
15524#1 M7	45.49893	49.00171	150	1940	89.06	15595 M6	48.99897	51.53799	120	1878	127.4
15533#1 M8E	44.95355	49.94103	200	1972	67.91	15604 M2	47.80029	52.84838	160	1653	84.3
15539#2 M8W	44.87236	49.64711	150	1842	166.36	15620 M3	46.03230	51.87041	80	1493	12.6
15543#2 M9	43.11740	47.18411	120	1719	83.0	15628 M3	46.04089	51.96060	80	2031	22.2
Station #	**Latitude (°S)**	**Longitude (°E)**	**Depth (m)**	**Volume filtered (L)**	**Mass collected (mg)**						
15773#3 M5	46.00383	56.26683	140	2169	94.2						
15773#41 M5	45.94017	56.42483	100	2278	57.2						
15775#9 M6	49.07383	51.24817	100	2339	147.6						
15775#29 M6	49.10717	51.20933	110	2359	38.8						
15776#2 Crozet	46.49917	51.91633	70	2434	21.7						
15776#2 Crozet	46.49917	51.91633	345	2313	36.4						
15777#1 Crozet	46.38067	51.82933	30	1647	43.8						

Table IV - 1: Details of SAPS deployments during 285 (no shading), D286 (light grey shading) and D300 (dark grey shading)

Station M3 immediately north of the islands was sampled on 7 occasions, providing an opportunity to examine the variation of trace metal content throughout a period of nearly 3 months. In addition, several other samples were taken in area north of the islands where natural iron fertilization was anticipated (M7, M10, M8E, M8W). Two particular sites, M8E and M8W were sampled because of their contrasts: the first site had low concentrations of Chl *a*, relatively high macronutrients (Si: 2.9 µmol L^{-1}) and a deep well mixed layer, whereas the second site had high concentrations of Chl *a*, depleted macronutrients (Si <0.1 µmol L^{-1}) and a shallower stratified surface layer (Read et al., 2007). These two sites were only 12 nautical miles apart. Southern sites (M2, M6) referred in the previous chapter as our "control sites" were sampled on different occasions too, over two austral summers. Finally, M9 to the north of the Polar Front Zone was sampled on two occasions.

Samples were treated by the two selective chemical digestions (Chapter Two) and concentrations of iron and aluminium were determined by ICP-MS, in both fractions: the acid leachable and the refractory fractions. POC concentrations were determined by the technique detailed in Appendix II by Bob Head at the Plymouth Marine Laboratory.

2 Results

Acid leachable fraction of aluminium and iron will be first presented, then total concentrations will be discussed .These results are necessary for the quantification of the vertical iron export (Chapter Five).

2.1 Distribution of SPM (>53 µm) and POC

SPM concentrations varied from 7.66 µg L^{-1} (Station 15554 M9) up to 90.31 µg L^{-1} (Station 15539#2, M8W) (see Figure IV-1 for the locations). The majority of the concentrations found between the three legs were lower than 30 µg L^{-1} representing nearly 60% of the samples (Figure IV - 2), which is a characteristic range for oligotrophic waters. On two occasions only did concentrations reach 90 µg L^{-1}. At M3, this concentration was measured 13 days after a maximum peak in Chl *a* of 2.5 µg L^{-1}.

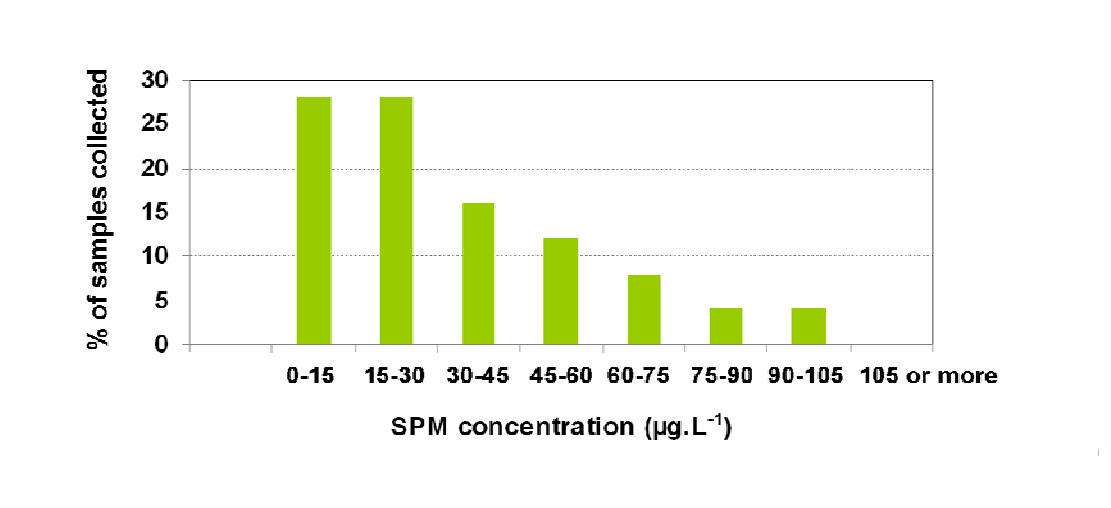

Figure IV - 2: Distribution of samples according to their SPM concentration.

Figure IV - 3 shows the variations of satellite derived surface Chl *a* concentration and SPM content of seawater below the mixed layer depth at Station M3. SPM concentrations follow very well the variation of Chl *a* and bracket the minimum and maximum values observed during the cruise.

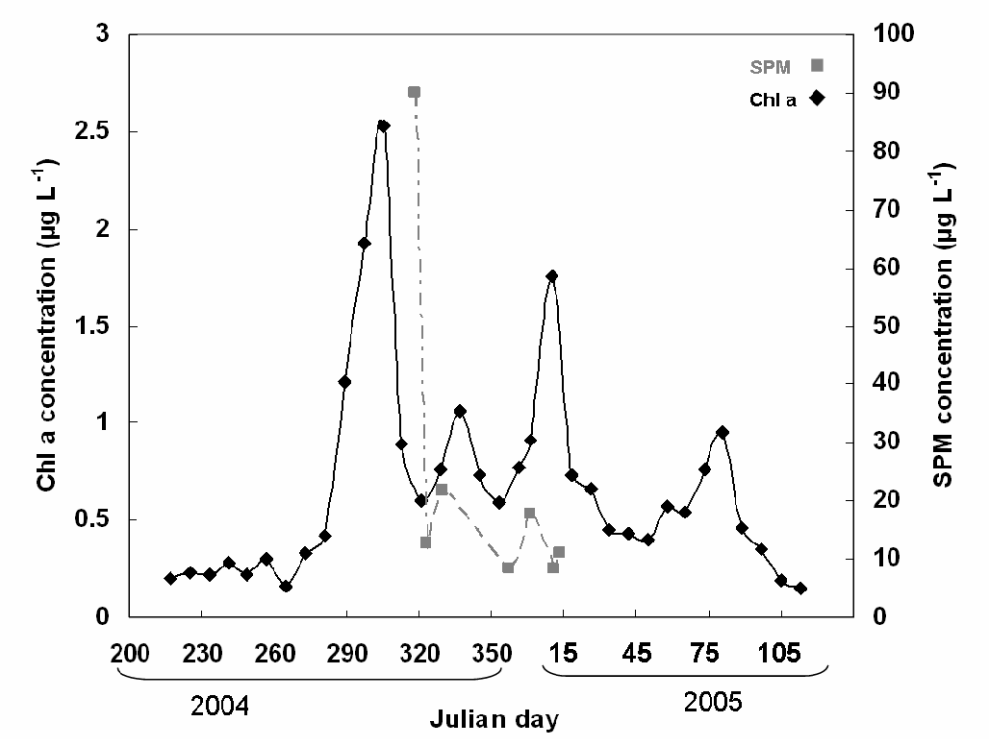

Figure IV - 3: Variation of surface chl *a* (black diamonds) and SPM (grey squares) concentrations obtained at the bottom of the mixed layer depth at station M3 during D285&D286

The southern sites that are not under the influence of the islands have similar concentrations of SPM with the northern sites (on average 38 µg L^{-1} and 32 µg L^{-1} respectively, Table IV-2). Therefore, it is difficult to distinguish the northern sites from the southern sites in terms of SPM concentrations. However, there is clear relationship between the SPM and POC concentrations at all sites, as shown in Figure IV - 4, indicating that the samples were mainly biogenic in origin.

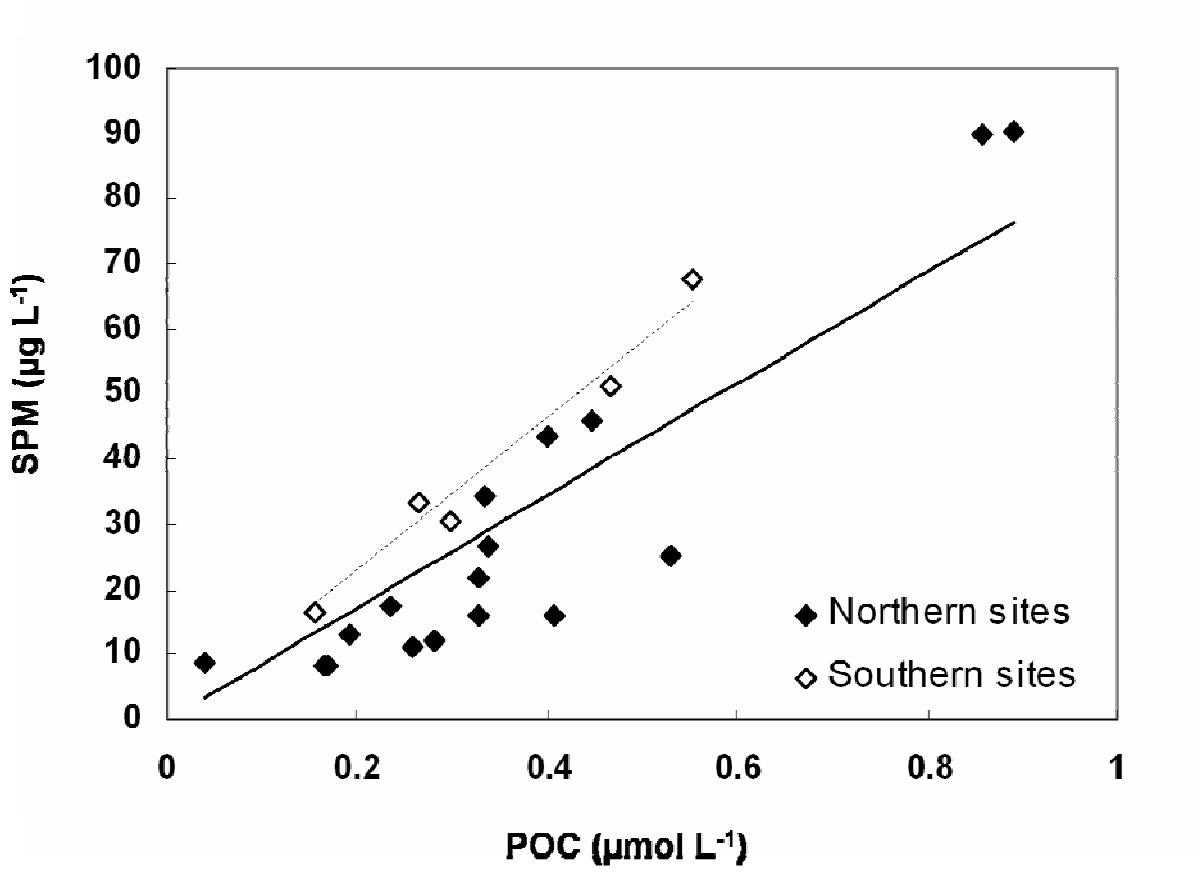

Figure IV - 4: POC versus SPM concentrations during D285, D286 and D300. A distinction is made between the Northern sites (♦, R^2 = 0.97), Southern sites (◊, R^2 = 0.94).

Stations sampled outside the Polar Front Zone (M9) will be left out of the discussion here as they are neither under of a possible influence of the Crozet Islands nor true HNLC sites as they can be under the influence of the Algulhas Return Current. Only the stations to the North (M3, M7, M8E, M8W, M10) and to the South (M2, M6) will be studied in detail.

Overall, there is good correlation between POC and SPM concentrations in both regions (South: r^2=0.97; North: r^2=0.94). POC concentrations ranged from 0.04 µmol L^{-1} (15776#1, Crozet) to 0.89 µmol L^{-1} (15539#2, M8W). Interestingly, the lowest POC

concentration was found at the closest station from Île de la Possession, confirming that the phytoplankton must have been inefficient due to high turbidity regimes and subsequent low light availability (Chapter Three). There was also no clear evidence of large differences in average POC concentrations between the two main regions (north, south) at the time of sampling. Various factors such as light regime, nutrients availability, or bioavailability of iron can explain this similarity in POC concentrations (Morris et al., 2007).

2.2 Acid leachable fraction of trace metals in SPM (>53 µm)

Although the scientific community is still not clear on which method best provides an estimate of the potentially biologically available iron, there is a consensus to define this fraction as the acid labile or reactive fraction (Johnson et al., 2005). In such a system where the "island effect" could have an influence on the distribution of iron, it is necessary to consider all forms of iron. Wells et al. (1991, 2000) demonstrated that the availability of iron to phytoplankton would be affected by the dissolution of solid forms as well as the colloidal influence on its uptake. Wells et al. (2000) applied a 25 % acetic leach (HAc) on their particulate samples. This treatment of suspended particles allows the determination of the labile or "acid leachable" fraction to phytoplankton by displacing adsorbed ions, dissolving Ca and Mg carbonates and some fraction of Al, Fe, Mn oxyhydroxides (Landing and Bruland, 1987). The second and final extraction by aqua regia and HF digests the remaining "refractory" particles that are considered to be unavailable to phytoplankton. Therefore, the HAc leach gives an operational measure of metals associated with the particles bound Fe-Mn oxides coatings that are potentially available to participate in short tern biogeochemical reactions (Hatje, 2003). The abundance of these HAc-soluble particulate forms should increase in areas where dissolved Fe is being scavenged to particulate forms.

The results of the first leach analyses in seawater of Al and Fe (HAc-Me in pmol L^{-1} and µg g^{-1}) are summarized in Table IV-2, which also gives SPM and POC concentrations at all sites.

The broad distributions of HAc-Me in the three regions of the study area are detailed below.

Station #	SPM µg L^{-1}	POC µmol L^{-1}	HAc-Al pmol L^{-1}	HAc-Al µg g^{-1}	HAc-Fe pmol L^{-1}	HAc-Fe µg g^{-1}
15494#2 M3	89.9	0.86	4.60	1.38	1.58	0.98
15499#2 M3	12.8	0.19	8.84	18.6	11.7	51.0
15503#2 M2	30.3	0.30	0.57	0.51	0.40	0.74
15511#1 M6	33.5	0.26	1.47	1.18	0.96	1.60
15517#2 M3	21.7	0.33	1.38	1.72	0.46	1.18
15524#1 M7	45.9	0.45	0.66	0.39	0.41	0.50
15533#1 M8E	34.4	0.34	4.98	3.91	2.68	4.35
15539#2 M8W	90.3	0.89	1.54	0.46	0.35	0.22
15543#2 M9	48.3	0.96	2.43	1.36	0.74	0.86
15554 M9	7.66	0.64	3.11	10.9	2.13	15.5
15563 M10	12.0	0.28	0.35	0.79	0.19	0.88
15573#2 M3	8.23	0.17	1.02	3.34	0.82	5.56
15580 M5	15.8	0.41	0.94	1.61	0.33	1.17
15591 M3	17.6	0.23	0.28	0.43	0.36	1.14
15595 M6	67.8	0.55	0.38	0.15	2.18	1.80
15604 M2	51.0	0.47	0.26	0.14	0.08	0.09
15620 M3	8.43	0.16	1.47	4.70	3.52	23.3
15628 M3	10.9	0.26	0.14	0.35	1.78	9.12
15773#3 M5	43.4	0.40	1.24	0.77	1.35	1.74
15773#4 M5	25.1	0.53	4.81	5.17	0.55	1.22
15775#29 M6	16.5	0.16	0.62	1.01	0.30	1.02
15776#1 Crozet	8.92	0.04	12.9	39.2	17.6	110
15776#2 Crozet	15.7	0.33	4.11	7.06	1.96	6.97
15777#1 BA	26.6	0.34	32.5	33.00	22.2	46.6
Average Northern sites	32.0	0.38	2.3	3.57	2.17	8.94
Average Southern sites	39.8	0.35	1.34	0.60	0.78	1.05
BA	17.0	0.34	32.5	33.00	22.2	46.6

Table IV - 2: Concentration of acid leachable Fe and Al (HAc-Me) in seawater and in particles. The % of HAc-Me relative to the total fraction, as well as the concentrations of POC and SPM at all stations during D285, D286, D300.

HAc-Me - Maximum concentrations of HAc-Fe were obtained at Baie Américaine, reaching 22.2 pmol L^{-1} and at another station close (14 kms) to Île de la Possession, where the HAc-Fe concentration was 17.6 pmol L^{-1}. These high values, 10 times greater than the average measured elsewhere support the hypothesis introduced in the previous chapter that the islands are a source of potentially bioavailable iron. In addition to these high concentrations of HAc-Fe, high concentrations of HAc-Al in seawater (up to 32.5 pmol L^{-1}) were observed at this station, which supports the hypothesis of an island source. The highest concentrations of leachable iron and aluminium in the particles were found at Station 15776#1 (Crozet, 75m) and at Baie Américaine. Particles were enriched by a

factor of almost 100 compared to the particles sampled at other sites. SPM at 340 m was much less enriched in Al (7.06 µg g^{-1}) and Fe (6.97 µg g^{-1}).

The northern region which is under the influence of the islands has higher average concentrations of metals than the Southern sites. However, this high average is due to elevated concentrations found at two particular stations, M8E and M3 (15499) reaching up to 18.6 µg g^{-1} for Al and 51 µg g^{-1} for Fe. Very low POC concentrations were found at these sites. If these points are removed from the calculation, then the difference between the northern sites and southern sites is less clear.

The southern sites have similar SPM concentrations to the northern sites and the maximum of HAc-Me concentrations were found at the beginning of the survey (Stations 15503 and 15511). It is therefore difficult to establish a difference between the fertilized sites and non fertilized sites by looking at only the acid-leachable fraction. It is necessary to study the total concentrations of both metals, which is the purpose of the next section.

2.3 Refractory and total trace metals concentrations in SPM (>53 µm)

The residues after the first leach were totally digested by aqua regia followed by HF concentrated solutions (Chapter Two and Appendix II) allowing the determination of the most refractory fraction (Ref-Me) of the trace metals studied here. HAc-Me and Ref-Me have been added to give the total concentrations.

In an analogous way than for the 1st leach results, concentrations will be presented in nmol L^{-1} (Table IV - 3) for the concentration in seawater and in mg g^{-1} in the particles.

Crozet – The Baie Américaine (BA) station had the highest concentrations of Al (25.8 nmol L^{-1}) and Fe (13.2 nmol L^{-1}). Concentrations in BA are 10 to 100 times greater than any northern or southern sites. The particles collected at this station have also the greatest concentrations of Al (25.8 mg g^{-1}) and Fe (27.7 mg g^{-1}). This is in line with the results of the 1st leach and confirms that the island is an iron source. Station 15776 presented enhanced values at 75m, in comparison with the concentrations observed near the bottom.

At 340m depth, Fe concentrations fell back to 0.81 nmol L^{-1}, which is about the average value of the Fe concentrations in the north (0.83 nmol L^{-1}).

Northern sites – The concentrations are highly variable throughout the period of the survey. For example, at station M3, total Al concentrations varied from 3.28 nmol L^{-1} (15494#2) down to 0.47 nmol L^{-1} (15517#2) whilst total iron varied from 1.74 nmol L^{-1} down to 0.25 nmol L^{-1} at the same stations. Another interesting feature is the difference between M8E and M8W stations: the main differences are noted in Fe (1.41 nmol L^{-1} at M8W versus 0.81 nmol L^{-1} at M8E). On average, concentrations of both trace metals in seawater are greater in the north than in the south, by at least a factor 3.

Southern sites – Although the southern sites are highly variable too in terms of concentrations, the trace metal content in seawater and in particles is much lower on average. For example, the lowest concentrations of Fe (0.15 nmol L^{-1}) are found in station M6 (15511#1) and M2 (15503#2) at the beginning of the survey.

In general, differences between the northern and southern sites are clearly visible in refractory and total concentrations of Al and Fe. The southern sites appear to be less concentrated in Al than the northern sites (6 times less) confirming that these sites are not under a lithogenic island influence.

Station #	SPM µg L^{-1}	POC µmol L^{-1}	Ref-Al nmol L^{-1}	Total Al nmol L^{-1}	Total Al mg g^{-1}	Ref-Fe nmol L^{-1}	Total Fe nmol L^{-1}	Total Fe mg g^{-1}
15494#2 M3	89.9	0.86	3.23	3.28	0.98	1.74	1.74	1.08
15499#2 M3	12.8	0.19	2.47	2.56	5.40	1.37	1.38	6.02
15503#2 M2	30.3	0.30	0.20	0.21	0.19	0.15	0.15	0.28
15511#1 M6	33.5	0.26	0.27	0.29	0.23	0.29	0.29	0.48
15517#2 M3	21.7	0.33	0.46	0.47	0.58	0.25	0.25	0.64
15524#1 M7	45.9	0.45	0.68	0.68	0.40	0.38	0.38	0.46
15533#1 M8E	34.4	0.34	1.61	1.66	1.30	0.80	0.81	1.32
15539#2 M8W	90.3	0.89	0.67	0.69	0.21	1.41	1.41	0.87
15543#2 M9	48.3	0.96	1.17	1.20	0.67	0.46	0.46	0.53
15554 M9	7.66	0.64	0.21	0.24	0.85	0.20	0.20	1.46
1556 3/0 M10	12.0	0.28	0.45	0.46	1.03	0.28	0.28	1.30
15573#2 M3	8.23	0.17	0.33	0.34	1.11	0.40	0.41	2.78
15580 M5	15.8	0.41	0.58	0.59	1.01	0.38	0.376	1.33
15591 M3	17.6	0.23	1.93	1.93	2.96	1.50	1.50	4.76
15595 M6	67.8	0.55	0.19	0.23	0.09	0.22	0.23	0.19
15604 M2	51.0	0.47	0.28	0.28	0.15	0.27	0.28	0.31
15620 M3	8.43	0.16	0.47	0.48	1.54	0.38	0.38	2.52
15628 M3	10.9	0.26	0.84	0.85	2.10	0.66	0.66	3.38
15773#3 M5	43.4	0.40	1.10	1.12	0.70	2.68	2.68	3.45
15773#41 M5	25.1	0.53	1.08	1.13	1.21	0.42	0.42	0.93
15775#29 M6	16.5	0.16	0.11	0.12	0.20	0.16	0.16	0.54
15776#1 Cro 75m	8.92	0.04	2.51	2.64	7.99	1.25	1.27	7.95
15776#2 Cro 340m	15.7	0.33	1.49	1.53	2.63	0.80	0.80	2.85
15777#1 BA	26.6	0.34	25.5	25.8	26.2	13.2	13.2	27.7
Average North	32.0	0.38	1.2	1.22	1.60	0.83	0.86	2.29
Average South	39.8	0.35	0.21	0.23	0.17	0.22	0.22	0.36
Baie Américaine	26.6	0.34	25.5	25.8	26.2	13.2	13.2	27.7

Table IV - 3: Detailed table of the concentrations of Ref-Me and total Me at all sites with SPM and POC concentrations.

It is also possible at this stage to establish some relationship between SPM or POC concentrations with total trace metal concentrations in the two main regions studied. This is illustrated on Figure IV - 5.

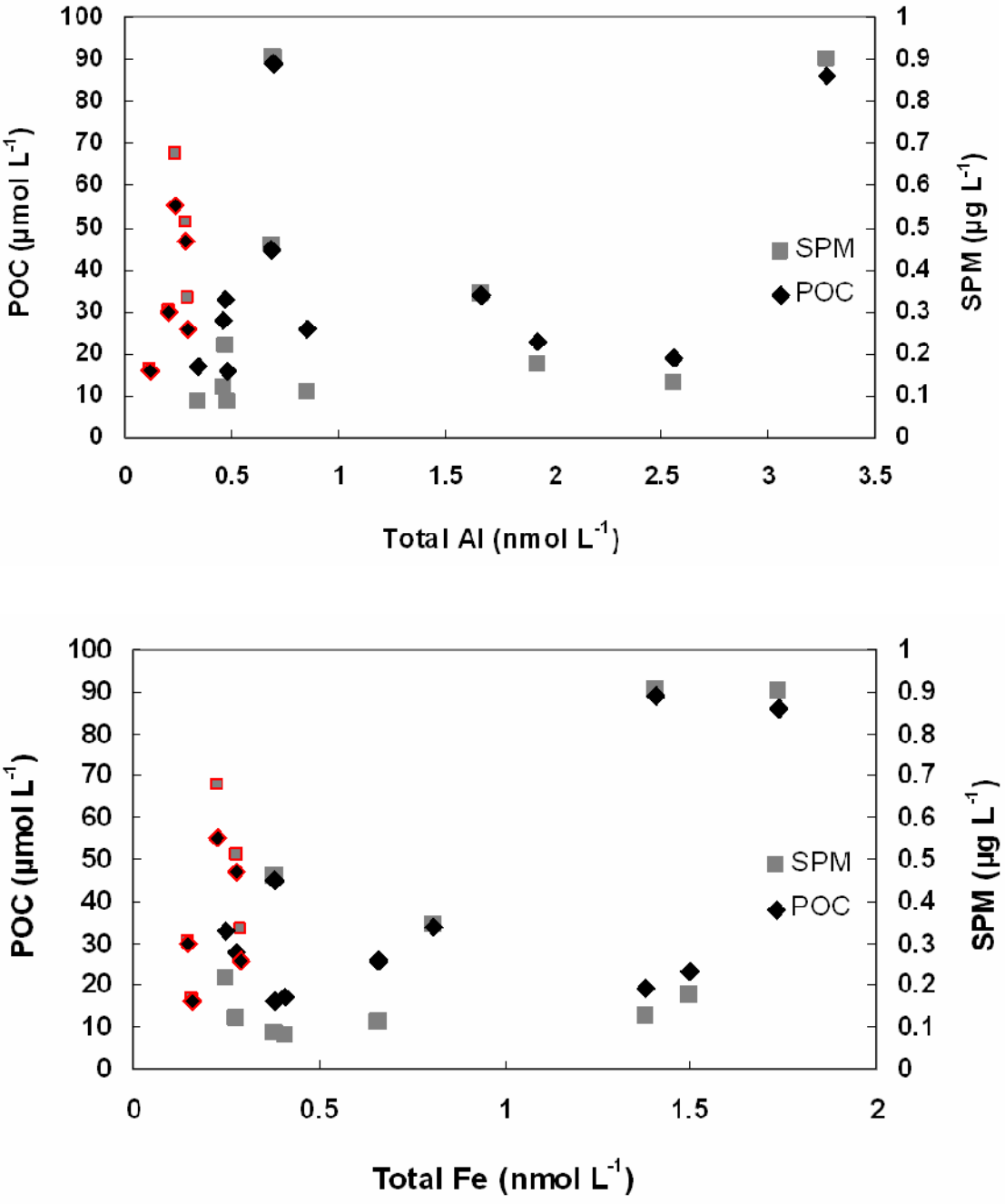

Figure IV - 5: Total Al and Fe versus POC (diamonds) and SPM (circles) concentrations.
Data points for southern sites have a red colour.

The difference between the northern sites and the southern sites appears clearly, in terms of concentrations, however, no correlation can be established between the concentrations of Al with POC or Fe with POC.

Similar average values for POC concentrations are found across the 3 regions studied, ranging from 0.34 to 0.38 whereas BA has much greater concentrations of Al and Fe. These low POC concentrations support the observation noticed and developed in Chapter Three, where a small phytoplankton community was observed at close proximity of the islands, despite a high concentration of DFe. This could be explained by the turbid waters due to suspended sedimentary material which could diminish the light availability in this area. Another explanation is that tidal and mean flows across the shallow topography may lead to enhanced mixing at the base of the mixed layer, resulting in mixed layers deeper than 150m (Venables et al., 2007).

The variability in acid leachable Fe and Al concentrations reveals the importance of biological processes during SPM formation. However, it appears clearly that there is a net difference between the northern and southern sites in terms of particle composition, the particles found in the north being enriched in Al and Fe.

In the following sections, this data set will be first compared with published results. Then, SPM images will be also used to examine the biogenic component of particles before using the molar ratio of Fe to Al to determine the relative importance of lithogenic material in comparison with the average upper continental basalt ratio.

2.4 Comparison with literature

The paucity of other data in the literature makes the comparison of the concentrations of Al and Fe obtained in this study difficult to make to a great extent. Studies conducted in the Southern Ocean are scarce and were mainly focused on the small (>0.2-0.4 μm) particulate metal fraction (e.g. Coale et al., 2005). However, a recent study by Lam et al. (2006) reported some results of the large fraction (>53 μm) in the Southern Ocean. All these studies are reported in Table IV - 4, including data from studies conducted in the Pacific (Landing and Bruland, 1987), Sargasso Sea (Sherrell and Boyle, 1992), Gulf of Maine and Labrador sea (Weinstein and Moran, 2004), in the Atlantic Ocean (Bishop et al., 1977; Bishop et Fleisher, 1987) and off the coast of California (Fitzwater et al., 2003).

Data reported prior to 1975 are not considered, due to the lack of trace metal clean sampling procedures and hence possible contamination.

Overall, both trace elements considered in this study are within the range of published data in the Southern Ocean (e.g. Lam et al., 2006). The highest values of total Fe obtained near Crozet are similar to the ones reported by Grotti et al. (2001) in Antactic coastal waters. Then values in Al and Fe found at BA station are greater than the results published for the open Southern Ocean, confirming a local island source of trace metals. PAl concentrations are in the same range of the concentrations observed by Dehairs et al. (1992) within the Polar Front Zone which provides the most convincing evidence of terrestrial input within this zone.

Location	Particle size *µm*	Depth *m*	SPM *mg L-1*	Total Al *nmol L-1*	Total Fe nmol L-1	HAc-Al *nmol L-1*	HAc-Fe *nmol L-1*	Reference
Southern Ocean: Pacific sector, 47°S-61°S	0.2	15			0.9			Tovar Sanchez et al., 2003
Pacific: 120-160°W; 20°S 40°N	0.3	15-4900	0.007-0.39	0.89-260	0.1-61.5	0.01-4.91	0.01-10.8	Landing and Bruland, 1987
California caostal waters	0.4	surface	0.24-4.31	1.0-2323	0.2-359	0.1-24	0.02-23.1	Fitzwater et al., 2003
Antarctic coastal water Ross Sea	0.4	2-380	0.15-4.31		1.1-58.5			Grotti et al., 2001
Polar front zone: 42-55°S 141.5-143°E	0.4	20-200		1.2-100				Cardinal et al., 2001
Polar Front zone: 59-68°S - 170°W	0.4	0.-500		0.05-0.47	0.02-0.24	0.01-0.17	0.006-0.13	Coale et al., 2005
Southern Ocean: 46.24°S-178°E	20	25		1.10-2.40	0.20-0.33			Frew et al., 2006
Sargasso sea	1.0-53	0-100		1.2-6.7	0.32			Sherrell and Boyle, 1992
Labrador Sea	53	0-250		0.1-1.5	0.1-1.2			Weinstein and Moran, 2004
Gulf of Maine	53	0-300	0.05-0.6	0.1-50	0.1-32			Weinstein and Moran, 2004
Equatorial Atlantic Ocean					1.9-3.8			Bishop and Fleisher, 1987; Bishop et al., 1977;
California coast: 36.36°N 122°W	53	0-80		60-850				Cullen and Sherrell, 1999
Subartic Pacific	53	12-900			0.005-2.476			Lam et al., 2006
Southern Ocean: 55°S 172°W	53				0.08-4			Lam et al., 2006
Southern Ocean: Crozet Islands	53	30-340	0.008-0.090	0.11-25.5	0.15-13.2	0.0002-0.03	0.0008-0.022	***This study***

Table IV - 4: Metal concentrations in suspended particulate matter from surface and shelf waters in diverse regions of the world ocean. Note that sampling depth and filter pore size may vary between studies.

3 Scanning Electron Microscopy (SEM) on selected samples

Three samples were selected for SEM imaging. Stations M3 (15517#2), M6 (15595) and Baie Américaine (15777) were chosen in order to investigate differences in particle composition between different zones around Crozet. The images are given in Figure IV - 6.

Different factors have an influence the composition of the phytoplankton community. For example, light, iron and silicate availability control the growth rates (e.g. Moore et al., 2007a) whilst the grazing pressure controls the mortality of the community (Smetacek et al., 2004). Depending on these factors, the phytoplankton species will adopt different strategies. For example, small cells tend develop under iron stress conditions but this has the consequence to put them under a higher grazing pressure. As a defense mechanism, they will tend to form long compact chains (Timmermans et al., 2004). By comparison, during iron replete conditions, picophytoplankton will shift towards nano and microplankton assemblages, leading potentially to export (Hoffmann et al., 2006).

The first plate (I) illustrates the particles at station M6 (15595). Small centric diatoms were observed, as well as another diatom, *Eucampia Antarctica*. M6 station had low dissolved iron concentrations (Chapter Three) that are probably limiting primary production as this station has been identified as a true HNLC site. This could explain the presence of small diatoms frustules that are typical of Fe stressed conditions (e.g. Timmermans et al., 2001).

The second plate corresponds to M3 (15517). The number of frustules is greater than the previous one, corresponding to a high export measured (See section 5 of this chapter). Various species can be found, such as the highly silicified *Eucampia Antarctica* (bottom left corner of Figure IV - 6, II-c), centric diatoms and *Chaetoceros Rostratus* (Figure IV - 6, II-b), this assemblage of phytoplankton being consistent with a recent iron supply as observed by Lam et al. (2006).

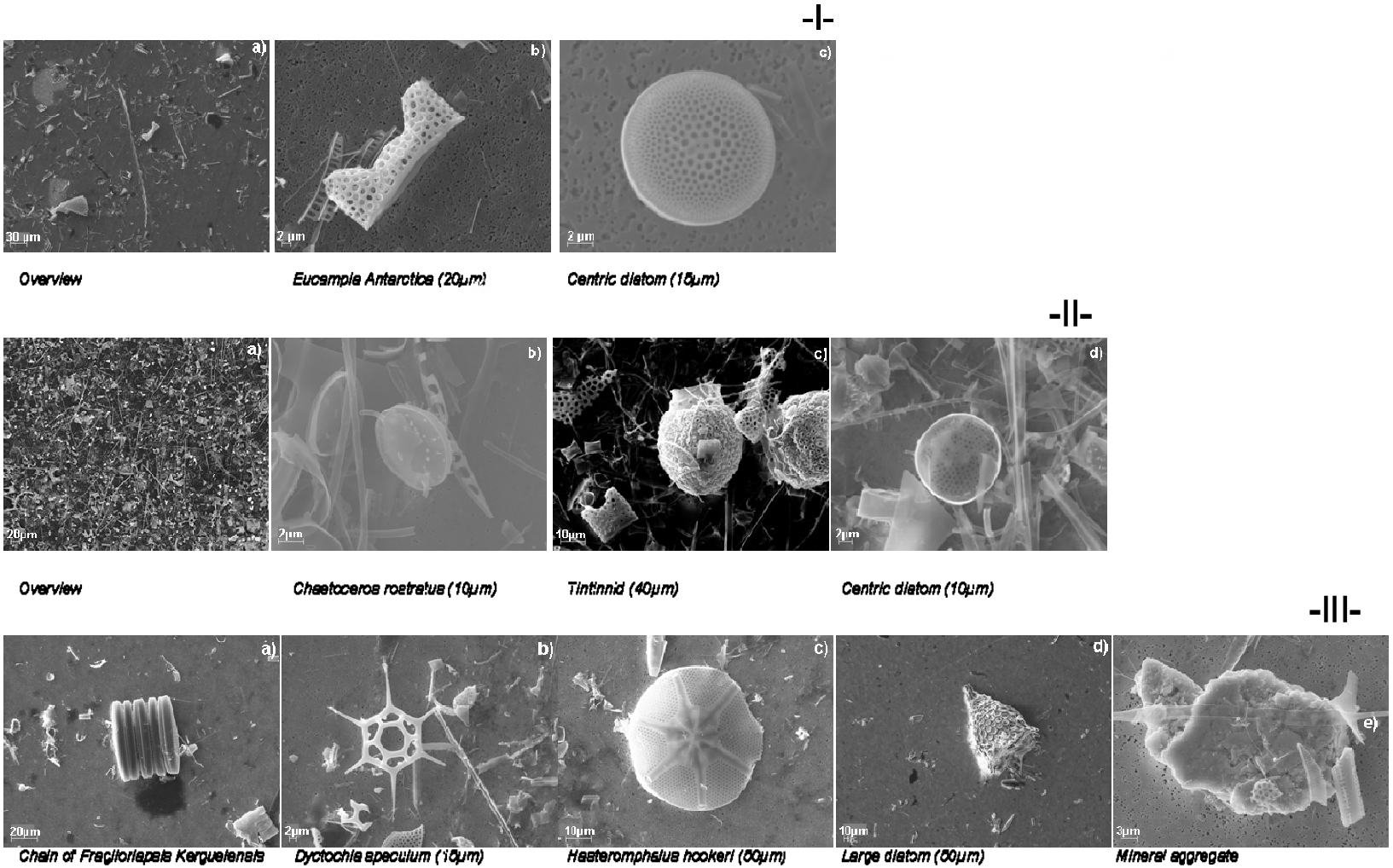

Figure IV - 6: SEM images of three selected samples: I- Station M6 (15595); II – Station M3 (15517) and III Baie Américaine (15777).

Finally, the last plate of images (Figure IV - 6, III) was obtained from a sample (30m depth) taken in Baie Américaine. The assemblage was composed of various species, including very large diatoms (>50µm), chains of pennate diatoms (*Fragiloriapsis Kerguelensis*), typical of an iron rich environment. The most interesting feature is one mineral particle found on the filter, (Figure IV - 6, III-e), that appeared to be composed mainly of Fe following its chemical identification by Extended X-Ray Absorption Fine Structure (EXAFS), which explains the high concentration of particulate iron found at this station. The presence of such a particle is not surprising given the volcanic nature of the Crozet Islands. Such particles, referred as "hot spots", were observed as well in the Southern Ocean by Lam et al. (2006).

4 Correlation between Al and Fe

At this stage, it is useful to consider the particulate trace metal partitioning, by studying the Fe/Al molar ratios. These ratios may indicate the relative importance of lithogenic material in a sample in comparison to the average basalt crust ratio of the Crozet Islands. Generally high ratios in suspended particles are expected because of the scavenging of dissolved trace elements on the outer surface of the frustules (Van Cappellen and Qiu, 1997a, 1997b). Using Fe and Al total concentrations, Fe/Al molar ratios were calculated and are reported for the northern and southern regions as well as in Baie Américaine in Table IV – 5.

Overall, the total particulate Fe/Al ratios were variable throughout the sampling period. On average, the southern sites have a higher ratio than the northern sites. At Baie Américaine stations the Fe/Al ratios approached the average lower estimate of the basalt crust ratio of 0.51 (Gunn et al., 1970; Marsh et al., 2007). Fe/Al ratios were lower in the Southern sites than in the Northern sites, supporting once again that the northern sites are under the influence of the islands. The high Fe/Al molar ratios in this area, up to 2.10 (Stn 15539#2, M8W) can be explained by a high diatom production transferring particulate matter out of the mixed layer which is reflected here by the POC concentration (0.89 µmol L^{-1}).

Also, the dissolution of lithogenic material out of the islands to North can stimulate the production of phytoplankton, which can then causes the removal of lithogenically derived iron from the mixed layer.

The basalt abundance molar ratio of 0.51 was used in a similar approach developed by Frew et al. (2006) for the calculation of the lithogenic component by assuming that all particulate aluminium derived from lithogenic material. The lithogenic component was calculated bymultiplying the total Aluminium concentrations by the basalt molar abundance ratio (Fe/Al) of 0.51. It is also possible to calculate the biogenic fraction, defined as the difference between the total concentration and the lithogenic fraction. It is also possible to calculate the biogenic fraction, defined as the difference between the total concentration and the lithogenic fraction. These results are reported in Table IV - 5.

These data indicate that a significant fraction of iron is of lithogenic origin, reaching up to 96% in the north (Station 15517#2 M3). The samples taken in the vicinity of Baie Américaine had a even greater percentage of lithogenic iron too. Interestingly, at M8W, the origin of iron seems mainly to be biogenic (75%, Table IV-5), suggesting that the bloom observed there was probably due to active recycling at this site. On average, the lithogenic particulate iron pool represents 68% of the total particulate iron pool which is in agreement with Frew et al. (2006), the lithogenic fraction being reported by Strzepek et al. (2005) as mainly lithogenic above 20 μm.

The biogenic fraction calculated by using the Fe/Al average basalt ratio is one order of magnitude greater than the HAc-Fe concentrations determined independently after the 1st leach. This result suggests that a significant fraction of the particles were available to the phytoplankton and that the HAc-Fe content may not reflect the sum of all potentially bioavailable iron.

Station #	Total Al nmol L^{-1}	Total Fe nmol L^{-1}	Fe/Al molar ratio	Lithogenic Fe nmol L^{-1}	Biogenic Fe nmol L^{-1}	% Lithogenic Fe	Enrichement factor
15494#2 M3	3.28	1.74	0.53	1.67	0.07	96	1.04
15499#2 M3	2.56	1.38	0.54	1.31	0.07	95	1.06
15503#2 M2	0.21	0.15	0.71	0.11	0.04	71	1.40
15511#1 M6	0.29	0.29	1.00	0.15	0.14	51	1.96
15517#2 M3	0.47	0.25	0.53	0.24	0.01	96	1.04
15524#1 M7	0.68	0.38	0.56	0.35	0.03	91	1.10
15533#1 M8E	1.66	0.81	0.49	0.85	-0.04	105	0.96
15539#2 M8W	0.69	1.41	2.04	0.35	1.06	25	4.01
1556 3/0 M10	0.46	0.28	0.61	0.23	0.05	84	1.19
15573#2 M3	0.34	0.41	1.21	0.17	0.24	42	2.36
15580 M5	0.59	0.376	0.64	0.30	0.08	80	1.25
15591 M3	1.93	1.5	0.78	0.98	0.52	66	1.52
15595 M6	0.23	0.23	1.00	0.12	0.11	51	1.96
15604 M2	0.28	0.28	1.00	0.14	0.14	51	1.96
15620 M3	0.48	0.38	0.79	0.24	0.14	64	1.55
15628 M3	0.85	0.66	0.78	0.43	0.23	66	1.52
15773#3 M5	1.12	2.68	2.39	0.57	2.11	21	4.69
15775#29 M6	0.12	0.16	1.33	0.06	0.10	38	2.61
15776#1 Cro 75m	2.64	1.27	0.48	1.35	-0.08	106	0.94
15776#2 Cro 340m	1.53	0.8	0.52	0.78	0.02	98	1.03
15777#1 BA	25.8	13.2	0.51	13.20	0.00	100	1.00
Average North	1.22	0.84	0.81	0.62	0.22	74	1.58
Average South	0.23	0.22	1.01	0.12	0.1	53	1.98
Baie Américaine	25.8	13.2	0.51	13.2	0.04	100	1

Table IV - 5: Total aluminium and iron concentrations and derived lithogenic and biogenic iron concentrations derived from the crustal ratio of Fe/Al as well as enrichment factors.

It is also possible to calculate the enrichment factor (Jickells et al., 1992), defined as:

$$EF_{Me} = [Me/Al]_{sample}/[Me/Al]_{basalt\ ratio}$$

The results of the averaged enrichment factors in the Northern sites and Southern sites, as well as at the Baie Américaine station are presented in Table IV – 5.

Baie Américaine concentrations are close to the basalt ratio as the enrichment factor equals to 1.

High Fe/Al ratio observed in particular in the south might indicate an external episodic input of particulate iron such as an atmospheric input (e.g. event CRO R 6 on the 24/11/2004 of 50 nmol L^{-1} of Fe, see Appendix Three).

Finally the major differences from both sites reside in the fact that the north is far more enriched in Fe than the south, as shown in Figure IV - 7:

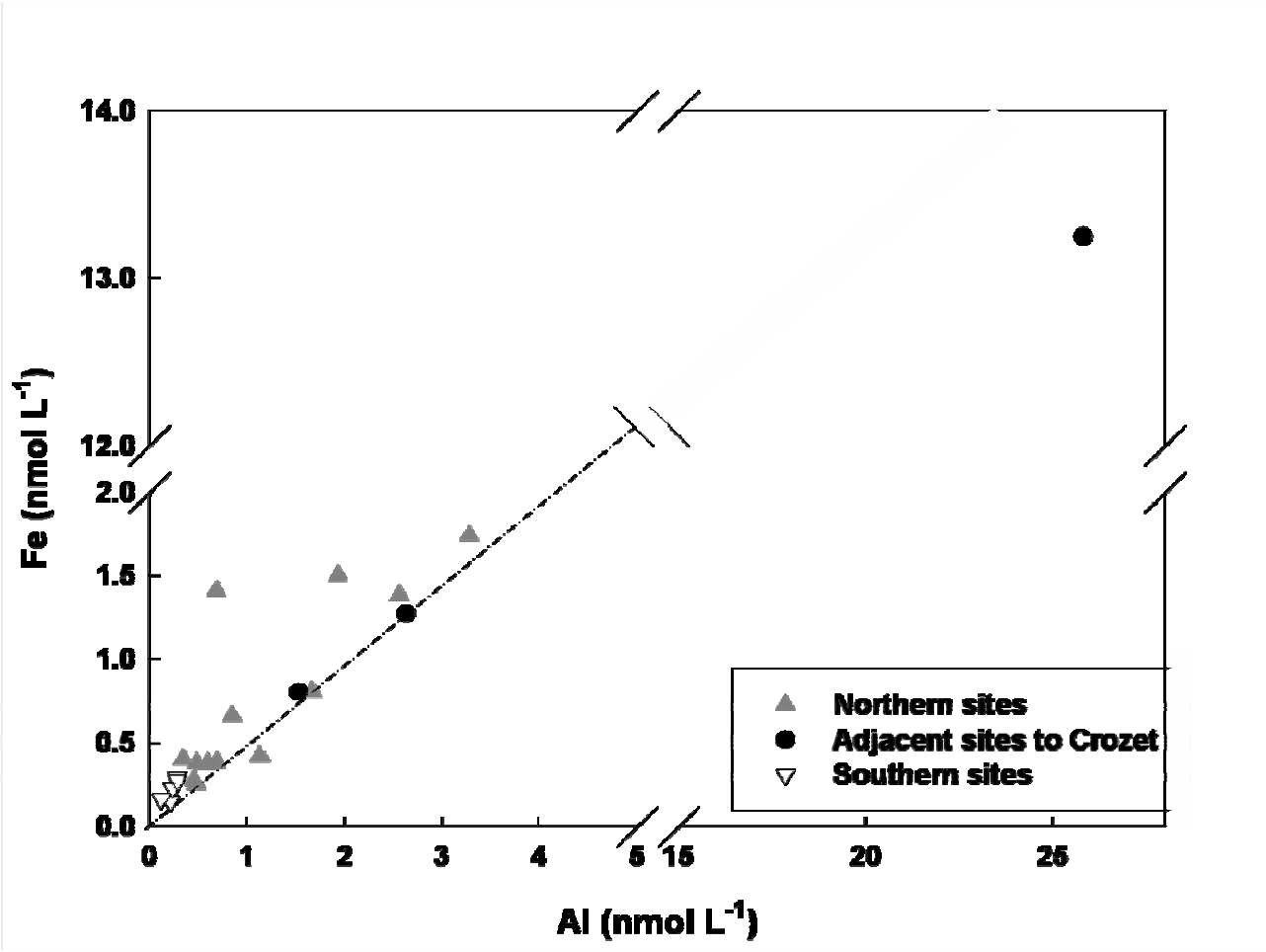

Figure IV - 7: Fe versus Al concentrations at both sites.
The basalt ratio is symbolized by the light black dashed line.

This figure infers that Fe is probably associated with aluminum inputs and supports the view that excess Fe (from the island system) has been delivered into this area, as thought previously when high concentrations of these metals were noticed in the particles.

5 Conclusions

A two step leaching technique was used in this work to assess the distribution of "labile" trace metals Al and Fe around the Crozet Islands in order to test the hypothesis of enhanced POC concentrations induced by enhanced bioactive Fe.

The content of SPM as well as the POC concentrations was highly variable during the survey, revealing the high complexity of processes occurring in this region. Hydrodynamics can allow the intrusion of HNLC water masses in the north, whilst variable atmospheric inputs can influence the distribution of Fe in the south. However, it is possible to distinguish some major trends.

Acid leachable fraction ranges from 0.02% to nearly 1% for Fe, typical of the large particles in the ocean (Wells et al., 1991). The largest concentration of total aluminium and iron were found at close proximity of the islands, reaching levels up to 150 times higher than the other sites, thus supporting the hypothesis of an island source. In the fertilized sites, the relationship etween Fe, Al and POC concentrations is clearly visible.

Fe/Al molar ratios gave the evidence that the northern sites are more enriched in these trace elements than the southern sites. Moreover the Fe/Al ratio calculated at Baie Américaine is similar to the basalt crustal ratio of the Crozet Islands, which confirms the hypothesis of the island source.

The next step is to calculate the vertical fluxes of these elements, by linking Fe with POC export using ^{234}Th derived export data. It will be then possible to establish an iron budget with the dissolved data presented in Chapter Three and the particulate data. This is the objective of the next chapter.

CHAPTER V:

BUILDING AN IRON BUDGET

In the two previous chapters, the concentrations of dissolved (<0.2µm) and particulate (>53µm) iron have been investigated. It is possible to link these two different pools in combination with atmospheric inputs in order to establish a budget of the sources and sinks of iron for waters surrounding the Crozet Islands. Firstly, using radium isotopes and dissolved iron data, lateral and vertical mixing inputs to the photic zone will be presented. Then, atmospheric inputs deduced from calcium and silicon concentrations as well as the downward flux of particulate iron in large particles will be calculated using ^{234}Th based C flux data and C/Fe molar ratios. Finally, all these fluxes will be considered in order to identify the main mechanisms that deliver iron to the waters surrounding the Crozet Islands.

1 Using radium mixing estimates in combination with dissolved iron data to estimate vertical and lateral advective inputs

In terms of lateral dispersion and vertical mixing, the use of natural radio-tracers presents a powerful tool to track a possible iron island input and its dispersion and mixing with adjacent waters. Short-lived radium isotopes have been used for this purpose

in collaboration with Matt Charette (WHOI) (Charette et al., 2007). Some essential information on the use of radium isotopes will be first introduced before presenting the calculations leading to the quantification of lateral and vertical inputs.

1.1 Background

The use of ratios of naturally occurring radium isotopes (respective half-life times: ^{226}Ra–$t_{1/2}$ = 1600 years, ^{228}Ra–$t_{1/2}$ = 5.75 years, ^{224}Ra–$t_{1/2}$ = 3.66 days, and ^{223}Ra–$t_{1/2}$ = 11.4 days) and their concentration gradients can provide estimates of the rates of their dispersion as they mix away from their source (Moore et al., 1980; Key et al., 1985; Moore et al., 1995). The Ra isotopes are produced by decay of particle bound thorium isotopes in sediments. Therefore, radium isotopes are continually added at ocean boundaries from sediments by both advective and diffusive processes, their source being located along the coastline and at any sediment water interface (Charette et al., 2007). Moereover, the only processes affecting their distribution are mixing and decay. Thus, radium isotopes, with their shelf-water source and wide-ranging half-lives, are ideally suited for evaluating the inputs of iron from islands into surface waters. In particular, the two short lived radium isotopes, ^{223}Ra and ^{224}Ra, are well suited for horizontal mixing studies, as their half-lives are short enough relative to seasonal changes in their input functions to satisfy the constant boundary condition assumption. This means that the variation of their activity over time depends only on the distance, as their inputs at the coastline are in steady-state (Moore, 2000). Variations of activity of these two short-lived isotopes follow this equation:

$$A_x = A_0 \exp\left[-x\sqrt{\frac{\lambda}{Kh}}\right] \qquad (1)$$

, where A_x is the activity at a distance x from the shore, A_0 is the activity at distance 0 from the coast, λ is the decay constant and Kh is the horizontal eddy diffusion coefficient.

^{228}Ra is also used for the study of the less rapid vertical mixing processes across the thermocline because the only processes controlling its distribution are vertical mixing and decay (Charette et al., 2007).

In this work, vertical ^{228}Ra and dissolved iron profiles at station M3 (Station 15622) about 55 km to the north of the islands and a surface water iron and ^{223}Ra and ^{224}Ra transect from Île de la Possession (referred as the "Baie Américaine" transect) towards the M3 station have been used to respectively estimate vertical and horizontal mixing rates.

1.2 Vertical transport of DFe to surface water

Details of radium sampling and analysis are not presented here as this work was performed by others. A full description can be found in Charette et al. (2007).

A simple one dimensional diffusive model of the vertical profile of ^{228}Ra at M3 (Station 15622) along with an average dissolved Fe gradient across the same depth interval was used to determine two mixing scenarios: a slow mixing regime between 1000m and 300m depth (Kz = 1.5 cm^2 s^{-1}) and a fast mixing regime between 5m and 300m depth (Kz = 11 cm^2 s^{-1}) using the following equation (for details, see Charette et al., 2007):

$$A_z = A_0 \exp\left[-z\sqrt{\frac{\lambda}{Kz}}\right] \qquad (2)$$

,where A_z is the activity at a depth z from the surface, A_0 is the activity at the surface, λ is the decay constant and Kz is the vertical eddy diffusion coefficient.

Dissolved iron data together with ^{228}Ra data are shown on Figure V - 1. The maximum contribution of entrainment of deep-water iron during turbulent vertical mixing is then obtained using the upper estimate of the mixing rate coefficient K_z (**11 cm^2 s^{-1}**) over the top three hundred meters.

The corresponding DFe gradient between these depths was calculated using 0.15 nmol L^{-1} at surface depth and 0.34 nmol L^{-1} at 300m depth, leading to a gradient of 0.00064 nmol L^{-1} m^{-1} or **0.64 nmol m^{-3} m^{-1}**.

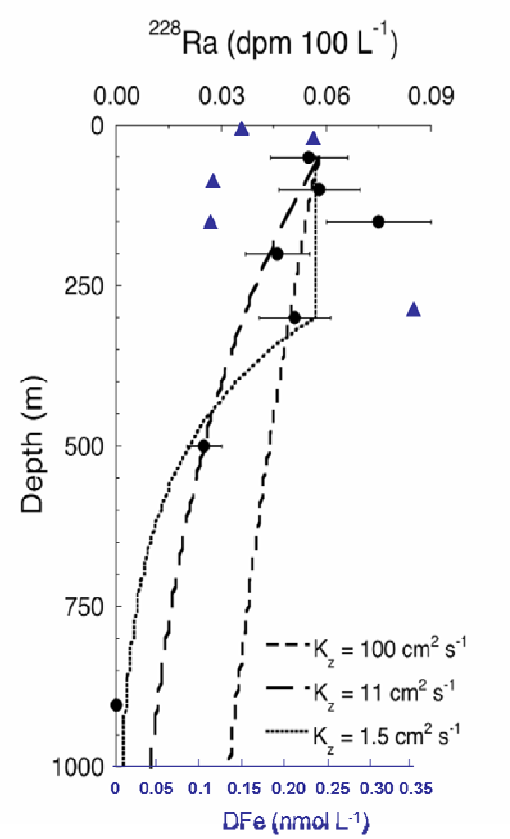

Figure V - 1: Model estimates of *Kz* fitted to the ^{228}Ra (black circles) and total dissolved iron (blue triangles) profiles at station M3 (adapted from Charette et al., 2007).

Combining the maximum value of the vertical diffusion coefficient K_z with this dissolved iron gradient (Equation 3) leads to a vertical input of dissolved iron DFe_v of:

$$\mathbf{DFe_{vmax}} = DFe_{grad} \,.\, K_z \qquad (3)$$

, where DFe_{grad} is the vertical dissolved iron gradient (0.64 nmol m^{-3} m^{-1}), K_z is the vertical diffusion coefficient (0.11 m^2 s^{-1}).

$$\mathbf{DFe_{vmax}} = 0.64 \,.\, 0.11.10^{-4} \,.\, 3600 \,.\, 24 = \mathbf{61\ nmol\ m^{-2}\ d^{-1}}$$

This estimate is the maximum vertical mixing rate of dissolved iron. Using the smaller estimate of the mixing rate coefficient, this flux equals to:

$$\mathbf{DFe_{vmin}} = 0.64 \,.\, 0.15.10^{-5} \,.\, 3600 \,.\, 24 = \mathbf{8\ nmol\ m^{-2}\ d^{-1}}$$

Blain et al (2007, *in press*) reported a Kz of 3.3 cm^2 s^{-1} over the Kerguelen Plateau, leading to a vertical input of 31 nmol m^{-2} d^{-1}. Few other studies give an estimation of the vertical mixing in the Southern Ocean, and they all calculated a smaller DFe vertical supply. For example, during FeCycle, Boyd et al. (2005) estimated the vertical flux to be 3 nmol m^{-2} d^{-1} and during SOIREE, the maximum vertical supply was calculated to be 8.3 nmol m^{-2} d^{-1}. The vertical input estimated in this study is higher than all values reported in the literature, suggesting that the vertical iron flux from deep waters around the Crozet plateau could contribute to the natural fertilization in the surface waters.

1.3 Horizontal advective transport of iron

Charette et al. (2007) used the short lived Radium isotopes ^{223}Ra and ^{224}Ra on the transect from Baie Américaine (Stations 567, 568 and 569) to provide an upper estimate of the horizontal flux of dissolved iron DFe_h. Details of Ra sampling and analysis can be found in Charette et al. (2007).

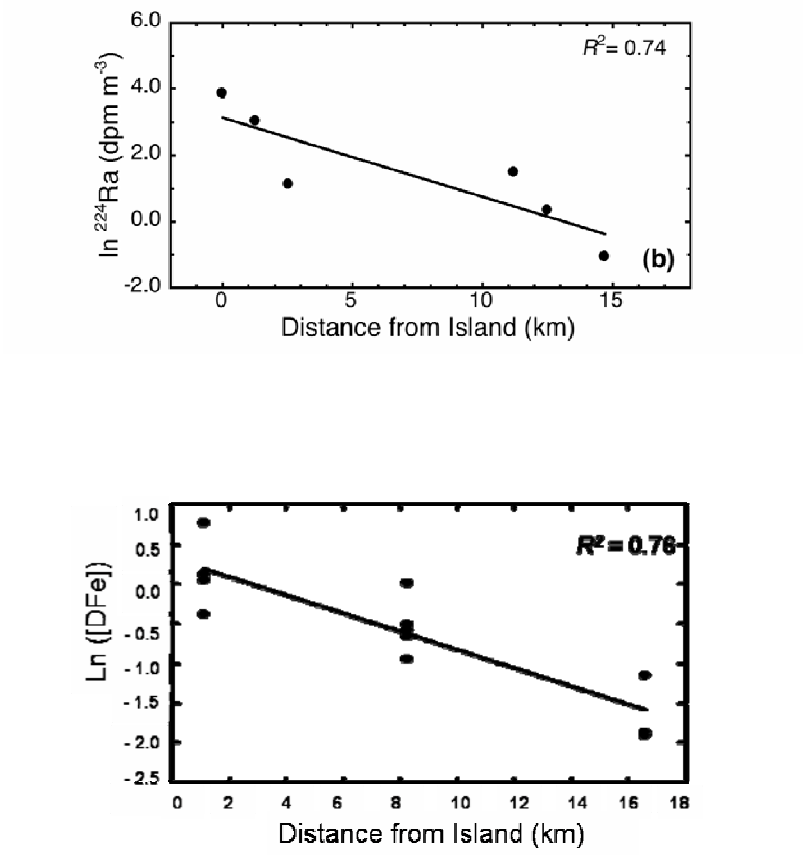

Figure V - 2: Off-island ^{224}Ra transect with ln transformed ^{224}Ra with slope used to estimate *Kh* (top) and off-island corresponding DFe transect in the upper 50m (Adapted from Charette et al., 2007).

The ^{224}Ra gradient was used to provide the upper estimate of the horizontal mixing coefficient *Kh* of **39 m^2 s^{-1}** (Equation 1), and the gradient of DFe in surface (upper 50m) presented in Chapter Three was equal to **0.07 nmol L^{-1} km^{-1}**. Both of these gradients are shown in Figure V-2.

Using ^{223}Ra, the lower estimate of horizontal diffusion coefficient K_h was equal to 6.6 m^{-2} s^{-1}.

Combining the maximum and minimum estimates of the horizontal diffusion coefficient K_h with the dissolved iron gradient (Equation 4 below), leads to a maximum and minimum horizontal flux of dissolved iron Fe_{hmax} and Fe_{hmin} of:

$$\mathbf{DFe_{hmax}} = DFe_{grad} \,.\, K_h \qquad (4)$$

, where DFe_{grad} is the vertical dissolved iron gradient (0.07 nmol L^{-1} km^{-1}), K_h is the horizontal diffusion coefficient (39 m^2 s^{-1}).

$$\mathbf{Fe_{hmax}} = 0.07 \,.\, 39^* \,.\, 3600 \,.\, 24 = \mathbf{236\ \mu mol\ m^{-2}\ d^{-1}}$$
$$\mathbf{Fe_{hmin}} = 0.07 \,.\, 6.6 \,.\, 3600 \,.\, 24 = \mathbf{40\ \mu mol\ m^{-2}\ d^{-1}}$$

It is now possible to estimate the cumulative effect of this horizontal flux over the fertilized area, if several parameters are assumed.

Firstly, Giret et al. (2002) reported a homogeneous mantle geochemical composition in this zone so it seems reasonable to assume that the two main islands are geochemically representative of the Archipelago and that the offshore gradient will be representative of the islands and shelf system as a whole.

Secondly, the shoreline length is estimated to be 600 km and the bloom area 90 000 km^2 (R. Pollard, *pers. comm.*, Charette et al., 2007). Finally, during winter, mixed layer depth can reach 250m and this horizontal flux can be integrated down to this value, and it is assumed the island released Fe is uniformly mixed into these waters (Figure V-3).

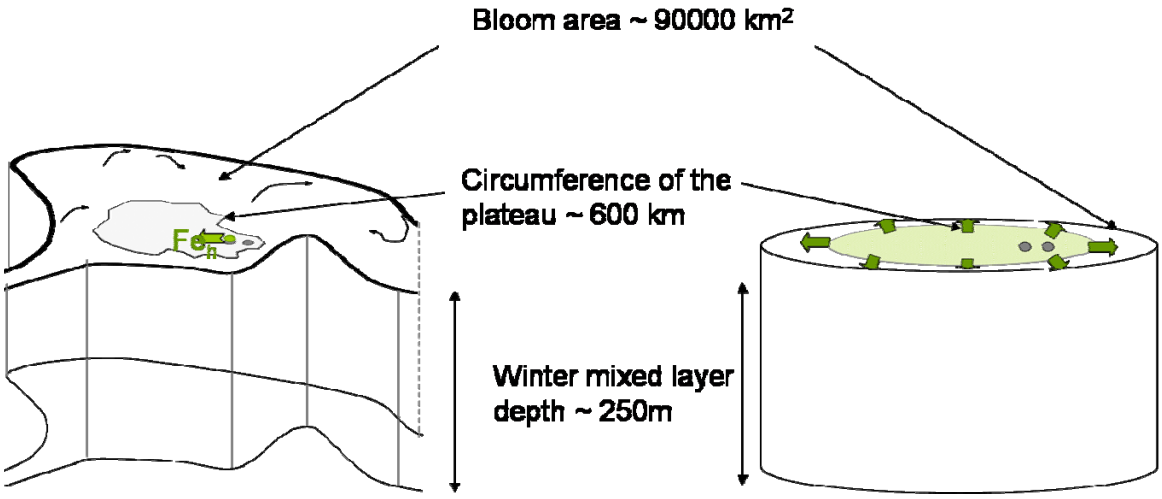

Figure V - 3: Schematic of cumulative effect of the horizontal flux of dissolved iron

The maximum and minimum resulting cumulative effects of this horizontal flux of dissolved iron DFe_{hmax} and DFe_{hmin} are calculated following the equation below:

$$\mathbf{DFe_h} = \frac{Feh.C.Mld}{A} \quad (5)$$

WhereFeh is the horiztonal flux of dissolved iron, C is the circumference of the Plateau, Mld is the winter mixed layer depth, and A is the bloom area. This leads to:

$$\mathbf{DFe_{hmax}} = (236 \,.\, 600\ 10^3 \,.\, 250)/\ (90\ 000\ 10^6) = \mathbf{390\ nmol\ m^{-2}\ d^{-1}}$$

$$\mathbf{DFe_{hmin}} = (40 \,.\, 600\ 10^3 \,.\, 250)/\ (90\ 000\ 10^6) = \mathbf{66\ nmol\ m^{-2}\ d^{-1}}$$

An important point is that the horizontal gradient of DFe is calculated in the upper 50m near the shore therefore does not include the deeper waters or the plateau itself. This DFe gradient could be enhanced further if the whole width of the continental shelf is considered (Luther and Wu, 1997).

2 Atmospheric inputs

Wet and dry deposition fluxes (F) were considered as one of the possible inputs over the Crozet area.

Air parcel back trajectories (Draxler and Rolph, 2003) for all rain and aerosol sampling periods show that air masses had no contact with any land masses apart from Antarctica for at least the 5 days prior to collection, and hence truly remote Southern Ocean air was sampled.

Atmospheric sampling was conducted on the deck above the bridge, the highest point of the ship well forward of ship emission sources. Samples were only collected when wind and ship movements guaranteed no contamination from the ship itself, but the filters were not cleaned for trace metal analysis. Therefore, iron concentrations in dust were derived from atmospheric concentrations of calcium and silicon by Alex Baker and Tim Jickells (UEA) (Planquette et al., 2007).

Rainwater samples (Table 3, Appendix III) were collected for trace metal analysis as described in Spokes et al. (2001). Full details are given in Appendix III (Sections 2.4 and 3.2)

Dry deposition fluxes were calculated by making the assumption that nitrate, excess Ca and silicate are associated with coarse mode aerosol and ammonium with fine mode and using deposition velocities of 2 cm s^{-1} and 0.1 cm s^{-1} respectively for the two modes (Baker et al., 2003).

These two approaches, using calcium and silicon, gave broadly similar results (0.16 and 0.32 g dust m^{-2} yr^{-1} respectively). A dust flux of 0.2 g m^{-2} yr^{-1}, which is the average of the two estimates rounded to one decimal place was therefore used. This dust flux corresponds to a **dry** deposition flux of Fe of **127 µmol m^{-2} yr^{-1}** assuming dust to be composed of 3.5 % Fe (see Section 4.2 of Appendix III for uncertainties).

Wet deposition is a more complicated exercise as it is difficult to estimate a precipitation rate in this oceanic region. No data appears to be available for Crozet. Taljaard and Loom

(1984) quote precipitation estimates for the two nearest islands (Marion and Kerguelen) as 2499 and 1117 mm yr^{-1} respectively so these were averaged and lead to a precipitation rate of 1808 mm yr^{-1}, which can be used for the determination of the wet deposition of Fe (Fw) flux defined as:

$$F_w = C\,P \quad (6)$$

where C is the volume weighted mean concentration of Fe in the rain samples (excluding CRO-R9, which was contaminated) and P is the precipitation rate for the region. The concentration of Fe within the samples ranged from 6 to 288 nmol L^{-1} (Table II, Appendix Three)

C was calculated from the Fe concentration (C_i) and volume (Vi) of each sample (Table II, Appendix Three) using:

$$C = \sum C_i V_i / \sum V_i \quad (7)$$

This translates to a **wet** deposition rate for total Fe of **198 µmol m^{-2} yr^{-1}.**

Combining both wet and dry deposition, the total Fe deposition is 325 µmol m^{-2} yr^{-1} with 61 % of this occurring as wet deposition. This corresponds to a daily flux of **89 nmol m^{-2} d^{-1}**. Southern Ocean dust and iron flux estimates from field campaigns are very limited but the fluxes here are substantially lower than those of Gaiero et al. (2003) from Patagonia and comparable to those seen in the very high rainfall regions of coastal South Island New Zealand (Halstead et al., 2000). Average rainwater iron concentrations from Halstead et al. (2000) and Croot et al. (2005) are similar to those reported here, but recent model estimates from Fan et al. (2006) are lower (~100 µmol m^{-2} yr^{-1}) by a factor of 3, highlighting the complexity of solubility ranges.

3 Estimation of DFe before the main bloom event

To constrain the potential of an island Fe source initiating the austral spring bloom, it is possible to estimate the DFe concentration that would have built up over the Austral winter.

This region under the island effect can be subjected to the three types of inputs that have been considered in this section: atmospheric, vertical and horizontal fluxes. During a

winter period of 100 days, these inputs can accumulate within the mixed layer depth down to 250m. However, when the stratification occurs at the beginning of austral spring, the depth of the mixed layer reduces down to ~100m. Therefore, the addition of these three fluxes multiplied by a winter period of 100 days, and over a pre-bloom mixed layer depth of 100 m, leads to a final concentration of $DFe_{endwinter}$ prior to the bloom of 0.54 nmol L^{-1}:

$$\mathbf{DFe_{endwinter}} = ((F_{atm} + DFe_{v} + DFe_{hmax}) \text{ x day / depth} = \mathbf{0.54\ nmol\ L^{-1}} \quad (8)$$

where F_{atm} is the atmospheric input, DFe_v and DFe_h are the vertical and horizontal inputs of total dissolved iron. Over the winter period when productivity is light limited, the concentration of Fe is therefore estimated to build up by ~0.54 nmol L^{-1} in waters to the north of the islands. As light levels increase gradually over the spring and summer, the bloom can be initiated and progress with this ambient DFe.

Interestingly, Lucas et al. (2007) have estimated a dissolved iron demand required to support the measured satellite derived seasonal estimates of new production rates. To do so, they have used upper in particular mid (0.06 mmol mol^{-1}) and lower (0.03 mmol mol^{-1}) estimates of intracellular DFe:N quotas required to support growth, recognising the variability in this quota as a function of differing taxa, Fe and light availability (Sunda and Huntsman, 1997; Twining et al., 2004). The seasonal DFe deman using DFe:N cell quota of 0.06 mmol mol^{-1} ranged between 0.25 and 0.75 nmol L^{-1}, with an overall minimum DFe demand in the south of 0.19 nmol L^{-1} at the lower quota.

This estimate of 0.54 nmol L^{-1} is therefore lower than, but of the same magnitude as, the demand derived independently by Lucas et al. (2007). Overall this calculation supports the view that DFe fluxes can support phytoplankton new production in the northern bloom region, but only by invoking DFe:N cell quotas of <0.06 mmol mol^{-1} (Lucas et al., 2007), which probably reflects the relative availability of ambient DFe and N.

The present estimates of the possible inputs investigated with the data available show that horizontal advection from the island system is the largest process adding dissolved Fe to the waters surrounding Crozet (Figure V-4), followed by the atmospheric and then the vertical mixing.

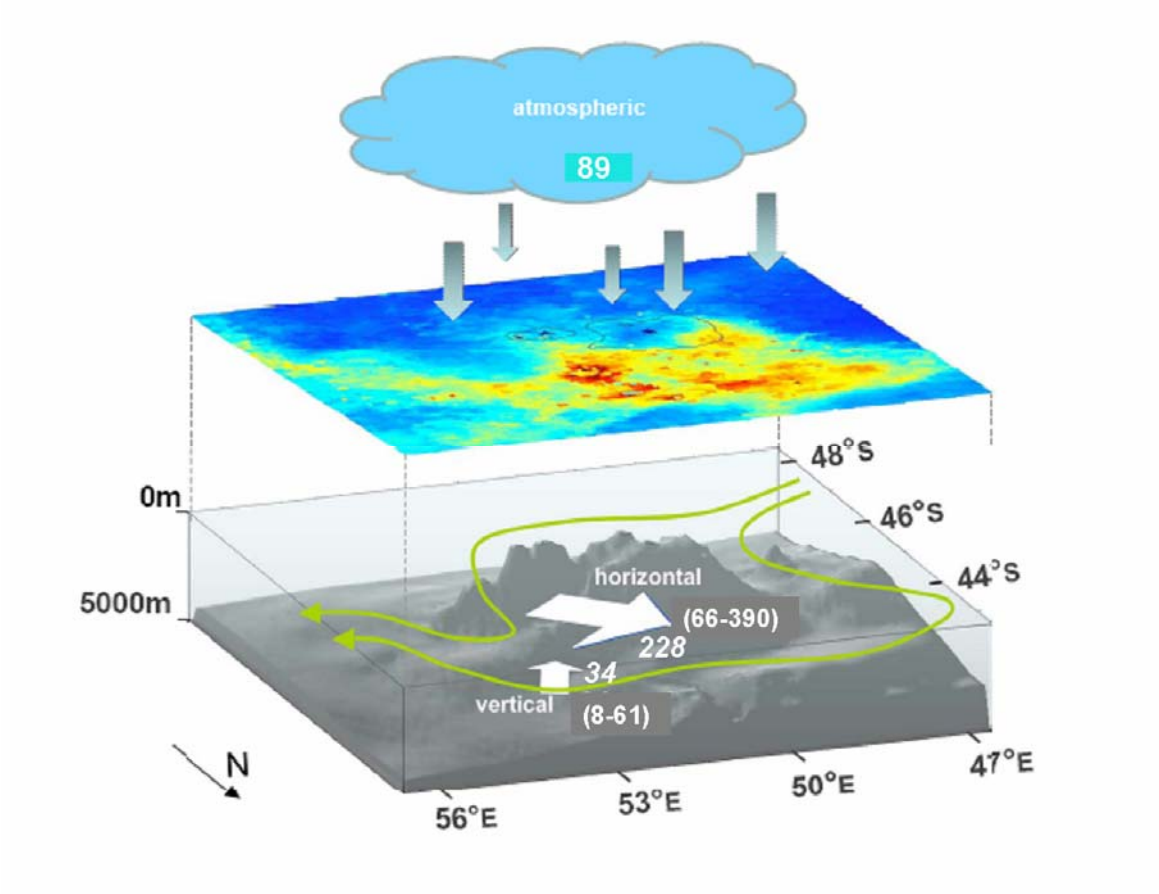

Figure V - 4 Main pathways of DFe in nmol m^{-2} d^{-1} into the bloom area around the Crozet Islands combining the main circulation paths (green lines), topography and a SeaWIFS chlorophyll *a* image for the austral summer 2004–2005.
The average of the fluxes are italicized, and the ranges are in brackets.

However, iron can be liberated from colloids (i.e. 0.2-0.8 µm) or adsorbed onto intermediate particles (0.4 µm - 10 µm). Unfortunately, it was not possible to sample these size ranges and the quantification of this pool remains unknown. It is also possible that colloidal iron may be released from sediments and added to iron advected to the bloom area. These additional sources could increase the iron budget at the end of the winter and will require further investigations. Nonetheless, this is the first estimate of Fe supply to the north of the Crozet islands, and it therefore provides a rationalization and an indication of the relative importance of different sources of Fe in these Sub-Antarctic island systems. Present significant uncertainties include the recycling and removal of Fe and the significance and availability of particulate Fe to the primary producers.

4 Estimation of the vertical fluxes of particulate Fe using ^{234}Th based C fluxes

4.1 Background

The radioactive particle tracer ^{234}Th (Bhat et al. 1969) can be used to estimate the amount of photosynthetically fixed CO_2 exported to the deep ocean as POC (Buesseler et al. 1992). ^{234}Th is the daughter isotope of naturally occurring ^{238}U, which is conservative in seawater and proportional to salinity (Chen et al. 1986).

Unlike ^{238}U, ^{234}Th tends to adhere to particles in the water column. As particles sink through the water column, scavenging Th as they go, a radioactive disequilibrium is formed between ^{238}U and ^{234}Th which can be used to quantify the rate of carbon export from the surface ocean when combined with data on the ratio of POC to particulate ^{234}Th activity. Morris et al. (2007) used the ^{234}Th flux and C:Th ratio to derive the POC flux using the relationship below:

$$POC\ flux = (POC{:}Th) * P \qquad (9)$$

where *POC flux* is the quantity of POC (μmol m^{-2} d^{-1}) falling out the surface ocean, *(POC:Th)* is the ratio of POC to ^{234}Th (μmol dpm^{-1}) on the large size class of particles (>50 μm), and *P* is the integrated ^{234}Th flux (dpm m^{-2} d^{-1}) calculated with the following equation (Morris et al., 2007):

$$P = \int_0^z \lambda(Au - At)dz \qquad (10)$$

, where λ is the decay constant of ^{234}Th (d^{-1}), A_u is the ^{238}U activity (dpm m^{-3}), A_t is the toal ^{234}Th activity (particulate and dissolved) and z is the depth.

It is then possible to calculate the vertical fluxes of particulate metals, like Fe or Al (PMe_v) using the relationship:

$$PMe_v = P*(POC{:}Th)*(Me{:}POC) \qquad (11)$$

where *(Me:POC)* is the molar ratio of Me/POC.

During D285 and D286, Stand Alone Pump Systems (SAPS were deployed simultaneously for Th and for DFe measurements (see Chapter Two). POC measured on the mesh dedicated for Th analysis was assumed to be equal to POC measured on the mesh collecting particles for trace metal analysis. POC concentrations were investigated in samples dedicated for the iron analysis and a comparison has been made (Figure V - 5).

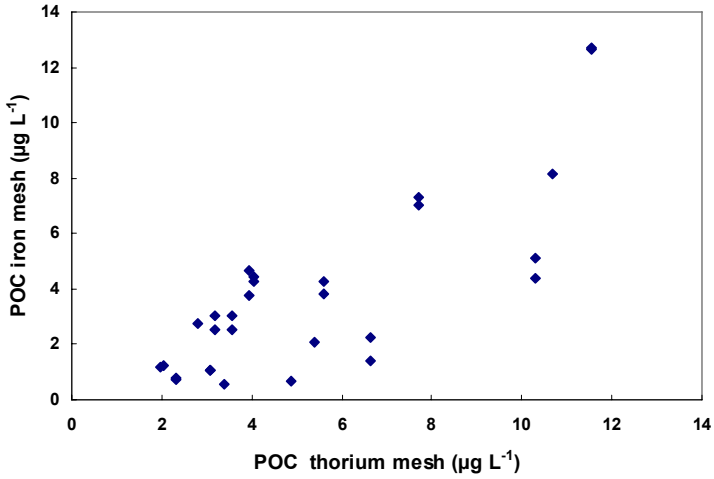

Figure V - 5: POC concentrations in µg L^{-1} obtained from the nylon meshes dedicated to Th and Fe analyses respectively.

For nearly half of the stations, POC concentrations obtained on the trace metal mesh are greater than the concentrations obtained on the Thorium mesh. Theses differences can be explained by the different masses of samples used for the analysis of POC. P. Morris used a typical mass of 5 mg of suspended particulate matter for the determination of POC as opposed to 1 mg due to analytical constraints. Moreover, 4 replicates were run by P. Morris for additional precision against 2 for the metal work. Therefore, choice has been made to use P. Morris's data for POC concentrations.

Vertical fluxes of POC, PMe_v were therefore calculated using equations 10 and 11, C:Th ratios and ^{234}Th fluxes derived for each station calculated by P. Morris (Morris et al., 2007). Results are reported in Table V - 1.

There are no flux data for the D300 cruise as no ^{234}Th sampling was done.

4.2 Results

POC export – Estimates of ^{234}Th derived POC export from the study region during D285 (Stations 15494#2 until 15563) showed a clear north-south gradient (Figure V - 6) with values of ranging from 15 mmol C m^{-2} d^{-1} in the north during the period immediately following the phytoplankton bloom, and 5 mmol C m^{-2} d^{-1} in the south prior to the small southern plankton bloom (Chapter Three) that occurred in late January when the light levels permitted it. During D286 no gradient was seen, once the modest bloom had occurred in the south (Morris et al., 2007). POC export then ranged between 16 and 28 mmol m^{-2} d^{-1} in the North and in the South.

Total particulate Al and Fe export

Values are reported in Table V - 1 for total values of the trace elements analyzed (see Chapter Four). The largest particulate iron export is found at station M3 (15491), reaching 164 µmol m^{-2} d^{-1}, which corresponds to a maximum of PAl_v export of 212 µmol m^{-2} d^{-1}. The lowest value was obtained at station M2 (2.43 µmol m^{-2} d^{-1}). There is a clear difference between the north and the south regions in terms of total particulate aluminium and iron exports (Figure V - 5). On average PFe_v equals 42.9 µmol m^{-2} d^{-1} in the north and 7.86 µmol m^{-2} d^{-1} in the south.

Overall the downward fluxes are quite high (100 times) compared to the vertical fluxes obtained by Frew et al. (2006) in the subantarctic waters southeast of New Zealand. It is important to notice that the PFe fluxes calculated by Frew et al. (2006) were not derived from ^{234}Th data, but were obtained using sediment traps. Their POC export ranged from 2.09 to 2.51 mmol m^{-2} d^{-1} which is at least 10 times lower than the POC exports measured around Crozet. This suggests that the PFe supply must have been more important in the Crozet area than in the region of open ocean subantarctic waters where Frew et al. (2006) conducted their sampling.

Station	^{234}Th flux dpm m^{-2} d^{-1}	C:Th µmol dpm^{-1}	POC mmol m^{-2} d^{-1}	PFe$_v$ µmol m^{-2} d^{-1}	PAl$_v$ µmol m^{-2} d^{-1}
15494#2 M3	1845	8.3	15.3	31.0	58.3
15499#2 M3	813	6	4.88	35.5	65.8
15503#2 M2	740	7.2	5.33	2.63	3.71
15511#1 M6	573	10.1	5.79	6.43	6.37
15517#2 M3	1965	7.1	13.9	10.7	20.1
15524#1 M7	2352	6.1	14.3	12.2	21.8
15533#1 M8E	1619	9.4	15.2	36.1	74.5
15539#2 M8W	2232	6.1	13.6	21.6	10.5
15563 M10	1933	7.2	13.9	13.8	22.8
15573#2 M3	2744	10.4	28.5	67.3	56.7
15591 M3	2550	9.9	25.2	164.6	212
15595 M6	2449	8.2	20.1	8.29	8.47
15604 M2	2734	8.8	24.1	14.1	14.6
15620 M3	2147	7.1	15.2	36.2	46.2
15628 M3	2235	7.5	16.8	42.7	54.5
North	2039	7.74	16.1	42.9	58.5
South	1624	8.58	13.8	7.86	8.28

Table V - 1: ^{234}Th export (dpm m^{-2} d^{-1}), C:Th (µmol dpm^{-1}) and POC export (nmol m^{-2} d^{-1}) from Paul Morris and calculated PFe$_v$ and PAl$_v$ (µmol m^{-2} d^{-1}) at each station during D285 and D286.

To illustrate the difference between the northern and the southern sites, POC, PFe$_v$ and PAl$_v$ are shown in Figure V - 6, where the distinction between D285 and D286 is made. These fluxes represent the total concentration of metals exported out of the mixed layer, as defined in Chapter Four.

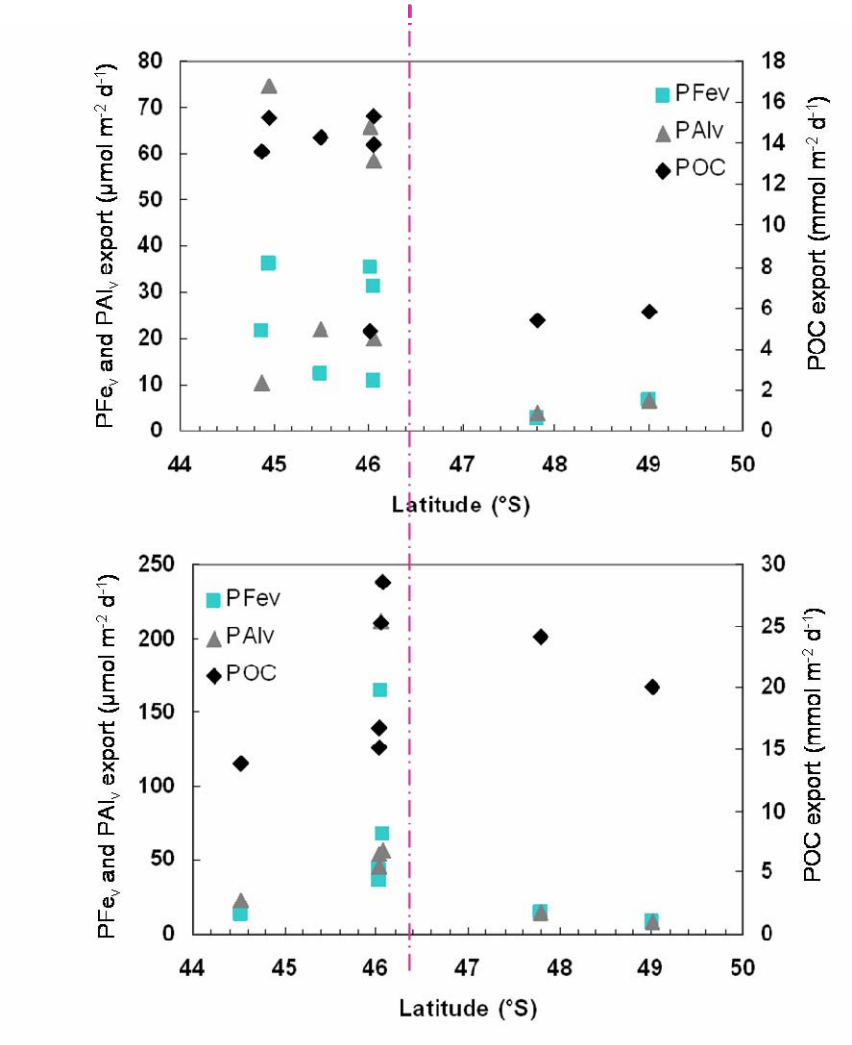

Figure V - 6: Latitudinal variation ^{234}Th derived POC export, PFe_v and PAl_v during D285 (top) and D286 (bottom). The purple long dash dotted line represents the latitude of the Crozet Islands.

In the next section, the labile fraction of the particulate export will be investigated in order to see if there is any relationship between the acetic acid leachable fraction exported and the carbon export. Also, these values, in particular for iron will be of use in the iron budget proposed later.

Labile particulate Al and Fe export

The labile concentrations calculated in Chapter Four may be considered to represent an estimate of the "bioactive" fraction (Landing and Bruland, 1987) of metals sinking out of the mixed layer. Therefore, they can be regarded as a sink of dissolved iron. The results are reported in Table V-2.

The highest export of labile iron occurred at Station M3 (15628) during the secondary bloom in January 2005, reaching up 336 nmol m^{-2} d^{-1}, and fluxes were overall greater in the north than in the south by a factor of 5. During SOIREE, Bowie et al. (2001) reported biogenic iron fluxes ranging between 19 to 47 nmol m^{-2} d^{-1} derived from POC export measured on 70 µm filters. Most of the values obtained in this work fall within this range, except for a few occasions (Stations M3 15449#2; M8E 15533#1 M3 15573#2, M3 15620 and 15628) where export was greater than 100 nmol m^{-2} d^{-1}. These values are consistent with an island source of Fe to the waters north of Crozet.

On average 102 nmol m^{-2} d^{-1} of acid leachable iron was exported in the north, whereas only 28 nmol m^{-2} d^{-1} were exported in the south. Another difference in export is noted for acid leachable aluminium, 0.91 µmol m^{-2} d^{-1} in the north relative to 0.49 µmol m^{-2} d^{-1} on average in the south.

Station	^{234}Th flux dpm m^{-2} d^{-1}	C:Th µmol dpm^{-1}	POC mmol m^{-2} d^{-1}	$LPFe_v$ nmol m^{-2} d^{-1}	$LPAl_v$ µmol m^{-2} d^{-1}
15494#2 M3	1845	8.3	15.3	28.1	0.82
15499#2 M3	813	6	4.88	302	2.27
15503#2 M2	740	7.2	5.33	7.06	0.10
15511#1 M6	573	10.1	5.79	21.4	0.33
15517#2 M3	1965	7.1	13.9	19.3	0.58
15524#1 M7	2352	6.1	14.3	12.9	0.21
15533#1 M8E	1619	9.4	15.2	120	2.23
15539#2 M8W	2232	6.1	13.6	5.32	0.24
15563 M10	1933	7.2	13.9	9.30	0.17
15573#2 M3	2744	10.4	28.5	138	1.71
15591 M3	2550	9.9	25.2	39.0	0.31
15595 M6	2449	8.2	20.1	79.4	1.39
15604 M2	2734	8.8	24.1	4.25	0.13
15620 M3	2147	7.1	15.2	336	1.40
15628 M3	2235	7.5	16.8	115	0.09
North	2039	7.74	16.1	102	0.91
South	1624	8.58	13.8	28	0.49

Table V - 2: ^{234}Th export (dpm m^{-2} d^{-1}), C:Th (µmol dpm^{-1}) and POC export (nmol m^{-2} d^{-1}) from Paul Morris and calculated $LPMe_v$ at each station during D285 and D286.

On Figure V - 7, the latitudinal variation of POC, $LPAl_v$ and $LPFe_v$ export is shown for the first two CROZEX cruise. During D285, it is clear that more acid leachable iron was exported at the northern sites. The same phenomena can be observed during D286, despite the POC export being similar in the two regions.

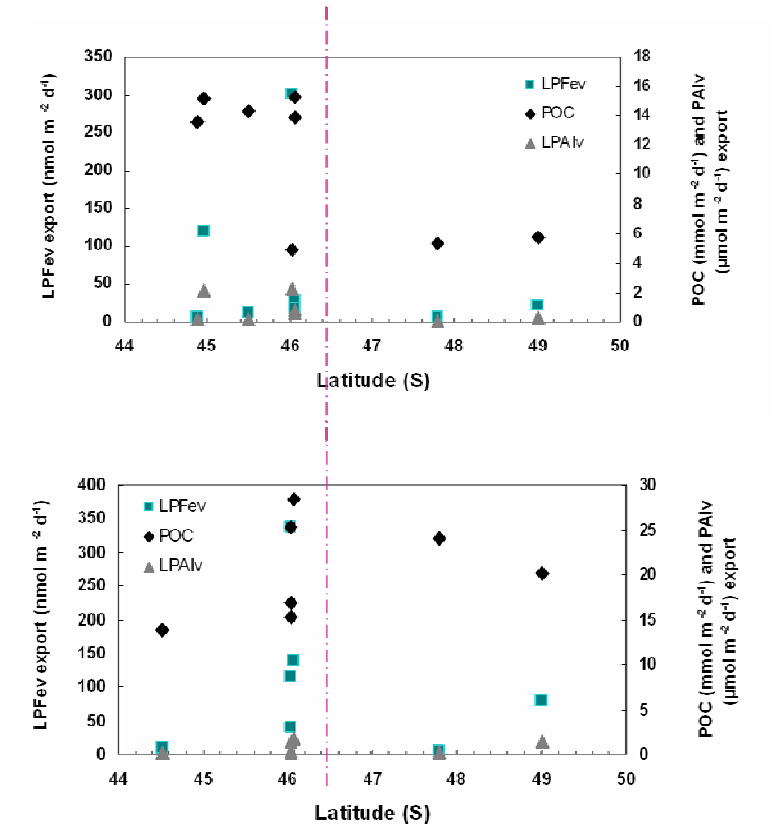

Figure V - 7: Latitudinal variation ^{234}Th derived POC export, $LPAl_v$ and LPFev during D285 (top) and D286 (bottom).
The purple long dash dotted line represents the latitude of the Crozet Islands.

In the following section, the relationship between POC export and $LPFe_v$ will be investigated together with an attempt to illustrate with the data available the various sources and sinks of iron in the Crozet system. Additionally, estimates of the residence time of iron in the upper water column will be described.

5 Discussion

The influence of iron enrichment from the Crozet Islands on downward POC export is a key issue in answering whether increased iron supply will elevate carbon sequestration to the deep ocean and this was one main biogeochemical hypothesis to be tested in this work.

5.1 Relationship between the export of POC and iron

By using calculated ^{234}Th fluxes, it was possible to estimate the POC and the total and acid leachable particulate metal exports combining C:Th and Me:Th ratios at a series of stations over the first two cruises. Large differences were visible between D285 and D286, the second leg being marked by a small bloom (0.6 µg L^{-1} of Chl *a*) occurring at M6 associated with a POC export of nearly 20 mmol m^{-2} d^{-1} in January 2005. During D285, it is clear that POC export is closely linked with LPFe and PFe exports (Figure V - 8) except for the second occupation of station M3 (Station 15499). Pollard et al. (2007b) demonstrated that this second occupation of M3 was characteristic of HNLC water advected from south of the Crozet Plateau, probably explaining the low POC export at this time.

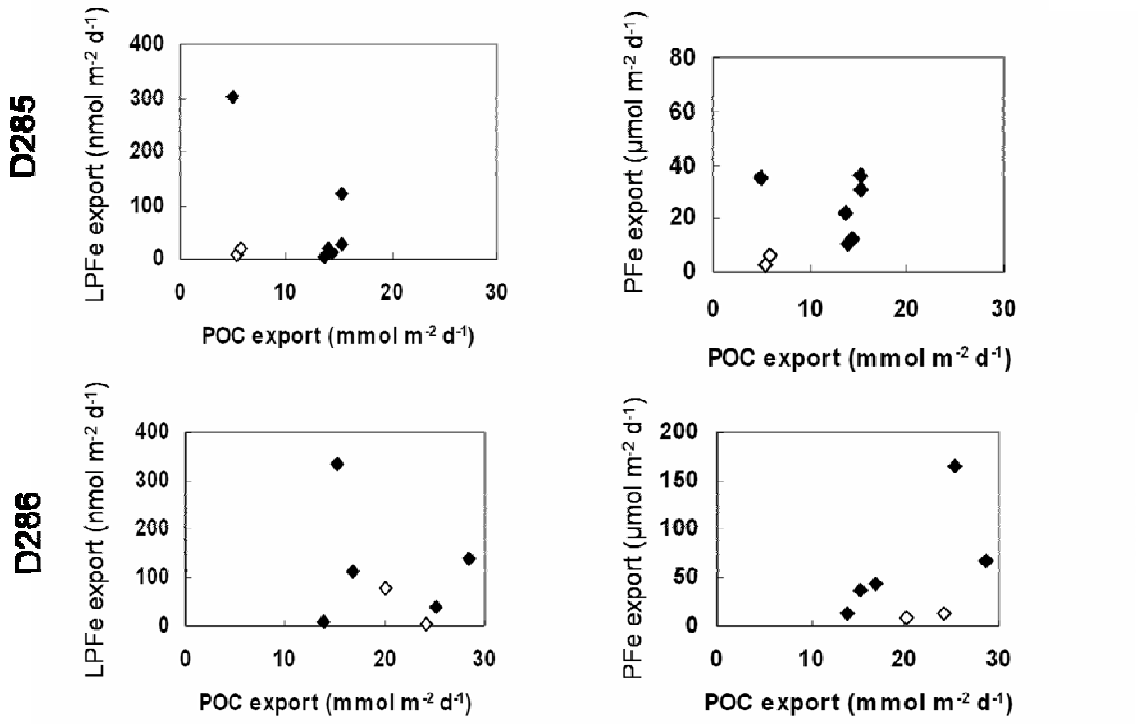

Figure V - 8: POC and LPFe export (left) and POC and PFe export (right) at all stations during D285 and D286. A distinction is made between Northern (♦) and Southern (◊) sites.

In addition to this, the last three occupations of M3 were centred in a blooming eddy close to the M3 location (Allen et al. 2006). It was hypothesised that the bloom was fuelled by entraining nutrient rich coastal waters from the local Île de la Possession which were then

vertically mixed with water in the centre of the eddy. Although the general residence time for water entering the bloom area to the north of the islands is typically 100 days, the area immediately north of the islands (M3) is probably experiencing more hydrodynamic variability, thus explaining these differences.

During the second leg, the relationship between POC and iron fluxes in less evident, although a relationship appears between the total Fe export and the POC export, suggesting that some of the refractory fraction could be available to the phytoplankton.

In Figure V - 9 is shown the latitudinal variation of the POC:LPFe ratio. This demonstrates that enhanced carbon export in the north is closely linked to the acid leachable iron export, except for the second occupation of M3 as mentioned just above.

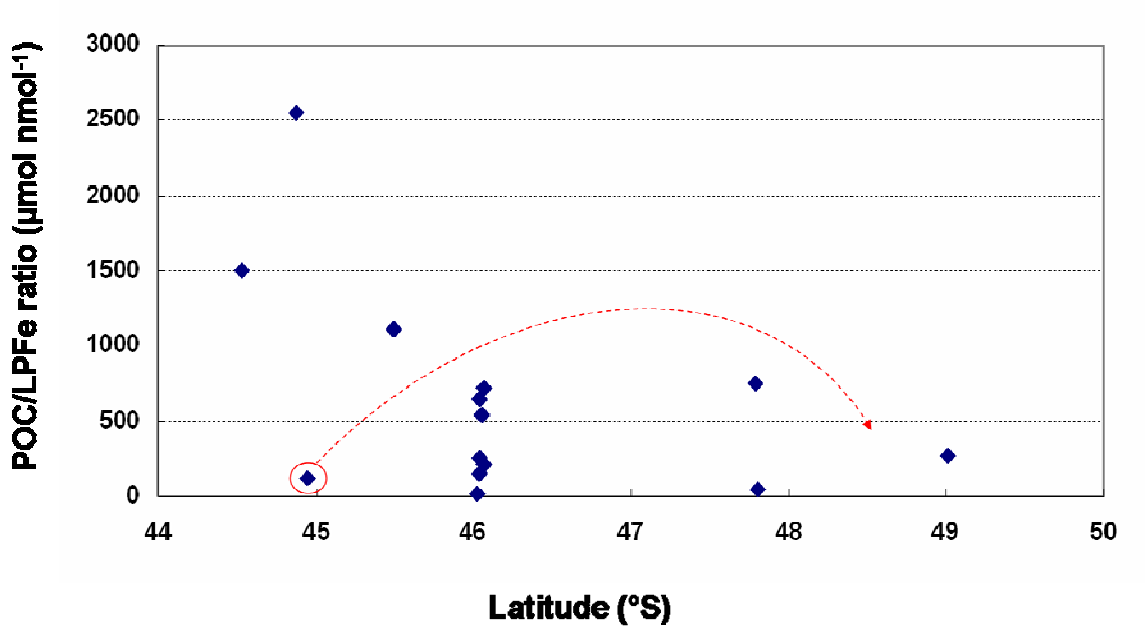

Figure V - 9: Latitudinal variation of POC:Fe ratio during D285.
The red circle highlights M8E station, which has a similar behaviour as HNLC waters (Read et al., 2007). The arrow indicates where the sample "should" fit on the plot.

5.2 Preliminary iron flux estimates for the surface waters to the North of the Crozet Islands

A budget for iron has been established using all the fluxes calculated in this study and is presented on Figure V - 10. It was impossible to build a budget for aluminium as no dissolved data is available to complement the particulate data.

This iron budget provides one of the first quantification of iron sources and sinks around the Crozet Islands. The greatest source of dissolved iron is from lateral advection from the islands, followed by atmospheric and vertical inputs. The major sink is by adsorption of acid leachable iron onto biogenic material that sinks out of the mixed layer.

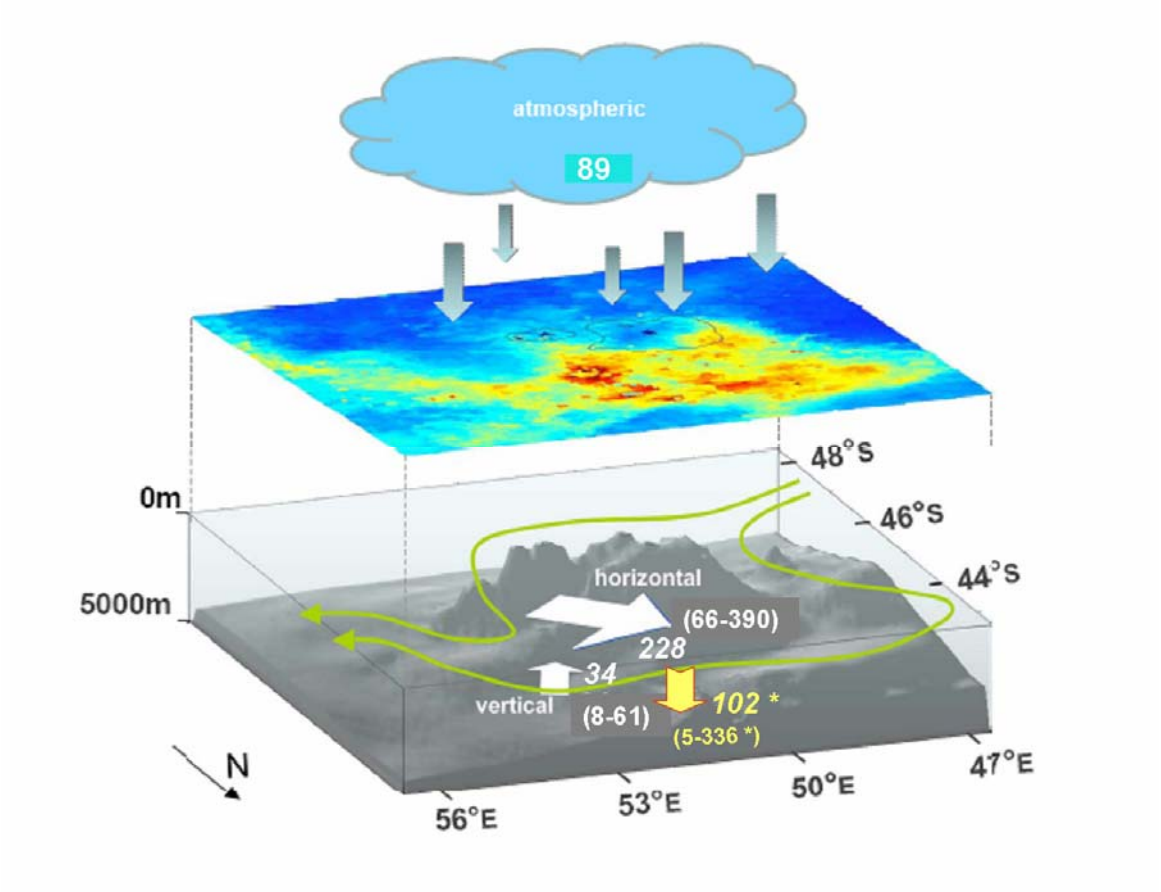

Figure V - 10: Main pathways of DFe in nmol m^{-2} d^{-1} into the bloom area around the Crozet Islands and labile iron removal term, combining the main circulation paths (green lines), and a SeaWIFS chlorophyll *a* image for the austral summer 2004-2005.

Note that the removal term in yellow font and marked with an asterisk represents the acetic acid leachable iron flux. The average fluxes are in italics, the ranges are in brackets.

However, unknown sources remain such as colloids and small particles that might be advected to the bloom area. There is also a substantial difference between the input and removal terms on average, but this difference is variable during the summer and the location. Station M3 is a good example of the variability as POC export ranged from 5 to 28 mmol m^{-2} d^{-1} and $LPFe_v$ ranged from 25 to 302 nmol m^{-2} d^{-1}.

Moreover, the acid leachable fraction may not represent the entire biogenic iron fraction as mentioned in Chapter Four. If the total Fe export is included in the removal processes, then the iron budget is largely unbalanced, as shown on Figure V – 11.

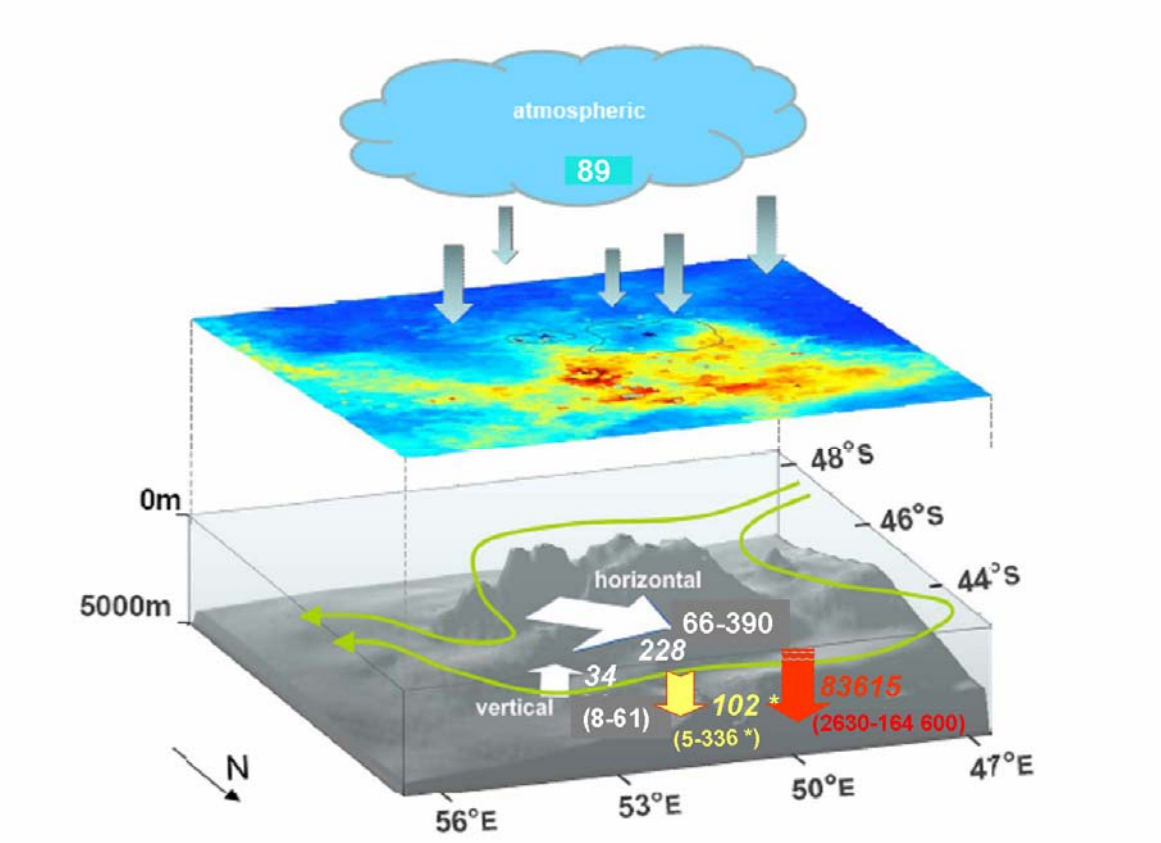

Figure V - 11: Main pathways of DFe in nmol m^{-2} d^{-1} into the bloom area around the Crozet Islands and removal terms combining the main circulation paths (green lines), and a summer averaged SeaWIFS chlorophyll *a* image for the austral summer 2004-2005.

Note that the removal term in red font represents the total particulate iron flux.

Nonetheless, as hypothesized previously, the particles are thought to originate from the islands, and this input of particles is not included in the horizontal dissolved iron flux. This leads to the conclusion that the majority of the particles advected to the bloom area are not in a bioavailable form to the phytoplankton and that only a small fraction is transformed (typically 1% if using the leachable iron flux as a "bioavailable" flux) and taken up by the organisms. Moreover, the flux of non bioavailable particles must be of the same order of magnitude than the total Fe vertical flux to balance the budget. This is illustrated in Figure V – 12.

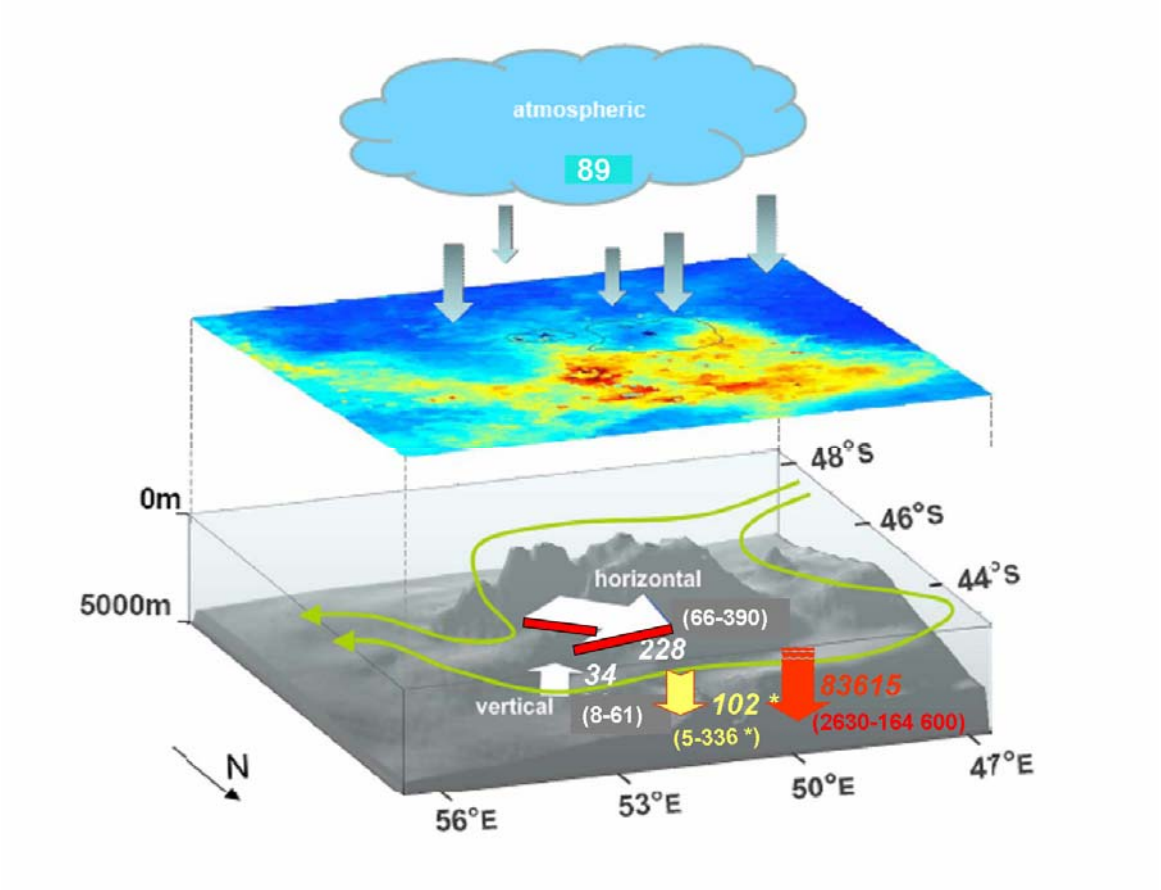

Figure V - 12: Main pathways of DFe and removal processes in nmol m^{-2} d^{-1} into the bloom area around the Crozet Islands combining the main circulation paths (green lines), and a summer averaged SeaWIFS chlorophyll *a* image for the austral summer 2004-2005.

5.3 Residence time of iron in surface waters

Finally, it is possible to estimate the residence time of iron in the waters surrounding the Crozet Islands. If POC:LPFe molar ratio found at the base of the mixed layer is considered to be similar to that in the overlying water column, then it is possible to calculate the LPFe concentrations by multiplying this ratio with the POC concentrations (S. Seeyave data) in the vertical profiles obtained at each station. Then, integrated LPFe concentrations can be calculated for the mixed layer, and the residence time estimated using the individual vertical fluxes calculated in the previous section. The detailed results are shown in Appendix IV and summarized in the table hereafter.

Site	Station	Depth m	Integrated LPFe nmol m^{-2}	LPFe flux nmol m^{-2} d^{-1}	Residence time days
M3	15494	200	2565	28.1	91
M3	15499	100	36824	302	122
M2	15504	150	1111	7.06	157
M6	15507	175	2873	21.4	134
M3	15518	175	1452	19.3	75
M7	15525	150	1125	12.9	87
M8E	15532	200	5553	120	46
M8W	15538	150	384	5.32	72
M10	15562	100	371	9.3	40
M3	15573	125	2718	138	20
M3	15589	100	1339	39	34
M6	15596	100	2892	79.4	36
M2	15606	150	199	4.25	47
M3	15623	80	12032	336	36
M3	15628	80	5512	115	48

Table V - 3 – Summary of results of integrated LPFe and iron residence time at all stations. See Appendix Four for detailed calculations of integrated DFe and LPFe.

The residence times are highly variable throughout the sampling period, highlighting the complexity of the processes occurring. Overall, these estimated values of iron residence time are consistent with the 100 days residence time of Fe estimated by Frew et al. (2006), in oligotrophic waters of the Sub-Antarctic Southern Ocean. The greatest

residence times were calculated in the southern sites reaching up to 160 days. The shortest was 20 days, at station M3.

The maximum residence time and integrated LPFe correspond to a minimum in carbon export and usually, an inverse relationship between the residence time and carbon export is observed as shown in Figure V-13.

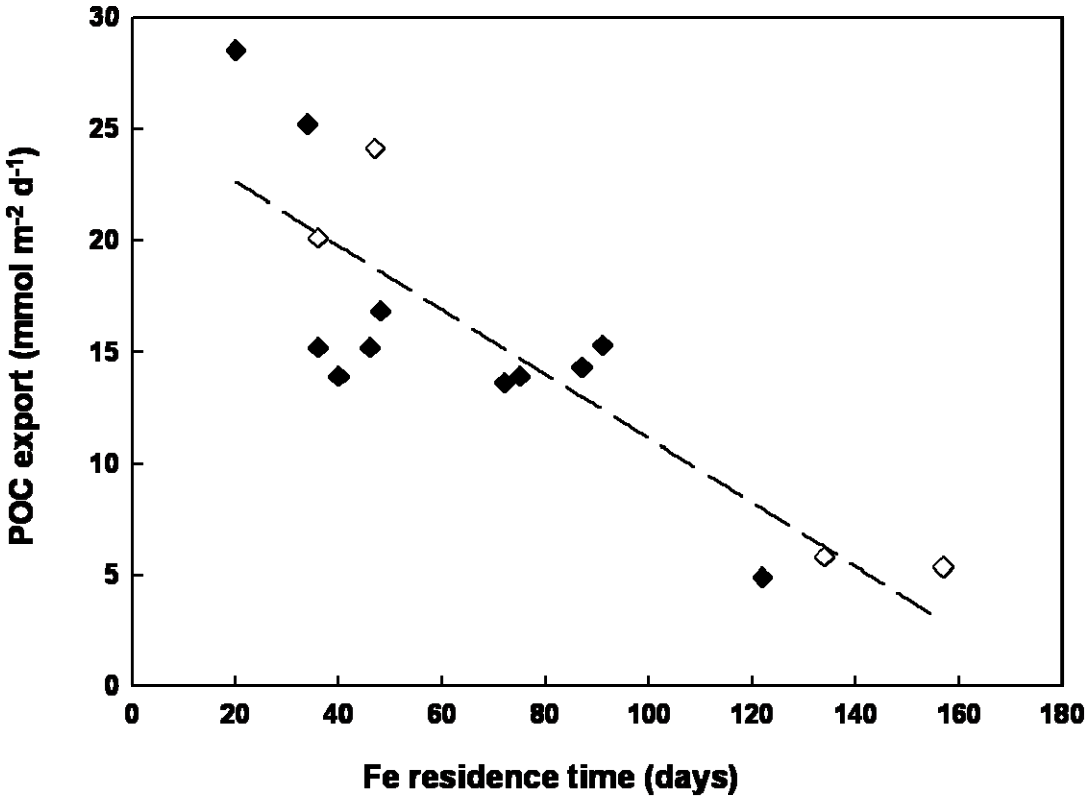

Figure V - 13: POC export (mmol m^{-2} d^{-1}) versus iron residence time (days) at the northern sites (♦) and the southern sites (◊).

This figure shows that the residence time of iron within the mixed layer is linked to the POC exported out of the mixed layer. The more iron is recycled in surface waters (i.e. the longer the residence time is) the less POC will be exported. Long residence times indicate recycling within the mixed layer by the bacterial community, which is confirmed by the study of Zubkov et al. (2007) based on Fe uptake and regeneration rates measurements using ^{55}Fe, that showed that relative iron uptake was 8 times lower in the north than in the south, suggesting a faster turnover of dissolved iron in the southern sites and less recycling. Total microbial iron uptake rates were computed at 0.12 nmol m^{-2} d^{-1} in the northern region and at 0.02 nmol m^{-2} d^{-1} in the southern region.

6 Conclusion

Three inputs mechanisms have been identified, leading to the natural fertilization of the northern sites and almost satisfying the Fe demand of the phytoplankton as estimated independently by Lucas et al. (2007). The combination of atmospheric, vertical and horizontal inputs leads to a final concentration of 0.54 nmol L^{-1}, and the demand was estimated at 0.75 nmol L^{-1}. The advection of smaller particles within the water column is likely to be another important internal source of DFe to cells, unfortunately no data were available to investigate this input.

The vertical removal fluxes of leachable iron in large suspended particles has been a key element in the determination of the residence time of iron, assuming that the POC:LPFe ratio found at the base of the mixed layer was similar in the surface waters. The residence times were found to be highly variable throughout the survey, however, a clear relationship between the POC exported out of the mixed layer and the residence time of iron has been shown, suggesting that iron balance must be primarily sustained by rapid recycling rather than advection in the north. This conclusion is in agreement with the results of an earlier artificial experiment in the Southern Ocean (Boyd et al., 2000), and that a slower recycling was occurring in the southern sites.

CHAPTER VI:

SUMMARY OF CONCLUSIONS AND FUTURE DIRECTIONS

The aims of this project was to test the hypothesis that natural iron fertilization was occurring north of the Crozet islands, to quantify the possible sources and sinks of dissolved iron in order to establish a budget and to see if enhanced primary production to the north of the plateau, leading to elevated carbon export was due to an "island mass effect".

To do so, processes influencing dissolved iron distributions around the Crozet islands have been investigated and the stations occupied at Baie Américaine were of particular importance for this study. The first objective was to build an iron analyzer to determine dissolved iron concentrations at sub-nanomolar concentrations (Chapter Two), a complete "user manual" can be found in Appendix I and sampling details are shown in Appendix III. The second objective was then to use this method to determined dissolved iron in vertical profiles collected around the Crozet islands (Chapter Three). The third objective was to determine the particulate iron concentrations in suspended particulate matter that was exported out of the mixed layer depth in both labile and refractory phases (Chapters Two and Four). Finally, the various fluxes into and out of the mixed layer, as well as iron residence times have been quantified and their influence on carbon export has been examined (Chapter Five). Each major step is considered in more detail below.

1 Analysis of iron in dissolved and suspended particulate phases

1.1 Flow injection analyzer

A flow injection analyser, using DPD catalytic spectrophotometric detection with preconcentration onto an NTA resin (FIA-NTA-DPD) was chosen to investigate the dissolved iron concentrations in the vertical profiles collected during the two first legs of the CROZEX program. This technique allows measurements of total dissolved iron down to picomolar levels such as those encountered in the HNLC waters of the Southern ocean. This analyser is light, portable and can be taken at sea, allowing near real time measurements. It was relatively easy to build, with the help of Matt Mowlem (OED, NOCS) for the software development. Some problems occurred, such as the reduction of the reagents blanks but they were solved by adding some extra columns to clean in-line the reagents. The analytical performance of the FIA-NTA-DPD analyzer was generally satisfactory despite difficulties with the spectrophotometer and some occasional backpressure problems. This technique has the main advantage that samples can be directly preconcentrated onto the NTA resin at pH 1.7 (recovery of iron is quantitative) without the need of a buffer and thus lowering the isnrtument blank. Additionally this resin is commercially available, therefore avoiding any problems in the preparation of the resin as encountered, for example with the preparation of 8-HQ resin (Nédélec, 2006). One slight inconvenient is that at pH 1.7, iron(II) cannot be collected and hydrogen peroxide must thus be added 10 mins before analysis to each sample to ensure that the determination of the total dissolved iron (Chapter II, Lohan et al., 2006).

This technique has been used successfully to determine the total dissolved iron (<0.2 μm) concentrations in the waters surrounding the Crozet Islands. The quality of the analysis was assessed using a standard approach examining the correlation of the calibration, precision of measurements, levels of blanks and limit of detection, values obtained for a certified reference material or internal seawater standard (Chapter II). The quality of the data was then examined by comparison with published data, and by their oceanographic consistency (Appendix III).

1.2 Two steps leaching technique

A two step leaching technique has been applied on the 28 samples of large suspended particles (>53 µm) collected with in-situ pumps in a variety of sites around the Crozet Islands. Aluminium and iron concentrations in both phases were determined using ICP-MS and are presented in Chapter Four.

The samples were firstly treated with a 25% acetic acid solution in order to release the labile fraction of iron. Then samples were totally digested with concentrated aqua regia and hydrofluoric acid. Blanks were processed in the same way as samples. The accuracy of this method has been tested using a wide range of certified reference materials, from lobster hepatopancreas (TORT-2) to marine mud (MAG-1, USGS). A detailed procedure can be found in Appendix II, as well as a description of all the techniques employed for the characterization of suspended particulate matter such as POC/PON analysis and SEM imaging.

1.3 Results

DFe - Very few problems of contamination were noticed (samples collected in the upper 15m of the water column where contamination from the ship was suspected) and the results of total dissolved iron in vertical profiles provide new insights into processes occurring around the Crozet Islands.

As mentioned in Chapter One, the Crozet islands are one of the few islands systems (Bouvet, South Georgia or Kerguelen) in the HNLC Southern Ocean where a bloom with a rather well defined spatial distribution can be observed annually. From earlier hydrographic surveys (Pollard & Read, 2001) it seemed highly likely that the bloom was constrained to the west and north by the SubAntarctic Front. However, only a small difference could be observed between the northern and the southern sites in the distribution of total dissolved iron concentrations, making the distinction between the supposed fertilized and non fertilized areas at first sight difficult. This difference appears to reflect the higher biomass to the north and its ability to remove Fe from solution. An important observation was that high DFeconcentrations, up to 4 nmol L^{-1} were measured

in close proximity of one of the main island, Île de la Possession. More interestingly, a gradient of 0.07 nmol L^{-1} m^{-1} was observed on moving away from the Baie Américaine, indicating that the islands and shelf systems were a natural source of iron. The present study thus provides one of the first iron data set supporting the "island mass effect" hypothesis around the Crozet Islands and the resulting paper is presented in Appendix III.

Iron and Aluminium in large suspended particles - SPM concentrations were typical of the concentrations reported for HNLC regions, varying from 7 to 90 µg L^{-1} and were quite variable depending on the time of sampling and sites. No general distinction could be made in terms of suspended particulate matter concentrations between the northern and southern sites. However, a clear relationship between the SPM and POC concentrations at all sites was found, indicating that the samples were mainly biogenic in origin.

SEM imaging was used to characterize some of the samples in terms of phytoplankton species. The southern sites were made of assemblages of small diatoms, characteristic of iron-stressed waters. The northern sites had a variable composition in phytoplankton depending on the sampling time, and were dominated sometimes by *Eucampia Antarctica* or small centric diatoms. Baie Américaine sample was poor in phytoplankton and large particle composed of mainly iron and silica was identified by EXAFS.

The maximum concentrations of Al and Fe were obtained at Baie Américaine, which were 100 times greater than the average measured elsewhere. This observation supports the hypothesis that the islands are a source of iron, among other elements. Moreover, total Fe and Al concentrations were greater by an order of magnitude in the north in comparison with the Southern sites. The fraction of the acid leachable fraction has been calculated and never exceeds 1% of the total fraction.

It was useful to investigate the concentrations of metals within the particles on a mol per mass basis as well as in the water column on a mol per volume basis. In particular, the particles content revealed clearly that those collected in Baie Américaine were metal enriched in aluminium (97.1 nmol g^{-1}) and in iron (498 nmol g^{-1}). Concentrations of all total trace metals in seawater (i.e. mol L^{-1} basis) are greater in the north than in the south, by at least a factor 3. The observations are consistent with an island source.

Overall, the concentrations considered in this study are within the range of published data. The highest values of Al and Fe obtained near Crozet are similar to the one reported by Grotti et al. (2001) in Antarctic coastal waters. If we remove BA station from the comparison, all the particulate trace metal data are in the range of those reported in the open Southern Ocean, confirming a local island source of trace metals.

Fe/Al ratios were investigated in the total fraction as these ratios may indicate the relative importance of lithogenic material in a sample in comparison to the average upper continental crust ratio. Fe/Al ratios were variable throughout the sampling period but they confirmed that the northern sites were more enriched in aluminium and iron than the southern sites. At Baie Américaine stations the Fe/Al ratios approached the average basalt crust ratio.

2 Fe budget and fluxes, and their impact on primary production

Using the total dissolved iron data and particulate trace metals concentrations, it was possible to calculate the sources and sinks of iron using radium and thorium isotopes in collaboration with Alex Baker, Tim Jickells, Matt Charette and Paul Morris. The main results were that the horizontal advection of dissolved iron is the main source of iron to the northern area of the Crozet islands, and the maximum contribution of this input was estimated to be nearly 400 nmol m^{-2} d^{-1}. Atmospheric inputs are not negligible as they can reach up to 90 nmol m^{-2} d^{-1} and can occur everywhere. This source may potentially explain the small bloom observed in the south during the austral summer 2004/2005. The present work also suggest that a very small fraction (1%) may actually be available to organisms from the large particles (>53 μm), although an important portion may be found in the intermediate particulate fraction (0.4-53 μm). Finally, vertical inputs represent at the maximum only 11% (61 nmol m^{-2} d^{-1}) of the identified sources in this work.

Scavenging of particles can be a major sink in the iron cycle (5-336 nmol m^{-2} d^{-1}). This was investigated too, and was averaged up to 100 nmol m^{-2} d^{-1} even if the vertical export of acid leachable iron can reach up 336 nmol m^{-2} d^{-1} at some times.

A fraction of atmospheric, vertical and horizontal inputs of iron can be potentially directly available to the phytoplankton population without additional transformation, except for the particulate fraction. However, whilst most of the particulate fraction appears to be refractory, to what extent this might be available to organism is unknown. The release of potentially bioavailable iron supplied from shelf sources in intermediate particles could be an important source for severely iron-stressed algal cells but has not been specifically addressed here. It was possible to estimate the concentration of bioavailable iron accumulated over the winter of 0.54 nmol L^{-1}. The residence time of iron has also been calculated for most of the stations occupied during the survey, ranging from 20 days at high productivity sites to 160 days at the southern sites.

From this work, it was evident that dissolved iron was transported from the Crozet Islands to the north and relieved the iron stressed phytoplankton community. This led to an enhanced primary production and carbon export, that was particularly evident during the first leg of CROZEX.

3 Future directions

The aim of this work was to determine whether the Crozet Islands were a source of iron to the surrounding waters. Several aspects of the iron cycle such as the speciation, and inputs of colloids and smaller particulate (0.4-53 μm) potential inputs could not be addressed in the scope of this study but the work here does provide a good basis for future investigations.

Samples have been collected for organic speciation work at a set of stations where total dissolved iron data is available. Speciation data could help to explain how the dissolved iron is maintained within the mixed layer and what concentrations of ligands are present.

All the samples taken for dissolved iron (typically 0.5 L) have been kept and they could be used for the determination of other bioactive metals, such as aluminium, copper, zinc and manganese. The solutions resulting from the two step leaching technique are also available for the quantification of these and other metals, and similar calculations would lead to the establishment of budgets of these elements. Incorporation of data obtained in the present work in models could help to gain a better understanding of the complex

progression of the bloom and its collapse by considering important driving factors (e.g. Silica drawdown, PON) and co-limitations.

Future directions of work should include as well the release processes leading to iron and other trace elements from sediments. It would be interesting to establish vertical profiles of particulate iron to investigate better the POC and PFe relationships, and availability of Fe to organisms, and in what phases the Fe resides. One could think as well of small particles incubations for the study of the mechanisms that release bioavailable iron from this pool. Such experiments are conducted for the atmospheric particles but it would be interesting to think about such experiments for suspended particles.

There is a need for a consensus in the determination of "labile" bioactive trace metals, as it is difficult to compare data sets due to the variety of techniques used by the scientific community.

Finally, in the context of natural island fertilization in the Southern Ocean, a crucial point would be as well to try to investigate the pre-bloom concentrations and sample before the austral spring begins. This may be difficult due to weather, but would really help to understand the natural iron fertilization processes.

REFERENCES:

Achterberg, E.P., T.W. Holland, A.R. Bowie, R. Fauzi C. Mantoura, P.J. Worsfold. 2001. Review: Determination of iron in seawater, Analytica Chimica Acta, 442, 1-14

Allen, J., Bakker, D., Read, J., Pollard, R., Charette, M., Venables, H., Planquette, H., Morris, P., Sanders, R., Moore, C.M. and Seeyave, S. (2006) An 'eddy-centric' bloom north of the Crozet Islands; sub-mesoscale entrainment of island nutrients or vertical diffusion? *Challenger Conference for Marine Science*, Oban, Scotland

Atkinson, A., Whitehouse, M.J., Priddle, J., C. C.G., Ward, P., and Brandon, M.A., 2001. South Georgia, Antarctica: a productive, cold water, pelagic ecosystem. Marine Ecology Progress Series, 216, 279-308

de Baar, H.J.W., de Jong, J.T.M., Nolting, R.F., Timmermans, K.R., van Leeuwen, M.A., Bathmann, U., van der Loeff, M.R., and Sildam, J., 1999. Low dissolved Fe and the absence of diatom blooms in remote Pacific waters of the Southern Ocean. Marine Chemistry, 66, 1-34

de Baar, H.J.W., and de Jong, J.T.M., 2001. Distributions, sources and sinks of iron in seawater. In: The Biogeochemistry of Iron in Seawater. Turner D.R., and Hunter K.A. eds, Chichester, John Wiley & Sons, IUPAC 7, 123-253

de Baar, H.J.W., Boyd, P.W., Coale, K. H. Landry, M. R., Tsuda, A., Assmy, P., Bakker, D.C.E., Bozec, Y., Barber, R.T., Brzezinski, M.A., Buesseler, K.O., Boyé, M., Croot, P. L. , Gervais, F., Gorbunov, M.Y., Harrison, P. J., Hiscock, W.T. , Laan, P., Lancelot, C., Law, C.S., Levasseur, M., Marchetti, A., Millero, F.J., Nishioka, J., Nojiri, Y., van Oijen, T., Riebesell, U., Rijkenberg, M.J.A., Saito H., Takeda S., Timmermans, K.R, Veldhuis, M. J.W., Waite A. and Wong C.S., 2005. Synthesis of Iron Fertilization Experiments: From the Iron Age in the Age of Enlightenment. Journal of Geophysical Research (Oceans), 110, C09S16, doi:10.1029/2004JC002601, 1-24

Baker, A. R., Kelly, S. D., Biswas, K. F., Witt, M. and Jickells, T. D., 2003. Atmospheric deposition of nutrients to the Atlantic Ocean. Geophysical Research Letters, 30, 2296, doi:10.1029/2003GL018518

Baker, A.R., Jickells, T.D., Witt, M, Linge, K.L., 2006. Trends in the solubility of iron, aluminium, manganese and phosphorus in aerosol collected over the Atlantic Ocean. Marine Chemistry, 98, 43-58

Baker, A.R. and Jickells, T.D., 2006. Mineral particles size as a control on aerosol solubility. Geophysical research letters, 33, L17608, doi:10.1029/2006GL026557

Banse, K., 1996. Low seasonality of low concentrations of surface chlorophyll in the Subantarctic water ring: underwater irradiance, iron or grazing? Progress in Oceanography 37, 241-291

Barbeau, K., Rue, E. L., Bruland, K. W., Butler, A., 2001. Photochemical cycling of iron in the surface ocean mediated by microbial iron(III)-binding ligands. Nature 413, 409–413

Barbeau, K., Rue, E.L., Trick, C.G., Bruland, K.W., Butler, A., 2003. Photochemical reactivity of siderophores produced by marine heterotrophic bacteria and cyanobacteria based on characteristic Fe(III) binding groups. Limnology and Oceanography, 48(3), 1069-1078

Berelson, W.M., McManus, J., Coale, K.H., Johnson, K.S., Burdige, D., Kilgore, T., Colodner, D., Chavez, F.P., Kudela, R.M., Boucher, J., 2003. A time series of benthic flux measurements from Monterey Bay, CA. Continental Shelf Research, 23, 457-481

Bhat, S.G., Krishnaswami, S., Lal, Rama, D. and Moore, W.S., 1969. $^{234}Th/^{238}U$ ratios in the ocean. Earth and Planetary Science Letters, 5, 483-491

Bishop, J.K.B., Edmond, J., Ketten, D.R., Bacon, M.P., Silker, W.B., 1977. The chemistry, biology, and vertical flux of particulate matter from the upper 400m of the Equatorial Atlantic Ocean, Deep-Sea Research I, 511-548

Bishop, J.K.B., Schupack, D., Sherrell, R.M., and Conte, M. 1985. A Multiple Unit Large Volume in-situ Filtration System (MULVFS) for sampling oceanic particulate matter in mesoscale environments. pp. 155-175 In: A. Zirino (ed.), Mapping Strategies in Chemical Oceanography, Advanced in Chemistry Series, Vol. 209, American Chemical Society, Washington, D.C.

Bishop, J.K.B., and Fleisher, M.Q., 1987. Particulate manganese dynamics in Gulf Stream warm-core rings and surrounding waters of the N.W. Atlantic. Geochimica Cosmochima Acta, 51, 2807-2825

Bishop, J.K.B., 1988. The barite-opal-organic carbon association in oceanic particulate matter. Nature, 332, 341-343

Blain, S. and Tréguer, P. 1995. Fe(II) and Fe(III) determination in sea water at the nanomolar level with selective on-liine preconcentration and spectrophotometric detection, Analytica Chemica Acta, 308, 425-432

Blain, S., Tréguer, P., Belviso, S., Bucciarelli, E., Denis, M., Desabre, S., Fiala, M., Jezequel, V.M., Lefèvre, J., Mayzaud, P., Marty, J.-C., and Razouls, S., 2001. A biogeochemical study of the island mass effect in the context of the iron hypothesis: Kerguelen Islands, Southern Ocean. Deep-Sea Research I, 48(1), 163- 187

Blain, S., Guieu, C., Clauste, H., Leblanc, K., Moutin, T., Quéguiner, B., Ras, J., Sarthou, G., 2004. Availability of iron and major nutrients for phytoplankton in the northeast Atlantic Ocean. Limnology and Oceanography, 49(6), 2095-2104

Blain, S., Quéguiner, B., Armand, L., Belviso, S., Bombled, B., Bopp, L., Bowie, A., Brunet, C., Brussaard, C., Carlotti, F., Christaki, U., Corbière, A., Durand, I., Ebersbach, F., Fuda, J-L, Garcia, N., Gerringa., L, Griffiths, B., Guigue, C., Guillerm, C., Jacquet, S., Jeandel, C., Laan, P., Lefèvre, D., Lo Monaco, C., Malits,

A., Mosseri, J., Obernosterer, I., Park, Y-H, Picheral, M., Pondaven, P., Remenyi, T., Sandroni, V., Sarthou, G., Savoye, N., Scouarnec, L., Souhaut, M., Thuiller, D., Timmermans, K., Trull, T., Uitz, J., van Beek, P., Veldhuis, M., Vincent, D., Viollier, E., Vong, L., Wagener, T., 2007. Effect of natural iron fertilization on carbon sequestration in the Southern Ocean, Nature, 446, 1070-1074

Blain, S., Sarthou, G., and Laan, P., *in press*. Distribution of dissolved iron during the natural iron fertilisation experiment KEOPS (Kerguelen Plateau, Southern Ocean). Deep-Sea Research II

Bonnet, S., and Guieu, C., 2004. Dissolution of atmospheric iron in seawater. Geophysical Research Letters, 31, L03303

Bowie, A.R., Maldonado, M.T., Frew, R.D., Croot, P.L., Acheterberg, E.P., Mantoura, R.F.C., Worsfold, P.J., Law, C.S., Boyd, P.W., 2001. The fate of added iron during a mesoscale fertilisation in the polar Southern ocean. Deep-Sea Research II, 48, 2703-2744

Bowie, A.R., Achterberg, E.P., Sedwick, P. N., Ussher, S., Worsfold, P.J. 2002. Real-time monitoring of picomolar concentrations of iron(II) in marine waters using automated flow injection-chemiluminescence instrumentation. Environmental Science and Technology, 36, 4600-4607

Bowie, A.R., Sedwick, P. N., and Worsfold, P.J. 2004. Analytical comparison between flow injection-chemiluminscence and flow injection-spectrophotometry for the determination of picomolar concentrations of iron in seawater. Limnology and oceanography, methods, 2, 42-54

Bowie, A.R., Achterberg, E.P., Croot, P.L., de Baar, H.J.W., Laan, P., Moffett, J.W., Ussher, S., Worsfold, P.J. 2006. A community-wide intercomparison exercise for the determination of dissolved iron in seawater. Marine Chemistry, 98, 81-99

Boyd, P.W., Watson, A.J., Law, C.S., Abraham, E.R., Trull, T., Murdoch, R., Bakker, D.C.E., Bowie, A.R., Buesseler, K.O., Chang, H., Charette, M.A., Croot, P.L., Downing, K., Frew, R.D., Gall, M., Hadfield, M., Hall, J.A., Harvey, M., Jameson, G., LaRoche, J., Liddicoat, M.I., Ling, R., Maldonado, M.T., McKay, R.M.,

Nodder, S., Pickmere, S., Pridmore, R., Rintoul, S., Safi, K.A., Sutton, P., Strzepek, R., Tanneberger, K., Turner, S., Waite, A., and Zeldis, J., 2000. A mesoscale phytoplankton bloom in the polar Southern Ocean stimulated by iron fertilization. Nature, 407, 695-702

Boyd, P.W., Law, C.S., Wong, C.S., Nojiri, Y., Tsuda, A., Levasseur, M., Takeda, S., Rivkin, R., Harrison, P.J., Strzepek, R., Gower, J., McKay, R.M., Abraham, E.R., Arychuk, M., Barwell-Clarke, J., Crawford, W., Crawford, D., Hale, M., Harada, K., Johnson, K.S., Kiyosawa, H., Kudo, I., Marchetti, A., Miller, W.L., Needoba, J., Nishioka, J., Ogawa, H., Page, J., Robert, M., Saito, H., Sastri, A., Sherry, N., Soutar, T., Sutherland, N., Taira, Y., Whitney, F., Wong, S.-K.E., and Yoshimura, T., 2004. The decline and fate of an iron-induced subarctic phytoplankton bloom. Nature, 428, 549-553

Boyd, P.W., Law, C., Hutchins, D.A., Abraham, E.R., Croot, P., Ellwood, M., Frew, R., Hadfield, M., Hall, J., Handy, S., Hare, C., Higgins, J., Hill, P., Hunter, K.A., Leblanc, K., Maldonado, M.T., McKay, R.M., Mioni, C., Olivier, M., Pickmere, S., Pinkerton, M., Safi, K., Sanders, S., Sanudo-Wilhelmy, S.A., Smith, M.H., Strzepek, R., Tovar- Sanchez, A., Wilhelm, S.W., 2005. FeCycle: attempting an iron biogeochemical budget from a mesoscale SF6 tracer experiment in unperturbated low iron waters. Global Biogeochemical Cycles, 19(GB4S20): doi: 10.1029/2005GB002494

Boyd, P.W., Jickells, T., Law, C.S., Blain, S., Boyle, E.A., Buesseler, K.O., Coale, K.H., Cullen, J.J., de Baar, H.J.W., Follows, M., Harvey, M., Lancelot, C., Levasseur, M., Owens, N.P.J., Pollard, R., Rivkin, R.B., Sarmiento, J., Schoemann, V., Smetacek, V., Takeda, S., Tsuda, A., Turner, S., Watson, A.J., 2007. Mesoscale Iron Enrichment Experiments 1993-2005: Synthesis and Future Directions. Science, 315, 612-617

Boye, M.B., Aldrich,A.P., van den Berg, C.M.G., deJong, J.T.M., Veldhuis, M.J.W., de Baar, H.J.W., 2003. Horizontal gradient of the chemical speciation of iron in surface waters of NE Atlantic Ocean. Marine Chemistry, 50, 129–143

Bruland, K.W., Orians, K.J. and Cowen, J.P., 1994. Reactive trace-metals in the stratified Central North Pacific. Geochimica et Cosmochimica Acta**,** 58(15), 3171–3182

Bruland K.W., and Rue E.L., 2001. Analytical methods for the determination of concentrations and speciation of iron. In: The Biogeochemistry of Iron in Seawater. Turner D.R., and Hunter K.A., Chichester, John Wiley & Sons, IUPAC 7: 255-289.

Bruland, K.W., and Lohan, M.C., 2004. Controls of trace metals in seawater. In: Treatise on Geochemistry, 6.02, 23-47, doi:10.1016/B0-08-043751-6/06105-3

Bucciarelli, E., Blain, S., and Tréguer, P., 2001. Iron and manganese in the wake of the Kerguelen Islands (Southern Ocean). Marine Chemistry, 73(1): 21-36

Buesseler, K.O., Bacon, M.P., Cochran, J.K. and Livingston, H.D., 1992. Carbon and nitrogen export during the JGOFS North Atlantic Bloom Experiment from ^{234}Th:^{238}U disequilibrium. Deep-Sea Research I, 39, 1115-1137

Buesseler K.O., and Boyd P.W., 2003. Will ocean fertilization work ? Science, 300, 67-68.

Buesseler, K.O., Andrews, J.E., Pike, S.M., and Charette, M.A., 2004. The effects of iron fertilization on carbon sequestration in the Southern Ocean. Science, 304, 414-417

Buesseler, K.O., Benitez-Nelson, C.R., Moran, S.B., Burd, A., Charette, M., Cochran, J.K., Coppola, L., Fisher, N.S., Fowler, S.W., Gardner, W.D., Guo. L.D., Gustafsson, O., Lamborg, C., Masque, P., Miquel, J.C., Passow, U., Santschi, P.H., Savoye, N., Stewart, G., Trull, T., 2006. An assessment of particulate organic carbon to thorium-234 ratios in the ocean and their impact on the application of ^{234}Th as a POC flux proxy. Marine Chemistry, 100, 213-233

Canfield, D.E., 1989. Reactive iron in marine sediments. Geochimica et Cosmochimica Acta, 53(3), 619-632

Cardinal, D., Dehairs, F., Cattaldo, T., André, L., 2001. Geochemistry of suspended particles in the Subantarctic and Polar Frontal Zones south of Australia: Constraints

on export and advection processes. Journal of geophysical research, 106 (C12), 31,637-34,656

Charette, M.A., Gonneea, M.E., Morris, P.J., Statham, P.J., Fones, G.R., Planquette, H., Salter, I., Naveira Garabato, A., 2007. Radium isotopes as tracers of iron sources fueling a Southern Ocean phytoplankton bloom. Deep-Sea Research II, 54, 1989-1998

Chen, J.H., Edwards, L. and Wasserburg, G.J., 1986. ^{238}U, ^{234}U and $_{232}Th$ in seawater. Earth and Planetary Science Letters, 80, 241-251

Chen, Y., and Siefert, R. L., 2004. Seasonal and spatial distribution and dry deposition fluxes of atmospheric total and labile iron over the tropical and subtropical North Atlantic Ocean. Journal of Geophysical Research, 109, D09305, doi:10.1029/2003JD003958

Chisholm, S.W., 2000. Oceanography: Stirring times in the Southern Ocean. Nature, 407, 685-687, doi:10.1038/35037696

Chisholm, S.W., Falkowski, P.G., and Cullen, J.J., 2001. Dis-crediting ocean fertilization. Science, 294, 309-310

Clegg, S.L. and Whitfield, M., 1990. A generalised model for the scavenging of trace metals in the open ocean. Deep-Sea Research I, 37, 809-832

Coale, K.H., Johnson, K.S., Fitzwater, S.E., Gordon, R.M., Tanner, S.J., Chavez, F.P., Ferioli, L., Sakamoto, C., Rogers, P., Millero, F.J., Steinberg, P., Nightingale, P., Cooper, D., Cochlan, W.P., Landry, M.R., Constantinou, J., Rollwagen, G., Trasvina, A., and Kudela R.M., 1996. A massive phytoplankton bloom induced by an ecosystem-scale iron fertilization experiment in the equatorial Pacific Ocean. Nature, 383, 495-501

Coale, K.H., Johnson, K.S., Chavez, F.P., Buesseler, K.O., Barber, R.T., Brzezinski M.A., Cochlan, W.P., Millero, F.J., Falkowski, P.G., Bauer, J.E., Wanninkhof, R.H., Kudela, R.M., Altabet, M.A., Hales, B.E., Takahashi, T., Landry, M.R., Bidigare,

R.R., Wang, X., Chase, Z., Strutton, P.G., Friederich, G.E., Gorbunov, M.Y., Lance, V.P., Hilting, A.K., Hiscock, M.R., Demarest, M., Hiscock, W.T., Sullivan, K.F., Tanner, S.J., Gordon, R.M., Hunter, C.N., Elrod, V.A., Fitzwater, S.E., Jones, J.L., Tozzi, S., Koblizek, M., Roberts, A.E., Hemdon, J., Brewster, J., Ladizinsky, N., Smith, G.J., Cooper, D., Timothy, D., Brown, S.L., Selph, K.E., Sheridan, C.C., Twining, B.S., and Johnson, Z.I., 2004. Southern Ocean iron enrichment experiment: Carbon cycling in high- and low-Si waters. Science, 304, 408-414

Coale, K.H., Gordon, M. and Wang, X., 2005. The distribution and behavior of dissolved and particulate iron and zinc in the Ross Sea and Antarctic circumpolar current along 170°W, Deep-Sea Research I, 52, 295-318

Collier R., and Edmond, J. 1984. The trace element geochemistry of marine biogenic particulate matter. Progress in Oceanography, 13, 113-199

Croot, P. L., and Laan, P. 2002. Continuous shipboard determination of Fe (II) in polar waters using flow injection analysis with chemiluminescence detection, Analytica Chimica Acata 466, 261-273

Croot, P.L., Andersson, K., Oztürk, M. and Turner, D.R., 2004a. The distribution and speciation of iron along 6ºE in the Southern Ocean. Deep-Sea Research II, 51, 2857-2879

Croot, P.L., Laan, P., Nishioka, J., Boyé, M., Timmermans, KR., Bellerby, R.G., Goldson, L., Nightingale P. and de Baar H.J.W., 2005. Spatial and temporal distribution of Fe(II) and H2O2 during EISENEX, an open ocean mesoscale iron enrichment. Marine Chemistry, 95, 65-88

Cullen, J.T. and Sherrell, T.M., 1999. Techniques for determination of trace metals in small samples of size-fractionated particulate matter: phytoplankton metals off central California. Marine Chemistry, 67, 233-247

Dehairs, F., Goeyens, L., Stroobants, N. and Mathot, S., 1992. Elemental composition of suspended matter in the Scotia-Weddell Confluence area during spring and summer 1988 (EPOS Leg 2). Polar Biology, 12, 25-33.

Draxler R.R. and Rolph G.D., 2003. HYSPLIT (Hybrid Single-Particle Lagrangian Integrated Trajectory) Model access via NOAA ARL READY website (http://www.arl.noaa.gov/ready/hysplit4.html) NOAA Air Resources Laboratory, Silver Spring MD

Duce, R.A., and Tindale, N.W., 1991. Atmospheric transport of iron and its deposition in the ocean. Limnology and Oceanography, 36, 1715–1726

Duce, R.A., Liss, P.S., Merrill, J.T., Atlas, E.L., Buat-Menard, P., Hicks, B.B., Miller, J.M., Prospero, J.M., Arimoto, R., Church, T.M., Ellis, W., Galloway, J.N., Hansen, L., Jickells, T.D., Knap, A.H., Reinhardt, K.H., Schneider, B., Soudine, A., Tokos, J.J, Tsunogai, S., Wollast R., Zhou, M., 1991. The atmospheric input of trace species to the world ocean. Global Biogeochemical Cycles**,** 5**,** 193–259

Eggiman, D.W., and Betzer, P.R. 1976. Decomposition and analysis of refractory oceanic suspended materials. Analytical chemistry, 48, 886-890

Elrod, V.A., Johnson, K., Coale, K.H. 1991. Determination of subnanomolar levels of iron(II) and total dissolved iron in seawater by flow injection analysis with chemiluminescence detection, Analytical Chemistry, 63, 893-898

Elrod, V.A., Berelson, W.M., Coale, K.H., Johnson, K.S., 2004. The flux of iron from continental shelf sediments: A missing source for global budgets. Geophysical Research Letters, 31(L12307), 1-4

Fan, S-M., Moxim, W.J., Levy II, H., 2006. Aelion input of bioavailable iron to the ocean. Geophysical research letters, 33, L07602, doi:10.1029/2005GL024852

Faust, B.C., 1994. A review of the photochemical redox reactions of iron(III) species in atmospheric, oceanic, and surface waters: Influences on geochemical cycles and oxidant formation. In: G.R. Helz, Zepp, R.G., Crosby, D.G. (Editor), Aquatic Surface Photochemistry. CRC Press, Inc., London, 3-37

Fitzwater, S.E., Johnson, K. S., Elrod, V.A., Ryan, J.P., Coletti, L., J., Tanner, S.J., Gordon, R.M., Chavez, F.P., 2003. Iron, nutrient and phytoplankton biomass relationships in upwelled waters of the California coastal system. Continental Shelf

Research, 23(16), 1523-1544Grotti, M., Soggia, F., Abelmoschi, M., Rivaro, P., Magi, E., Frache, R., 2001. Temporal distribution of trace metals in Antarctic coastal waters. Marine Chemistry 76, 189-209

Foucart, S., 2007. L'épandange de fer dans l'océan ne favoriserait pas l'absorption de CO_2 par le plankton. Le Monde, édition du 27 Avril 2007

Frew, R.D., Hutchins, D.A., Nodder, S., Sanudo-Wilhelmy, S., Tovar-Sanchez, A., Leblanc, K., Hare, C.E., Boyd, P.W., 2006. Particulate iron dynamics during FeCycle in subantarctic waters southeast of New Zealand. Global Biogeochemical cycles, 20, GB1S93, doi:10.1029/2005GB002558

Gaiero, D.M., Probst, J. -L., Depetris, P. J., Bidart, S. M. and Leleyter, L., 2003. Iron and other transition metals in Patagonian riverborne and windborne materials: geochemical control and transport to the southern South Atlantic Ocean. Geochimica et Cosmochimica Acta, 67 (19), 3603-3623

GEOTRACES. An international study of the marine biogeochemical cycles of trace elements and their isotopes. International council for science. Scientific committee on oceanic research (SCOR) publishers, 2006.

German, C., and Von Damm, K.L., 2004. Hydrothermal processes. In: Treatise on Geochemistry, Chapter 6, Pages 181-222, doi:10.1016/B0-08-043751-6/06109-0

Gerringa, L.J.A., de Baar, H.J.W., Timmermans, K.R., 2000. A comparison of iron limitation of phytoplankton in natural oceanic waters and laboratory media conditioned with EDTA. Marine Chemistry, 68, 335-346

Gerringa, L.J.A., Rijkenberg, M.J.A., Wolterbeek, H.Th., Verburg, T.G., Boye, M., de Baar, H.J.W., 2007. Kinetic study reveals weak Fe-binding ligand, which affects solubility of Fe in the Scheldt estuary. Marine Chemistry, 103, 30-45

Gervais, F., Rievesell, U., and Gorbunov, M.Y., 2002. Changes in primary productivity and chlorophyll *a* in response to iron fertilization in the Southern Polar Frontal Zone. Limnology and Oceanography, 47(5), 1324-1335

Giret, A., Tourpin, S., Marc, S., Verdier, O., Cottin, J-Y, 2002. Volcanisme de l'île aux Pingouins, archipel Crozet, témoin de l'hétérogénéité du manteau fertile au sud de l'océan Indien. Penguins Island, Crozet archipelago, volcanic evidence for a heterogeneous mantle in the southern Indian Ocean. Comptes Rendus Geosciences, 334, 481-488

Gledhill, M., McCormack, P., Ussher, S., Achterberg, E.P., Fauzi, R., Mantoura, C., Worsfold, P.J., 2004. Production of siderophore type chelates by mixed bacterioplankton populations in nutrient enriched seawater incubations. Marine Chemistry, 88, 75-83

Gran, H.H., 1931. On the conditions for the production of plankton in the sea. Conseil Permanent pour l'exploration internationale de la mer. Rapports et Procès verbaux, 75, 37-46

Gregg, W. W., Ginoux, P., Schopf, P.S., Casey, N.W., 2003. Phytoplankton and iron: Validation of a global three-dimensional ocean biogeochemical model. Deep Sea Research II, 50, 3143–3169

Grotti, M., Soggia, F., Abelmoschi, M.L., Rivaro, P., Magi, E., Frache, R., 2001. Temporal distribution of trace metals in Antarctic coastal waters. Marine Chemistry, 76 (3), 189-209

Grotti, M., Soggia, F., Dalla Riva, S., Magi, E., Frache, R, 2003. An *in situ* filtration system for trace element determination in suspended particulate matter. Analytica Chimica Acta, 498, 165-173

Guéguen C., Belin C., Thomas B.A., Monna F., Favarger P.-Y., and Dominik J., 1999. The effect of freshwater UV-irradiation prior to resin preconcentration of trace metals. Analytica Chimica Acta, 386, 155-159

Gunn, B.M., Coy-Yll, R., Watkins, N.D., Abranson, C.E., Nougier, J., 1970. Geochemistry of an Oceanite-Ankaramite Basalt Suite from East Island, Crozet Archipelago. Contributions to Mineralogy and Petrology, 28, 319-339

Halstead, M.J.R., Cunninghame, R.G., Hunter, K.A., 2000. Wet deposition of trace metals to a remote site in Fiordland, New Zealand. Atmospheric Environment 34 (4), 665-676

Hart, T.J., 1934. On the phytoplankton of the southwest Atlantic and the Bellingshausen Sea 1921-31, Discovery Reports, VIII, 1-268, 1934

Harvey, H. W., 1938. The supply of iron to diatoms. Journal of Marine Biology Association U.K., 22, 205-219

Hatje, V., 2003. Particulate trace metal and major element distributions over consecutive tidal cycles in Port Jackson Estuary, Australia. Environmental geology, 44, 231-239

Helmers, E., 1996. Trace metals in suspended particulate matter of Atlantic Ocean surface water (40°N to 20°S). Marine Chemistry, 53, 51-67

Henjes, J., Assmy, P., Klaas, C., Verity, P., Smetacek, V., 2007. Response of microzooplankton (protists and small copepods) to an iron-induced phytoplankton bloom in the Southern Ocean (EisenEx). Deep-Sea Research I, 54, 363–384

Hirata, S., Yoshihara, H., Aihara, M. 1999. Determination of iron(II) and total iron in environmental water samples by flow injection analysis with column preconcentration of chelating resin functionalized with N-hydroxyethylethylenediamine ligands and chemiluminescence detection. Talanta, 49, 1059- 1067

Hirayama, K., and Unohara, N. 1988. Spectrophotometric catalytic determination of an ultratrace amount of iron (III) in water based on the oxidation of N,N-dimethyl-p-phenylenediamine by hydrogen peroxide. Analytical Chemistry, 60, 2573-2577.

Hoffmann, L.J., Peeken, I., Lochte, K., Assmy, P., Veldhuis, M., 2006. Different reactions of Southern Ocean phytoplankton size classes to iron fertilization. Limnology and Oceanography, 51, 1217-1229

Holeton, C.L., Nédélec, F., Sanders, R., Brown, L., Moore, C. M. M., Stevens, D.P., Heywood, K.J., Statham, P.J., and Lucas, C., 2005. Physiological state of phytoplankton communities from the Southwest Atlantic sector of the Southern Ocean, as measured by fast repetition rate fluorometry. Polar Biology, 29: 44-52.

Honjo, S., Francois, R., Manganini, S., Dymond, J., Collier, R., 2000. Particle fluxes to the interior of the Southern Ocean in the Western Pacific sector along 170 degrees W. Deep-Sea Research II, 47, 3521–3548

Hutchins, D. A., DiTullio, G. R., and Bruland, K. W., 1993. Iron and regenerated production: evidence for biological iron recycling. Limnology and Oceanography, 38, 1242–1255

Hutchins, D.A., Witter, A.E., Butler, A., and Luther III, G.W., 1999. Competition among marine phytoplankton for different chelated iron species. Nature, 400, 858-861

Jickells, T.D., and Spokes, L.J., 2001. Atmospheric iron inputs to the oceans. In: The Biogeochemistry of Iron in Seawater. Turner D.R., and Hunter K.A., Chichester, John Wiley & Sons, IUPAC 7, 85-121

Jickells, T.D., An, Z.S., Anderson, K.K., Baker, A.R., Bergametti, G., Brooks, N., Cao, J.J., Boyd, P.W., Duce, R.A., Hunter, K.A., Kawahata, H., Kubilay, N., La Roche, J., Liss, P.S., Mahowald, N., Prospero, J.M., Ridgwell, A.J., Tegen, I., Torres, R., 2005. Global Iron Connections between desert dust, ocean biogeochemistry and climate. Science 308, 67–71

Johnson, K.S., Gordon, R.M., and Coale, K.H., 1997. What controls dissolved iron concentrations in the world ocean? Marine Chemistry, 57(3-4): 137-161

Johnson, K.S., Chavez F.P., Friederich, G.E., 1999. Continental-shelf sediment as a primary source of iron for coastal phytoplankton. Nature, 398,697-700

Johnson, K.S., and Karl, D.M., 2002. Is ocean fertilization credible and creditable? Science, 296, 467-468

Johnson, W.K., Miller, L.A., Sutherland, N.E., Wong, C.S., 2005. Iron transport by mesoscale Haida eddies in the Gulf of Alaska. Deep-Sea Research II, 52, 933-953

Johnson, K.S., Boyle, E., Bruland, K., Coale, K., Measures, C., Moffett, J., Aguilar-Islas, A., Barbeau, K., Bergquist, B., Bowie, A., Buck, K., Cai, Y., Chase, Z., Cullen, J., Doi, T., Elrod, V., Fitzwater, S., Gordon, M., King, A., Laan, P., Laglera-Baquer, L., Landing, W., Lohan, M., Mendez, J., Milne, A., Obata, H., Ossiander, L., Plant, J., Sarthou, G., Sedwick, P., Smith, G.J., Sohst, B., Tanner, S., Van den Berg, S., and Wu., J. 2007. Developing standards for dissolved iron in seawater. EOS, 88, 130-131

De Jong, J.T.N., Den Das, J., Bathmann, U., Stoll, M.H.C., Kattner, G., Nolting, R.F., De Baar, H.J.W, 1998. Dissolved Fe at sub-nanomolar levels in southern ocean as determined by ship-board analysis, Analytica Chimica Acta 377, 113-124

Key, R.M., Stallard, R.F., Moore, W.S., J.L. Sarmiento, J.L., 1985. Distribution and flux of ^{226}Ra and ^{228}Ra in the Amazon River estuary. Journal of Geophysical Research, 90(C4), 6995-7004

Kinugasa, M., Ishita, T., Sohrin, Y., Okamura, K., Takeda, S., Nishioka, J., Tsuda, A., 2005. Dynamics of trace metals during the subarctic Pacific iron experiment for ecosystem dynamics study (SEEDS2001). Progress in Oceanography, 64, 129-147

Korb R.E., and Whitehouse M.J., 2004. Contrasting primary production regimes around South Georgia, Southern Ocean: large blooms versus high nutrient, low chlorophyll waters. Deep-Sea Research I, 51, 721-738

Laës, A., Vuillemin, R., Leilde, B., Sarthou, G., Bournot-Marec, C., Blain, S. 2005. Impact of environmental factors on in-situ determination of iron in seawater by flow injection analysis. Marine Chemistry, 97, 347-356

Lam, P.J., Bishop, J.K.B., Henning, C.C., Marcus, M.A., Waychunas, G.A., Fung, I.Y., 2006.Wintertime phytoplankton bloom in the Subarctic Pacific supported by

continental margin iron. Global Biogeochemical Cycles, Vol. 20, No. 1, GB1006, doi:10.1029/2005GB002557

Lancelot, C., Hannon, E., Becquevort, S., Veth, C., de Baar, H.J., 2000. Modeling phytoplankton blooms and carbon export production in the Southern Ocean: dominant controls by light and iron in the Atlantic sector in Austral spring 1992. Deep-Sea Research I,47, 1621-1662

Landing, W. M., and Bruland, K.W. 1987. The contrasting biogeochemistry of iron and manganese in the Pacific Ocean. Geochimica Cosmochimica Acta, 51, 29-43

Lewis, B.L., Landing, W.M. 1992. The investigation of dissolved and suspended particulate trace metal fractionation in the Black Sea. Marine Chemistry, 40, 105-141

Lohan M.C., Aguilar-Islas A.M., Franks R.P., and Bruland K.W., 2005. Determination of iron and copper in seawater at pH 1.7 with a new commercially available chelating resin, NTA Superflow. Analytica Chimica Acta, 530, 121-129

Lohan, M.C., Aguilar-Islas, A. M., Bruland, K.W. 2006. Direct determination of iron in acidified (pH 1.7) seawater samples by flow injection analysis with catalytic spectrophotometric detection: application and intercomparison. Limnology and oceanography, methods, 4, 164-171

Löscher, B.M. 1999. Relationships among Ni, Cu, Zn, and major nutrients in the Southern Ocean. Marine Chemistry, 67: 67-102

Lucas, M., Seeyave, S., Sanders, R., Moore, C.M.M., Williamson, R., Stinchcombe, M., 2007. Nitrogen uptake responses to a naturally Fe-fertilised phytoplankton bloom during the 2004/5 CROZEX study. Deep-Sea Research II, 54, 2138-2173

Luther, G.W., Wu, J, 1997. What controls dissolved iron concentrations in the world ocean? A comment. Marine Chemistry, 57, 173-179

Macrellis, H.M., Trick, C.G., Rue, E.L., Smith, G.J., Bruland, K. W., 2001. Collection and detection of natural iron-binding ligands from seawater. Marine Chemistry 76, 175–187.

Mahowald, N., Baker, A.R., Bergametti, G., Brooks, N., Duce, R.A., Jickells, T.D., Kubilay, N., Prospero, J., Tegen, I., 2005. Atmospheric global dust cycle and iron inputs to the ocean. Global biogeochemical cycles, 19, GB4025, doi:10.1029/2004GB002402

Maldonado, M. T. and Price, N. M., 1999. Utilization of iron bound to strong organic ligands by plankton communities in the subarctic Pacific Ocean. Deep-Sea Research II, 46, 2447–2473.

Maldonado, M. T. and Price, N. M., 2000. Nitrate regulation of Fe reduction and transport by Fe-limited Thalassiosira oceanica. Limnology and Oceanography, 45(4): 814-826

Marsh, R., Mills, R.A., Green, D.R.H., Salter, I., Taylor, S., 2007. Controls on sediment geochemistry in the Crozet region. Deep-Sea Research II, 54, 2260-2274

Martin, J.H., and Gordon, R.M., 1988. Northeast Pacific iron distributions in relation to phytoplankton productivity. Deep-Sea Research I, 35, 177-196.

Martin, J.H. and Fitzwater, S.E., 1988. Iron deficiency limits phytoplankton growth in the North-East Pacific subarctic. Nature, 331: 341-343.

Martin, J.H., 1990a. Glacial-interglacial CO_2 change : The iron hypothesis. Paleoceanography, 5: 1-13.

Martin, J.H., Gordon, R.M., and Fitzwater, S.E., 1990b. Iron in Antarctic waters. Nature, 345,156-158

Martin, J.H., Fitzwater, S.E. and Gordon, R.M., 1991a. We Still Say Iron Deficiency Limits Phytoplankton Growth in the Subarctic Pacific. Journal of Geophysical Research-Oceans, 96(C11): 20699-20700

Martin, J.H., Gordon, R.M. and Fitzwater, S.E., 1991b. The Case For Iron. Limnology and Oceanography, 36(8): 1793-1802

Martin, J.H., Fitzwater, S.E., Gordon, R.M., Hunter, C.N., and Tanner, S.J., 1993. Iron, primary production and carbon-nitrogen flux studies during the JGOFS North Atlantic Bloom Experiment. Deep-Sea Research II, 40, 115-134

Martin, J.H., Coale, K.H., Johnson, K.S., Fitzwater, S.E., Gordon, R.M., Tanner, S.J., Hunter, C.N., Elrod, V.A., Nowicki, J.L., Coley, T.L., Barber, R.T., Lindley, S., Watson, A.J., van Scoy, K., Law, C.S., Liddicoat, M.I., Ling, R., Stanton, T.P., Stockel, J., Collins, C., Anderson, A., Bidigare, R.R., Ondrusek, M., Latasa, M., Millero, F.J., Lee, K., Yao, W., Zhang, J.Z., Friederich, G.E., Sakamoto, C., Chavez, F.P., Buck, K., Kolber, Z., Greene, R.M., Falkowski, P.G., Chisholm, S.W., Hoge, F., Swift, R., Yungel, J., Turner, S., Nightingale, P., Hatton, A., Liss, P.S., and Tindale, N.W., 1994. Testing the iron hypothesis in ecosystems of the equatorial Pacific Ocean. Nature, 371, 123-129

Measures, C. I., Yuan, J., Resing, J.A.. 1995. Dtemrination of Fe in sea water by flow injection analysis using in-line preconcentration and spectrophotometric detection, Marine Chemistry, 50, 3-12

Metzl, N., Tilbrook, B. and Poisson, A., 1999. The annual fCO_2 cycle and the air-sea CO_2 flux in the sub-Antarctic Ocean. Tellus, 51B, 849-861

Millero, F.J., 1989. Effect of Ionic Interactions on the Oxidation of Fe(II) and Cu(I) in Natural Waters. Marine Chemistry, 28, 1-18.

Moffett, J.W., 2001. Transformations among different forms of iron in the ocean. In: The Biogeochemistry of Iron in Seawater. Turner D.R., and Hunter K.A., Chichester, John Wiley & Sons, IUPAC 7: 343-372

Moody J.R., 1982. The sampling, handling and storage of materials for trace analysis. Philosophical Transactions of the Royal Society of London. Series A, Mathematical and Physical Sciences, 305, 669-680.

Moore, W.S., Feely, H.W., Li, Y-H, 1980. Radium isotopes in subarctic waters. Earth and Planetary Science Letters, 49, 329-340

Moore, W.S., Astwood, H., Lindstrom, C., 1995. Radium isotopes in coastal waters on the Amazon shelf. Geochimica Cosmochimica Acta, 59(20), 4285-4298

Moore, W.S., 2000. Determining coastal mixing rates using radium isotopes. Continental Shelf Research, 20, 1993-2007

Moore, J. K., Doney, S.C., Lindsay, K., 2004. Upper ocean ecosystem dynamics and iron cycling in a global three-dimensional model. Global Biogeochemical Cycles, 18, GB4028, doi:10.1029/2004GB002220

Moore, C.M., Seeyave, S., Hickman, A.E., Allen, J.T., Lucas, M.I., Planquette, H., Pollard, R.T., Poulton, A.J., 2007*a*. Iron-light interactions during the CROZet natural iron bloom and EXport experiment (CROZEX) I: phytoplankton growth and photophysiology. Deep-Sea Research II, 54, 2045-2065

Moore, C. M. M., Hickman, A.E. Poulton, A.J., Seeyave, S. and Lucas, M.I., 2007*b*. Iron-light interactions during the CROZet natural iron bloom and EXport experiment (CROZEX) II: taxonomic responses and elemental stoichiometry. Deep-Sea Research II, 54, 2066-2084

Morel, F.M.M. and Price, N.M. 2003. The biogeochemical cycles of trace metals in the oceans. Science 300:944-947

Morris, P.J., Sanders, R., Turnewitsch, R., Thomalla, S.J., 2007. ^{234}Th derived particulate organic carbon export compared to new production from an island induced phytoplankton bloom in the Southern Ocean. Deep-Sea Research II, 54, 2208-2232

Ndung'u K., Francks R.P., Bruland K.W., and Flegal A.R., 2003. Organic complexation and total dissolved trace metal analysis in estuarine waters: comparison of solvent-extraction graphite furnace atomic absorption spectrometric and chelating resin flow injection inductively coupled plasma-mass spectrometric analysis. Analytica Chimica Acta, 481,127-138.

Nédélec F. 2006. Implementation of a method to determine sub-nanomolar concentrations of iron in seawater and its application to the study of marine iron biogeochemistry at the ocean – shelf interface. Thesis. University of Southampton

Nishioka J., Takeda S., Wong C.S., and Johnson W.K., 2001. Size-fractionated iron concentrations in the northeast Pacific Ocean: distribution of soluble and small colloidal iron. Marine Chemistry, 74(2-3): 157-179.

Obata, H., Karatani, H., Nakayama, E. 1993. Automated determination of iron in seawater by chelating resin concentration and chemiluminescence detection. Analytical Chemistry, 65, 1524-1528.

Obata H., Karatani H., Matsui M., and Nakayama E., 1997. Fundamental studies for chemical speciation of iron in seawater with an improved analytical method.Marine Chemistry, 56(1-2), 97-106

Pazan, S. E. and Niiler, P. P. 2004. New global drifter data set available. Eos, Transactions, American Geophysical Union, 85 (2), 17

Perissinotto, R., Laubscher, R.K., Mc Quaid, C.D., 1992. Marine productivity enhancement around Bouvet and the South Sandwich Islands (Southern Ocean). Marine Ecology Progress Series, 88, 41-53

Planquette, H., Statham, P.J., Fones, G.R., Charette, M.A., Moore, C.M.M., Salter, I., Nédélec, F.H., Taylor, S.L., French, M., Baker, A.R., Mahowald, N., Jickells, T.D., 2007. Dissolved iron in the vicinity of the Crozet Islands, Southern Ocean. Deep-Sea Research II, 1999-2019

Pollard, R.T., Lucas, M.I., Read, J.F., 2002. Physical controls on biogeochemical zonation in the Southern Ocean. Deep-Sea Research II, 49, 3289-3305

Pollard, R.T., Sanders, R., Lucas, M.I. and Statham, P.J., 2007a. The Crozet Natural Iron Bloom and Export Experiment (CROZEX). Deep-Sea Research II, 54, 1905-1914

Pollard, R.T. Venables, H.J., Read, J.F., Allen, J.T., 2007b. Large scale circulation around the Crozet Plateau controls an annual phytoplankton bloom in the Crozet Basin. Deep-Sea Research II, 54, 1915-1929

Poulton, A., J., Moore, C.M.M., Seeyave, S., Lucas, M.I., Fielding, S., Ward, P., 2007. Phytoplankton community composition around the Crozet Plateau, with emphasis on diatoms and *Phaeocystis*. Deep-Sea Research II, 54, 2085-2105

Price N.B., 2005. The elemental stoichiometry and composition of an iron-limited diatom. Limnology and Oceanography, 50(4), 1159-1171

Read, J.F., Pollard, R.T., Allen, J.T., 2007. Crozet station M8: development of a physical environment conducive to productive success. Deep-Sea Research II, 1930-1948

Rijkenberg, M.J.A., Fischer, A.C., Kroon, J.J., Gerringa, L.J.A., Timmermans, K.R., Wolterbeck, H.Th., de Baar, H.J.W., 2005. The influence of UV irradiation on the photoreduction of iron in the Southern Ocean. Marine Chemistry, 93, 119-129

Rijkenberg, M.J.A., Gerringa, .J.A., Carolus, V.E., Velzeboer, I. and de Baar, H.J.W., 2006. Enhancement and inhibition of iron photoreduction by individual ligands in open ocean seawater. Geochimica et Cosmochimica Acta, 70(11), 2790-2805. doi:10.1016/j.gca.2006.03.004

Rose, A.L. and Waite, T.D., 2002. Kinetic model for Fe(II) oxidation in seawater in the absence and presence of natural organic matter. Environmental Science & Technology, 36(3), 433-444

Rue, E.L. and Bruland K.W., 1995. Complexation of iron(III) by natural organic ligands in the central North Pacific as determined by a new competitive ligand - quilibration/adsorptive cathodic stripping voltammetry method. Marine Chemistry, 50, 117–138

Rue, E.L. and Bruland, K.W., 1997. The role of organic complexation on ambient iron chemistry in the equatorial Pacific Ocean and the response of a mesoscale iron addition experiment. Limnology and Oceanography, 42, 901–910

Saito, C., Noriki, S., Tsunogai, S., 1992. Particulate flux of Al, a component of land origin in the western North Pacific. Deep-Sea Research, 39, 1315-1327

Saito, M.A., G. Rocap and J.W. Moffett. 2004. Cobalt and Nickel in the Peru upwelling region: A major flux of labile cobalt utilized as a micronutrient. Global Biogeochemical Cycles, 18, doi:10.1029/2003GB002216

Sanders, R., Morris, P.J., Stinchcombe, M., Seeyave, S., Venables, H.J., Lucas, M.I., 2007. New production and the *f*-ratio around the Crozet Plateau in austral summer 2004-5 diagnosed from seasonal changes in inorganic nutrient levels. Deep-Sea Research II, 54, 2191-2207

Sarthou, G., Jeandel., C., Brisset, D., Amouroux, D., Besson, T., Donard, O.F.X., 1997. Fe and H2O2 distributions in the upper water column in the Indian sector of the Southern Ocean. Earth and Planetary Science Letters, 147, 83-92

Sarthou, G., Baker, A.R., Blain, S., Achterberg, E.P., Boye, M., Bowie, A.R., Croot, P.L., Laan, P., de Baar, H.J.W., Jickells, T.D., Worsfold, P.J., 2003. Atmospheric iron deposition and sea-surface dissolved iron concentrations in the eastern Atlantic Ocean. Deep-Sea Research I, 50, 1339-1352

Sedwick, P.N., and DiTullio, G.R., 1997. Regulation of algal blooms in Antarctic shelf waters by the release of iron from melting sea ice, Geophysical Research Letters, 24, 2515–2518

Sedwick P.N., Blain, S., Quéguiner, B., Griffiths, F.B., Fiala, M., Bucciarelli, E., Denis, M. 2002. Resource limitation of phytoplankton growth in the Crozet Basin, Subantarctic Southern Ocean. Deep-Sea Research II, 49, 3327-3349

Seeyave, S., Lucas, M.I., Moore, C.M., and Poulton, A.J., 2007. Phytoplankton productivity and community structure across the Crozet Plateau during summer 2004/2005. Deep-Sea Research II, 54, 2020-2044

Sherrell, R.M., and Boyle, E.A., 1992. The trace metal composition of suspended particles in the oceanic water column near Bermuda. Earth and Planetary Science Letters, 111, 155-174

Sholkovitz E.R., 1978. The flocculation of dissolved Fe, Mn, Al, Cu, Ni, Co and Cd during estuarine mixing. Earth and Planetary Science Letters, 41(1), 77-86

Spokes, L., Jickells, T.D. and Lim, B., 1994. Solubilization of aerosol trace-metals by cloud processing – a laboratory study. Geochimica et Cosmochimica Acta, 58, 3281 – 3287

Spokes, L., Jickells, T.D. and Jarvis, K., 2001. Atmospheric inputs of trace metals to the northeast Atlantic Ocean: the importance of southeasterly flow. Marine Chemistry, 76, 319-330

Statham, P.J., German, C.R., Connelly, D.P., 2005. Iron (II) distribution and oxidation kinetics in hydrothermal plumes at the Kairei and Edmond vent sites, Indian Ocean. Earth and Planetary Science Letters, 236(3-4), 588-596

Stumm, W. 1992., Chemistry of the Solid-Water interface. Wiley, New York, 780pp.

Sulzberger, B. and Laubscher, H., 1995. Reactivity of various types of iron(III) (hydr)oxides towards light-induced dissolution. Marine Chemistry, 50(1-4): 103-115

Sunda, W.G., and Huntsman, S.A., 1995. Iron uptake and growth limitation in oceanic and coastal phytoplankton. Marine Chemistry, 50(1-4), 189-206

Sunda, W.G., and Huntsman, S.A., 1997. Interrelated influence of iron, light and cell size on marine phytoplankton growth. Nature, 390, 389-392

Sunda W.G., 2001. Bioavailability and bioaccumulation of iron in the sea. In: The Biogeochemistry of Iron in Seawater. Turner D.R., and Hunter K.A., Chichester, John Wiley & Sons, IUPAC 7, 41-84

Tagliabue, A., and Arrigo, K.R., 2006. Processes governing the supply of iron to phytoplankton in stratified seas, Journal of Geophysical Research, 111, C06019, doi:10.1029/2005JC003363

Takeda, S., and Tsuda, A., 2005. An *in situ* iron-enrichment experiment in the western subarctic Pacific (SEEDS): Introduction and summary. Progress in Oceanography, 64, 95-109

Taljaard, J.J. and Loom, H.V., 1984. Climatology of the Indian Ocean south of 35ºS. In Climate of the Ocean. In: H.v. Loom (Editor), 505-601. Elsevier, pp. 716pp.

Timmermans, K.R., Gerringa, L.J.A., de Baar, H.J.W., van der Wagt, B., Veldhuis, M.J.W., de Jong, J.T.M, Croot, P.L., Boye, M., 2001. Growth rates of large and small Southern Ocean diatoms in relation to availability of iron in natural seawater. Limonology and Oceanorgaphy, 46(2), 260-266

Timmermans, K.R., van der Wagt, B., de Baar, H.J.W., 2004. Growth rates, half-saturation constants, and silicate, nitrate, and phosphate depletion in relation to iron availability of four large, open-ocean diatoms from the Southern Ocean. Limnology and Oceanography, 49(6), 2141-2151

Tovar-Sanchez, A., Sañudo-Wilhelmy, S.A., Garcia-Vargas, M., Weaver, R.S., Popels, L.C., Hutchins, D.A., 2003. A trace metal clean reagent to remove surface-bound iron from marine phytoplankton. Marine Chemistry, 82, 91-99

Twining, B.S., Baines, S.B., Fisher, N.S., 2004. Elemental stoichiometries of individual plankton cells collected during the Southern Ocean Iron Experiment (SOFeX). Limnology and Oceanography 49, 2115–2128

Ussher, S.J., Achterberg, E.P., Worsfold, P., 2004. Marine biogeochemistry of iron. Environmental chemistry, *1*(2), 67-80, doi:10.1071/EN04053

Ussher S.J., Yaqoob M., Achterberg E.P., Nabi A., and Worsfold P.J., 2005. Effect of model ligands on iron redox speciation in natural waters using flow injection with luminol chemiluminescence detection. Analytical Chemistry, 77, 1971-1978

Van Cappellen, P. and Qiu, L., 1997a. Biogenic silica dissolution in sediments of the SouthernOcean. II. Kinetics. Deep-Sea Research II, 44, 1109-1128

Van Cappellen, P. and Qiu, L., 1997b. Biogenic silica dissolution in sediments of the Southern Ocean. I. Solubility. Deep-Sea Research, II, 44, 1129-1149

Van den Berg, C.M.G., 1995. Evidence for organic complexation of iron in seawater. Marine Chemistry, 50(1-4), 139-157

Venables, H.J., Pollard, R.T., Popova, E.E.,2007. Physical conditions controlling the early development of a regular phytoplankton bloom north of the Crozet Plateau, Southern Ocean. Deep-Sea Research II, 54, 1949-1965

Verado, D.J., Froelich, P.N., McIntyre, A., 1990. Determination of organic carbon and nitrogen in marine sediments using the Carlo-Erba NA-1500 analyser. Deep Sea Research I, 37: 157-165

Waite, D.T. and Morel, F.M.M., 1984. Photoreductive dissolution of colloidal iron oxides in natural waters. Environmental Science and Technology, 18, 860-868

Watson, A.J., 2001. Iron limitation in the Oceans. In: Biogeochemistry of iron in seawater. Turner D.R., and Hunter K.A., Chichester, John Wiley & Sons, IUPAC 7: 9-39

Weeks, D. A. and Bruland, K.W. 2002. Improved method for shipboard determination of Fe in sea water by flow injection analysis, Analytica Chimica Acta, 453, 21-32

Weinstein, S.E. and Moran, S.B. 2004. Distribution of size-fractionated particulate trace metals collected by bottles and in-situ pumps in the Gulf of Maine-Scotian shelf and Labrador sea. Marine Chemistry, 87, 121-135

Wells, M. L., Zorkin, N. G. and Lewis, A. G., 1983. The role of colloid chemistry in providing a source of iron to phytoplankton. Journal of Marine Research, 41, 731-746.

Wells M.L., and Goldberg E.D., 1991. Occurence of small colloids in sea water. Nature, 353, 342-344

Wells, M.L., Mayer, L.M., Guillard, R.R.L., 1991. A chemical method for estimating the availability of iron to phytoplankton in seawater. Marine chemistry, 33, 23-40

Wells, M.L., Smith, G.,J., Bruland, K.W. 2000. The distribution of colloidal and particulate bioactive metals in Narrangansett Bay, RI. Marine chemistry, 71, 143-163

Westerlund, S.F.G., Anderson, L.G., Hall, P.O.J., Iverfeldt, A., Vanderloff, M.M.R., Sundby, B., 1986. Benthic fluxes of cadmium, copper, nickel and lead in coastal environments. Geochimica and. Cosmochimica Acta, 50, 1289–1296

Whitfield M., 2001. Interactions between phytoplankton. Advances in Marine Biology, 41, 1-128

Wu J., Boyle E.A., Sunda W.G., and Wen L.-S., 2001. Soluble and colloidal iron in the oligotrophic North Atlantic and North Pacific. Science, 293, 847-849

Zeebe, R.E., and Archer, D., 2005. Feasibility of ocean fertilization and its impact on future atmospheric CO_2 levels. Geophysical Research Letters, 32, doi:10.1029/2005GL022449

Zubkov, M.V., Holland, R.J., Burkill, P.H., Croudace, I.W., Warwick, P.E., 2007. Microbial abundance, activity and iron uptake in vicinity of the Crozet Isles in November 2004–January 2005, Deep-Sea Research II, 54, 2126-2137

APPENDIX I:

PROTOCOL FOR THE DETERMINATION OF TOTAL DISSOLVED IRON WITH THE FIA-DPD-NTA ANALYSER

As explained in Chapter Two, the method developed is based on the catalytic oxidation of DPD by H_20_2 prior to a preconcentration step on a NTA chelating resin, this reaction being monitored with a spectrophotometer (UNICAM 7825). The behaviour of the system during a long analytical sequence may change with time due, for instance, to an increasing temperature in the laboratory which may enhance the sensitivity and induce more bubbles in the reagents stream, potential contamination of the system after analysing a contaminated sample and peristaltic tubing use.

In this appendix the instrumentation and the reagents are first described before going through the analytical process. All materials and procedures are described in great detail and some examples are also given. The instrumentation section should serve as a guideline for anybody wishing to build a similar analyser whereas the process and examples constitutes a detailed user guide.

1 Instrumentation and consumables

Peristaltic Pump: Gilson Minipuls 3, 8 channels

Peristaltic tubing: Pharmed Masterflex

Green-Green 1.85 mm (*ref*: 95706-40, Cole Palmer)

Orange-Orange 0.89 mm (*ref*: 95706-26, Cole Palmer)

Orange-Yellow 0.51 mm (*ref*: 95706-18, Cole Palmer)

Injection Valves: Two 6-ports Cheminert low-pressure valves model C22-31860 with microelectric 2-position actuator and ¼-28 fittings (VICI Valco Instruments, Thames Restek)

3 Tee-pieces Peek 3-way junctions

Tubing PTFE 1/16"od x 0.030" (0.75mm) id (M/1) (Kinesis PT 7)

Heating unit Laboratory made thermostated heating system (at 25 ± 1^{o}C)

NTA columns (Qiagen) made in Perspex (1.6 mm long, 2 mm i.d.) packed with NTA (Qiagen) resin, except for the preconcentration column, which is FIALAB factory made column (mini column assembly 2cm long MC-2CNME, and C-2CNME)

Acetic acid glacial*:* 1L, *ref* A/0410/PB15 (Fisher Scientific)

DPD: Biokemica- (HPLC) 25g (FLUKA) *ref* 07767 (Sigma Aldrich)

HCl: 2.5L, *ref* H/1190/PB17 (Fisher Scientific)

SBDW: obtained with sub-boiled Milli-Q water

Hydrogen Peroxide: 1L, *ref* H/1820/15 (Fisher Scientific)

Instrument control: National Instruments USB-6009 card

Laptop: Toshiba satellite Pro

Communication software: Software written in LabVIEW 7.1 (National Instruments Corp.) by Dr. Matt Mowlem (OED, NOCS)

Data processing Software: written in LabVIEW 6.1 (National Instruments Corp.) by Dr. F. Nédélec

2 Reagents

All reagents must be prepared in a clean wet station because of the hazards associated with them (please refer to COSHH & Risk Assessment forms for more detail). They are stored in acid-washed low density polyethylene bottles (LDPE) and prepared with sub-boiled distilled water (SBDW) to minimize contamination.

2.1 Monthly

Prepare high purity acids and water by:

Sub-boiling distilled hydrochloric acid: Q-HCl

Sub-boiling distilled acetic acid: Q-HAc

Sub-boiling distilled Milli-Q water: SBDW

High purity ammonia (Q-NH_3) and ammonium acetate (Q-NH_3Ac) solutions are made by bubbling high purity ammonia gas through water and high purity acetic acid (Q-HAc). Please follow these instructions (courtesy of Pr. P. Statham):

Before opening any valves check that tubing from ammonia cylinder to the clean wet station is in place and intact.

a) *That there is a flow of air from the lab into the clean wet station (use a light piece of tissue against the gap below the front of to check this is so*
b) *The inline PTFE filter is secured and that the perforated bubbler is sitting within the plastic bottle of SBDW in the clean wet station*

Operation:

1) *Fill 1L Teflon bottle with 750mL of SBDW*
2) *Open main valve quarter of a turn*
3) *Adjust second stage pressure to no more that 0.5 bar.*
4) *Gradually open secondary valve (attached to tube going to the bubbler) until there is a steady gentle stream of ammonia bubbles passing through the water in the bottle*
5) *Keep bubbling until saturation of the solution occurs (typically about 2.5 hours)*
6) *Periodically (every few months) check couplings to ensure they are tight*
7) *To close down the system, shut off valve to the bubbler first, then main valve to the cylinder.*

Changing cylinders:

The gas regulator should be changed outside the building, so that any trace of ammonia can be vented to the atmosphere.

Emergency procedure:

If the tubing to the wet station breaks or there is some other catastrophic leak of ammonia into the laboratory immediately vacate the room and:

1. *Activate the fire alarm*
2. *Inform the security office that there is a leak of ammonia and the fire brigade will need to be informed to bring protective clothing and breathing apparatus*
3. *Alert the safety officer.*
4. *Ask estates staff to immediately switch of makeup air to the clean lab (as this will force ammonia into the building)*

Ammonium acetate crystals are prepared in the same way, except that the Teflon bottle must be weighed prior the procedure and is then is filled with 500 mL of Q-HAc. Make sure that the Teflon tubing is down about ¾ of the way of the bottle. The crystals take a few hours to form, and be careful towards the end point otherwise the Teflon tubing will get stuck in the bottle. Once the crystals are formed, weigh the bottle and prepare a saturated solution (Q-NH_3HAc) by adding SBDW in order to get a concentration of ~16.5 M.

2.2 Daily:

The volumes of reagents below are designed for~9hours of use.

Q-HCl 1.5M: this eluting acid (1.5N) is prepared by a single distillation of trace metal grade HCl 6N followed by a dilution with SBDW, typically add 30mL of Q-HCl to 220 mL of SBDW

***0.05 M DPD*:** DPD crystals must be kept in the fridge. Add 0.55g of DPD in 50 mL of SBDW and add 75 µL of Q- HCl to slow down the oxidation.

***H_2O_2 5%*:** add 16.5 mL of 30% (v/v) H_2O_2 in 100 mL of SBDW

Acetic Acid/Ammonia buffer solution*:*

Quartz-Acetic acid (Q-HAc) is prepared by a single distillation of trace metal grade of glacial acetic acid (Fisher). Ammonia is prepared by dissolving high purity gaseous ammonia in sub-boiling distilled water, using the procedure above established by Pr. P. Statham.

Rinsing solution: add 13.5 mL of Q-NH_3HAc to 136.5 mL of SBDW and adjust to pH 3.2 with Q-HAc (typically 30mL)

Buffer: add 27 mL of Q-NH_3HAc to 123 mL of SBDW and adjust to pH 9.3 with Q-NH_3 (typically 10mL)

3 Preparation of the standards

10 µM Fe stock solution: in a polystyrene tube, add:

- 167 µL 1000 ppm Fe(III) stock standard solution (SPEX)
- 29.733 mL of SBDW
- 100 µL of Q-HCl

100 nM Fe(III) standard: add 300 µL of 10 µM to 29.7 mL of SBDW

Standard addition to LISW. Pour some LISW in a 50 mL LDPE bottle. Then prepare the standards as wanted using the 100 nM standard solution.

4 General Procedure

4.1 Cleaning the manifold

Empty the waste bottle.
Flush 1.5N Q-HCl through the manifold using the different polystyrene tubes provided (one for each tube marked as “rinse sample”, “rinse rinse”, “rinse HCl”, “rinse buffer”, “rinse DPD”, “rinse H_2O_2”). Adjust the pressure on each tube, one by one, starting with the buffer and DPD line, then HCl, then H_2O_2 and finally rinse and sample lines, increasing the pressure gradually and slowly to avoid any back pressure problem.

Flush for:
20 min at the beginning of each analysis
20 min at the end of the analysis, followed by a 10 mins rinse with SBDW.
20 min after changing anything in the manifold, e.g. columns, fitting, tubing

4.2 Warming-up

Switch on the spectrophotometer and all the valves. Make sure the wavelength is set at 514 nm. Adjust it by pressing “edit” then press the arrows to get the appropriate wavelength.

Switch on the laptop and make sure that the USB cable is plugged in correctly. Make sure that the green light of the DAQ-MX card is flashing.

Place all the reagent bottles in-line, and check that the pressure is well adjusted on each tube (4.5 rpm on the peristaltic pump).
Open LabView 7.1 and the vi entitled “IronIII_MX_II”.

The timing sequence (in ms) menu should appear and look likeFigure AI- 1: Screenshot of LAbView 7 interface Figure AI- 1. If the last two lines are still activated, then right-click on each of them, go to “Data operations” then click on “Delete Row”

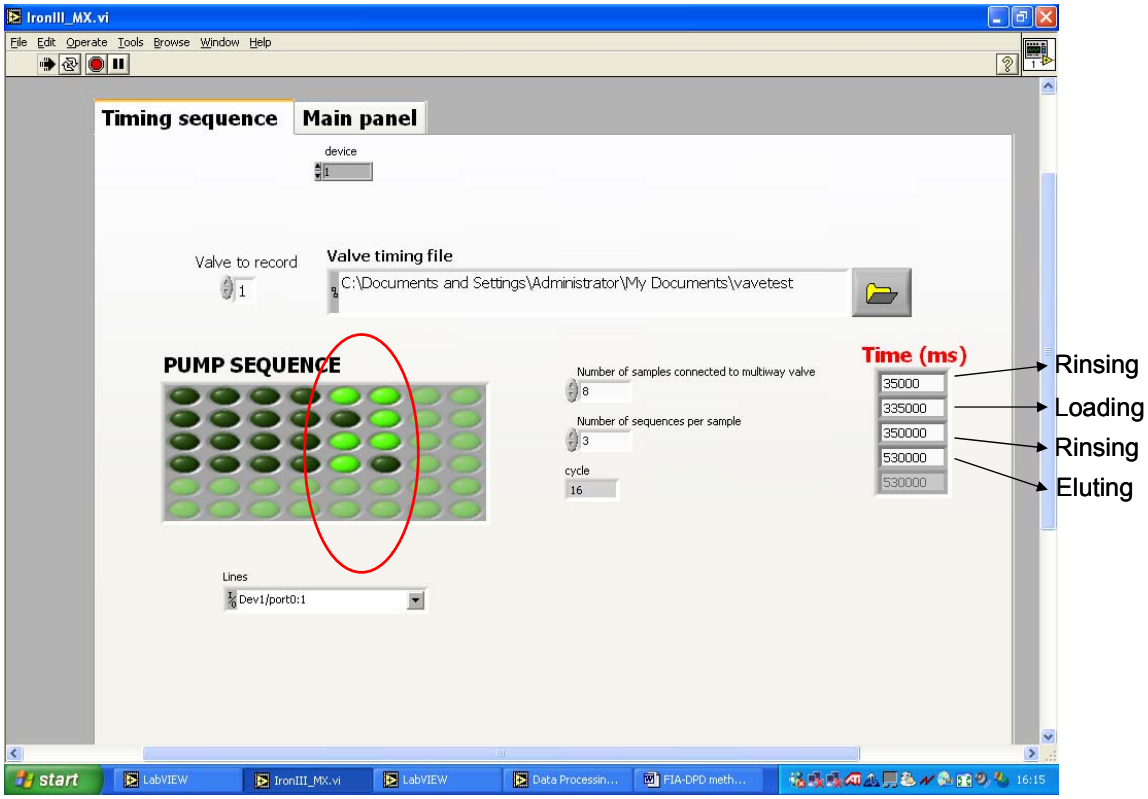

Figure AI- 1: Screenshot of LAbView 7 interface

You can change the loading time (in ms) depending on the concentration of the samples. The time of each step must be added to the previous one. Therefore make sure that you change as well the rinsing and eluting times if you change the loading time.

Example a: currently, the sequence is set up as follow:

35 000 msec rinsing

5 mins (300 000 msec) loading

25 000 msec rinsing

3 mins (180 000 msec) eluting

If you want to change the loading time to 3 mins, then the sequence to enter will be:

35000 msec rinsing

215000 msec loading

240000 msec rinsing

420000 msec eluting

Do not modify the valve sequence (circled in red) as it controls the position of the two valves between loading, eluting or rinsing modes.

In the main panel, specify a file name and make sure that the box is ticked.
Then save the "vi" by pressing on Crtl + S.

To start the analyzer, click on the arrow ("run") on the top left of the main panel. If you want to modify the loading time, click on stop (top left, next to run) and don't forget to save and specify another file name otherwise, it will be overwritten.

Use the appropriate sequence in the LabView program, depending on the range of concentrations you are working with, referring to the following indications:

RANGE	**0.05-1nM**	**1-2nM**	**2-5nM**	**5-10 nM**
Loading time	**7 min**	**4 min**	**1 min**	**15 s**

Let blanks run until the baseline is well-stabilized (typically wait for 20 min). The typical baseline value is around 0.18V and should never exceeds 0.25V.

Check that the pH of the stream is between 5.5 and 6; ideal pH is 5.6.
If not, then adjust it by adding either Q-HAc or Q-NH_3 to the buffer depending on which pH is measured.

4.3 Running the samples

Run a calibration (3 replicates), starting with two blanks, and then the lowest standard.
10 min before running a sample, add 250 µL of 30% H_2O_2 to 25mL of sample to ensure that all Fe(II) is oxidised to Fe(III).
After the calibration, run the SAFe deep certified reference material then the samples. Periodically, run the LISW internal standard.
Stop the system by clicking firstly on the **"START"** button and then on the **"STOP"** button at the end of a cycle.
If for one reason or another, some contamination is observed, then change the reagents and their bottles and start the whole procedure again (see Section 5 of this appendix for troubleshooting).

After each day of analysis, wash the whole system following the procedure described above. Release the pressure on all the peristaltic pump tubes after removing the tubing from the reagent bottles
Switch off everything (Gilson, heating, white extension lead, laptop)

5 Troubleshooting

This section presents 3 typical problems that may occur with the analyser.

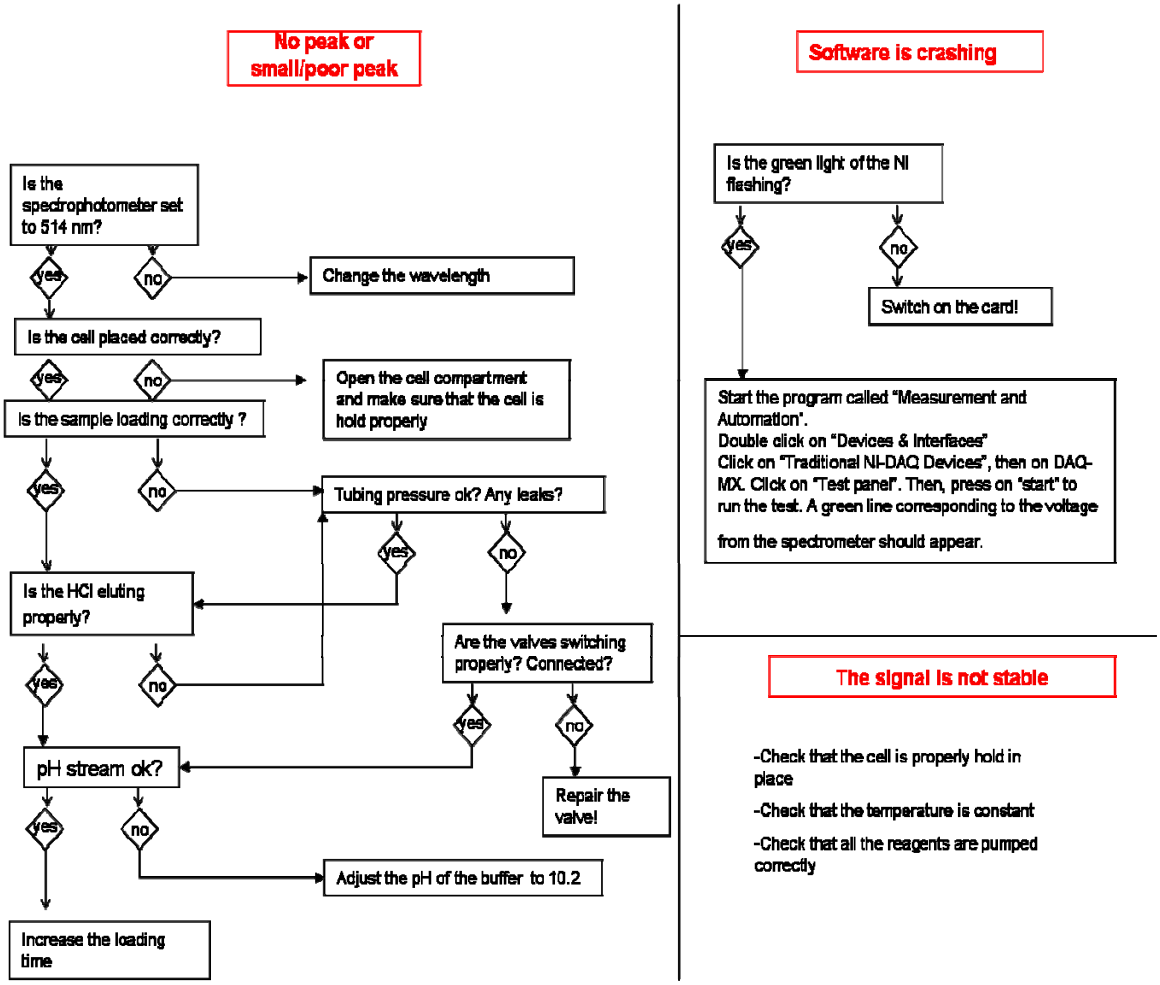

6 Alternative version of the analyser

If only one valve is available (or the second one broken!), it is still possible to do some analysis, by modifying slightly the manifold and the Labview sequence, by reducing the number of lines by two and using just one valve (i.e use the first column in the LabView program). For this you will need to deselect the second column: right-click on it, go to "Data operations" then click on "Delete entire column". Follow the same procedure for deselecting the two last rows.

The reagents remain the same.

The modified manifold is drawn on the figure below:

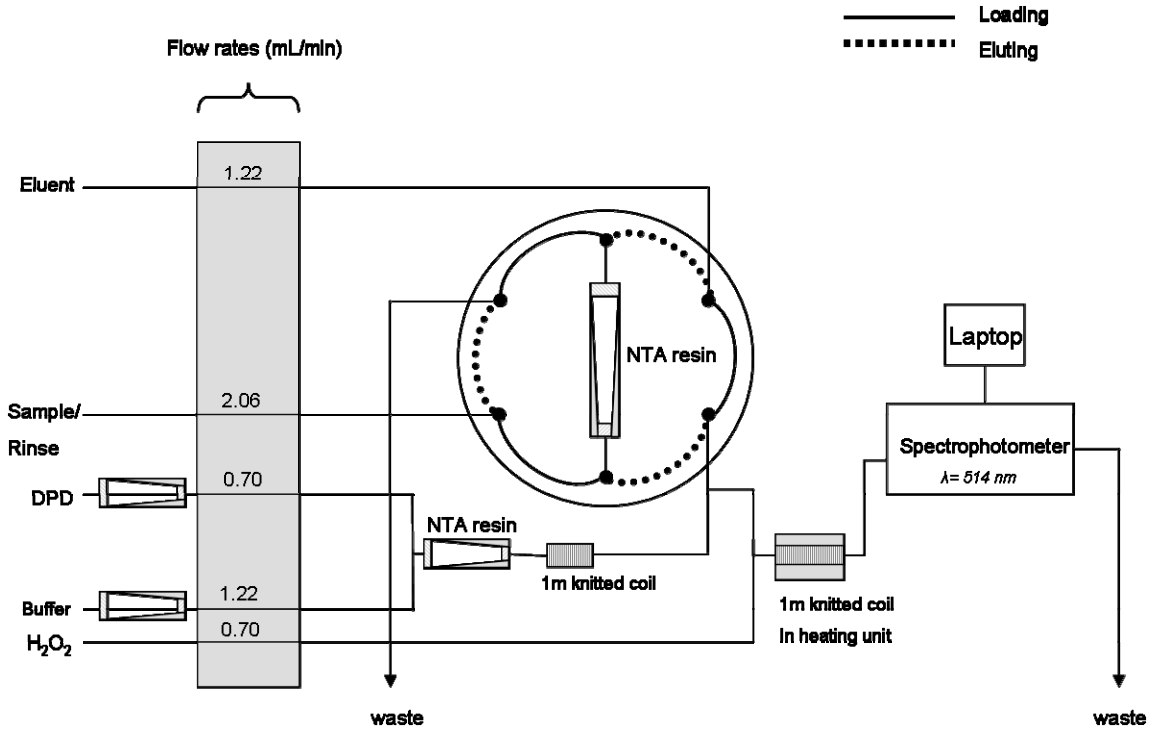

The sequence remain the same, there is just the need to change the sample and the rinse lines to match the sequence loading/rinsing.

Example b: if you want to apply the same sequence as in example a, you will enter:

-385000 msecs which corresponds to a rinsing/loading/rinsing sequence of 35000, 300000 msec and 25 000 msec during which you will have to: let the rinsing line for 35000 msec (35 s), change to the sample line for 300000 msecs (5 mins) then let the rinsing line for 25000 msec (25s). Which is equals to let the rinsing line in place for 230 sec (1min 50') and the sample line for 5 mins after the 1st cycle.

-530000 msecs, which corresponds to 180s eluting time.

7 Data processing (after Nédélec et al., 2006)

All files generated by the LabView program are text files. These files can easily be imported in Excel.

Raw data files produced during analyses are 1-column data files, where the first column is the spectrophotometer signal (in Volts). These files can be very big and would have to be split in several files before being imported in Excel as Excel spreadsheets are limited in the number of rows (32000). The LabView 6.1 software designed by Dr. Nédélec during

her PhD is used here as an alternative to calculate the peak area before being imported in Excel.

Open “Data processing area” from the LabView 6.1 menu. The chart space should be empty (black) when opening the vi.
Click on the white arrow on top-right of the screen, a window then opens asking which file to open, select a file, click OK, the data is then loaded. The screen should look like this:

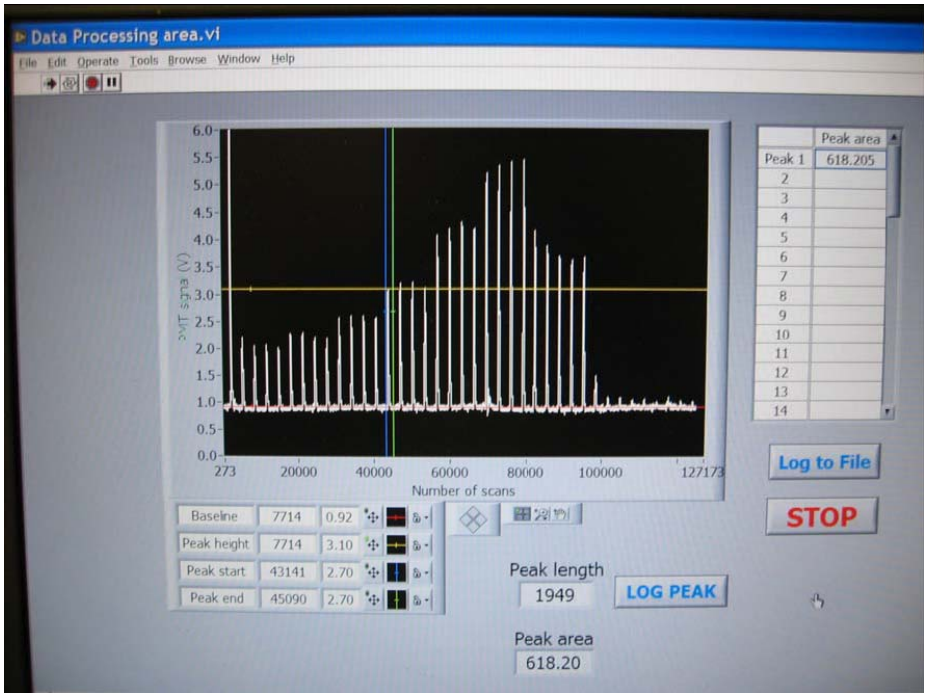

On the bottom left of the chart are the readings of the different axes:

- Red line = Baseline
- Yellow line = Peak height
- Blue line = Peak start
- Green line = Peak end

Under the chart is a small display of the different options :

- The cross + is to drag the axis to the position wanted
- The middle one is a zoom function
- The hand is to go from one peak to another by dragging the chart

In the bottom middle of the screen are: “**peak length**” corresponding to the number of scans between [peak start] and [peak end]; the instant reading of “**peak area**”; a button to “**LOG PEAK**” in a table when axis are placed properly on the chart.

In the top right of the screen is the table where logged peaks are displayed.
Under the table are: the button to save the table in a file ("**Log To File**"); and to stop the program when finished ("**STOP**")

Click on the middle button of the chart options to zoom on one peak (*only the base of the peak is needed*)
Click on the cross icon to be able to drag the axis. If the axis is not shown after zooming, call it: left-click on the cross of the axis wanted in the chart caption and select "**bring to center**"
Drag the axis at their position :

- The baseline (red) at the baseline level after the peak;
- The peak start (blue) where the signal increases from the baseline level;
- The peak end (green) where the signal comes back to the baseline level.

The peak length should not exceed 834 (end of detection for a 5 mins loading sequence) and it is preferable to avoid taking in account bubbles shown in the baseline after the peak and take the end of the peak before the bubble if the signal was already back to the baseline level.
When axes are positioned, click on the "**LOG PEAK**" button once to record the peak area measured in the table. The value saved is then shown for peak 1 in the table at the top right corner.
*NB: If the "**LOG PEAK**" button is pressed twice then the peak area will be logged twice. There is no way to erase this, the alternative is to start from the beginning again or taking notes that the peak was logged by mistake twice or if the wrong peak was measured* **!!**

Click then on the "hand" icon to drag the chart to the next peak and start the same procedure. When all peaks have been logged in the table, click on the "**Log To File**" button. A window will appear asking where to save the file. The file should be named as: **Calib*[date]*ToExcel** for a calibration, and **Samples*[location]* To Excel** for samples

*NB: It is possible to open a new file afterwards, but the table needs to be emptied before logging new peaks otherwise new data will be logged on the same file. To empty the table, left-click on the table and select "**Empty Table**". Then start logging peaks.*

When finished, press the "**STOP**" button and close the program.The new file is a text file of 1 column with peak areas which can be imported in Excel.

Open **Excel** and the file "**Calib_spreadsheet.xls**" or "**CTDSamples_spreadsheet.xls**" (My documents/CROZEX/data/)
Open the file prepared as "**Calib*[date]*ToExcel**" or "**Samples*[location]*ToExcel**" (Select "All files" for "Files of Type:"). Press "**Finish**" at the Text Import Wizard.
Copy the column of data of the imported file in column A of the spreadsheet.
Then using the notes taken during analysis, copy and paste the peak area to the right solution analysed.
For the calibration, also check that the standards concentrations are right and the calibration will be drawn automatically. Don't forget to save the file with a new name.

APPENDIX II:

ANALYTICAL METHODS FOR DETERMINING THE ELEMENTAL COMPOSITION OF SUSPENDED PARTICULATE MATTER (SPM)

In this appendix the two-step acid attack for the release into solution of trace metals in SPM followed by ICP-MS analysis, the analytical processes for POC/PON and the preparation for SEM imaging are described. The rationale for the choice of leach methods is given in Chapter Two. All these methods were applied in this thesis and led to the results presented in Chapter Four.

1 Consumables

Acetic acid glacial*:* 1L, 99.8%, Primar grade (Fisher Scientific)
Hydrofluoric acid: 500 mL, 49%, Optima grade (Fisher Scientific)
Nitric Acid: 1L, Primar grade (Fisher Scientific)
Sub Boiled Distilled Water: obtained with sub-boiled distilled Milli-Q water

Sulphurous acid: 2.5L, Laboratory reagent grade (Fisher Scientific)

Centrifuge tubes: box of 500, 10 mL (Sarstedt)

Cyclopore filters: Whatman Cyclopore 0.4 µm pore size, box of 100 (Fisher Scientific)

Standards for ICP-MS analysis (SPEX)

Silver cups: box of 200, 12.5 x 5 mm (Elemental Microanalysis Ltd)

Polysulfone filtering unit

Clean Teflon pots

Gridded tray: Microplate Millipore MultiScreen 96 well polypropylene tray cell (Fisher Scientific)

Tweezers: clean plastic (for trace metals) and stainless steel (POC/PON)

Foil

1. Sequential Leaching – detailed protocol

After collection, the folded filters were stored frozen until analysis. All the following operations were performed in a clean laboratory (Class 100), A general overview of the processes is shown in the figure below.

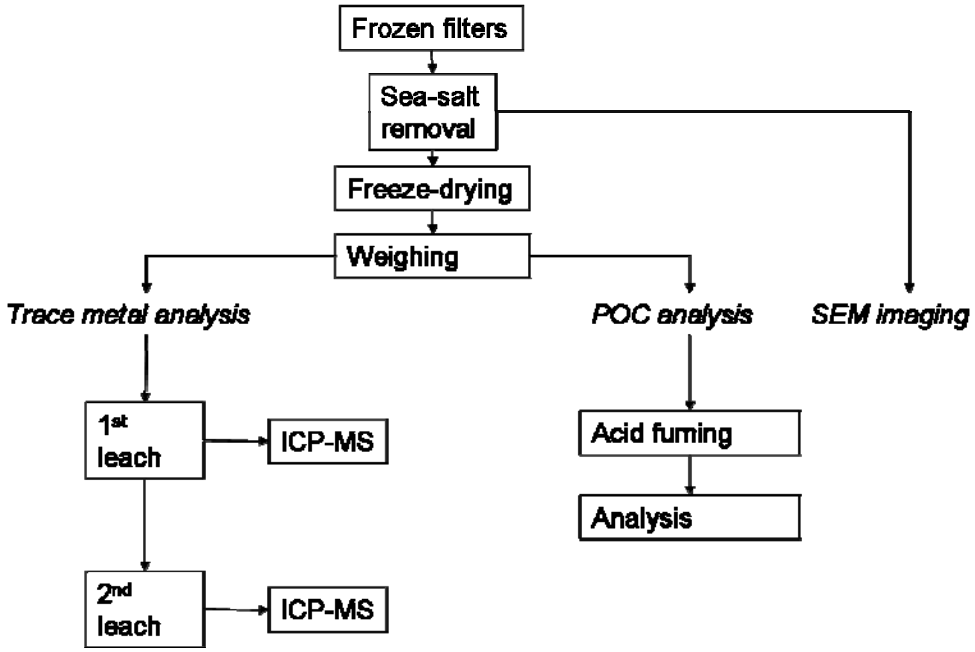

Figure AII- 1 Flow diagram of the processes involved for the determination of the elemental composition of SPM

1.1 Sea salt removal

- Wash off all the material from the nylon mesh with a known volume of SBDW using clean plastic tweezers above a polysulfone filtration unit loaded with a 0.4 µm clean and pre-weighed Cyclopore filter. Whilst rinsing, pipette out 20 µL onto another Cyclopore filter (0.2 µm pore size) for Scanning Electron Microscopy (see Section 5 of this appendix), that will be kept in the fridge until analysis.
- Freeze dry the nylon mesh overnight then weigh it and by comparison with the initial dry weight determine if there is any significant loss of material that may have been locked up in the pores of the filter.
- Freeze dry the Cyclopore filter for 12 hours and weigh it to determine the mass of material collected (m). Take a small sub-sample, typically 1.5 mg into a pre-ashed and pre-weighed silver cup for particulate organic carbon and nitrogen (POC/PON) analysis, and reweigh to have an accurate mass of SPM.

1.2 1st Leach: 25% acetic acid leach

- 25 % Acetic acid solution is made from some sub-boiled distilled acetic acid and sub-boiled distilled water
- In clean Teflon pots (15 mL), add a known volume of 25% Acetic acid to the Cyclopore filter that will fully cover the filter and leave it for 2 hours at room temperature.
- Pour the solution into a 10 mL clean centrifuge tube and centrifuge at 2500 rpm for 15 minutes.
- Transfer the overlying solution to clean Teflon pots (30 mL screw cap) and take it to dryness on a hotplate (110°C). Add 4 mL of 2% Q-HNO_3 to the residues then keep this solution for analysis on the ICP-MS.
- Pre-weigh another series of clean Teflon pots that are going to be used to contain the refractory residue from the 1st leach. Rinse out the tube the refractory residue with SBDW directly into the pot (15 mL; screw cap) then dry it on a hot plate at 140°C, to be ready for the second leach.

1.3 Total digest

- After the 1st leach, the refractory fraction is brought into solution by a total digestion using aqua regia and hydrofluoric acid (HF), which completely releases the trace elements including those in the aluminosilicate phases
- The reagents (HCl, HNO_3, HF) used in the dissolution procedures must be all high purity, or double-sub-boiled distilled acids (HCl, HNO_3). All operations must be performed in a clean room.
- Add 2.4 mL of concentrated aqua regia, and heat for 24 hours at 140°C, Teflon pots capped.
- Taken to dryness at 140°C on a hot plate
- Add 2 mL of concentrated hydrofluoric acid (HF) and 0.3 mL of nitric (HNO_3) acid. Let the solution dissolve at 140°C for 24 hours.
- If any residual organic matter after the previous step is noted, further digest it by a heating evaporation cycle with more HNO_3 and HF as necessary
- Add 2mL of 6M HCl and heat for 24 hours at 140°C to drive off the fluorides, Teflon pots capped.
- Take the solution to dryness at 140°C on a hot plate
- Prepare the final digest solutions: add a known mass of 2% HNO_3 to the residues and keep the resulting solution in clean 15mL LDPE bottles (Nalgene) until analysis.
- Prepare some blank solutions (4) and treat them in the same manner as the samples.

The solutions are ready for inductively coupled plasma mass spectrometry (ICP-MS) analysis.

2 ICP-MS analysis

The analyses of the solutions were performed on a AGILENT 7500cx series mass spectrometer with an integrated auto sampler and an octopole reaction cell.

Because the response of the mass spectrometer in counts per second is directly proportional to the concentration of a given element in a sample, it is relatively easy to calibrate the system using a series of external standards of differing concentrations. It is therefore crucial to determine which elements are to be determined then to prepare a mixed standard solutions containing every element that are to be analyzed and within the range of concentrations expected.

2.1 Preparation of mixed standards and internal standard solutions

For this work, the mixed standards were prepared in the range of 0.1 to 200 ppb .To do so, prepare the following solutions:

- 2% nitric acid solution: 10 mL of concentrated sub-boiled distilled nitric acid + 490 mL of SBDW

- 50 ppm mixed standard solution from 1000 ppm stock standards: 0.5 mL of each standard made up to 10mL with SBDW

- 1 ppm mixed standard solution from 50 ppm mixed standard: 200 µL of 50 ppm + 9.80 mL of 2% nitric acid solution

- 100 ppb solution from 1 ppm mixed standard: 100 µL of 1 ppm + 9.9 mL of 2% nitric acid solution

- finally, make up *0.1 and 1 ppb using 10 ppb solution*; 5 and 10 ppb using 100 ppb standard and **50,100 and 200 ppb from 1ppm solution**. The volumes to use are shown in the table below:

	Blank	*0.1 ppb*	*1 ppb*	5 ppb	10 ppb	**50 ppb**	**100 ppb**	**200 ppb**
Mixed standard	-	*100 µL*	*1 mL*	0.5 mL	1 mL	**0.5 mL**	**1 mL**	**2 mL**
2% nitric acid solution	10 mL	*9.9 mL*	*9 mL*	9.5 mL	9 mL	**9.5 mL**	**9 mL**	**8 mL**

Table AII- 1 Volumes of mixed standard solution and 2% nitric solution necessary for the preparation of the calibration.

Tuning solution was a 10 ppb solution of Li, Y, Ce, Tl and Co in 2% HNO_3 solution and the rinsing solution was (2.5% HNO_3 + 0.5 HCl solution The argon flow was set up at 0.95L min^{-1}.This series was designed to cover the range of concentrations encountered with the samples from CROZEX. If one sample is found to fall significantly outside of this range, it will be diluted by a greater factor and run again.

It is also necessary to prepare an internal standard which consists of one or more elements that are known to be absent or present at negligible concentrations in the sample. They are added to each sample at a known concentration so that any variation in the intensity of their signal can be used to correct the data for other elements. This correction is usually

made automatically by the software. To prepare the internal standard, follow this protocol:

- Prepare the internal standard solution: 400 ppb of Rh and Bi.
    - Prepare first a 100 ppm Rh/Bi solution from 1000 ppm stock standard: 1mL of each + 8 mL of 2% nitric solution
    - 400 ppb solution from 100 ppm standard: 0.2 mL of 100 ppm standard + 49.8 mL of 2% nitric solution.

2.2 Running the samples on the ICP-MS

The first thing to do is to load the method where the calibration parameters and interference corrections are defined. The pumping times are also set up at this stage. The pumping times were: the sample was loaded for 30 s followed by a stabilization time of 30s. The pump speed was 30 rps (round per second). After analysis, the sample line was rinsed for 30 s in SBDW then for 60 s in 5% nitric solution to ensure no carry over of sample or standard.

The analytical ICP-MS sequence was programmed as follows:

- Run two blanks
- Run the series of standards
- Run two blanks
- Run the samples
- Every 15 samples run one blank, one standard (e.g. 10 ppb), one blank

The data processing procedure includes linear drift correction, interference corrections, instrument blank subtraction, calibration with international standards and a dilution correction. All these corrections are done automatically by the software provided.

Usually a dilution factor of 10 was applied to the first leach samples, and a dilution between 40 to 1600 for the total leach samples. Note that the mass of material removed for POC/PON analysis must be subtracted for the final calculation of concentrations. Accuracy, precision and blanks are reported in Chapter Two.

3 Particulate Organic Carbon and Nitrogen analysis

As seen in Section 1 of this appendix, the samples were collected directly in pre weighed and combusted silver cups. The samples need to be manipulated with tweezers above a surface covered with combusted foil to get a clean surface to work on.

Based on a modified version of the Verado et al. method (1990), samples are first fumigated with concentrated sulphorous acid in a vacuum desiccator for 48 hours. To do so, in a plastic desiccator (without the desiccant), pour some concentrated sulphurous acid (fresh) directly in the bottom of the desiccator, then place the silver cups on the plastic tray above the acid. As this acid is very noxious, this work has to be done in a fume hood. The silver cups containing the samples must be fumed under vacuum for 48h.
After this, dry samples again at 60°C for a further 48 hours but leave them in the drying oven until you are ready to pellet them.
Pellet the silver cup at the correct size to get the sample into the POC analyzer auto sampler.
Once samples have been pelleted, keep them in a gridded tray (96 places).
POC and PON were measured using a Carlo-Erba NA-1500 elemental analyzer by Bob Head from Plymouth Marine Laboratory, after standardization with acetanilide. The relative standard deviation of analytical replicates was <13% (n = 3) for both POC and PON. Procedural blanks for C and N demonstrated that sample contamination was negligible (<1%) (B. Head, pers. comm.).

4 Scanning Electron Microscopy

Prior to examination under the SEM, aliquots (typically 60 µL) are gently pipetted onto 25mm polycarbonate filters (pore size – 0.2µm) whilst rinsing out the cyclopore filters with SBDW. The filters are then sliced into quarters and mounted onto 25mm aluminium SEM stubs layered with an adhesive carbon coating. The samples are subsequently coated with 20nm of gold using a Hummer VI-A gold sputter coater.
Imaging and analysis are undertaken using a Leo 1450VP Scanning electron microscope. Backscatter electron images are obtained with operating conditions using a voltage of 20kV with a nominal probe current of 500pA, and a working distance of 19mm.

APPENDIX III:

PUBLISHED PAPER IN DEEP-SEA RESEARCH II

DISSOLVED IRON IN THE VICINITY OF THE CROZET ISLANDS, SOUTHERN OCEAN

Available online at www.sciencedirect.com
ScienceDirect
Deep-Sea Research II 54 (2007) 1999–2019
DEEP-SEA RESEARCH PART II
www.elsevier.com/locate/dsr2

Dissolved iron in the vicinity of the Crozet Islands, Southern Ocean

Hélène Planquette[a,*], Peter J. Statham[a], Gary R. Fones[b], Matthew A. Charette[c], C. Mark Moore[d], Ian Salter[a], Florence H. Nédélec[a], Sarah L. Taylor[a], M. French[e], A.R. Baker[e], N. Mahowald[f], T.D. Jickells[e]

[a]National Oceanography Centre, University of Southampton, Southampton SO17 3ZH, UK
[b]School of Earth and Environmental Sciences, University of Portsmouth, Burnaby Building, Burnaby Road, Portsmouth PO1 3QL, UK
[c]Woods Hole Oceanographic Institution, Woods Hole, MA 02543, USA
[d]University of Essex, Colchester CO4 3SQ, UK
[e]School of Environmental Sciences, University of East Anglia, Norwich NR4 7TJ, UK
[f]National Centre for Atmospheric Research, P.O. Box 3000, Boulder, CO 80307, USA

Received 17 October 2006; received in revised form 30 March 2007; accepted 26 June 2007
Available online 27 September 2007

Abstract

The annual phytoplankton bloom occurring north of the Crozet Plateau provides a rare opportunity to examine the hypothesis that natural iron fertilization can alleviate high-nutrient low-chlorophyll (HNLC) conditions normally associated with the Southern Ocean. Therefore, during CROZet natural iron bloom and EXport experiment (CROZEX), a large multidisciplinary study performed between November 2004 and January 2005, measurements of total dissolved iron ($D_{Fe} \leqslant 0.2\,\mu m$) were made on seawater from around the islands and atmospheric iron deposition estimated from rain and aerosol samples.

D_{Fe} concentrations were determined by flow injection analysis with *N*,*N*-dimethyl-*p*-phenylenediamine dihydrochloride (DPD) catalytic spectrophotometric detection. D_{Fe} concentrations varied between 0.086 and 2.48 nM, with low values in surface waters. Enrichment of dissolved iron (>1 nM) at close proximity to the islands suggests that the plateau and the associated sediments are a source of iron. Waters farther north also appear to be affected by this input of coastal and shelf origin, although dissolved iron concentrations decrease as a function of distance to the north of the plateau with a gradient of ~0.07 nM km^{-1} at the time of sampling. Using lateral and vertical diffusion coefficients derived from Ra isotope profiles and also estimates of atmospheric inputs, it was then possible to estimate a D_{Fe} concentration of ~0.55 nM to the north of the islands prior to the bloom event, which is sufficient to initiate the bloom, the lateral island source being the largest component. A similar situation is observed for other Sub-Antarctic Islands such as Kerguelen, South Georgia, that supply dissolved iron to their surrounding waters, thus enhancing chlorophyll concentrations.

Keywords: Dissolved iron, Crozet Islands, Southern Ocean, HNLC

1. Introduction

The hypothesis that iron (Fe) can act as a limiting micro-nutrient in high-nutrient low-chlorophyll

*Corresponding author.
E-mail address: hfp@noc.soton.ac.uk (H. Planquette).

0967-0645/$ - see front matter © 2007 Elsevier Ltd. All rights reserved.
doi:10.1016/j.dsr2.2007.06.019

(HNLC hereafter) regions is now generally accepted and has been investigated on a number of occasions (Boyd et al., 2000, 2007; de Baar et al., 2005). The Fe hypothesis originally proposed by Martin (1990) has led to numerous studies that all demonstrate that the addition of Fe to HNLC waters causes an increase in phytoplankton productivity. Subsequent investigations into Fe's role in phytoplankton physiology also have revealed important findings. Among them, one can cite its role in photosynthetic and respiratory electron transport, nitrate reduction, and chlorophyll synthesis (Sunda and Huntsman, 1995, 1997). The broader implication is that in HNLC waters, the presence of Fe can increase the efficiency of the biological pump and promote drawdown of atmospheric carbon dioxide (CO_2) (Bakker et al., 2001, 2005; Boyd et al., 2004; Law et al., 2006; Martin, 1990).

The Southern Ocean is subjected to these HNLC conditions and is depicted as the largest potential sink of anthropogenic CO_2 in the global ocean (Martin, 1990; Tréguer and Pondaven, 2001) and as a key system in the context of climate change (Sarmiento et al., 1998). However, due to the existence of distinct regional sub-systems differing in their physical and biological properties (Arrigo et al., 1998; Tréguer and Jacques, 1992), this ocean should not be viewed as one entity.

There have been numerous scientific investigations conducted over the last decade to try and understand the relationship between Fe and the biogeochemical functioning of HNLC regions. Recently, several *in situ* Fe-enrichment experiments in the Southern Ocean (e.g., SOIREE (Bakker et al., 2005; Boyd et al., 2000), SOFEX (Buesseler et al., 2004; Coale et al., 2004), EISENEX (Boyé et al., 2005; Croot et al., 2005)), that are summarized by de Baar et al. (2005) and Boyd et al. (2007), have highlighted the importance of Fe availability for phytoplankton communities in this region. However, as pointed out by Chisholm (2000), such artificial enrichments cannot represent natural processes effectively, since the perturbation could lead to many unintended side effects such as changing the structure of the marine ecosystem, or generating greenhouse gases other than CO_2.

Most Fe inputs to the remote global surface waters are derived from aeolian dust, with the largest sources (e.g., Saharan desert) being in the northern hemisphere (Sarthou et al., 2003). However, such atmospheric inputs are estimated to be small in the Southern Ocean (Jickells et al., 2005) although very few data exist for this region.

Sites of natural and continuous fertilization of Fe do exist where there is permanent interaction between water masses and margins of landmasses; this phenomenon is generally called "the island mass effect". Several previous studies (Croot et al., 2004a; de Baar et al., 1999; de Jong et al., 1998; Löscher, 1999; Sarthou et al., 1997) have inferred Fe-fertilized phytoplankton blooms around island systems in the Southern Ocean such as South Georgia (Korb et al., 2004; Moore and Abbott, 2002), Kerguelen (Blain et al., 2001, 2002, 2007; Bucciarelli et al., 2001), Bouvet (Croot et al., 2004a) and the Crozet Islands (Metzl et al., 1999; Sedwick et al., 2002).

Therefore, the two-leg CROZet natural Fe bloom and EXport experiment (CROZEX) cruise on *RRS Discovery* in the austral summer of 2004/2005 in the waters surrounding the Crozet Islands provided an excellent opportunity to examine how the natural sources of Fe, originating either from the islands directly or from the relatively shallow surrounding sediments, could relieve Fe stress and therefore promote phytoplankton growth, particularly by the larger cells typically responsible for the export of particulate carbon and nitrogen.

Within the Sub-Antarctic region of the Southern Ocean, between the Polar and Subtropical water masses, the volcanic Crozet archipelago located on a shallow plateau on the eastern flank of the southwest Indian Ocean ridge comprises two main islands in the east and three smaller islands 100 km to the west. The Crozet area exhibits high concentrations of chlorophyll during austral spring and summer (Fiala et al., 2003) to the north of the islands, and is particularly suited to a study of Fe distributions, because of the way in which the topography and the zonal winds constrain the local circulation patterns and the extent of the bloom (Pollard and Read, 2001; Pollard et al., 2002).

In the present paper, new data on dissolved Fe ($D_{Fe} \leqslant 0.2\,\mu m$) distributions around the Crozet Islands are presented. Particular emphasis has been placed on the sources of Fe to the upper water column, and on the different processes that drive the distribution of Fe, such as biological uptake, mixing with deeper waters, advection of Fe-rich waters from the islands and atmospheric inputs.

2. Sampling and methods

2.1. Study area

Seawater and atmospheric samples were collected during the CROZEX cruises (D285 and D286) on

board *RRS Discovery* between 3 November 2004 and 21 January 2005. The research area was located around the Îles Crozet (45°95′ and 46°50′S, 50°33′ and 52°58′E), which are the surface projections of the Crozet Plateau (~1220 km × ~600 km) situated approximately 2000 km south east of South Africa on the edge of the Southern Ocean. Stations were established for water sampling and physical observations at strategic points in areas to the north-west, north-east, in close proximity and directly south of the two main islands, Île de la Possession and Île de l'Est. The stations sampled and their positions are shown in Fig. 1 and Table 1. Station M3 was sampled several times, providing an opportunity to assess the temporal evolution of conditions at one site.

2.2. Sampling and cleaning procedures

2.2.1. Chlorophyll-a

Samples for chlorophyll-*a* (Chl *a*) analysis (100–200 mL) were filtered onto Whatman GF/F filters then extracted into 90% acetone for 24 h in a dark refrigerator before measurement on a Turner designs fluorometer (Welschmeyer, 1994).

2.2.2. D_{Fe}

Prior to the cruise, storage sample bottles were soaked in ~2% (v/v) aqueous Decon detergent for 3 days and subsequently soaked for 3 days each in 50% HCl (v/v) and 50% (v/v) HNO_3 (Fisher Scientific). In between steps, the bottles were rinsed with Milli-Q water. After removal from the acid bath, the sample bottles were rinsed with sub-boiled distilled water. The sample bottles were filled with Milli-Q water acidified with quartz sub-boiling distilled HCl (Q-HCl) and stored in clean zipper seal polyethylene bags in a class-100 clean-air laboratory. Polycarbonate filters were soaked for 2 weeks in 10% v/v Q-HCl, rinsed and stored in sub-boiled distilled water.

Water-column samples were collected with a trace-metal clean Titanium CTD (conductivity, temperature, depth) rosette system in 10-L Ocean Technical Equipment (OTE) bottles modified for trace metal sampling and processed on board in a container equipped with a class 100 laminar flow bench. After pressurizing the OTE bottles with filtered high-purity nitrogen (BOC Gases), the valves were opened and seawater was directed through an acid-washed 0.2-μm polycarbonate filter

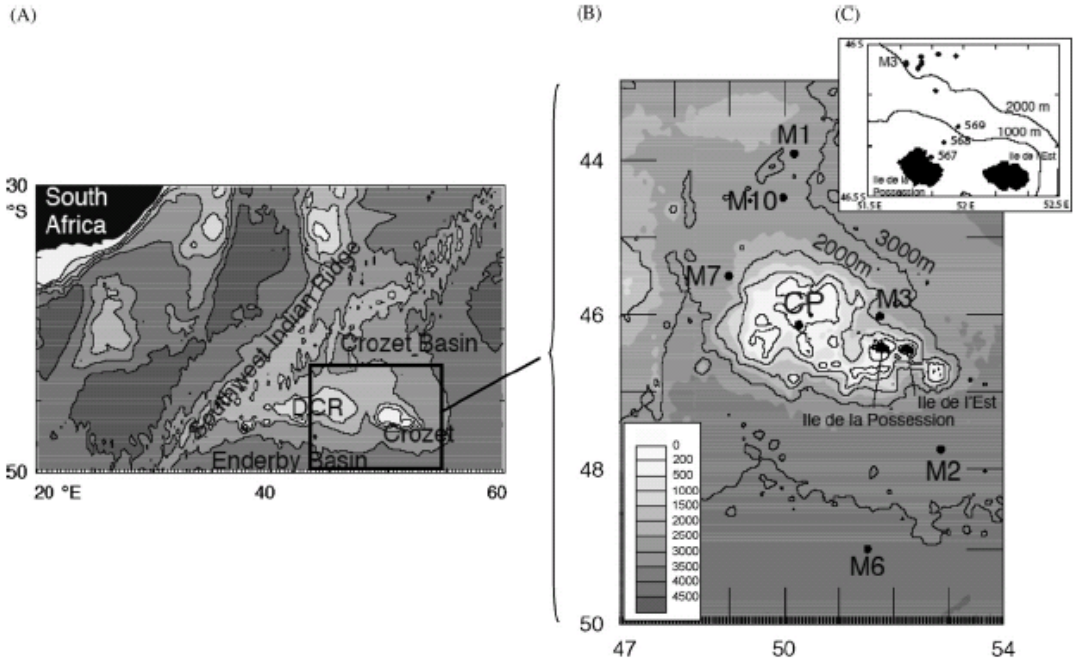

Fig. 1. (A) Location of the Crozet Islands relative to South Africa. (B) Stations sampled for D_{Fe} during D285 and D286 North and South of the Crozet plateau. (C) Detail of stations between Baie Américaine (567) on Île de la Possession and M3.

Table 1
Station locations, depth, dissolved iron concentrations (<0.2 μm), temperature, salinity, density, and Chl *a* concentrations during D285 and D286

Station details	Depth (m)	D_{Fe} (nM)	Temperature (°C)	Salinity	Density (σ_0)	Chl *a* (mg m^{-3})
M1 (491)	5	0.22	5.813	33.727	26.566	0.90
11/11/2004	10	–	5.803	33.727	26.566	0.76
43.92049°S	20	0.31	5.802	33.727	26.566	0.79
50.26742°E	40	–	5.801	33.727	26.567	0.77
3118 m	50	0.34	5.761	33.726	26.570	–
	60	–	5.769	33.727	26.571	0.73
	70	–	5.746	33.730	26.576	0.76
	110	0.38	4.417	33.890	26.882	–
	250	0.30	3.135	34.085	27.117	–
	500	0.29	2.741	34.301	27.347	–
M3.1 (496)	5	–	4.368	33.828	26.822	0.61
13/11/2004	10	–	4.371	33.829	26.822	0.87
46.06809°S	15	0.10	4.370	33.829	26.822	0.68
51.78529°E	42	0.09	4.227	33.828	26.839	1.1
2287 m	65	–	3.752	33.828	26.839	1.03
	175	0.09	3.125	33.876	26.938	–
	218	0.10	2.990	33.856	26.981	–
	300	0.12	2.858	34.008	27.114	–
M2.1 (502)	5	0.27	3.279	33.793	26.871	0.34
19/11/2004	10	0.24	3.155	33.787	26.881	0.39
47.79537°S	20	–	3.174	33.790	26.890	0.35
52.86216°E	40	0.24	3.159	33.791	26.903	0.42
3870 m	60	(4.38)a	3.160	33.801	26.912	0.43
	80	0.22	3.161	33.805	26.914	0.43
M6.1 (511)	5		2.710	33.794	26.948	0.27
22/11/2004	10	0.20	2.687	33.794	26.948	0.25
49.00557°S	20	–	2.705	33.809	26.960	0.25
51.50046°E	40	0.25	2.530	33.811	26.966	0.45
4275 m	60	–	2.572	33.812	26.974	0.27
	80	0.21	2.469	33.820	26.976	0.38
	250	0.40	1.661	33.911	27.129	–
M3.3 (516)	5	–	4.368	33.842	26.826	0.47
25/11/2004	10	–	4.370	33.842	26.826	0.48
46.05961°S	20	(2.08)a	4.369	33.842	26.826	0.49
51.79093°E	40	0.19	4.227	33.841	26.841	0.49
3986 m	60	(0.40)	3.875	33.862	26.894	0.49
	80	0.28	3.621	33.872	26.928	0.41
M7 (524)	5	–	5.530	33.816	26.675	1.34
27/11/04	10	(1.65)a	5.533	33.816	26.675	1.34
45.49943°S	15	(0.63)	5.533	33.816	26.675	1.39
49.00242°E	25	(0.73)	5.533	33.817	26.675	1.41
2749 m	35	0.29	5.528	33.818	26.677	1.38
	55	0.27	5.044	33.837	26.748	1.22
	75	0.44	3.897	33.897	26.920	–
	100	0.34	3.444	33.906	26.971	–
	125	0.23	3.132	33.921	27.013	–
	150	0.46	3.008	33.939	27.038	–
	200	0.20	2.969	34.016	27.103	–
	300	0.26	2.872	34.143	27.214	–
	400	0.46	2.706	34.223	27.293	–
	500	0.23	2.650	34.294	27.355	–

Table 1 (*continued*)

Station details	Depth (m)	D_{Fe} (nM)	Temperature (°C)	Salinity	Density (σ_0)	Chl *a* (mg m^{-3})
M10.1 (563)	5	0.48	6.126	33.786	26.578	0.80
21/12/2004	10	–	6.132	33.786	26.577	0.73
44.52528°S	15	0.40	6.142	33.786	26.576	–
49.96059°E	25	–	6.125	33.786	26.578	0.8
2943 m	35	0.31	5.998	33.787	26.595	0.81
	55	–	5.432	33.790	26.666	–
	75	0.30	4.459	33.806	26.789	0.20
	125	0.16	3.700	33.902	26.943	–
	200	0.30	3.195	34.007	27.075	0.037
BA (567)	5	1.05	4.563	33.871	26.830	0.57
22/12/2004	25	0.68	4.520	33.872	26.834	0.56
46.36854°S	50	2.16	4.370	33.883	26.863	0.54
51.82754°E	80	1.13	4.248	33.889	26.874	0.47
83 m						
BA + 1 (568)	5	0.60	4.633	33.870	26.819	0.60
22/12/2004	25	0.52	4.644	33.870	26.819	0.62
46.32332°S	50	0.56	4.605	33.870	26.823	0.62
51.89459°E	100	0.39	3.956	33.908	26.924	0.27
379 m	200	1.01	3.435	33.982	27.034	0.30
	300	2.08	2.986	34.075	27.151	0.19
	376	0.56	2.760	34.190	27.262	0.06
BA + 2 (569)	5	0.16	4.662	33.855	26.796	0.88
22/12/2004	25	0.15	4.678	33.864	26.810	1.00
46.26997°S	50	0.32	4.049	33.898	26.899	0.45
51.97083°E	100	0.15	3.669	33.962	27.007	0.18
1491 m	300	0.42	2.803	34.112	27.199	0.04
	750	0.29	2.606	34.438	27.476	–
M3.4 (572)	5	(1.71)a	5.211	33.826	26.720	1.01
22/12/2004	10	–	5.211	33.831	26.725	0.948
46.06223°S	15	–	5.211	33.831	26.725	1.01
51.78169°E	25	0.26	5.211	33.831	26.725	0.95
2375 m	35	0.38	5.212	33.831	26.725	0.97
	55	–	4.960	33.835	26.756	0.82
	75	0.26	4.427	33.852	26.829	–
	175	0.31	3.108	33.931	27.023	–
	500	0.22	2.614	34.243	27.316	–
M3.5 (592)	5	0.24	5.039	33.807	26.725	0.61
31/12/2004	10	–	5.027	33.826	26.741	0.62
46.05134°S	15	–	5.022	33.832	26.747	0.72
51.77591°E	25	0.27	4.992	33.848	26.763	0.78
2404 m	35	–	4.914	33.851	26.774	0.73
	55	0.12	4.773	33.857	26.795	0.79
	100	0.41	3.912	33.915	26.933	–
	200	0.15	3.022	34.010	27.094	–
M2.2 (605)	10	(0.52)	5.043	33.764	26.690	0.26
06/01/2005	20	–	5.041	33.764	26.691	0.30
47.80111°S	40	–	4.843	33.765	26.714	0.32
52.84952°E	50	0.09	4.809	33.766	26.719	–
3883 m	60	–	4.681	33.767	26.734	0.43
	80	–	4.212	33.773	26.789	0.72
	100	0.16	3.719	33.783	26.846	0.35
	150	–	2.488	33.844	27.008	0.13
	160	0.17	2.349	33.855	27.027	–
	200	0.11	2.035	33.910	27.097	–

Table 1 (*continued*)

Station details	Depth (m)	D_{Fe} (nM)	Temperature (°C)	Salinity	Density (σ_0)	Chl *a* (mg m^{-3})
M3.7 (622)	5	0.15	6.075	33.831	26.619	4.94
10/01/2005	10	–	6.075	33.831	26.620	5.10
46.03412°S	20	0.23	6.075	33.831	26.619	4.95
51.86656°E	40	–	5.661	33.838	26.705	3.94
2322 m	50	–	4.742	33.871	26.833	0.88
	60	–	4.288	33.897	26.889	–
	80	0.10	3.881	33.925	26.945	0.29
	100	–	3.711	33.961	27.006	–
	150	0.09	3.313	33.997	27.057	–
	200	–	3.002	34.056	27.133	–
	300	0.34	2.742	34.117	27.205	–
	400	–	2.700	34.187	27.264	–
	500	0.20	2.641	34.270	27.337	–

A dash indicates that no sample was collected; (a) denotes the sample was grossly contaminated from OTE bottle; ( ) denotes the sample is thought to be contaminated from the ship by a specific comparison with the rest of the profile. It is suggested that for future projects, CTD sampling should not be conducted so close to the stationary or slowing ship (< 30 m).

housed in a Teflon filtration unit. Clean low-density polyethylene bottles (1 L, 500 mL, Nalgene) were used to store samples after being rinsed twice with the seawater sample. After collection, samples were acidified to pH 1.7 with Q-HCl and stored for at least 2 months prior to analysis.

2.3. Analysis of total dissolved iron in seawater samples

2.3.1. Apparatus

Total dissolved Fe concentrations (D_{Fe} hereafter) were measured in acidified (pH 1.7) seawater samples, using flow injection analysis (FIA) with in-line preconcentration and spectrophotometric detection (Lohan et al., 2006; Measures et al., 1995). This method is based on the in-line preconcentration of Fe(III) on a nitriloacetic acid (NTA, Quiagen) resin, placed in a Global FIA 2-cm mini-column. Eluted Fe(III) then catalyzes the oxidation of *N*,*N*-dimethyl-*p*-phenylenediamine dihydrochloride (DPD, Sigma-Aldrich) by hydrogen peroxide (H_2O_2, Trace metal Grade, Fisher Scientific). It is assumed that all Fe(II) is oxidized to Fe(III) by the addition of H_2O_2 to a final concentration of 10 μM in the sample prior to the DPD oxidation step.

The manifold (Fig. 2) consisted of a 8-channel peristaltic pump (Gilson) with PharMed® tubes (Cole Palmer) of various internal diameters to obtain the appropriate flow rates. A 6-port valve (VICI, Valco instruments) was used in two different positions: loading/rinsing and eluting. All connecting tubing used was 0.8 mm internal diameter Teflon. The buffer/DPD and the rinsing solutions were cleaned in-line using 2 × 1 cm Global-FIA mini-columns packed with NTA Superflow resin. The pH of the solution stream was maintained at pH 5.6 with an ammonium acetate buffer, prepared with ammonium acetate crystals obtained by bubbling filtered high-purity gaseous ammonia (BOC) through sub-boiled distilled acetic acid in an ice bath. To minimize contamination, sample and reagent bottles were positioned within a class-100 laminar flow bench. Prior to analysis, the entire manifold was rinsed for 2 h with 1.5 N Q-HCl. Hydrogen peroxide solution (5%) and DPD solution (0.05 M) were prepared daily.

Absorbance was measured using a UNICAM 7825 spectrophotometer fitted with a 1-cm flow through cell. The entire system, including signal acquisition and data processing, was controlled by a Lab-VIEW (version 7.2, National Instruments Corp.) programme. The time for one analytical cycle was approximately 15 min and a minimum of two replicate analyses per sample were made.

2.3.2. Calibration and performance

The instrument was calibrated daily by analyzing acidified (pH 1.7) low-Fe seawater samples from the study area that had been spiked with a diluted Fe(III) standard solution (SPEX plasma standard). Standard additions were typically in the range 0.1–0.8 nM. Results were calculated from integration of the peak areas. Replicate analyses ($n = 2$–3) were performed for all samples and standard

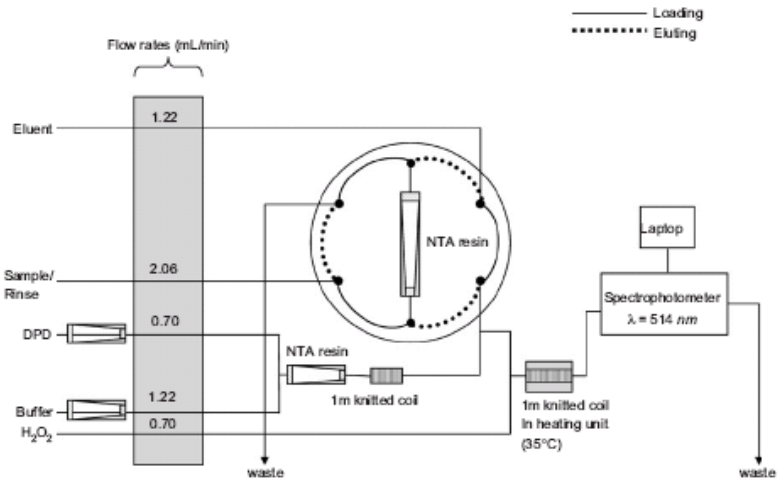

Fig. 2. FIA manifold used for the preconcentration and determination of iron in seawater.

Table 2
Aerosol sample collection details during D286 and non-sea-salt Ca (nss Ca) and soluble Si concentrations

Event	Start date	Start position	Volume collected (mL)	Fe concentration (nmol L^{-1})
CRO-R2	08/11/2004	40.63°S, 41.98°E	60	187
CRO-R3	08/11/2004	40.95°S, 43.37°E	100	6
CRO-R4	09/11/2004	41.25°S, 44.69°E	520	56
CRO-R5	18/11/2004	46.06°S, 51.79°E	250	288
CRO-R6	22/11/2004	49°S, 51.50°E	200	50
CRO-R7	30/11/2004	44.95°S, 49.94°E	130	121
CRO-R9	03/12/2004	43.12°S, 47.19°E	130	1858

solutions. Blank values varied between 0.058 and 0.09 nM, with a mean of 0.073 ± 0.016 nM and the detection limit was 0.048 nM. NASS-5 (3.71 ± 0.63 nM; our value: 3.67 ± 0.18 nM) and the reference seawater from the recent Fe intercomparison exercise (Sampling and Analysis of Fe (SAFe) SAFe deep (0.91 ± 0.09 nM; our value: 0.95 ± 0.11 nM) seawaters taken in the North Pacific at 1000 m were used for the validation of the technique and values obtained fell within the quoted ranges. As our samples were acidified for a long period of time, the risk of bias caused by a fraction of the Fe being unavailable to the resin is low as confirmed by Lohan et al. (2006) using the same technique.

2.4. Atmospheric sampling and analysis

Atmospheric sampling (Table 2) was conducted on the deck above the bridge, the highest on the ship and well forward of ship emission sources. Samples were only collected when wind and ship movements guaranteed no contamination from the ship itself. Rainwater samples (Table 3) were collected for trace metal analysis as described previously (Spokes et al., 2001) using a clean polypropylene 40-cm diameter funnel attached to a clean LDPE sample bottle. Samples were frozen immediately after collection until return to the laboratory. Before analysis by inductively coupled plasma optical emission spectroscopy (ICP-OES), defrosted samples were acidified with concentrated HNO_3 (Aristar, BDH) to an amount equivalent to 1 mL L^{-1} of sample (pH < 2) for at least 2 weeks and hence represent an estimate of total wet deposition. Aerosols were collected using a high-volume (1 m^3 min^{-1}) air sampler (Graseby-Anderson) onto cellulose (Whatman 41) 25 × 20-cm collection substrates. One-quarter of each filter was extracted in ultrapure water using

Table 3
Fe concentrations and deposition fluxes obtained from the rain samples collected during D285

Sample	Start date and time (UTC)	Start position	End date time (UTC)	End position (m^3)	Air volume ($nmol\,m^{-3}$)	nss Ca ($nmol\,m^{-3}$)	Si
CRO I 01	15/12/2004 11:00	37.47°S, 34.31°E	18/12/2004 08:43	42.50°S, 42.46°E	4049.0	0.5	0.015
CRO I 02	19/12/2004 10:58	43.07°S, 47.15°E	21/12/2004 11:10	44.77°S, 50.51°E	4497.6	2.6	0.081
CRO I 04	25/12/2004 06:55	45.94°S, 56.51°E	27/12/2004 06:55	46.00°S, 56.15°E	2897.6	0.2	0.017
CRO I 05	29/12/2004 07:10	46.00°S, 55.11°E	31/12/2004 07:35	46.06°S, 51.78°E	3027.3	0	0.015
CRO I 07	04/01/2005 07:10	49.00°S, 51.33°E	06/01/ 2005 07:45	48.23°S, 52.28°E	3004.6	0	0.011
CRO I 08	06/01/2005 07:45	48.30°S, 52.18°E	08/01/2005 07:30	46.41°S, 51.91°E	3190.7	0	0.022

1 h of ultrasonic agitation and major ions determined by ion chromatography (Jickells et al., 2003). A separate quarter was similarly extracted with 1 mM $NaHCO_3$ buffer (pH 7) for determination of soluble Si (Baker et al., 2006a). Throughout the sampling and analyses, appropriate blank and quality control procedures were used (Spokes et al., 2001; Baker et al., 2006a).

Air parcel back trajectories (Draxler and Rolph, 2003) for all rain and aerosol sampling periods show air masses had no contact with any land masses apart from Antarctica for at least the 5 days prior to collection, and hence we were sampling truly remote Southern Ocean air.

3. Results

Salinity, temperature, Chl *a* and Fe concentrations are reported in Table 1.

3.1. Hydrography, Chl a and macronutrients

3.1.1. Hydrography

Large-scale and mesoscale circulation is described in detail by Pollard et al. (2007) and Read et al. (2007) and summarized in Fig. 3. Briefly, the topography of the plateau (Park et al., 2002; Pollard and Read, 2001) significantly influences the general circulation. HNLC water masses of the Sub-Antarctic Front (SAF) intrude northwards to the west of Crozet, and are retroflected eastwards at 42°S. As a consequence, the area to the north (42°S–46°S) of the Crozet Plateau is semi-enclosed, and water that has been in contact with the Plateau is rarely transported south as indicated by trajectories of Argo profiling Floats (Pollard et al., 2007). Consequently, the spatially large bloom observed in this HNLC area is clearly constrained to the north and west by the SAF, which separates it from higher Chl *a* concentrations farther north associated with the Sub-Tropical Front and the Agulhas Return Current.

3.1.2. Chl a and nutrients

Satellite imagery based on MODIS and SeaWIFS data (Venables et al., 2007) demonstrates that the peak of the bloom occurred prior to our arrival. Commencing in mid-September, the bloom was constrained mainly to the north of the islands, bounded by the SAF, with Chl *a* concentrations reaching a local maximum of $8\,\mu g\,L^{-1}$ at the beginning of November (Venables et al., 2007).

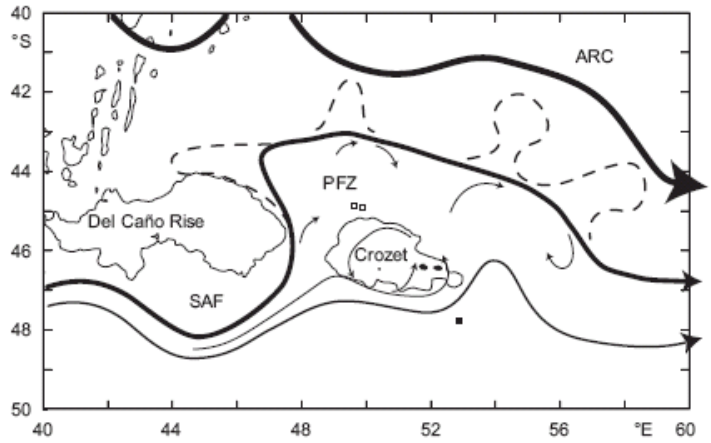

Fig. 3. Main features of circulation around the Crozet Plateau, taken from Pollard et al. (2007). *ARC: Agulhas Return Current. PFZ: Polar Frontal Zone. SAF: Sub-Antarctic Front.*

The bloom declined by the end of November, and surface Chl *a* values reached their lowest concentrations, $0.6\,\mu g\,L^{-1}$, with a maximum of $1.4\,\mu g\,L^{-1}$ close to the islands. However, in late January, further blooms were observed north of the islands.

Nitrate concentrations decreased from 24 μM south to 18 μM north of the plateau over the sampling period, and initial silicate concentrations of 18.5 μM became almost totally depleted (0.2 μM) in the region to the north of the plateau by mid-January (Sanders et al., 2007).

Phytoplankton productivity for the region followed the same general pattern as for Chl *a* distribution (Seeyave et al., 2007). Low rates ($<0.5\,gC\,m^{-2}\,d^{-1}$) were measured at Stations M2 and M6 to the south of the islands in HNLC waters, and $\sim 3\,gC\,m^{-2}\,d^{-1}$ was measured at the M3 site just to the north of the islands during the bloom in January.

3.2. Atmospheric inputs

3.2.1. Dry deposition

Aerosol samples were not specifically collected for trace metals due to sampling constraints, so we inferred atmospheric dust deposition flux (F_{dust}) using two approaches. Firstly, we used excess (non-sea-salt), aerosol calcium (nss Ca hereafter) and assumed this was associated with crustal dust (Ca content of dust $A_{Ca} = 1.6$ wt%, assuming excess Ca is 100% soluble (Croot et al., 2004b),

Table 4
Estimated terrestrial dust fluxes to the region

Analyte	Concentration ($nmol\,m^{-3}$)	Deposition flux ($nmol\,m^{-2}\,d^{-1}$)
NO_3^-	1.0±0.3	1730
NH_4^+	3.6±0.9	320
nss Ca^{2+}	0.1±0.2*	172*
	0.55±1	
Sol_{Si}	0.016±0.004*	28*
	0.027±0.027	

$n = 6$ except $^*n = 5$, one apparently anomalous result excluded.

RAM = relative atomic mass):

$$F_{dust} = \frac{F_{nss\,Ca}\,RAM_{Ca}}{A_{Ca}}. \quad (1)$$

Secondly, we used estimates of aerosol soluble Si, which we assumed to be entirely of terrestrial origin (an upper limit since seawater Si may have contributed significantly), with an assumed Si solubility (Sol_{Si}) of 0.3% (Baker et al., 2006a) and assuming the abundance of Si in (A_{Si}) dust to be 30 wt%

$$F_{dust} = \frac{F_{Si}\,RAM_{Si}}{A_{Si}\,Sol_{Si}}. \quad (2)$$

Deposition fluxes (F) were calculated from atmospheric concentrations (Table 4) assuming nitrate, excess Ca and silicate are associated with coarse-mode aerosol and ammonium with fine mode and using deposition velocities of 2 and $0.1\,cm\,s^{-1}$, respectively,

for the two modes (Baker et al., 2003). Atmospheric N deposition estimates are provided for the sake of completeness; given residual N is available in seawater throughout the season in this region, this supply from the atmosphere is not needed to support productivity.

These two approaches, using calcium and silica, gave broadly similar results (0.16 and 0.32 g dust $m^{-2} yr^{-1}$, respectively), and we therefore used a dust flux of 0.2 g $m^{-2} yr^{-1}$, which is the average of the two estimates rounded to one decimal place. This dust flux corresponds to a dry deposition flux of Fe of 127 μmol $m^{-2} yr^{-1}$, assuming dust to be 3.5% Fe (see Section 4.2 for uncertainties).

3.2.2. Wet deposition

Wet deposition of Fe (F_w) was estimated using $F_w = C\ P$, where C is the volume weighted mean concentration of Fe in the rain samples (excluding CRO-R9, which was contaminated) and P is the precipitation rate for the region. C was calculated from the Fe concentration (C_i) and volume (V_i) of each sample using

$$C = \frac{\sum C_i V_i}{\sum V_i}. \quad (3)$$

Estimating precipitation rate in this oceanic region is complicated by orographic rainfall on the islands, and no data appear to be available for Crozet. Taljaard and Loom (1984) quote precipitation estimates for the two nearest islands (Marion and Kerguelen) as 2499 and 1117 mm yr^{-1}, respectively, so we averaged these and assumed a precipitation of 1808 mm yr^{-1}. Some precipitation may fall as snow and may scavenge dust differently from rain, but we have no quantitative information with which to address this, so chose to apply this precipitation rate to the rain samples collected. This translates to a wet deposition rate for total Fe of 198 μmol $m^{-2} yr^{-1}$. The total Fe deposition is thus calculated at 325 μmol $m^{-2} yr^{-1}$ with 61% of this occurring as wet deposition. Uncertainties in these fluxes are considered in Section 4.2. Southern Ocean dust and Fe flux estimates from field campaigns are very limited, but the fluxes here are substantially lower than those of Gaiero et al. (2003) from Patagonia and comparable to those seen in the very high rainfall regions of coastal South Island, New Zealand (Halstead et al., 2000). Average rainwater Fe concentrations from Halstead et al. (2000) and Croot et al. (2005) are similar to those reported here.

3.3. Dissolved iron

Vertical profiles of D_{Fe} are shown in Figs. 4–6, and detailed in Table 1. The profiles are grouped together for three broad locations: an oligotrophic control area south of the plateau (Station M6 [511]; Fig. 4A, Station M2 [502] and [605]; Fig. 4B and C), Station M3 northeast of the plateau (Fig. 5), and Baie Américaine (BA) stations in close proximity to the plateau (569, 568, 567; Figs. 6A–C). With the exception of Baie Américaine stations, D_{Fe} concentrations for all vertical profiles are characteristically low (<1 nM), ranging from ~0.1 to 0.5 nM. The inshore stations of Baie Américaine are characterized by generally higher D_{Fe} concentrations, with maxima of ~2 nM at 50 m (Station 567, Fig. 6A) and 300 m (Station 568, Fig. 6B), respectively. Typically, we observe some D_{Fe} depletion in surface waters, while below the surface mixed layer (usually ~80 m, Venables et al., 2007), D_{Fe} concentrations were higher.

3.3.1. Southern sites (M6 and M2)

Station M6 (511, Fig. 4A) is located south of the islands in HNLC water masses that are not believed to be influenced by the plateau (Fig. 3, Pollard et al., 2007). Surface-water temperatures were close to 2 °C and the constant density down to ~125 m implies deep mixing. Consequently, D_{Fe} concentrations above this depth exhibit little variability (range 0.21–0.25 nM) while Chl *a* concentrations are also low (0.18–0.26 μg L^{-1}), both typical of Southern Ocean HNLC regions (Sedwick et al., 2002). However, below the pycnocline, there is a D_{Fe} maximum value of 0.4 nM at 250 m depth.

Station M2 (502, Fig. 4B and 605, Fig. 4C) is located northeast of M6. Surface-water temperatures varied from 3.3 and 5 °C. Between mid-November (4B) and early January (4C), Chl *a* values varied between 0.26 and 0.35 μg L^{-1}, whilst D_{Fe} decreased from 0.22 to 0.09 nM during this period in the top 100 m. This decrease corresponds to a small bloom (Venables et al., 2007) that occurred in late December, with the phytoplankton community presumably removing the available Fe.

Overall, these values are consistent with this being a typical HNLC region in contrast to the north of the plateau.

3.3.2. Station M3

M3 (Station 496; Fig. 5A, Station 572 Fig. 5B; Station 592 Fig. 5C, Station 622, Fig. 5D) is located

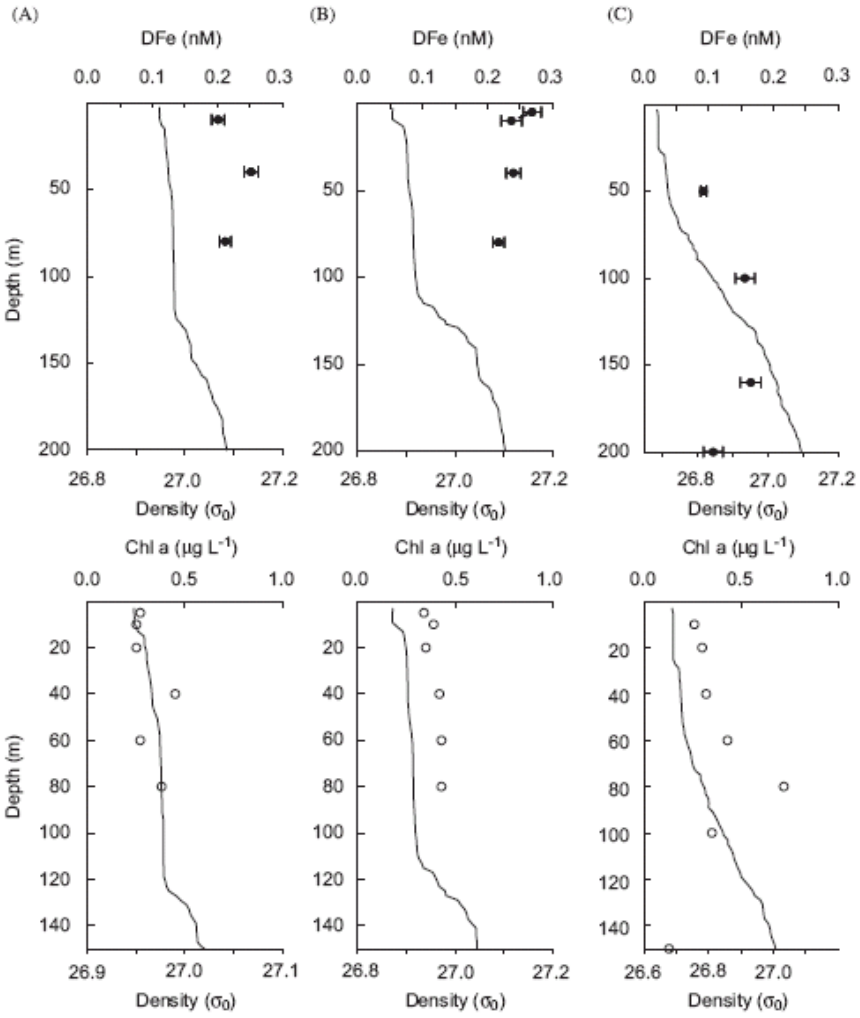

Fig. 4. Water-column profiles of D_{Fe}, salinity, temperature and Chlorophyll *a* at: (A) M6, Station 511 (22/11/2004); (B) M2.1, Station 502 (19/11/2004) and (C) M2.2, Station 605 (06/01/2005).

~35 km north of the plateau in an area where it was hypothesized that the bloom developed in direct response to an input of dissolved Fe from the islands. This station was occupied five times. Only four stations are shown on Fig. 5 as too few data were available for Station 516 (Table 1). Sea-surface temperature varied from 4.4 °C at the beginning of the sampling period (13/11/2004, Station 496) to 6.1 °C at the end (Station 622). The mixed-layer depths were relatively shallow (40–70 m) for all the occupations.

The first occupation (496, Fig. 5A) was after the main bloom event (Venables et al., 2007) in mid-October and appeared to be under the influence of an influx of new water coming from the HNLC south (Pollard et al., 2007). Consequently, surface chlorophyll concentrations were lower than expected at this station, with a maximum of 0.15 μg L^{-1} at 42 m depth. D_{Fe} concentrations above the mixed-layer depth were very low with a mean value of 0.1 nM. The later two occupations (Stations 572 (Fig. 5B) and 592 (Fig. 5C)) exhibit low chlorophyll concentrations, varying from 0.58 to 0.85 μg L^{-1}. In parallel, D_{Fe} concentrations in the upper water column varied with time, and had a mean value of 0.26 nM within the mixed layer. At Station 592, a D_{Fe} maximum of 0.4 nM was

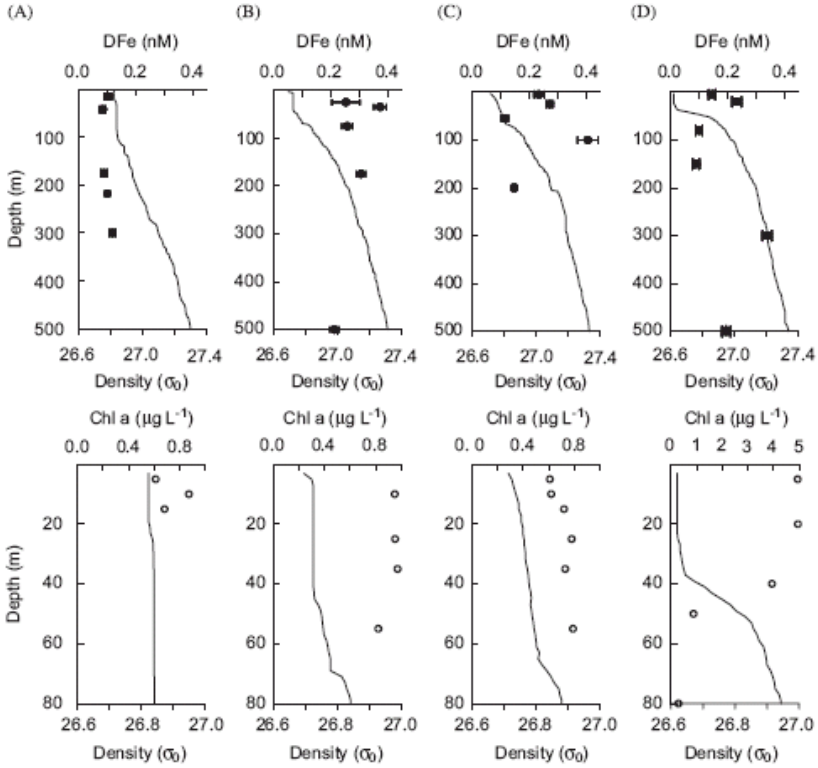

Fig. 5. Water column profiles of D_{Fe}, salinity, temperature and Chlorophyll *a* at M3: (A) Station 496 (13/11/2004); (B) Station 572 (22/12/2004); (C) Station 592 (31/12/2004) and (D) Station 622 (10/01/2005).

observed just below the pycnocline. The last occupation in January 2005 (Station 622, Fig. 5D) was during a secondary bloom event, with chl *a* concentrations reaching 5 μg L^{-1}, with D_{Fe} concentrations depleted down to 0.1 nM within the mixed layer. Another D_{Fe} maximum of 0.34 nM was observed at 300 m. No values as high were found at the Southern sites.

3.3.3. *Baie Américaine*

Three stations were occupied: 567 (Fig. 6A), 568 (Fig. 6B), and 569 (Fig. 6C), which were located progressively further away from the shore. Station 567 was approximately 1 km from the shore, in shallow waters (80 m). At this station, D_{Fe} concentrations were remarkably high (>0.5 nM), with a 2.16 nM peak at 50 m depth and surface values were close to 1 nM (Fig. 6A). Interestingly, Chl *a* concentration within this mixed, and potentially turbid, water column were low, with a mean value of 0.5 μg L^{-1}, suggesting the potential for light limitation within near-shore waters.

Station 568, is located northeast of 567 and at ~8.2 km distance from the shore. Within the mixed layer (80 m), D_{Fe} and Chl *a* concentrations were relatively constant, at around 0.5 nM and 0.5 μg L^{-1}, respectively. Elevated D_{Fe} concentrations of 1 nM at 200 m then 2 nM at 300 m, and a lower value of 0.5 nM near the bottom (376 m) were observed. The last station (569) offshore in this transect was located 16 km away from the shore. Here again, within the mixed layer (50 m) D_{Fe} and Chl *a* were relatively constant. An increase in the D_{Fe} concentration of 0.4 nM was observed at 300 m depth. Chl *a* concentration were higher at Station 569, up to 1.67 μg L^{-1}, which corresponded to a low D_{Fe} concentration (0.18 nM) in surface waters.

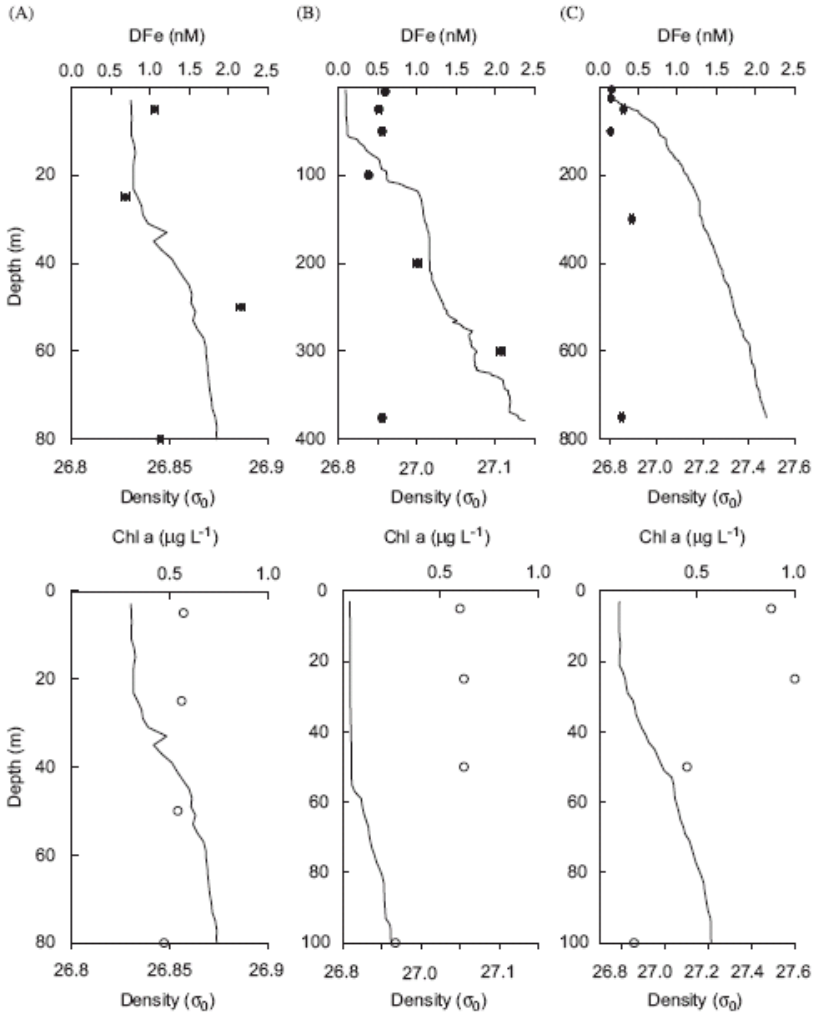

Fig. 6. Water column profiles of D_{Fe}, salinity, temperature and Chlorophyll *a* along a transect from Baie Américaine on 22/12/2004: (A) BA, Station 567; (B) BA + 1, Station 568 and (C) BA + 2, Station 569.

3.3.4. Other stations: M1 (491), M10 (563), M7 (524)

Vertical profiles (Table 1) obtained downstream of the islands (Stations M1, M10, M7) exhibit similar concentrations to those reported by Croot et al. (2004a) and Sedwick et al. (2002) for the 0.4-µm filtered fraction, with concentrations ranging from 0.1 nM in surface waters to 0.5 nM at greater depths. A low-level variability is evident between these stations, with concentrations ranging from 0.2 to 0.4 nM in the upper water column.

M1 and M7 were sampled in November; when the concentrations of Chl *a* were quite high for both, 0.79 for M1 and up to 1.20 µg m^{-3} at M7, respectively. D_{Fe} concentrations were very similar, around 0.3 nM in the upper water column with no depth related trends evident. M10 was sampled after the major blooms in late December. Concentrations

of Fe are higher, around 0.5 nM, and chlorophyll concentrations are very low, 0.3 μg L^{-1}.

4. Discussion

Examining the supply of Fe and the mechanisms that drive the annual phytoplankton bloom north of the Crozet Plateau are of great interest for understanding how natural Fe fertilization may alleviate HNLC conditions normally associated with the Southern Ocean. The present study will discuss briefly the relationship between Chl *a* and D_{Fe} distribution then focus on the relative importance of atmospheric, lateral and upwelling mixing processes in the supply of D_{Fe} to surface waters by using a variety of approaches.

4.1. Upper water column (50 m) distributions of D_{Fe} and their relationship to Chl a

Overall, the surface concentrations of D_{Fe} are similar to recently reported values in this sector of the Southern Ocean. Conducted in the late summer 1998, Croot et al. (2004a) using chemiluminescence detection found dissolved Fe (< 0.4 μm) concentrations from 0.04 to 0.58 nM along a 6°E transect. Sedwick et al. (2002), during ANTARES IV (January–February 1999) around the Crozet Islands, reported D_{Fe} concentrations varying between 0.09 and 0.50 nM over the top 300 m (< 0.4 μm) using catalytic spectrophotometric detection (Measures et al., 1995.). More recently, Blain et al. (2007) reported a mean concentration around the Kerguelen Islands of 0.09 ± 0.034 nM over the top 500 m.

However, a study conducted around the Kerguelen Islands (Bucciarelli et al., 2001) observed considerably higher concentrations of D_{Fe}, in the order of 7 nM. This difference may be explained by the time of sampling, which was prior to the bloom event in October, therefore prior to the main uptake by the phytoplankton, as well as there being a high concentration of lithogenic material (Blain et al., 2001). As Fe is considered to be the main limiting nutrient, one might expect that a high input of Fe will promote a bloom, which will cause an increase in chlorophyll and gradually a decrease in Fe concentrations. However, we do not expect a simple relationship between D_{Fe} and Chl *a*. This may reflect changes in Fe uptake and the fact that the phytoplankton community is affected by other factors such as light availability and grazing (Lancelot et al., 2000). For example, the fact that the Chl *a* concentrations are low very close distance to the shore (Station 567) and where D_{Fe} are the highest could indicate that the light mixing regime is not favourable to the phytoplankton community in these likely turbid waters.

Repeated occupations of Station M3 provide a quasi time series and highlight the complexity of the processes influencing the bloom which is occasionally influenced by advection of near-surface waters from the south (Pollard et al., 2007). Fig. 7

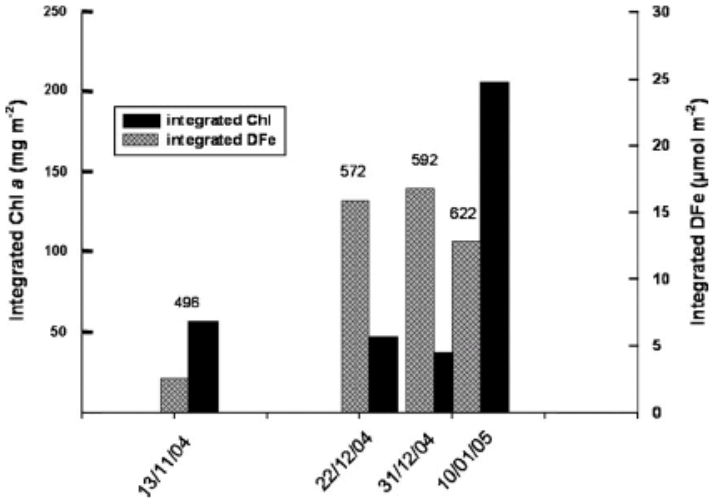

Fig. 7. Variation of integrated Chl *a* and D_{Fe} at Station M3.

represents the variation of integrated Chl *a* and D_{Fe} over time at M3. The first occupation of this Station (572) was sampled at the end of the main bloom, when biological uptake has probably reduced the bioavailable D_{Fe} to a concentration resulting in limitation of the phytoplankton population by mid-November. A temporally and spatially variable Fe resupply proximal to the Plateau may have occurred and reinitiated or maintained small bloom regions. It is also likely that some D_{Fe} recycling processes occur. A combination of these factors may thus explain the high-integrated Chl *a* observed in mid-January and simultaneous decrease in integrated D_{Fe} (Station 622). An additional factor of importance seems to be the ambient irradiance, which appeared to control the bloom initiation and early development (Venables et al., 2007).

Another approach to the link between primary production and D_{Fe} that has been taken by Moore et al. (2007a, b) is to calculate growth rates on addition of D_{Fe}. The reported values to the north of the plateau were of comparable magnitudes to estimates of maximal growth rates for natural population around the Kerguelen Islands (Blain et al., 2001). They also present evidence for Fe limitation within declining stages of the bloom to the north of the islands. Some relationships between enhanced phytoplankton photochemical efficiencies (F_v/F_m) and higher D_{Fe} were also observed *in situ*. At any particular time the relationship between D_{Fe} and Chl *a* will also depend on the stage of bloom progression and the amount of biological Fe uptake that has occurred.

4.2. Sources of dissolved iron

In the following section using the data available, estimates of the various sources of Fe to surface waters around the Crozet Islands and their relative importance are investigated.

4.2.1. Atmospheric inputs

Model estimates based on composites of dust models (Jickells et al., 2005; Mahowald et al., 2005) give annual dust fluxes (wet and dry) of $0.2\,g\,m^{-2}\,yr^{-1}$ in this region, which corresponds to total Fe deposition, assuming an Fe content 3.5% (Jickells and Spokes, 2001) of $132\,\mu mol\,m^{-2}\,yr^{-1}$. There are limited data available for model calibration in the Southern Ocean region and many caveats associated with the aerosol and rainwater calculations (see Section 3.2). However, the two separate approaches (model and field sampling) agree within a factor of three, lending confidence to the estimates. Model estimates suggest little seasonality in dust deposition, although fluxes are lower than the average by about a factor of 2 in the period March–June. During the phytoplankton productive season fluxes are similar to the annual average.

To estimate soluble Fe inputs we used our field data (Section 3.2) and assumed a solubility for dry deposition of 8% (Baker et al., 2006b) and 14% for wet deposition (Jickells and Spokes, 2001), yielding a soluble Fe input of $38\,\mu mol\,m^{-2}\,yr^{-1}$, equivalent to a dissolved Fe flux (F_{atm}) of 104 (rounded to 100) $nmol\,m^{-2}\,d^{-1}$ (Fig. 9). Since the review by Jickells and Spokes (2001), Willey et al. (2004) and Kieber et al. (2005) have reported the active photochemical production of soluble Fe(II) and also higher Fe solubilties in North Atlantic rains, while Halstead et al. (2000) report similar solubilities to those of Jickells and Spokes (2001). The solubility of Fe in rainwater is clearly an important uncertainty in these calculations and merits further study.

It is not straightforward to estimate uncertainties on the overall soluble Fe flux presented in Table 4. This uncertainty will have three main components—physical flux (precipitation/deposition velocity), concentration variation and solubility, plus analytical uncertainties that are generally small by comparison. Deposition velocities are considered to have an uncertainty of a factor of 3 (Duce et al., 1991), and our estimate of rainfall amount in 3.2 has a 50% uncertainty. The overall variability of aerosol concentrations is 25–100% (Table 4) among the suite of samples we collected, but of course this set is from a limited field campaign and it is unlikely we captured the full range of variability seen in this area. Our rainwater concentrations have been volume-weighted, which provides a more reliable average but means we cannot directly provide an estimate of variability. Since total soluble Fe fluxes are dominated by wet deposition, the uncertainties in precipitation amount (factor of 2), volume weighted concentration and solubility dominate. Thus it seems likely that the uncertainty in fluxes is of the order of a factor 2–5. Mahowald et al. (2005) suggest uncertainties in model based dust fluxes are probably an order of magnitude.

4.2.2. Vertical transport of D_{Fe} to surface water

Charette et al. (2007) used a simple one-dimensional diffusive model on the vertical profile of

^{228}Ra at M3 along with an average dissolved Fe gradient across the same depth interval, and determined two mixing scenarios: a slow mixing situation between 1000 and 300 m depth ($K_z = 1.5\,cm^2\,s^{-1}$) and a fast mixing situation between 5 and 300 m depth ($K_z = 11\,cm^2\,s^{-1}$). The maximum contribution of this potential source is then obtained using the upper estimate of the mixing rate ($11\,cm^2\,s^{-1}$) over the top 300 m and a D_{Fe} gradient of $0.64\,nmol\,m^{-3}\,m^{-1}$ (0.15 nM at 5 m depth, 0.34 nM at 300 m) and the maximum D_{Fe} vertical mixing rate would be $F_z = 61\,nmol\,m^{-2}\,d^{-1}$ (Fig. 9). Blain et al. (2007) reported a K_z of $3.3\,cm^2\,s^{-1}$ over the Kerguelen Plateau, leading to a vertical input of $31\,nmol\,m^{-2}\,d^{-1}$.

4.2.3. Lateral sources of Fe from the island system

The last input one can consider in this system with the data available is the lateral transport of dissolved Fe from the islands to the surrounding waters.

The average water-column D_{Fe} concentrations found immediately in the vicinity of Baie Américaine are 1.25 nM at Station 567 (closest to the islands) and 0.81 nM at Station 568. These are the highest concentrations found during our study and give us reasonable confidence that the island system is a source of Fe. This source can be from sediments on the shelf (Elrod et al., 2004), direct runoff, and there is also the possibility that soluble Fe can be leached from suspended particles as they are laterally advected through the water column (Lam et al, 2006).

Moreover, Stations 567, 568, 569 (Baie Américaine) and 572 (M3) show a clear decreasing gradient (Fig. 8) of D_{Fe} concentrations at all depths. Using the same approach as Johnson et al. (1997), it is possible to estimate a scale length, which is defined as "the distance over which concentrations drop to $1/e$ of the initial value". Looking at the upper 50 m, our scale length is 25 km, which is considerably lower than the scale length of 151 km estimated by Bucciarelli et al. (2001) in the vicinity of Kerguelen Islands in the near-shore waters. This difference may be explained by a different circulation pattern around the two islands but more importantly by the difference between the respective surface areas of the islands. The Kerguelen Islands have a surface area of 7000 km^2 and the Crozet Islands only 350 km^2; thus the magnitude of natural Fe fertilization could be lowered. Significant loss of horizontally advected Fe from the sediments and shelf can occur too, in particular with scavenging onto sinking particles before all of this Fe can be distributed to the entire bloom region, which extends well north of M3.

The circulation as described by Pollard et al. (2007) has the consequence of semi-enclose the area

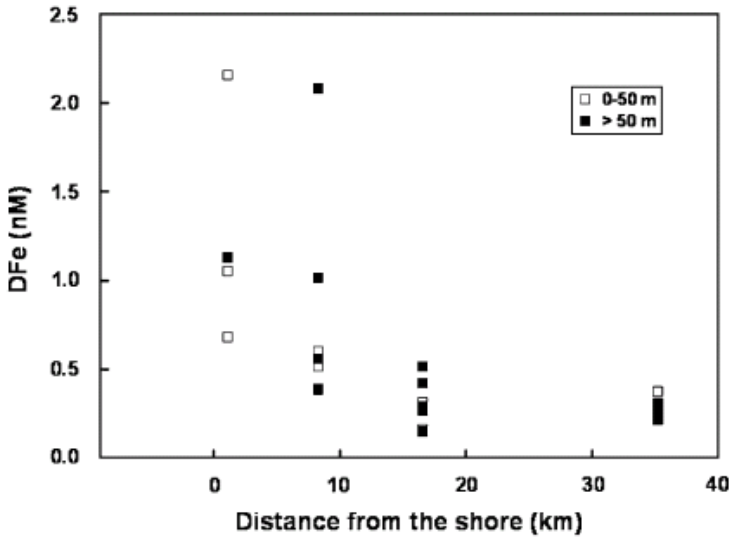

Fig. 8. D_{Fe} versus distance from the shore along the Baie Américaine transect extended out to M3 (Station 572).

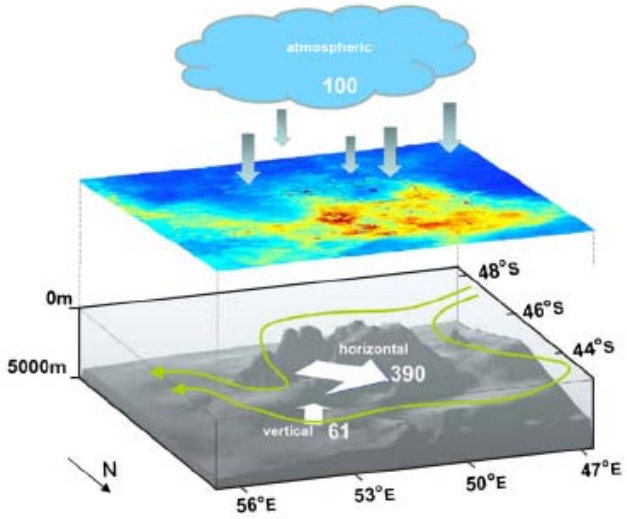

Fig. 9. Main pathways of D_{Fe} in nmol $m^{-2} d^{-1}$ into the bloom area around the Crozet Islands combining the main circulation paths (green lines), topography and a SeaWIFS chlorophyll a image for the austral summer 2004–2005.

to the north of the Crozet Plateau (Fig. 3), where the residence time of surface water is ~60 days. Consequently the large bloom observed in this HNLC area is clearly constrained by this northern branch, as well as any dissolved Fe from the islands and the associated plateau.

If one considers the island and the plateau systems to be a source of Fe throughout the year, then during the low light conditions of the winter when primary production is low, the concentration of Fe can build up and disperse laterally and then be readily available in springtime. Charette et al. (2007) used short-lived Radium isotopes ^{223}Ra and ^{224}Ra on the transect from Baie Américaine (Stations 567, 568 and 569) to provide an upper estimate of this horizontal flux (F_h) of 236 μmol $m^{-2} d^{-1}$ using a linear gradient of 0.07 nM km^{-1} (average of D_{Fe} in the upper 50 m). Giret et al. (2002) reported a homogeneous mantle geochemical composition in this zone, so it seems reasonable to assume that the two main islands are geochemically representative of the Archipelago and that the offshore gradient will be representative of the islands and shelf system as a whole.

Using a 600-km shoreline and a bloom area of 90 000 km^2 (Charette et al., 2007), the cumulative effect of this horizontal flux is estimated to be up to 390 nmol $m^{-2} d^{-1}$, which is considerably higher than either the atmospheric or vertical inputs (Fig. 9). Another important fact is that the horizontal gradient of D_{Fe} was calculated in the upper 50 m near the shore therefore not including the deeper waters nor the plateau itself. This D_{Fe} gradient would be enhanced further if the whole width of the continental shelf is considered (Luther and Wu, 1997).

4.3. Estimation of D_{Fe} before the main bloom event

To constrain the potential of an island Fe source initiating the austral spring bloom, it is possible to estimate the D_{Fe} concentration that would have built up over the Austral winter.

This region under the island effect can be subjected to the three types of inputs that have been considered in this work: atmospheric, vertical and horizontal fluxes. The addition of these three fluxes multiplied by a winter period of 100 days, and over a winter mixed-layer depth of 100 m (Eq. (4)), leads to a final concentration of D_{Fe} prior to the bloom of 0.55 nM:

$$\frac{(F_{atm} + F_z + F_h) \times 100}{100}. \quad (4)$$

This estimate is lower than but of the same magnitude as the 0.75 nM demand derived independently by Lucas et al. (2007). Overall our calculations support the view that our D_{Fe} fluxes can

support phytoplankton new production in the northern bloom region, but only by invoking D_{Fe}:N cell quotas of $<0.06\,mmol\,mol^{-1}$ (Lucas et al., 2007), which probably reflects the relative availability of ambient D_{Fe} and N.

In addition to Fe sources so far discussed, it is also important to look at the potential role of suspended particles. Soluble Fe can be leached from suspended particles as they are laterally advected through the water column, as recently described by Lam et al. (2006). It is also possible that colloidal Fe may be released from sediments and added to Fe advected to the bloom area. These additional sources could increase the Fe budget at the end of the winter and require further investigation.

5. Summary and conclusions

The area investigated by CROZEX covers a broad range of hydrographic and biogeochemical conditions and therefore allows a comparison between a low-productivity low-Fe zone and a high-productivity, relatively high-Fe zone at the edge of the Southern Ocean. Overall, the concentrations of D_{Fe} found are low in surface waters because we sampled after the main bloom event, and they are in the range of values reported in other studies from this area (Sedwick et al., 2002. Croot et al., 2004a).

This data set allows us to propose a scenario for the bloom initiation and maintenance northwards of the Crozet Archipelago during the austral summer. The transect of stations from Baie Américaine shows a distinct concentration gradient, thus providing strong evidence for the island shelf system being a source of Fe. Other input terms to the surface water considered included atmospheric deposition input and vertical mixing. However, the present estimate shows that horizontal advection is the largest term, followed by the atmospheric and then the vertical mixing. Over the winter period when productivity is light limited, the concentration of Fe is estimated to build up to ~0.55 nM in waters to the north of the islands. As light levels increase gradually over the spring and summer, the bloom can be initiated and progress with this ambient D_{Fe}.

This first overall estimate of Fe supply fuelling the bloom to the north of the Crozet Islands therefore provides a rationalization and an indication of the relative importance of different sources of Fe in these Sub-Antarctic Island systems. Present significant uncertainties include the recycling and removal of Fe and the significance and availability of particulate Fe to the primary producers.

Acknowledgments

We would like to thank the Captain, officers, engineers, technicians and crew of the *RRS Discovery* for their enthusiasm and their professional assistance. These cruises were the two first of the Crozex project, which was a contribution to a British BICEP (Biophysical Interactions and Control of Export Production)—NERC program. This work was also supported by NERC Grant NE/B502844/1 and a NERC Ph.D. studentship for M.F.

We also acknowledge R. Pollard and E. Popova for their help with illustrations, and the thoughtful and constructive comments of three anonymous referees who greatly improved the quality of this paper.

References

Arrigo, K.R., Worthen, D., Schnell, A., Lizotte, M.P., 1998. Primary production in Southern Ocean waters. Journal of Geophysical Research 103 (C8), 15,587–15,600.

De Baar, H.J.W., de Jong, J.T.M., Nolting, R.F., van Leeuwe, M.A., Timmermans, K.R., Templin, M., Rutgers van der Loeff, M.M., Sildam, J., 1999. Low dissolved Fe and the absence of diatom blooms in remote Pacific waters of the Southern Ocean. Marine Chemistry 66, 1–34.

De Baar, H.J.W., Boyd, P.W., Coale, K.H., Landry, M.R., Tsuda, A., Assmy, P., Bakker, D.C.E., Bozec, Y., Barber, R.T., Brzezinski, M.A., Buesseler, K.O., Boyé, M., Croot, P.L., Gervais, F., Gorbunov, M.Y., Harrison, P.J., Hiscock, W.T., Laan, P., Lancelot, C., Law, C.S., Levasseur, M., Marchetti, A., Millero, F.J., Nishioka, J., Nojiri, Y., van Oijen, T., Riebesell, U., Rijkenberg, M.J.A., Saito, H., Takeda, S., Timmermans, K.R., Veldhuis, M.J.W., Waite, A., Wong, C.S., 2005. Synthesis of iron fertilization experiments: from the Iron Age in the age of enlightenment. Journal of Geophysical Research (Oceans) 110 (C09S16), 1–24.

Baker, A.R., Kelly, S.D., Biswas, K.F., Witt, M., Jickells, T.D., 2003. Atmospheric deposition of nutrients to the Atlantic Ocean. Geophysical Research Letters 30, 2296.

Baker, A.R., French, M., Linge, K.L., 2006a. Trends in aerosol nutrient solubility along a west-east transect of the Saharan dust plume. Geophysical Research Letters 33, L07805.

Baker, A.R., Jickells, T.D., Witt, M., Linge, K.L., 2006b. Trends in the solubility of iron, aluminium, manganese and phosphorus in aerosol collected over the Atlantic Ocean. Marine Chemistry 98, 43–58.

Bakker, D.C.E., Watson, A.J., Law, C.S., 2001. Southern Ocean iron enrichment promotes inorganic carbon drawdown. Deep-Sea Research II 48, 2483–2507.

Bakker, D.C.E., Bozec, Y., Nightingale, P.D., Goldson, L., Messias, M.-J., De baar, H.J.W., Liddicoat, M., Skjelvan, I., Strass, V., Watson, A.J., 2005. Iron and mixing affect

biological carbon uptake in SOIREE and EISENEX. Two Southern Ocean iron fertilisation experiments. Deep-Sea Research I 52, 1001–1019.

Blain, S., Tréguer, P., Belviso, S., Bucciarelli, E., Denis, M., Desabre, S., Fiala, M., Martin Jézéquel, V., Le Fèvre, J., Mayzaud, P., Marty, J.-C., Razouls, S., 2001. A biogeochemical study of the island mass effect in the context of the iron hypothesis: Kerguelen Islands, Southern Ocean. Deep-Sea Research I 48 (1), 163–187.

Blain, S., Sedwick, P.N., Griffiths, F.B., Quéguiner, B., Bucciarelli, E., Fiala, M., Pondaven, P., Tréguer, P., 2002. Quantification of algal iron requirements in the Subantarctic Southern Ocean (Indian sector). Deep-Sea Research II 49 (16), 3255–3273.

Blain, S., Quéguiner, B., Armand, L., Belviso, S., Bombled, B., Bopp, L., Bowie, A., Brunet, C., Brussaard, C., Carlotti, F., Christaki, U., Corbière, A., Durand, I., Ebersbach, F., Fuda, J.-L., Garcia, N., Gerringa, L., Griffiths, B., Guigue, C., Guillerm, C., Jacquet, S., Jeandel, C., Laan, P., Lefèvre, D., Lo Monaco, C., Malits, A., Mosseri, J., Obernosterer, I., Park, Y.-H., Picheral, M., Pondaven, P., Remenyi, T., Sandroni, V., Sarthou, G., Savoye, N., Scouarnec, L., Souhaut, M., Thuiller, D., Timmermans, K., Trull, T., Uitz, J., van Beek, P., Veldhuis, M., Vincent, D., Viollier, E., Vong, L., Wagener, T., 2007. Effect of natural iron fertilization on carbon sequestration in the Southern Ocean. Nature 446, 1070–1074.

Boyd, P.W., Watson, A.J., Law, C.S., Abraham, E.R., Trull, T., Murdoch, R., Bakker, D.C.E., Bowie, A.R., Buesseler, K.O., Chang, H., Charette, M., Croot, P., Downing, K., Frew, R., Gall, M., Hadfield, M., Hall, J., Harvey, M., Jameson, G., LaRoche, J., Liddicoat, M., Ling, R., Maldonado, M.T., McKay, R.M., Nodder, S., Pickmere, S., Pridmore, R., Rintoul, S., Safi, K., Sutton, P., Strzepek, R., Tanneberger, K., Turner, S., Waite, A., Zeldis, J., 2000. A mesoscale phytoplankton bloom in the polar Southern Ocean stimulated by iron fertilization. Nature 407, 695–702.

Boyd, P.W., Law, C.S., Wong, C.S., Nojiri, Y., Tsuda, A., Levasseur, M., Takeda, S., Rivkin, R., Harrison, P.J., Strzepek, R., Gower, J., McKay, R.M., Abraham, E., Arychuk, M., Barwell-Clarke, J., Crawford, W., Crawford, D., Hale, M., Johnson, K., Kiyosawa, J., Kudo, I., Marchetti, A., Miller, W., Needoba, J., Nishioka, J., Ogawa, J., Page, J.T., Robert, M., Saito, H., Sastri, A., Sherry, N., Soutar, T., Sutherland, N., Taira, Y., Whitney, F., Wong, S.K.E., 2004. The decline and fate of an iron-induced Subarctic phytoplankton Bloom. Nature 428, 549–553.

Boyd, P.W., Jickells, T., Law, C.S., Blain, S., Boyle, E.A., Buesseler, K.O., Coale, K.H., Cullen, J.J., de Baar, H.J.W., Follows, M., Harvey, M., Lancelot, C., Levasseur, M., Owens, N.P.J., Pollard, R., Rivkin, R.B., Sarmiento, J., Schoemann, V., Smetacek, V., Takeda, S., Tsuda, A., Turner, S., Watson, A.J., 2007. Mesoscale iron enrichment experiments 1993–2005: synthesis and future directions. Science 315, 612–617.

Boyé, M., Nishioka, J., Croot, P.L., Laan, P., Timmermans, K.R., de Baar, H.J.W., 2005. Major deviations of iron complexation during 22 days of a mesoscale iron enrichment in the open Southern Ocean. Marine Chemistry 96 (3–4), 257–271.

Bucciarelli, E., Blain, S., Tréguer, P., 2001. Iron and manganese in the wake of the Kerguelen Islands (Southern Ocean). Marine Chemistry 73 (1), 21–36.

Buesseler, K.O., Andrews, J.E., Pike, S.M., Charette, M.A., 2004. The effects of iron fertilization on carbon sequestration in the Southern Ocean. Science 304, 414–417.

Charette, M.A., Gonneea, M. E., Morris, P.J., Statham, P.J., Fones, G.R., Planquette, H.F., Salter, I., Naveira Garabato, A., 2007. Radium isotopes as tracers of iron sources fueling a Southern Ocean phytoplankton bloom. Deep-Sea Research II, this issue [doi:10.1016/j.dsr2.2007.06.003].

Chisholm, S.W., 2000. Oceanography: stirring times in the Southern Ocean. Nature 407, 685–687.

Coale, K.H., Johnson, K.S., Chavez, F.P., Buesseler, K.O., Barber, R.T., Brzezinski, M.A., Cochlan, W.P., Millero, F.J., Falkowski, P.G., Bauer, J.E., Wanninkhof, R.H., Kudela, R.M., Altabet, M.A., Hales, B.E., Takahashi, T., Landry, M.R., Bidigare, R.R., Wang, X., Chase, Z., Strutton, P.G., Friederich, G.E., Gorbunov, M.Y., Lance, V.P., Hilting, K.A., Hiscock, M.R., Demarest, M., Hiscock, W.T., Sullivan, K.F., Tanner, S.J., Gordon, M.R., Hunter, C.N., Elrod, V.A., Fitzwater, S.E., Jones, J.L., Tozzi, S., Koblizek, M., Roberts, A.E., Herndon, J., Brewster, J., Ladizinsky, N., Smith, G., Cooper, D., Timothy, D., Brown, S.L., Selph, K.E., Sheridan, C.C., Twining, B.S., Johnson, Z.I., 2004. Southern Ocean iron enrichment experiment: carbon cycling in high- and low-Si waters. Science 304 (5669), 408–414.

Croot, P.L., Andersson, K., Öztürk, M., Turner, D.R., 2004a. The distribution and speciation of iron along 6ºE in the Southern Ocean. Deep-Sea Research II 51, 2857–2879.

Croot, P.L., Streu, P., Baker, A.R., 2004b. Short residence time for iron in surface water impacted by atmospheric dry deposition from Saharan dust events. Geophysical Research Letters 31, L32S08.

Croot, P.L., Laan, P., Nishioka, J., Boyé, M., Timmermans, K.R., Bellerby, R.G., Goldson, L., Nightingale, P., de Baar, H.J.W., 2005. Spatial and temporal distribution of Fe(II) and H_2O_2 during EISENEX, an open ocean mesoscale iron enrichment. Marine Chemistry 95, 65–88.

Draxler, R.R., Rolph, G.D., 2003. HYSPLIT (Hybrid Single-Particle Lagrangian Integrated Trajectory) Model access via NOAA ARL READY website 〈http://www.arl.noaa.gov/ready/hysplit4.html〉 NOAA Air Resources Laboratory, Silver Spring, MD.

Duce, R.A., Liss, P.S., Merrill, J.T., Atlas, E.L., Buat-Ménard, P., Hicks, B.B., Miller, J.M., Prospero, J.M., Arimoto, R., Church, T.M., Ellis, W.E., Galloway, J.N., Hansen, L., Jickells, T.D., Knap, A.H., Reinhardt, K.H., Schneider, B., Soudine, A., Tokos, J.J., Tsunogai, S., Wollast, R., Zhou, M., 1991. The atmospheric input of trace species to the world ocean. Global Biogeochemical Cycles 5, 193–259.

Elrod, V.A., Berelson, W.M., Coale, K.H., Johnson, K.S., 2004. The flux of iron from continental shelf sediments: a missing source for global budgets. Geophysical Research Letter 31, L12307, doi:10.1029/2004GLO20216.

Fiala, M., Delille, B., Dubreuil, C., Kopczynska, E., Leblanc, K., Morvan, J., Quéguiner, B., Blain, S., Caillau, C., Conan, P., Corvaiser, R., Denis, M., Frankignoulle, M., Oriol, L., Roy, S., 2003. Mesoscale surface distribution of biogeochemical characteristics in the Crozet Basin frontal zones (South Indian Ocean). Marine Ecology Progress Series 249, 1–14.

Gaiero, D.M., Probst, J.-L., Depetris, P.J., Bidart, S.M., Leleyter, L., 2003. Iron and other transition metals in Patagonian riverborne and windborne materials: geochemical

control and transport to the Southern South Atlantic Ocean. Geochimica et Cosmochimica Acta 67 (19), 3603–3623.

Giret, A., Tourpin, S., Marc, S., Verdier, O., Cottin, J.-Y., 2002. Volcanisme de l'île aux Pingouins, archipel Crozet, témoin de l'hétérogénéité du manteau fertile au sud de l'océan Indien. Penguins Island, Crozet archipelago, volcanic evidence for a heterogeneous mantle in the Southern Indian Ocean. Comptes Rendus Geosciences 334, 481–488.

Halstead, M.J.R., Cunninghame, R.G., Hunter, K.A., 2000. Wet deposition of trace metals to a remote site in Fiordland, New Zealand. Atmospheric Environment 34 (4), 665–676.

Jickells, T.D., An, Z.S., Andersen, K.K., Baker, A.R., Bergametti, G., Brooks, N., Cao, J.J., Boyd, P.W., Duce, R.A., Hunter, K.A., Kawahata, H., Kubilay, N., laRoche, J., Liss, P.S., Mahowald, N., Prospero, J.M., Ridgwell, A.J., Tegen, I., Torres, R., 2005. Global iron connections between desert dust, ocean biogeochemistry and climate. Science 308, 67–71.

Jickells, T.D., Spokes, L.J., 2001. Atmospheric iron inputs to the Oceans. In: Turner, D.R., Hunter, K.A. (Eds.), The Biogeochemistry of Iron in Seawater. IUPAC Series on Analytical and Physical Chemistry of Environmental Systems. Wiley, Chichester, pp. 85–121.

Johnson, K.S., Gordon, R.M., Coale, K.H., 1997. What controls dissolved iron concentrations in the world ocean? Marine Chemistry 57, 137–161.

Jickells, T.D., Kelly, S.D., Baker, A.R., Biswas, K., Dennis, P.F., Spokes, L.J., Witt, M., Yeatman, S.G., 2003. Isotopic evidence for a marine ammonia source. Geophysical Research Letters 30 (7), 1374.

De Jong, J.T.M., den Das, J., Bathmann, U., Stoll, M.H.C., Kattner, G., Nolting, R.F., de Baar, H.J.W., 1998. Dissolved iron at subnanomolar levels in the Southern Ocean as determined by shipboard analysis. Analytica Chimica Acta 377, 113–124.

Kieber, R.J., Skrabal, S.A., Smith, B.J., Willey, J.D., 2005. Organic complexation of Fe(II) and its impact on the redox cycling of iron in rain. Environmental Science and Technology 39 (6), 1576–1583.

Korb, R.E., Whitehouse, M.J., Ward, P., 2004. SeaWIFS in the Southern Ocean: spatial and temporal variability in phytoplankton biomass around South Georgia. Deep-Sea Research II 51 (1–3), 99–116.

Lam, P.J., Bishop, J.K.B., Henning, C.C., Marcus, M.A., Waychunas, G.A., Fung, I.Y., 2006. Wintertime phytoplankton bloom in the Subarctic Pacific supported by continental margin iron. Global Biogeochemical Cycles 20 (1).

Lancelot, C., Hannon, E., Becquevort, S., Veth, C., De Baar, H.J.W., 2000. Modeling phytoplankton blooms and carbon export production in the Southern Ocean: dominant controls by light and iron in the Atlantic sector in Austral spring 1992. Deep-Sea Research I 47 (9), 1621–1662.

Luther, G.W., Wu, J., 1997. What controls dissolved iron concentrations in the world ocean?—A comment. Marine Chemistry 57, 173–179.

Law, C.S., Crawford, W.R., Smith, M.J., Boyd, P.W., Wong, C.S., Nojiri, Y., Robert, M., Abraham, E.R., Johnson, W.K., Forsland, V., Arychuk, M., 2006. Patch evolution and the biogeochemical impact of entrainment during an iron fertilisation experiment in the sub-Arctic Pacific. Deep-Sea Research II 53, 2012–2033.

Löscher, B.M., 1999. Relationships among Ni, Cu, Zn, and major nutrients in the Southern Ocean. Marine Chemistry 67, 67–102.

Lohan, M.C., Aguilar-Islas, A., Bruland, K.W., 2006. Direct determination of iron in acidified (pH 1.7) seawater samples by flow injection analysis with catalytic spectrophotometric detection: application and intercomparison. Limnology and Oceanograph (Methods) 4, 164–171.

Lucas, M., Seeyave, S., Sanders, R., Moore, C.M.M., Williamson, R., Stinchcombe, M., 2007. Nitrogen uptake responses to a naturally Fe-fertilised phytoplankton bloom during the 2004/5 CROZEX study. Deep-Sea Research, this issue [doi:10.1016/j.dsr2.2007.06.017].

Mahowald, N.M., Baker, A.R., Bergametti, G., Brooks, N., Jickells, T.D., Duce, R.A., Kubilay, N., Prospero, J.M., Tegen, I., 2005. The atmospheric global dust cycle and iron inputs to the ocean. Global Biogeochemical Cycles 19, GB4025.

Martin, J.H., 1990. Glacial–interglacial CO_2 change: the iron hypothesis. Paleoceanography 5 (1), 1–13.

Measures, C.I., Yuan, J., Resing, J.A., 1995. Determination of iron in seawater by flow injection analysis using in-line preconcentration and spectrophotometric detection. Marine Chemistry 50 (1–4), 3–12.

Metzl, N., Tilbrook, B., Poisson, A., 1999. The annual *f*CO2 cycle and the air–sea CO_2 flux in the sub-Antarctic Ocean. Tellus 51B, 849–861.

Moore, C.M.M., Seeyave, S., Hickman, A.E., Allen, J.T., Lucas, M.I., Planquette, H., Pollard, R.T., Poulton A.J., 2007a. Iron-light interactions during the CROZet natural iron bloom and EXport experiment (CROZEX) I: phytoplankton growth and photophysiology. Deep-Sea Research (II), this issue [doi:10.1016/j.dsr2.2007.06.011].

Moore, C.M.M., Hickman, A.E., Poulton, A.J., Seeyave, S., Lucas, M.I., 2007b. Iron-light interactions during the CROZet natural iron bloom and EXport experiment (CROZEX) II: taxonomic responses and elemental stoichiometry. Deep-Sea Research (II), this issue [doi:10.1016/j.dsr2.2007.06.015].

Moore, J.K., Abbott, M.R., 2002. Surface chlorophyll concentrations in relation to the Antarctic Polar Front: seasonal and spatial patterns from satellite observations. Journal of Marine Systems 37, 69–86.

Park, Y.-H., Pollard, R.T., Read, J.F., Leboucher, V., 2002. A quasi-synoptic view of the frontal circulation in the Crozet Basin during the Antares-4 cruise. Deep-Sea Research II 49 (9–10), 1823–1842.

Pollard, R.T., Read, J.F., 2001. Circulation pathways and transports of the Southern Ocean in the vicinity of the Southwest Indian Ridge. Journal of Geophysical Research 106 (C2), 2881–2898.

Pollard, R.T., Lucas, M.I., Read, J.F., 2002. Physical controls on biogeochemical zonation in the Southern Ocean. Deep-Sea Research Part Ii—Topical Studies in Oceanography 49 (16), 3289–3305.

Pollard, R.T., Venables, H.J., Read, J.F., Allen, J.T., 2007. Large scale circulation around the Crozet Plateau controls an annual phytoplankton bloom in the Crozet Basin. Deep-Sea Research II, this issue [doi:10.1016/j.dsr2.2007.06.012].

Read, J.F., Pollard, R.T., Allen, J.T., 2007. Sub-mesoscale structure and the development of an eddy in the Subantarctic Front north of Crozet Islands. Deep-sea Research II, this issue [doi:10.1016/j.dsr2.2007.06.013].

Sanders, R., Morris, P.J., Stinchcombe, M., Seeyave, S., Venables, H.J., Lucas, M.I., 2007. New production and the

f-ratio around the Crozet Plateau in austral summer 2004-5 diagnosed from seasonal changes in inorganic nutrient levels. Deep-Sea Research II, this issue [doi:10.1016/j.dsr2.2007.06.007].

Sarmiento, J.L., Hughes, T.M.C., Stouffer, R.J., Manabe, S., 1998. Simulated response of the ocean carbon cycle to anthropogenic climate warming. Nature 393 (6682), 245–249.

Sarthou, G., Jeandel, C., Brisset, L., Amouroux, D., Besson, T., Donard, O.F.X., 1997. Fe and H_2O_2 distributions in the upper water column in the Indian sector of the Southern Ocean. Earth and Planetary Science Letters 147, 83–92.

Sarthou, G., Baker, A.R., Blain, S., Achterberg, E.P., Boyé, M., Bowie, A.R., Croot, P.L., Laan, P., de Baar, H.J.W., Jickells, T.D., Worsfold, P., 2003. Atmospheric iron deposition and sea-surface dissolved iron concentrations in the eastern Atlantic Ocean. Deep-Sea Research I 50 (10–11), 1339–1352.

Sedwick, P.N., Blain, S., Quéguiner, B., Griffiths, F.B., Fiala, M., Bucciarelli, E., Denis, M., 2002. Resource limitation of phytoplankton growth in the Crozet Basin, Subantarctic Southern Ocean. Deep-Sea Research Part II 49 (16), 3327–3349.

Seeyave, S., Lucas, M.I., Moore, C.M., Poulton, A.J., 2007. Phytoplankton productivity and community structure across the Crozet Plateau during summer 2004/2005. Deep-Sea Research, this issue [doi:10.1016/j.dsr2.2007.06.010].

Spokes, L., Jickells, T.D., Jarvis, K., 2001. Atmospheric inputs of trace metals to the northeast Atlantic Ocean: the importance of southeasterly flow. Marine Chemistry 76, 319–330.

Sunda, W.G., Huntsman, S.A., 1995. Iron uptake and growth limitation in oceanic and coastal phytoplankton. Marine Chemistry 50 (1–4), 189–206.

Sunda, W.G., Huntsman, S.A., 1997. Interrelated influence of iron, light and cell size on marine phytoplankton growth. Nature 390, 389–392.

Taljaard, J.J., Loom, H.V., 1984. Climatology of the Indian Ocean south of 35°S. In: Loom, H.V. (Ed.), Climate of the Ocean. Elsevier, Amsterdam, pp. 505–601, 716pp.

Tréguer, P., Jacques, G., 1992. Dynamics of nutrient and phytoplankton and cycles of carbon, nitrogen and silicon in the Southern Ocean: a review. Polar Biology 12, 149–162.

Tréguer, P., Pondaven, P., 2001. Preface: climatic changes and the carbon cycles in the Southern Ocean: a step forward. Deep-Sea Research II 49, 1597–1600.

Venables, H., Pollard, R.T., Popova, E.E., 2007. Physical conditions controlling the early development of a regular phytoplankton bloom north of the Crozet Plateau, Southern Ocean. Deep-Sea Research II, this issue [doi:10.1016/j.dsr2.2007.06.014].

Welschmeyer, N.A., 1994. Fluorometric analysis of chlorophyll-a in the presence of chlorophyll-*b* and pheopigments. Limnology and Oceanography 39 (8), 1985–1992.

Willey, J.D., Kieber, R.J., Avery Jr., G.B., 2004. Effects of rainwater iron and hydrogen peroxide on iron speciation and phytoplankton growth in seawater near Bermuda. Journal of Atmospheric Chemistry 47 (3), 209–222.

APPENDIX IV:

INTEGRATED ACID LEACHABLE IRON IRON DATA AT ALL STATIONS DURING D285 AND D286

In this appendix, detailed calculation of integrated concentrations of LPFe (Table I) is presented.

Site	Station	Depth m	POC µmol L^{-1}	LPFe:C ratio	LPFe pmol L^{-1}	Integrated LPFe nmol m^{-2}
M3	15494	5	7.4	1.842E-06	13.64	76.89
M3	15494	10	9.3	1.842E-06	17.11	141.98
M3	15494	20	6.1	1.842E-06	11.28	257.11
M3	15494	40	7.8	1.842E-06	14.43	300.40
M3	15494	60	8.5	1.842E-06	15.61	318.04
M3	15494	80	8.8	1.842E-06	16.19	304.79
M3	15494	100	7.8	1.842E-06	14.29	344.68
M3	15494	125	7.2	1.842E-06	13.29	314.52
M3	15494	150	6.4	1.842E-06	11.88	283.39
M3	15494	175	5.9	1.842E-06	10.80	223.09
M3	15494	200	3.8	1.842E-06	7.05	
M3	***15494***	***200***				***2565***
M3	15499	10	7.9	6.134E-05	487.35	4280.60
M3	15499	20	6.0	6.134E-05	368.77	7607.87
M3	15499	40	6.4	6.134E-05	392.02	8557.72

M3	15499	60	7.6	6.134E-05	463.75	54.56	7570.82
M3	15499	80	4.8	6.134E-05	293.33	34.51	8805.56
M3	15499	100	9.6	6.134E-05	587.22	69.08	
M3	***15499***	***100***				***total***	***36824***
M2	15504	5	5.9	1.341E-06	7.93	2.94	134.52
M2	15504	20	7.5	1.341E-06	10.00	3.71	388.64
M2	15504	60	7.0	1.341E-06	9.43	3.50	182.69
M2	15504	80	6.6	1.341E-06	8.84	3.28	157.04
M2	15504	100	5.1	1.341E-06	6.86	2.55	146.53
M2	15504	125	3.6	1.341E-06	4.86	1.80	101.78
M2	15504	150	2.4	1.341E-06	3.28	1.22	
M2	***15504***	***150***				***total***	***1111***
M6	15507	5	4.7	3.647E-06	17.16	5.14	89.78
M6	15507	10	5.1	3.647E-06	18.75	5.62	550.63
M6	15507	40	4.9	3.647E-06	17.95	5.38	410.07
M6	15507	60	6.3	3.647E-06	23.05	6.91	457.11
M6	15507	80	6.2	3.647E-06	22.66	6.79	812.53
M6	15507	125	3.7	3.647E-06	13.45	4.03	298.83
M6	15507	150	2.9	3.647E-06	10.45	3.13	253.88
M6	15507	175	2.7	3.647E-06	9.86	2.96	
M6	***15507***	***175***				***total***	***2873***
M3	15518	5	6.5	1.386E-06	9.07	5.05	46.54
M3	15518	10	6.9	1.386E-06	9.55	5.32	291.58
M3	15518	40	7.1	1.386E-06	9.89	5.51	227.23
M3	15518	60	9.3	1.386E-06	12.83	7.15	225.44
M3	15518	80	7.0	1.386E-06	9.71	5.41	189.30
M3	15518	100	6.6	1.386E-06	9.22	5.13	202.28
M3	15518	125	5.0	1.386E-06	6.97	3.88	151.43
M3	15518	150	3.7	1.386E-06	5.15	2.87	117.76
M3	15518	175	3.1	1.386E-06	4.27	2.38	
M3	***15518***	***175***					***1452***
M7	15525	5	11.8	9.05E-07	10.71	10.08	56.75
M7	15525	10	13.2	9.05E-07	11.99	11.28	108.74
M7	15525	20	10.8	9.05E-07	9.76	9.18	214.85
M7	15525	40	13.0	9.05E-07	11.73	11.03	242.36
M7	15525	60	13.8	9.05E-07	12.51	11.77	192.86
M7	15525	80	7.5	9.05E-07	6.78	6.38	116.57
M7	15525	100	5.4	9.05E-07	4.88	4.59	193.27
M7	15525	150	3.1	9.05E-07	2.85	2.68	
M7	***15525***	***150***				***total***	***1125***

M8E	15532	5	5.6	7.98E-06	44.98	13.54	229.17
M8E	15532	10	5.9	7.98E-06	46.69	14.05	495.49
M8E	15532	20	6.6	7.98E-06	52.41	15.77	947.17
M8E	15532	40	5.3	7.98E-06	42.31	12.73	785.79
M8E	15532	60	4.5	7.98E-06	36.27	10.92	979.10
M8E	15532	80	7.7	7.98E-06	61.64	18.55	742.17
M8E	15532	100	1.6	7.98E-06	12.58	3.78	643.23
M8E	15532	150	1.6	7.98E-06	13.15	3.96	731.31
M8E	15532	200	2.0	7.98E-06	16.10	4.85	
M8E	***15532***	***200***				***total***	***5553***
M8W	15538	5	7.9	3.906E-07	3.07	12.43	15.66
M8W	15538	10	8.2	3.906E-07	3.20	12.96	34.57
M8W	15538	20	9.5	3.906E-07	3.71	15.06	71.76
M8W	15538	40	8.9	3.906E-07	3.46	14.03	70.83
M8W	15538	60	9.3	3.906E-07	3.62	14.68	55.79
M8W	15538	80	5.0	3.906E-07	1.96	7.94	42.31
M8W	15538	100	5.8	3.906E-07	2.27	9.22	92.77
M8W	15538	150	3.7	3.906E-07	1.44	5.83	
M8W	***15538***	***150***				***total***	***384***
M9	15553	5	8.5	3.316E-06	28.33	2.64	141.80
M9	15553	10	8.6	3.316E-06	28.39	2.64	291.93
M9	15553	20	9.0	3.316E-06	29.99	2.79	601.12
M9	15553	40	9.1	3.316E-06	30.12	2.80	496.57
M9	15553	60	5.9	3.316E-06	19.54	1.82	434.42
M9	15553	80	7.2	3.316E-06	23.90	2.22	444.83
M9	15553	100	6.2	3.316E-06	20.58	1.92	
M9	***15553***	***100***				***total***	***2411***
M10	15562	5	7.6	6.637E-07	5.07	7.54	25.24
M10	15562	10	7.6	6.637E-07	5.02	7.47	53.46
M10	15562	20	8.5	6.637E-07	5.67	8.43	101.64
M10	15562	40	6.8	6.637E-07	4.50	6.69	79.46
M10	15562	60	5.2	6.637E-07	3.45	5.13	65.43
M10	15562	80	4.7	6.637E-07	3.09	4.60	45.38
M10	15562	100	2.2	6.637E-07	1.44	2.15	
M10	***15562***	***100***				***total***	***371***
M3	15573	10	5.5	4.893E-06	26.68	12.98	280.71
M3	15573	20	6.0	4.893E-06	29.47	14.34	614.03
M3	15573	40	6.5	4.893E-06	31.94	15.54	575.65
M3	15573	60	5.2	4.893E-06	25.63	12.47	477.12
M3	15573	80	4.5	4.893E-06	22.08	10.75	400.60

M3	15573	100	3.7	4.893E-06	17.98	8.75	369.75
M3	15573	125	2.4	4.893E-06	11.60	5.65	
M3	***15573***	***125***				***total***	***2718***
M3	15589	5	9.3	1.516E-06	14.11	59.59	69.70
M3	15589	10	9.1	1.516E-06	13.77	58.12	136.30
M3	15589	20	8.9	1.516E-06	13.49	56.97	274.56
M3	15589	40	9.2	1.516E-06	13.96	58.94	269.43
M3	15589	60	8.6	1.516E-06	12.98	54.80	313.07
M3	15589	80	12.1	1.516E-06	18.33	77.37	275.89
M3	15589	100	6.1	1.516E-06	9.26	39.11	
M3	***15589***	***100***				***total***	***1339***
M6	15596	5	7.9	3.93E-06	30.94	3.23	156.40
M6	15596	10	8.0	3.93E-06	31.62	3.30	320.98
M6	15596	20	8.3	3.93E-06	32.58	3.40	643.73
M6	15596	40	8.1	3.93E-06	31.79	3.32	700.72
M6	15596	60	9.7	3.93E-06	38.28	4.00	619.72
M6	15596	80	6.0	3.93E-06	23.69	2.47	450.21
M6	15596	100	5.4	3.93E-06	21.33	2.23	
M6	***15596***	***100***				***total***	***2892***
M2	15606	5	7.8	1.782E-07	1.38	4.59	7.91
M2	15606	10	10.0	1.782E-07	1.78	5.91	20.37
M2	15606	20	12.9	1.782E-07	2.29	7.61	45.60
M2	15606	40	12.7	1.782E-07	2.27	7.52	38.99
M2	15606	60	9.2	1.782E-07	1.63	5.42	34.89
M2	15606	80	10.4	1.782E-07	1.86	6.16	25.01
M2	15606	100	3.6	1.782E-07	0.64	2.14	25.98
M2	15606	150	2.2	1.782E-07	0.39	1.31	
M2	***15606***	***150***				***total***	***199***
M3	15623	5	14.9	2.146E-05	319.12	34.41	1273.34
M3	15623	10	8.9	2.146E-05	190.21	20.51	1787.78
M3	15623	20	7.8	2.146E-05	167.34	18.04	3724.29
M3	15623	40	9.6	2.146E-05	205.08	22.11	1951.33
M3	15623	50	8.6	2.146E-05	185.18	19.97	1528.25
M3	15623	60	5.6	2.146E-05	120.47	12.99	1767.37
M3	15623	80	2.6	2.146E-05	56.27	6.07	
M3	***15623***	***80***				***total***	***12032***
M3	15628	5	20.5	6.942E-06	142.35	52.95	686.18
M3	15628	10	19.0	6.942E-06	132.12	49.15	1241.73
M3	15628	20	16.7	6.942E-06	116.22	43.23	1722.96
M3	15628	40	8.1	6.942E-06	56.07	20.86	997.83

M3	15628	60	6.3	6.942E-06	43.71	16.26	863.09
M3	15628	80	6.1	6.942E-06	42.60	15.85	
M3	***15628***	***80***				***total***	***5512***

Table AIV- I. Integrated LPFe data during D285 and D286.